



HAL
open science

GABAergic signaling in cortical feedback to the olfactory bulb

Camille Mazo

► **To cite this version:**

Camille Mazo. GABAergic signaling in cortical feedback to the olfactory bulb. *Neurons and Cognition [q-bio.NC]*. Université Pierre et Marie Curie - Paris VI, 2017. English. NNT : 2017PA066066 . tel-01609874

HAL Id: tel-01609874

<https://theses.hal.science/tel-01609874>

Submitted on 4 Oct 2017

HAL is a multi-disciplinary open access archive for the deposit and dissemination of scientific research documents, whether they are published or not. The documents may come from teaching and research institutions in France or abroad, or from public or private research centers.

L'archive ouverte pluridisciplinaire **HAL**, est destinée au dépôt et à la diffusion de documents scientifiques de niveau recherche, publiés ou non, émanant des établissements d'enseignement et de recherche français ou étrangers, des laboratoires publics ou privés.



Université Pierre et Marie Curie

Ecole Doctorale Cerveau, Cognition et Comportement
Laboratoire "Gènes, Synapses et Cognition", CNRS UMR3571
Laboratoire "Perception et Mémoire", Institut Pasteur

GABAergic Signaling in Cortical Feedback
to the Olfactory Bulb

par Camille Mazo

Thèse de doctorat de l'Université Pierre et Marie Curie

Dirigée par Pierre-Marie Lledo et encadrée par Gabriel Lepousez

Présentée et soutenue publiquement le 23 Juin 2017

Devant le jury composé de :

Dr. Andreas Schaefer	Rapporteur
Dr. Didier De Saint Jan	Rapporteur
Dr. Hannah Monyer	Examinatrice
Dr. Karim Benchenane	Examineur
Pr. Alain Trembleau	Examineur
Dr. Pierre-Marie Lledo	Directeur de Thèse



Université Pierre et Marie Curie

Ecole Doctorale Cerveau, Cognition et Comportement
Laboratoire "Gènes, Synapses et Cognition", CNRS UMR3571
Laboratoire "Perception et Mémoire", Institut Pasteur

GABAergic Signaling in Cortical Feedback
to the Olfactory Bulb

par Camille Mazo

Thèse de doctorat de l'Université Pierre et Marie Curie

Dirigée par Pierre-Marie Lledo et encadrée par Gabriel Lepousez

Présentée et soutenue publiquement le 23 Juin 2017

Devant le jury composé de :

Dr. Andreas Schaefer	Rapporteur
Dr. Didier De Saint Jan	Rapporteur
Dr. Hannah Monyer	Examinatrice
Dr. Karim Benchenane	Examineur
Pr. Alain Trembleau	Examineur
Dr. Pierre-Marie Lledo	Directeur de Thèse

Abstract

Cortical feedback is instrumental for sensory perception. Feedforward inputs convey information from the perpetually evolving external world and feedback is believed to gate sensory perception to relevant inputs. In the olfactory system, odorants are never experienced in isolation by the nose, and they might be meaningful to the animal or not depending on the context. Feedback inputs onto early processing stages are poised to permit selective attention to the relevant odorants in the olfactory scene. During my thesis work, I focused on understanding the key role that inhibitory GABAergic signaling plays in the cortical feedback to the olfactory bulb in mice.

The fact that the olfactory cortex sends excitatory projections back to the olfactory bulb is well-known, and the first part of my work started with the discovery that excitatory transmission between cortical feedback inputs and the olfactory bulb is modulated by metabotropic receptors for GABA. Surprisingly, a differential modulation of cortical feedback transmission was found, based on the postsynaptic targets. Building on this finding, we investigated the impact of this regulation on the olfactory bulb network, and in particular the functional impact on the output cells. We found that GABAergic signaling at cortical feedback axons profoundly changes the response of the olfactory bulb output cells to odor stimulation.

In the second part of my thesis, I found that the cortical projections to the olfactory bulb not only comprises of excitatory components, but also inhibitory components. The accurate origin of this GABAergic feedback has been characterized and the functional connectivity between the projections and olfactory bulb neurons is currently assessed. We also observed that manipulating this GABAergic feedback activity perturbs olfactory behavior. To better appreciate how it does so, we are currently investigating when this inhibitory feedback is activated and what functional consequences cortico-bulbar GABAergic feedback has on the olfactory bulb.

Résumé

Les retours corticaux sont essentiels pour la perception sensorielle. Les afférences sensorielles transmettent l'information provenant d'un monde en perpétuel changement, alors que les signaux de retour semblent nécessaires à la sélection des informations sensorielles pertinentes. En ce qui concerne l'olfaction, l'information sensorielle est constituée d'une multitude de molécules odorantes, et c'est ce mélange complexe qui pénètre dans la cavité nasale. En fonction du contexte, c'est une partie ou une autre de cet ensemble de molécules qui va être importante d'un point de vue comportemental. Les retours corticaux transmis vers les étapes précoces du traitement de l'information permettent vraisemblablement de faire particulièrement attention aux odeurs pertinentes de l'environnement. Durant mon doctorat, je me suis attaché à comprendre le rôle clé joué par l'inhibition GABAergique dans les retours corticaux vers le bulbe olfactif.

Il a été décrit que le cortex olfactif envoie des projections excitatrices en retour sur le bulbe olfactif. C'est pourquoi la première partie de mon travail a commencé avec la découverte d'une modulation métabotropique et GABAergique du retour cortical excitateur. De façon surprenante, nous avons trouvé une modulation différentielle en fonction des cibles post-synaptiques. Fort de ces résultats, une étude de l'impact de cette modulation sur le réseau du bulbe olfactif, et en particulier sur les neurones de projections, a été conduite. Nous avons démontré que la signalisation GABAergique au niveau de retours corticaux change de manière profonde la réponse du bulbe olfactif aux odeurs.

Dans un deuxième temps, j'ai trouvé que le cortex olfactif envoie non seulement des projections de retour excitatrices, mais aussi des retours inhibiteurs. La localisation précise de ce retour GABAergique a ensuite été caractérisée, ainsi que la connectivité fonctionnelle entre les fibres de retour et les neurones du bulbe olfactif. Nous avons également observé qu'en manipulant l'activité de ces fibres GABAergiques, nous pouvions modifier le comportement olfactif. Afin de mieux connaître comment cela se produit, nous étudions actuellement les périodes auxquelles ce retour GABAergique est actif, et quelles sont les conséquences fonctionnelles de son activation dans le bulbe olfactif.

Acknowledgements

Many people contributed to the development of these four years of work. I wish to thank particularly my thesis director Pierre-Marie Lledo and my supervisor Gabriel Lepousez for their support in all aspects during my graduate training. I am also grateful to Matt Valley who supervised my work during my Master training and guided my first steps in my PhD. I thank all the members of the laboratory for their thoughtful comments, constructive discussion and precious help. I am deeply grateful to my thesis committee and to the Jury. I thank the thesis committee, Drs. Andreas Schaefer, Karim Benchenane and Dominique Debanne, for their excellent advice, for their constructive comments and for their mentoring. I thank the thesis reviewers, Drs. Andreas Schaefer and Didier De Saint Jan for accepting the burden of reading this thesis, but I especially thank them for their insightful inputs. I wish to thank also the other member of the Jury: Drs. Hannah Monyer, Alain Trembleau, Karim Benchenane for accepting to be part of the Jury and their enthusiasm about my work.

I am grateful to all the members of the laboratory, and I especially thank Julien and Enzo, trainees in the lab I had the great opportunity to supervise and work with. I also particularly thank Laurent, Damien, Antoine, Gilles who are more than colleagues to me, Sharim (thanks for the English edits in the manuscript!), Oriana, Mathilde, Mariana, Carine, Kurt, Mariane, my co-PhD trainees (good luck to you guys!) Soham, Anne, Maud, Marie. I am again grateful to Pierre-Marie and Gaby. Listing all my colleagues I had insightful or joyful discussion with will be too long and I apologize for those who are not cited. I also wish to thank members of the Neurosciences department here in Pasteur for their thoughtful comments.

Finally, I would like to switch in French to thank my family and friends. Merci à ma famille pour les nécessaires moments de détente et de repos, d'efforts et de réconforts ! C'est toujours un plaisir de se retrouver. Merci aussi à mes amis, Alice, Guigui, Marie, Marina, Clément, Ahmed. Merci en particulier à Florian, a.k.a. kiki, pour les pauses café, les pauses bières, les discussions, plaintives ou constructives, sérieuses ou drôles, scientifique ou non. Ça a été un plaisir/défouloir de partager le quotidien de thésard avec toi. Travailler avec un ami a aussi été plaisant et une vraie source de motivation. Finalement, merci à Céline pour partager mes galères sur cette fin de thèse. Merci pour ta compréhension et pour ta relecture de ma thèse à la chasse aux coquilles et autres erreurs de grammaire !

Contents

I	Introduction	1
1	GABAergic signaling in the brain	5
1.1	Inhibition in the brain	5
1.1.1	GABAergic receptors	6
1.1.2	Mechanisms of inhibition	9
1.1.3	Activation of GABAergic receptors	11
1.1.4	Inhibitory neuron diversity	13
1.2	Inhibitory neurons in brain circuits: functions of inhibition . .	19
1.2.1	Inhibition in microcircuits	19
1.2.2	Inhibitory neuron activity in behavior	20
1.2.3	"Balanced" inhibition and excitation	22
1.2.4	Inhibition narrows opportunity window for input inte- gration	23
1.2.5	Inhibition shapes tuning properties of excitatory neurons	23
1.2.6	Inhibition controls the gain of neurons	24
1.2.7	Inhibition of inhibition	28
1.2.8	Cell assembly recruitment	28
1.2.9	Oscillations	29
1.2.10	Inhibition in plasticity and learning	30
1.3	Functional role GABA _B R-mediated inhibition	31
1.4	Long-range GABAergic projections in the brain	35
1.5	Conclusion on the role of inhibition in brain circuits	39
2	Introduction to the olfactory system	41
2.1	Signal transduction: from the nose to the brain	41
2.2	Synaptic organization in the Olfactory Bulb	44
2.2.1	Microcircuits in the Glomerular Layer	44
2.2.2	Olfactory bulb output neurons: routing the informa- tion to the olfactory cortex	48
2.2.3	Reciprocal connection with Granule cells	51

2.2.4	Additional microcircuits	54
2.3	From the Olfactory Bulb to the Olfactory Cortex	57
3	Top-down to the Olfactory Bulb	63
3.1	Glutamatergic feedback from the olfactory cortex	64
3.1.1	Projections originating from the anterior olfactory nucleus	65
3.1.2	Projections originating from the anterior piriform cortex	68
3.1.3	Topography of cortical feedback projections	73
3.1.4	Conclusion on glutamatergic cortical feedback	73
3.2	Top-down inputs from neuromodulatory regions	74
3.2.1	Serotonergic neuromodulation	74
3.2.2	Inputs from the locus cœruleus	78
3.2.3	Cholinergic inputs from the basal forebrain	80
3.2.4	Conclusion on neuromodulatory top-down	81
3.3	GABAergic top-down	82
3.4	Conclusion on top-down inputs to the olfactory bulb	83
4	Olfactory Coding in the Olfactory Bulb	85
4.1	Large scale temporal coding in the olfactory bulb	86
4.2	Transformation in the Glomerular Layer	90
4.3	Transformation by Granule cells	93
4.4	Transformation by other Olfactory Bulb neurons	96
4.5	Odor responses in M/T cells	97
4.6	Olfactory code in the Olfactory Bulb	101
4.7	Cortical influences on olfactory coding and behavior	106
II	Results	111
1	Cortical top-down inputs to the olfactory bulb are regulated by GABA_BRs (Article 1)	115
1.1	Results from the article	115
1.2	Supplementary results	133
2	GABAergic cortico-bulbar projections to the olfactory bulb alter olfactory perception (Article 2, in preparation)	135
2.1	Results from the article in preparation	135
2.2	Preliminary results	163
III	Discussion	165
0.1	Extended discussion on Article 1	168
0.2	Discussion on Article 2 and future directions	175
0.3	General discussion	180

Bibliography	185
Appendices	227
Appendix A- Genetic tools to label, monitor and manipulate cell- type specific activity	227
Appendix B- GABA _B Rs form large complexes.	231
Appendix C- Supplemental methods.	233

List of Figures

1.1	GABA _B Rs: structure and signaling pathways	9
1.2	Inhibitory neuron diversity	17
1.3	Main forms of inhibitory microcircuits	21
1.4	Main functions of inhibition in the brain	26
2.1	Connectivity in the early olfactory system	43
2.2	Cytoarchitecture and Circuits of the Olfactory Bulb	45
2.3	Periglomerular and Granule cells structures and functions	47
2.4	The MC-GC dendrodendritic synapse	53
2.5	Outputs and inputs to the Olfactory Bulb	59
2.6	Cytoarchitecture and Circuits of the Anterior Piriform Cortex	61
3.1	Relative densities of centrifugal fibers across olfactory bulb layers	75
4.1	Spontaneous and Odor-evoked activity in Granule Cells	95
4.2	Multiple Odor response properties in Mitral and Tufted cells	99
2.1	Cortico-bulbar GABAergic axon activity discriminates odor values	164
1	Dual conditional labeling of cortico-bulbar GABAergic neurons	177

Part I

Introduction

Introduction

Information processing requires an interplay between the several billions of neurons in the mammalian brain. Each single neuron is heavily interconnected through 1,000 to 10,000 synapses and together form a vast and complex neuronal network. This network is arranged into many individual processing units, and notably microcircuits, that allow massive parallel processing of information. Excitation and inhibition are balanced in microcircuits in order to shape the information that the brain has to encode and decode. Sensory input from the nose, for example, is transmitted to the brain, where information is first locally processed by an interplay between local excitatory and inhibitory connections. Then, the formatted information is forwarded to downstream brain regions that will perform additional computations to further extract more complex features from the signal. However, this simplistic view of feedforward flow of information does not reflect the complexity of brain functioning. Feedback and "top-down" flows of information are thought to convey signals relative to the internal or brain state of the animal, and/or information on sensory expectation based on the animal's previous experience. This would imply that top-down inputs are a *prior* or prediction signal to incoming information, and depend on the sensory "context", rather than on the sensory "content". Thus, they are thought to be essential for the salience of sensory information and selective attention. However, at present, these potential functions of top-down inputs need to be further clarified. At minima, top-down inputs deeply influence sensory perception, as will be described in this thesis.

Both feedforward and feedback influences are heavily regulated, either by local circuit processing, plasticity mechanisms or neuromodulation. Therefore, understanding how microcircuits operate under influences from different brain regions is a fundamental challenge.

From here-in this introduction will focus on four chapters. Firstly, the role of inhibition in the brain will be reviewed. Then I will describe the organization of the olfactory system (the brain regions that encode smell). Thirdly, I will detail how centrifugal inputs impact early sensory processing. Lastly, I will expose and discuss how neurons respond to odors and what code they might use for transmitting olfactory information to downstream regions. Throughout the introduction, data from the rodent literature will be mainly reviewed.

Chapter 1

GABAergic signaling in the brain

1.1 Inhibition in the brain

Neurons in the brain are extensively connected. Indeed, a 1mm^3 volume of neocortex spanning the 6 layers contains $\sim 10^5$ neurons, $\sim 4\text{km}$ of axon, $\sim 0.4\text{km}$ of dendrite, and $\sim 10^9$ synapses. Presynaptic axons typically connect to postsynaptic neurons *via* multiple contacts and inhibitory neurons can inhibit $> 50\%$ of their neighboring excitatory cells within a radius of $100\mu\text{m}$ and receive excitatory inputs from a large fraction of them (Harris and Shepherd, 2015). In the cortex, the external part of the brain, inhibitory neurons represent $\sim 20\%$ of the neurons, the other 80% being excitatory. An exception to this rule is provided by the olfactory bulb (OB), which is very special as GABAergic cells largely outnumber the glutamatergic cell (in the order of 100:1).

Excitation in the brain is mainly driven by the neurotransmitter glutamate, whilst γ -aminobutyric acid (GABA) is the main inhibitory neurotransmitter. Glutamatergic neurons are referred to as "principal" neurons because they are excitatory and often constitute the output channel of a brain region. GABAergic neurons, in contrast, mainly extend their axonal arborization locally, therefore they are referred to as "interneurons". However, some local neurons are glutamatergic and some inhibitory neurons are projecting to distal brain structures, as we will see in this thesis. For which reason I will strictly use the word interneurons for locally innervating neurons and not as a synonym for inhibitory neurons.

GABA was found to be the major inhibitory transmitter in higher brain centers in the 1970s. GABA is produced from the decarboxylation of glutamate by two distinct enzymes: the glutamic acid decarboxylase (GAD) 65 and GAD 67. Although both GAD 65 and 67 participate in GABA synthesis, their different subcellular localizations (GAD 67 is found throughout the cell while GAD 65 is enriched in synaptic terminals), biochemistry, and knock-

out phenotypes suggest that they play different roles in synaptic physiology. Following synthesis, GABA is loaded in the vesicles by the vesicular GABA transporter (VGAT) and is released in the synaptic cleft in a phenomenon called exocytosis.

GABAergic neurons also release neuropeptides (some of which are used for their identification, see below). Neuropeptides are known to have profound effects on network dynamics and functions, but this is beyond the focus of the study and will not be detailed here. In summary, neuropeptides are stored in distinct vesicles from neurotransmitters, and are detected throughout the compartments of the cell, notably in the soma and dendrites. Neuropeptide release is believed to require high-frequency firing at extrasynaptic sites and receptor binding would be achieved through diffusion (for reviews on that subject, see van den Pol, 2012).

This chapter introduces general concepts about inhibition at multiple levels: from the molecular to the circuit levels, with emphasis on the metabotropic and long-distance transmissions.

1.1.1 GABAergic receptors

Inhibitory synapse is a synapse that has the capacity of reducing the probability of action potential emission by the postsynaptic cell. Inhibitory neurons release GABA that binds GABA receptors expressed at the postsynaptic cell membrane.

Iontropic receptor for GABA GABA type A receptors (GABA_ARs) are ionotropic receptors for GABA, composed of five subunits arranged around a central axis to form an ion channel, permeable to chloride and bicarbonate ions (for a review, see Fritschy and Panzanelli, 2014). In mammals, 19 different subunits of GABA_ARs have been identified, and classified in eight families comprising several members and potentially different isoforms (α 1-6, β 1-3, γ 1-3, δ , ϵ , θ , π and ρ 1-3). The diversity of subunits fosters the possibility for a very large number of permutations (over a million), but in reality, most mammals receptors are composed of two members of the α and two of the β family, and one member of the γ family, limiting the naturally expressed receptors to $\sim 30 - 40$. The GABA binding site is located between the α and β subunits. Binding of GABA transiently stabilizes the complex in an open configuration, allowing ionic flux. In addition to GABA, GABA_ARs possess a variety of allosteric sites at which a number of agents act, such as benzodiazepines and alcohol. Different combinations of subunits have differing pharmacological and physiological properties, and are heterogeneously distributed throughout the brain, and within subcellular domains. For example, α 1, 2 or 3 subunits interact with scaffold proteins (such as gephyrin) to localize mainly at the synaptic cleft on the postsynap-

tic neuron, while $\alpha 4$ and 6 or δ ϵ -containing receptors exclusively localize peri- or extrasynaptically. $\alpha 5$ -containing receptors can localize both synaptically and outside of the synapse. Peri- and extrasynaptic receptors respond to "spill-over" or volume transmission, much like GABA_BRs (see below). Many different subunit compositions of GABA_ARs are more or less associated with distinct subcellular localizations and will not be reviewed in further details here.

Metabotropic receptor for GABA In addition to GABA_ARs, GABA can bind type B receptors (GABA_BRs).

Indeed in the 1980s, a series of elegant studies by Norman Bowery suggested the existence of a second type of GABA receptors (see Bowery, 2010 for a review on the history of the discovery of GABA_BRs). GABA was able to decrease neurotransmitter release as predicted, but the surprise came when looking at the pharmacology: GABA binding was unaffected by the competitive GABA agonists bicuculline, isoguvacine or muscimol, and it was activated by β -chlorophenylGABA (baclofen) which was inactive in classical sites for GABA. The structure of the receptor was revealed in the late 1980s, more than 10 years after GABA_AR structure. The terms GABA_A and GABA_B receptors were proposed by Dr Bowery in 1981 to distinguish the classic from the unconventional sites for GABA binding (Bowery, 2010). GABA_BRs are widely distributed in the brain, although there are regional variations. GABA_BRs are metabotropic receptors for GABA, members of the superfamily of G protein-coupled receptors (GPCRs), a group of receptors that include metabotropic glutamate and olfactory receptors. All GPCRs have a common structure: seven transmembrane domains, ligand-binding domains in the extracellular space, and a G protein-activation domain in the cytosolic region (Figure 1.1,A1). GABA_BRs belong to the class C of GPCRs, a class of structurally more complex GPCRs than the other classes. Functional GABA_BRs are obligate heterodimers of type 1 and type 2 subunits (GABA_{B1} and GABA_{B2}; GABA_BRs were the first GPCRs to be shown to function as heterodimer; Pin and Bettler, 2016). GABA_{B1} subunit possesses binding sites for the agonist and antagonist while GABA_{B2} binds G proteins and increase affinity for ligand binding. Recently, crystal structures revealed the structural mechanism of ligand activation in GABA_BRs (Figure 1.1,A2; Geng et al., 2013). Several isoforms of GABA_{B1} exist, the most prominent being GABA_{B1a} and GABA_{B1b}. In contrast to GABA_{B1b}, GABA_{B1a} contains two sushi domains at its extracellular N terminal that traffic GABA_{B(1a,2)}-containing receptors to axon terminals (Figure 1.1,A1; Gassmann and Bettler, 2012; Pin and Bettler, 2016). In addition, several recent studies showed that GABA_BRs form larger complexes than dimers (Pin and Bettler, 2016; see Appendix 0.3 for further details).

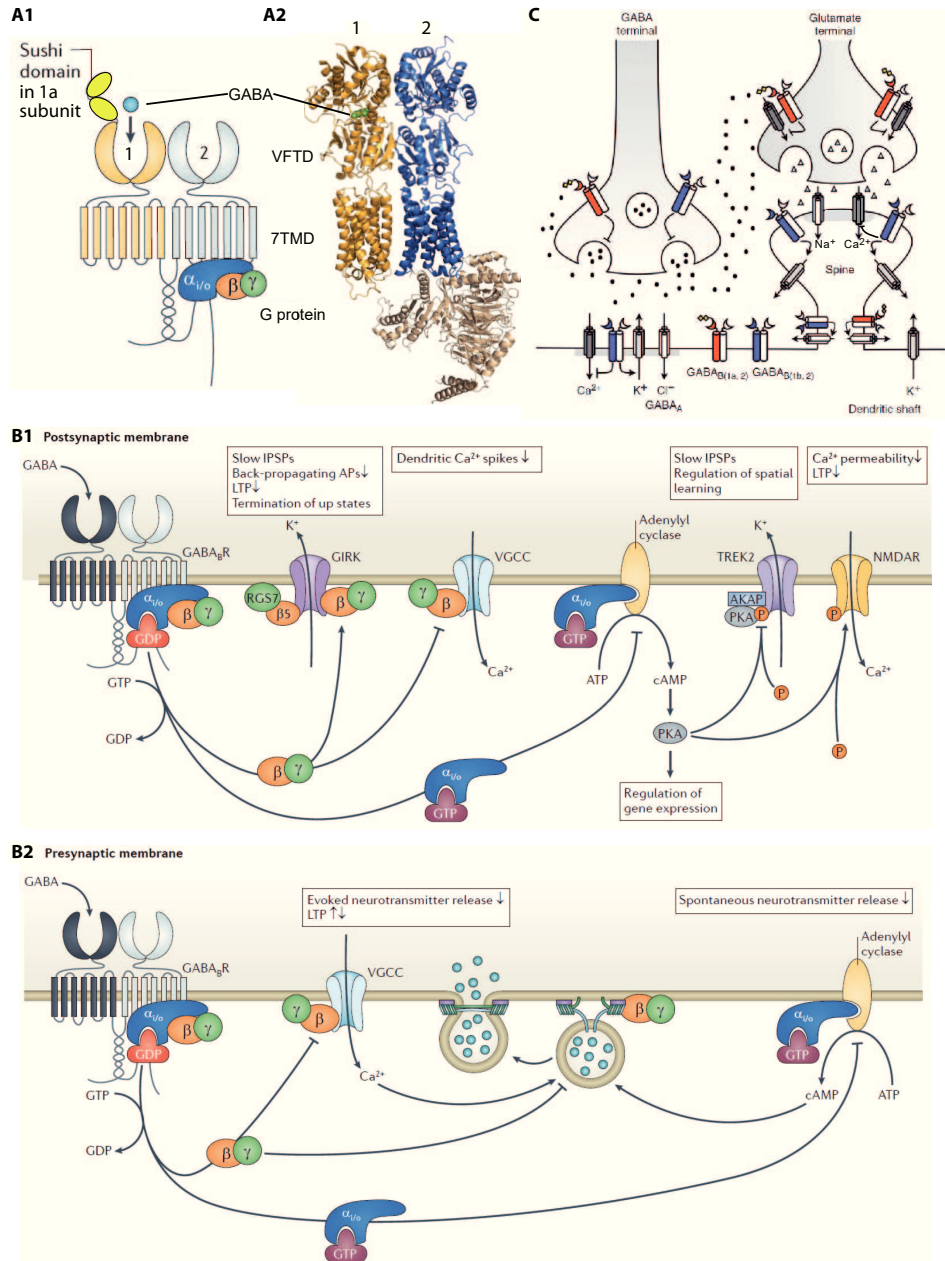


Figure 1.1 – GABA_BRs: structure and signaling pathways.

A. Structure of GABA_BRs. GABA_BRs are heterodimers of B1 (in yellow) and B2 subunits (in blue). Each subunit is a GPCR made of seven-transmembrane domain (7TMD) and a large extracellular venus flytrap domain (VFTD). GABA binding site is confined to the VFTD of the GABA_{B1} subunit, while GABA_{B2} subunit docks the G_{i/o}-type G protein at its C terminus. GABA_{B1a} contains two extracellular Sushi domains at its N terminus. A1 is a schematic representation adapted from (Gassmann and Bettler, 2012). A2 is a representation based on the crystal structure adapted from (Pin and Bettler, 2016).

Figure 1.1 (Continued) – B. Signaling pathways downstream GABA_BR activation. GABA_BR activates heterotrimeric G_{i/o}-type G proteins that split into the $\alpha_{i/o}$ and $\beta\gamma$ subunits. At postsynaptic membranes (B1), released $\beta\gamma$ subunit opens G protein-activated inwardly rectifying potassium (GIRK) channels and inhibits voltage-gated calcium channels (VGCCs). The $\alpha_{i/o}$ subunit inhibits adenylyl cyclase activity and thereby the activity of the protein kinase A (PKA). Reduction of PKA activity has several effects: 1) diminution of the inhibition of potassium channels, 2) inhibition of the Ca²⁺ permeability of NMDARs, and 3) modification of gene expression. At presynaptic membranes (B2), $\beta\gamma$ subunit also inhibits VGCCs, thus leading to a reduction of evoked Ca²⁺-dependent neurotransmitter release. In addition, $\beta\gamma$ directly binds SNARE complex required for vesicle fusion. $\alpha_{i/o}$ subunit negatively regulates the adenylyl cyclase and thereby prevents vesicle fusion and spontaneous neurotransmitter release. Finally, GABA_BR-mediated inhibition of neurotransmitter release regulates LTP processes. See text for further details. Adapted from (Gassmann and Bettler, 2012).

C. Distribution of GABA_BRs to neuronal compartments. Schematic of a glutamatergic terminal contacting a dendritic spine and a GABAergic terminal contacting the dendritic shaft. GABA_BRs are localized extrasynaptically, on glutamate and GABA terminals presynaptically, and on dendritic shafts and spines postsynaptically. Autoreceptors inhibit the release of GABA while heteroreceptors inhibit the release of other neurotransmitters, such as glutamate. GABA_BRs containing the 1a subunit are believed to be enriched at presynaptic terminals. Adapted from (Pinard et al., 2010).

AKAP: A-kinase anchoring protein; cAMP: cyclic adenosine monophosphate; GPCR: G protein-coupled receptor; SNARE: Soluble N-ethylmaleimide-sensitive factor attachment protein receptor; TREK2, or KCNK10: subtype of potassium channel.

1.1.2 Mechanisms of inhibition

GABA_AR-mediated inhibition GABA_ARs are expressed in both neurons and glia in the central nervous system. Reversal potential of Cl⁻ is close to the resting membrane potential of the cell in the adult brain ($\sim -70mV$), thus GABA_AR activation produces little net current across the membrane, however the conductance of the cell is greatly increased and therefore Na⁺ or Ca²⁺ entry has reduced impact on the voltage membrane potential. This type of inhibition is called "shunting" inhibition (as we will see later in this paragraph, GABA_BRs, can also mediate shunting inhibition). In the neonate brain however, internal chloride concentration in the cell is higher, bringing the reversal potential to $\sim -45mV$, and therefore Cl⁻ flux depolarizes the cell. Although the depolarizing role of GABA is fundamental in the developing brain (Ben-Ari, 2014), this work focuses on adult brain in which GABA has mainly an inhibitory action.

GABA_BR-mediated postsynaptic inhibition. As classical neurotransmitter receptors, GABA_BRs are expressed at postsynaptic sites. Upon activation, GABA_BRs recruit a G_{ai/o}-type G protein that has multiple actions inside the postsynaptic cell (Figure 1.1,B1,C). The α_i subunit inhibits adenylyl cyclase, leading to reduced cyclic adenosine monophosphate (cAMP) production and downregulation of the protein kinase A. Protein kinase A

phosphorylates a subunit of NMDARs (GluN2B or NR2B), which enhances Ca^{2+} permeability. Upon GABA_{B} R activation and protein kinase A down-regulation, NMDARs are less permeable to Ca^{2+} . G proteins associated with GABA_{B} Rs have other sites of action. β/γ subunits inhibit voltage-gated Ca^{2+} channels (and notably L-type Ca^{2+} channels) and enhance the activity of a subtype of K^{+} channels, namely the G protein-coupled inward rectifying K^{+} channels (GIRKs), whose reversal potential is about -90mV . Although the cell resting membrane potential vary across cells and is determined by the combination of inhibitory and excitatory conductances, it is generally situated around -70mV and therefore, GABA_{B} R-mediated inhibition is called "hyperpolarizing" inhibition. Spike threshold, the membrane potential at which a cell fire action potential, is determined by the properties, density and distribution of the ion channels in regard to the action potential initiation zone. Together with the cell resting membrane potential and its conductance, threshold to spike determines whether the cell is far or close to action potential emission.

Shunting inhibition can be highly compartmentalized. Both GABARs can mediate shunting inhibition located at precise sites on postsynaptic cells. For instance, in addition to the axon initial segment, pyramidal cells can generate Ca^{2+} spikes in their distal dendrites through an array of voltage-gated calcium channels (Larkum et al., 2001). Rather than passively relaying synaptic inputs to the soma, these dendritic spikes sum in a supralinear fashion in the cell body and can generate somatic burst firing. In addition, anatomical work revealed that glutamatergic and GABAergic axon terminals can contact individual dendritic spines (a highly specialized structure of a dendrite, which forms a protrusion tethered to the dendrite by the spine neck). Both types of GABARs can mediate shunting inhibition, thereby preventing Ca^{2+} spike initiation (see Higley, 2014 for a review). GABA_{A} Rs, through the opening of Cl^{-} permissive channels, trigger shunting inhibition that prevents membrane voltage from reaching threshold to spike. Interestingly, the high electrical resistance of a spine neck isolates the shunt in one spine from the neighboring ones. Thus, GABARs can mediate highly compartmentalized inhibition within the dendritic arbor. In addition, by direct inactivation of Ca^{2+} channels, GABA_{B} R activation can also shunt excitatory conductance on the dendritic spine (Palmer et al., 2012). GABA_{B} Rs were also found to decrease Ca^{2+} influx through NMDARs by a protein kinase A-dependent pathway. Therefore, GABA_{B} Rs inhibition is not restricted to hyperpolarizing inhibition of a cell membrane voltage but can also mediate shunting inhibition in the dendritic arborization.

Kinetics of ionotropic vs. metabotropic inhibition. In addition to having distinct net effects on the cell membrane potential, GABA_{A} and

GABA_B receptors-mediated inhibition varies in terms of kinetics. Indeed, GABA_ARs are fast ion channels receptors, leading to Cl⁻ flux inside the cell in a few milliseconds, while GABA_BRs are slow metabotropic receptors coupled to G proteins and subsequent cell effectors. Hyperpolarization triggered by postsynaptic GABA_BR activation peaks after $\sim 100ms$. Therefore GABA_A and GABA_B receptors-mediated inhibition are often associated with different functions. However, accumulating evidence points towards a role for GABA_BRs in fast network activity (see below).

GABA_BRs also mediate presynaptic inhibition. Beside activation of postsynaptic receptors as a classical neurotransmitter, GABA can bind presynaptic GABA_BRs and regulate synaptic transmission (Figure 1.1, B2, C). Therefore, through activation of GABA_BRs, GABA can be considered as a neuromodulator too. Similarly to its action at postsynaptic sites, presynaptic GABA_BRs activation leads to inhibition of adenylyl cyclase by αi subunit and consequent reduction of cAMP production. Because cAMP is involved in the process leading to vesicle fusion, αi subunit depresses neurotransmitter release *via* that mechanism. $G\alpha i/o$ subunit decreases exocytosis by increasing the energy barrier for vesicle fusion (Rost et al., 2011). In addition to diminishing cAMP production, GABA_BRs inhibit neurotransmitter release *via* its β/γ subunits by inhibiting voltage-gated Ca²⁺ channels in one hand, and directly interfering with SNARE proteins (proteins of the docking vesicle docking complex) in the other hand. Thus, presynaptic GABA_BRs depress neurotransmitter release by decreasing the number of vesicle released by action potentials. Presynaptic GABA_BRs can be expressed at GABA and glutamatergic terminals, forming respectively auto- and heteroreceptors and preventing GABA or glutamate release (example of both are find in the olfactory bulb, Figure 1.1, C).

Cross activations. Finally, data suggests that GABA_BRs engage in intracellular signaling crosstalks with NMDARs and mGluRs (respectively ionotropic and metabotropic receptors for glutamate; Gassmann and Bettler (2012); Morrisett et al. (1991)), thereby revealing the complex function of GABA_BRs.

1.1.3 Activation of GABAergic receptors

A single action potential evokes neurotransmitter release in the synaptic cleft, which rapidly diffuses and binds to postsynaptic receptors. In the case of inhibitory synapses, GABA binds GABA_ARs very briefly in spite of its high concentration (1 – 10mM), owing to the low affinity of GABA_ARs for GABA and active transport mediated by GABA transporters (GAT, expressed at axon terminals and glial cells). This type of rapid transmission is

called synaptic or phasic transmission.

In addition, immunohistochemical studies localized GABA_BRs at the peri- and extrasynaptic plasma membrane (Figure 1.1,C; Kohl and Paulsen, 2010). Due to their extrasynaptic location, GABA_BRs are thought to be activated in periods of high GABAergic neuron activity, leading to saturation of GABA uptake, accumulation and spilling over of GABA out of the synaptic cleft, allowing it to reach and bind extrasynaptic GABA_BRs. In a seminal hippocampal slice work, Scanziani (2000) showed that rhythmic activity, engaging simultaneously and repetitively several inhibitory neurons, is necessary to activate GABA_BRs. GABA has to pool to overcome uptake and reach GABA_BRs outside the synaptic cleft. This transmission involving diffusion of neurotransmitter outside the synaptic cleft is known as "spill over" or "volume transmission". However, recent studies suggest that volume transmission can not be restricted as a simple homogeneous diffusion of GABA. For instance, Pan et al. (2009) demonstrated differential functional recruitment of presynaptic GABA_BRs at cortico- or thalamo-amygdalar synapse. Indeed, pharmacology studies previously showed the presence of presynaptic GABA_BRs at cortical and thalamic axon terminals on both inhibitory and excitatory amygdalar neurons. Cortical or thalamic afferent rhythmic stimulation, however, led to cross-activation of GABA_BRs at thalamic or cortical presynaptic terminals, respectively, when synapsing onto principal, but not inhibitory, neurons (Pan et al., 2009). This study shows a target-specific activation of GABA_BRs at presynaptic terminals. GABA diffusion in the extracellular space depends on the number of molecules of GABA released, GABA uptake and 3D-morphology of the extracellular space. Volume transmission is thus a more complex phenomenon than originally thought. Furthermore, NGs are a well-known exception for this need for synchrony since they can release GABA from many boutons simultaneously (Oláh et al., 2009; Tamas, 2003) and GABA_BRs can be activated with a single action potential (Tamas, 2003). Similarly in the OB, a single sensory neuron stimulation was sufficient to induce GABA release from postsynaptic GABAergic neurons, in turn activating GABA_BRs at sensory axons (Aroniadou-Anderjaska et al., 2000). Notably, GABA_BRs are high affinity receptors for GABA (The EC50 of GABA_BRs is half the EC50 for GABA_ARs) and in the appropriate context, can play an important role in circuits, network dynamics and behavior.

Some types of GABA_ARs also localize outside the synapse (Brickley and Mody, 2012), where they mediate a persistent form of inhibition called tonic inhibition. The ambient (extracellular) level of GABA is rather low and is set by the balance between GABA spilling over from surrounding synapses and the activity of GABA uptake. Non-vesicular GABA release, particularly *via* GABA permeation through bestrophin in astrocytes also influences the level of extrasynaptic GABA. Two properties are thus necessary for GABA_ARs

to induce tonic inhibition: high affinity for GABA, and little desensitization – a mechanism by which a receptor closes even though it still binds its ligand. δ and $\alpha 5$ -GABA_ARs are classical receptors associated with tonic inhibition, although other types of GABA_ARs have also been shown to mediate tonic inhibition (ϵ and $\alpha\beta$ -only; Brickley and Mody, 2012). Interestingly, GABAergic neurons do not seem to bear $\alpha 5$ -containing GABA_ARs (Ferando and Mody, 2014).

The level of tonic inhibition is crucial for brain function and has been associated with changes in behaviors during puberty and with a variety of debilitating neurological and psychiatric disorders, such as sleep disorders, epilepsy, generalized anxiety disorders and stress disorders (Brickley and Mody, 2012)

In the next section, I will highlight the tremendous diversity of GABAergic neurons in the brain.

1.1.4 Inhibitory neuron diversity

Given the neuron diversity, they have been classified in different subtypes based on several criteria: morphology and localization of their soma, morphology of their dendritic or axonal arborization, connectivity matrix of their inputs and outputs, developmental origin, gene expression pattern, intrinsic electrical properties, and the strategy they use to encode information *in vivo* (such as the famous "place" and "grid" cells of the hippocampus and entorhinal cortex, respectively). Classification methods have given rise to different categorization of cortical excitatory neurons, but generally these neurons have a pyramidal-shaped soma, thick apical dendrite branching out in upper cortical layers, and profuse basal dendrites. Their axonal arborization differs to a larger extent between subtypes but the pattern is generally similar between neurons whose soma is located in the same layer. Moreover, axonal arborization was not fully accessible with early Golgi staining techniques and therefore historical classification rarely takes into account axon morphology. Pyramidal cell subtypes are often named after the position of their somas for instance. In the neocortex, layer 2/3 pyramidal cells have their somas in the layer 2/3 and extend their dendrites in layer 1, receive input from the thalamus and send their axon to the contralateral cortex or higher-order cortical areas. In the olfactory cortex, layer 2b pyramidal cells are called superficial pyramidal (SP) cells, whereas layer 3 pyramidal cells are known as deep pyramidal (DP) cells. Both SP and DP cells extend their apical dendrites throughout the cortical layers, but they differ in their local and distant projections patterns, as we will see in further details in section 3. Pyramidal neurons typically express the gene CaMKII. Other examples of excitatory cells are semi-lunar (SL) cells from the olfactory cortex, with soma shape of a half-moon, two apical dendrites, none or poor basal dendritic

arborization (Suzuki and Bekkers, 2006, 2011).

Inhibitory neurons have been found to be much more diverse than their excitatory counterparts: hundreds of types can potentially be described. Almost all inhibitory neurons are born in the medial or caudal ganglionic eminence in the subpallium region, and were first reported to exhibit a large diversity of intrinsic electrical and synaptic properties (Figure 1.2,A). Briefly, cells were reported to have spontaneous regular or irregular spiking activity (i.e, regular or irregular interspike interval), or low or fast spiking (up to 120 Hz). In response to depolarization, cell firing can exhibit an adaptative behavior (i.e, increase in the interspike interval), accelerating behavior (decrease in the interspike interval) or no adaptation of their interspike interval. GABAergic neurons can also show a burst-firing behavior following depolarization. Intrinsic voltage-gated conductances also set the cell threshold to spike and regulate after spike properties, such as after-hyperpolarization or after-depolarization. Lastly, GABAergic neurons were also found to exhibit different forms of short-term plasticity in response to train stimulation. Synaptic currents can either facilitate or depress upon repeated stimulation, and this property is often dependent on the frequency of stimulation. In addition, GABAergic cell diversity is also represented in their neurochemical composition: they can express a variety of neuropeptides (somatostatin, SOM; vasoactive intestinal peptide, VIP; neuropeptide Y, NPY; cholecystokinin, CCK), calcium-binding proteins (parvalbumin, PV; calbindin, CB; calretinin, CR) and receptors (such as the 5-hydroxy-tryptamine receptor 3a, 5-HT3aR; Figure 1.2,A,B)). GABAergic cells are diverse in terms of morphology as well. Their dendritic arborization, and especially their innervation pattern of the postsynaptic principal cell (Figure 1.2,A,B), is particularly striking: somatic or perisomatic, axon initial segment or dendrite-targeting (basket, chandelier and Martinotti cells, respectively). More recently, the development of transgenic mouse lines and optogenetics have shed light on inhibitory neurons preferentially targeting other inhibitory neurons (namely VIP-expressing neurons). Finally, electrophysiological evidence supports the existence of inhibitory neurons mediating their function through volume transmission (neurogliaform cells, NG cells).

Facing the diversity. Inhibitory neurons diversity results in highly specific and precise spatiotemporal inhibitory control of principal cells, thought to maximize computations supported by the network. However, no clear consensus exists regarding the classification of inhibitory neurons across brain regions. In the hippocampus *cornu ammonis* region 1 (CA1), a GABAergic neuron classification has been elaborated, using mainly morphological features such as the location of the soma (Klausberger and Somogyi, 2008). In contrast, efforts to achieve a consensus on GABAergic neuron classification in the neocortex did not succeed in accomplishing this goal, and only

led to the identification of features that can be used as a basis for separating inhibitory neurons into subtypes (Ascoli et al., 2008; DeFelipe et al., 2013). Nevertheless, recent advances in molecular genetics lead to an emerging classification of inhibitory neurons in three main types: PV-, SOM- and 5HT3aR-expressing neurons (Figure 1.2,A; Harris and Mrsic-Flogel, 2013; Kepecs and Fishell, 2014; Tremblay et al., 2016). Although these molecular markers do not reflect the complexity of GABAergic neurons and are not directly related to the cell physiology, they have been proven useful because 1) they are expressed in largely non-overlapping populations, 2) they account for nearly 100% of GAD67-expressing neurons in somatosensory cortex, and 3) they permit the use of transgenic mice for cell type-specific studies. However, it is worth noting that some brain regions contain large fractions of inhibitory neurons that do not fall in any of these categories. For instance in the olfactory cortex, more than 90% of the GAD67-expressing cells in layer 1a were not labeled by any of the marker tested (PV, SOM, CB, CR, CCK, NPY and VIP Suzuki and Bekkers, 2010). In addition, these clusters are not necessarily mutually exclusive, such that a cell can have characteristics of multiple classes.

Genetically engineered mice, together with recent developments in activity imaging and optogenetic tools permit to label, monitor and manipulate specific GABAergic populations and allow tremendous insight into the specific role of an inhibitory neuron population on the computations of the network they are embedded in.

Below, I will briefly review the characteristics of the three types of GABAergic neurons from the aforementioned classification, before giving an overview of the function of inhibition in brain circuits.

Parvalbumin neurons. The PV group includes fast-spiking basket cells and chandelier cells, mainly targeting principal neurons (Figure 1.2,A,B). Basket cells are soma and perisomatic targeting neurons, with axonic arborization forming a basket around the postsynaptic neuron. Chandelier cells have axons targeting the axon initial segment. Because of their proximal inhibition, PV cells are thought to powerfully influence spike generation in the postsynaptic cell. Within a subtype, cells remain heterogeneous. For instance, PV basket cells whose cell bodies are located in different layers in the hippocampus show distinct characteristic regarding their dendrite and axon organization, stimulus selectivity and spiking activity with regards to different oscillatory rhythms (Tremblay et al., 2016). PV basket cells are the largest population of neocortical GABAergic neurons and have been extensively studied recently, perhaps because of their intriguing fast-spiking behavior. Indeed, PV basket cells exhibit numerous morphological, biophysical and molecular specializations responsible for their speed, efficiency, and temporal precision (Figure 1.2,A; for a review see Hu et al., 2014). For

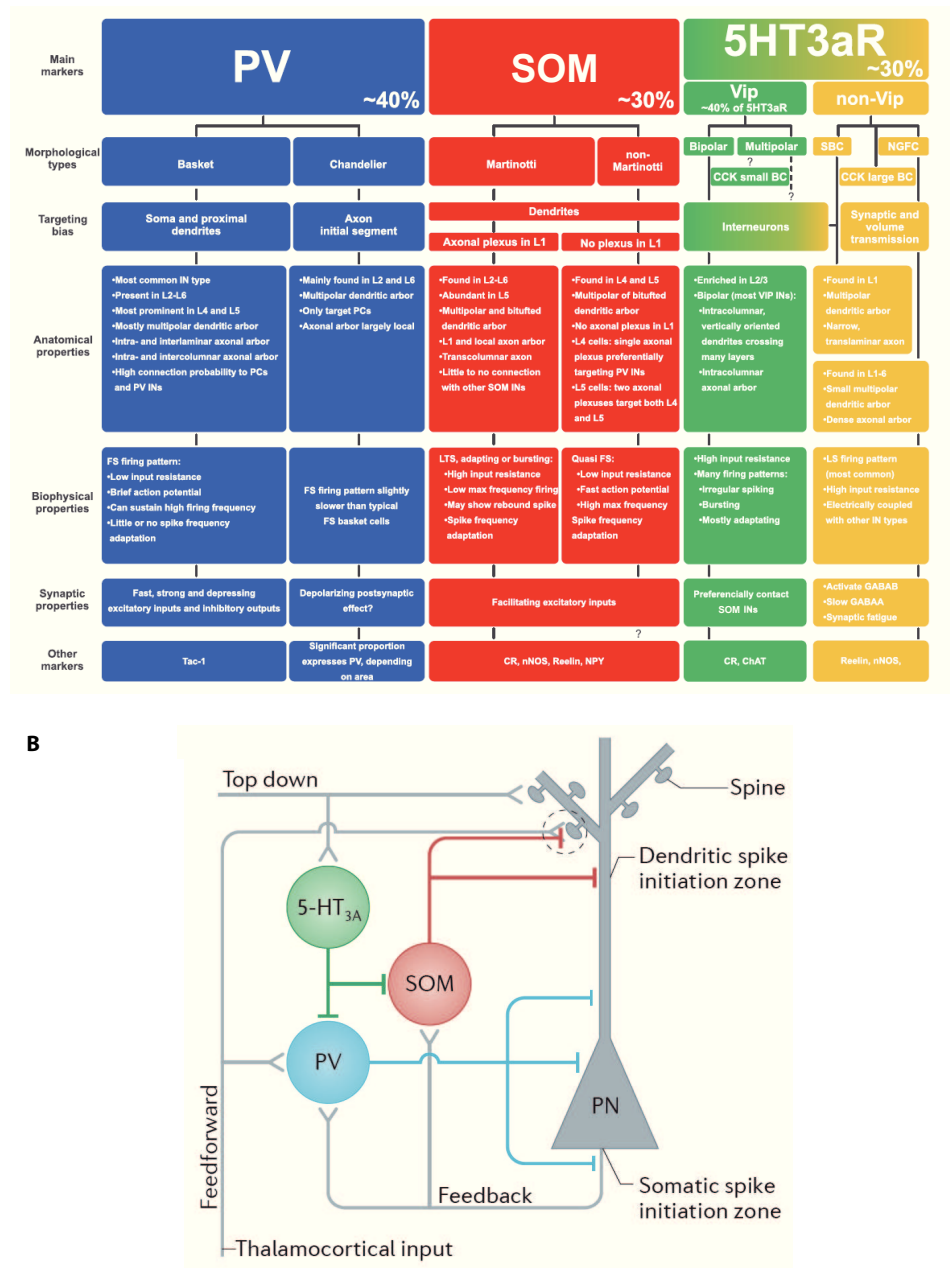


Figure 1.2 – Inhibitory neuron diversity.

A. Diversity, classification, and properties of Neocortical GABAergic neurons. Nearly all the GABAergic neurons in neocortex express one of the main three non-overlapping markers: parvalbumin (PV, blue), somatostatin (SOM, red), and the ionotropic serotonin receptor 5HT3a (green and yellow). Further subdivisions within each molecular group are revealed by morphological features, cellular and subcellular targeting biases, and expression of other markers, as well as some known anatomical, electrophysiological, and synaptic properties. From (Tremblay et al., 2016).

Figure 1.2 (Continued) – B. Synaptic organization of the three main type of GABAergic neurons within cortical circuits. Perisomatic-targeting PV⁺ neurons are activated by feedforward and feedback excitation and sharply curtail the generation of somatic action potentials in response to afferent inputs. Dendrite-targeting SOM⁺ neurons are strongly engaged by recurrent excitation originating from local cortical pyramidal neurons. SOM⁺ neurons are also engaged by external inputs in the olfactory cortex. They form synapses on both dendritic shafts and spines that converge with excitatory inputs (dashed circle) to regulate synaptic integration and dendritic spike initiation. GABAergic neurons expressing 5-HT3a mainly target other GABAergic neurons and receive excitatory inputs from top-down intracortical projections. From (Higley, 2014).

BC: Basket Cell; ChAT: Choline acetyltransferase; CR: Calretinin; FS: Fast Spiking; IN: Interneuron (i.e. GABAergic neuron); LTS: low-threshold spiking; PC and PN: Principal Cell and Pyramidal neuron; nNOS: neuronal nitric oxide synthase; NPY: Neuropeptide Y; NGFC: Neurogliaform cell; SBC: Single Bouquet Cell; 5HT3aR: Neurons expressing the 5-hydroxytryptamine receptor 3A

instance, they receive converging input onto their dendrites that are expressing a particular set of AMPAR (GluA1 and GluA4, Ca²⁺ permeable) and K⁺ channels (Kv3), responsible for provoking excitatory postsynaptic potentials (EPSPs) with fast kinetics. Because of these characteristics, PV cells are thought to be detectors of coincident inputs. Moreover, PV basket cells express "supercritical" Na₊ channels allowing fast axonal propagation of action potential, fast presynaptic Ca²⁺ channels (P/Q type) and tight coupling between these channels and release machinery as well as fast release sensors (synaptotagmin 2) for speed and temporal precision of synaptic transmission. PV basket cells also provide massive divergent outputs onto principal cells and have been associated with complex network operations, such as expansion of dynamic range, establishment of a critical window for cortical plasticity, pattern separation, gain modulation, and modulation of place and grid field shapes and phase procession in the hippocampus and entorhinal cortex (see below; Hu et al., 2014).

Somatostatin neurons. A second cluster consists of SOM-expressing neurons. In contrast to PV cells, SOM cells target dendrites. They are composed of a morphologically defined interneuron class, the Martinotti cells (that target apical dendritic tufts), and an heterogeneous group simply referred to as non-Martinotti cells (Figure 1.2,A,B). SOM neurons are regular-spiking and inputs to SOM neurons were shown to be facilitating, while inputs to PV neurons are depressing (Figure 1.2,A). This short-term plasticity property might be determined by the expression at the GABAergic neuron membrane of a protein (an extracellular leucine-rich repeat fibronectin-containing 1 protein), which regulates the release probability of the presynaptic cell (Tremblay et al., 2016). In contrast to PV neurons, SOM neurons appear to respond best to burst-firing of a single or a small group of presynaptic cells. Therefore, while PV cells seem to be coincidence detectors, SOM cells

seem to integrate local network activity over longer time scales, maybe to normalize the network (see below). Interestingly, a subgroup of SOM cells in deep cortical layers expresses the neuronal nitric oxide synthase (nNOS) and are thought to be the main source of long-range projections from the neocortex (Tamamaki and Tomioka, 2010).

Because SOM+ cells synapse onto distal dendrites of principal cells and PV+ neurons onto the soma or proximal dendrites (Figure 1.2,B), SOM+ and PV+ cells are conceptually thought to mediate different types of inhibitions. SOM-expressing cells would control dendritic integration and Ca^{2+} spike generation and therefore control burst firing, while PV-containing neurons would prevent spike output and thereby control spike timing. In a recent work, Royer and colleagues (2012) selectively inhibited SOM+ or PV+ cells of the hippocampus and observed that SOM+ cell inhibition led to increased burst firing of pyramidal cells without altering the theta phase of spikes, while PV+ cells inhibition led to a shift in theta phase spike modulation with no change of burst firing. Similarly, SOM+ cell inhibition in the barrel cortex led to increased burst firing of principal cells (Gentet et al., 2012). Therefore, these two studies seem to confirm that dendritic-targeting GABA neurons control the postsynaptic cell burst firing, while PV+ cells regulate spike timing.

5HT3aR neurons. A third and last group is composed of neurons expressing 5HT3aR (Figure 1.2,A,B). This group is more heterogeneous than the PV and SOM groups. Remarkably, 5HT3aR neurons seem to be strongly impacted by neuromodulatory signals such as serotonin and acetylcholine. This group contains VIP-expressing neurons, which mainly inhibit other interneurons, resulting in disinaptic inhibition onto principal cells (Figure 1.2,B). Indeed, VIP-expressing neurons seem to preferentially synapse onto SOM neurons. VIP+ neurons have a high input resistance, a property that makes them particularly responsive to incoming inputs (Figure 1.2,A). Another subtype of 5HT3aR neurons are NG cells. NG cells have very dense axons and exhibit high release-site density, not necessarily associated with synapses. Therefore NG cells are thought to mediate volume GABA transmission and seem to be specialized in long-lasting inhibition (Figure 1.2,A).

GABAergic neuron diversity and their differential functions.

GABAergic neurons from the same type, but not between distinct types, are greatly interconnected *via* electrical synapses mediated by GAP junctions. Electrical synapses are bidirectional synapses permissive to both anions and cations, resulting in both inhibitory and excitatory PSPs. They act as low-pass filter and are responsible for slow membrane potential variations. They are thought to enable high synchrony between interconnected neurons.

Recently, growing amount of studies report distinct roles for different

types of interneurons within a circuit of interest, but independent work sometimes fails to observe similar functions for the same set of neurons (compare for example Zhang et al., 2014, Wilson et al., 2012 and Atallah et al., 2012). For example, one study reported that in the visual cortex, SOM neurons sharpen orientation tuning, while PV neurons control the response gain. Another similar work found that PV neurons sharpens tuning, whilst SOM cells do not (Tremblay et al., 2016). This observation suggest that different functions can be attributable to a GABAergic neuron group and these functions are flexible, probably depending on how these neurons are engaged by sensory inputs or brain states. Activity pattern, and therefore function of inhibitory neurons can vary greatly depending on the context. In addition, GABAergic neuronal diversity is simplified using the molecular markers for the three main inhibitory types. This point is well illustrated by the data from the Allen Institute for Brain Science, where recording intrinsic electrical characteristics from several hundred of cells was achieved (see <http://celltypes.brain-map.org/>). For a better understanding of GABAergic neuron function, more selective labeling, monitoring and manipulation of GABAergic subtypes would be useful. To address this issue, genetic intersectional approach, in which genetic manipulation depends on the action of two recombinases, is a promising technique that could allow more restricted manipulations and finer dissections of GABAergic neuron subpopulation functions (He et al., 2016). In addition, high-throughput single-cell mRNA sequencing methods, allowing unbiased transcriptomic analysis of individual neurons could become a useful tool to better elucidate the diversity of GABAergic neurons.

In the next section, I will briefly review the canonical circuits GABAergic neurons are embedded in, the circuit operations they permit and eventually the consequences on behavior.

1.2 Inhibitory neurons in brain circuits: functions of inhibition

1.2.1 Inhibition in microcircuits

Inhibitory neurons can mediate several types of inhibition within local circuits. When GABAergic neurons are excited by an external source and in turn inhibit glutamatergic neurons, this inhibition is called "feedforward inhibition" (1.3,A). In contrast, when excitatory neurons drive their own inhibition, one refers to this inhibition as "feedback inhibition" (1.3,B). In other words, from the point of view of a principal neuron population, if inhibition is self-generated the inhibition is termed "feedback", however it is called "feedforward" when inhibitory neurons are externally driven. Feedforward

and feedback inhibition can be mediated by separate groups of inhibitory neurons. For instance, in the anterior piriform cortex (APC), afferent inputs stimulate layer 1a horizontal and NG cells, which in turn mediate feedforward inhibition mainly onto SL cells. SL cells then drive SP cells, that recruit fast-spiking multipolar (fMP) cells of layer 3 and induce feedback inhibition onto both SL and SP cells (Suzuki and Bekkers, 2012). Interestingly, at the network level, feedforward inhibition onto SP cell dendrites dominates for a weak stimulation, while a stronger stimulation produced mainly somatic feedback inhibition (Stokes and Isaacson, 2010). This shift from dendritic to somatic inhibition can be explained by short-term plasticity mechanism at afferent synapse to GABAergic neurons: while synapse between afferent axons to layer 1a GABAergic neuron depresses, the synapse onto layer 3 inhibitory neurons facilitates. In the neocortex and in the hippocampus however, a train of excitatory stimuli first elicit somatic inhibition mediated *via* PV+ cells, and progressively shift distally, where SOM+ neuron synapses are formed (Tremblay et al., 2016). This can similarly be explain by the depressing and facilitating nature of inputs to PV and SOM cells, respectively.

Feedback inhibition can be further divided in two classes of microcircuits. If an external drive excite a subpopulation of excitatory neurons, which in turn drive their own inhibition, this form of inhibition is termed "recurrent" (Figure 1.3,B'), however the inhibition is called "lateral" when the first excited population recruit inhibition onto another subset of principal neurons, within the same functional circuit (Figure 1.3,B"). In the APC, afferent inputs are first recruiting SL cells, which in turn drives fMP cells and therefore trigger recurrent inhibition onto SL cells and lateral inhibition onto SP cells.

Lastly, inhibition can also come from an external source, termed "direct inhibition" (Figure 1.3,C) and, finally, inhibition of inhibitory neurons results in "disinhibition" onto principal cells (Figure 1.3,D).

The fundamental question that remains open is which type of GABAergic neuron contributes to specific brain circuit functions, behavior and the alteration of which function can lead to disease. Inhibitory activity is likely to depend on the network activity pattern in addition to neuronal characteristics. In this introduction, I will now focus on the synaptic physiology of GABA, the main functions supported by local inhibitory neurons, and finally I will review the literature and some new functions supported by long-range projecting inhibitory neurons.

1.2.2 Inhibitory neuron activity in behavior

Recent development in genetically engineered mice and calcium activity sensors has allowed investigation of specific neuronal types in behaving mice. Since anesthesia greatly impacts the function, I will mainly focus on data from the awake literature in this section and the following ones (Haider

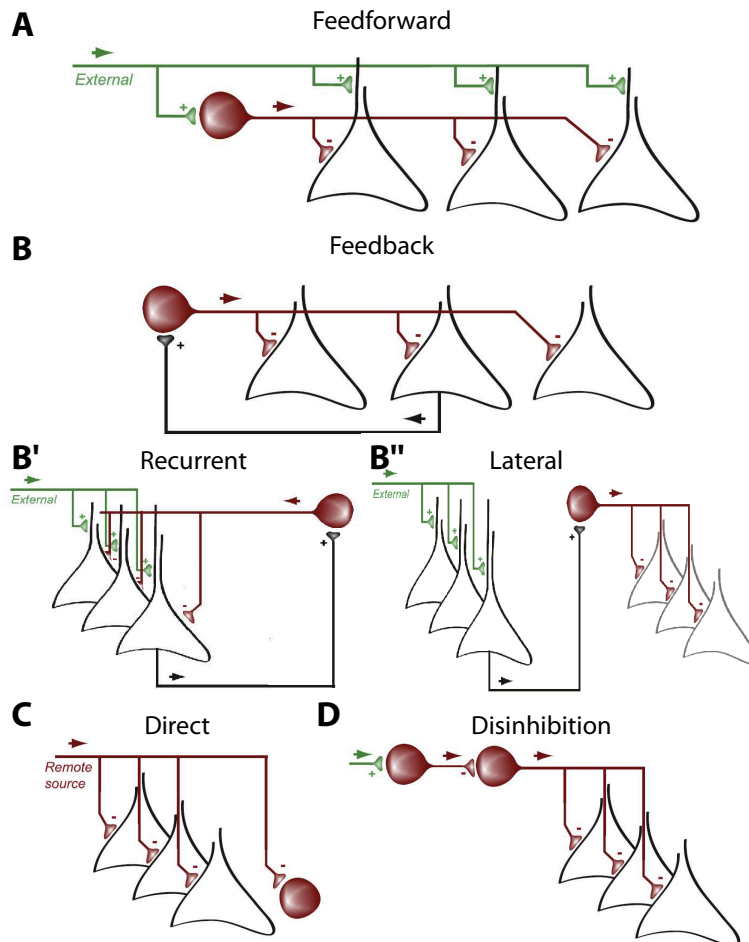


Figure 1.3 – Main forms of inhibitory microcircuits.

A. Feedforward inhibition. An external source (green) mediates disynaptic inhibition on excitatory neurons (black) through the activation of local GABAergic neurons (red).

B. Feedback inhibition. Principal cells drive their own inhibition. B'. External inputs drive an assembly of principal cells, which in turn inhibits itself. This is the strict form of feedback inhibition. B''. Within the same functional circuit, lateral inhibition allows a first assembly of principal cells, recruited by an external drive, to suppress the activity of another assembly of principal cells. In networks, lateral inhibition usually mediates competition between cell assemblies recruited by similar stimuli.

C. Direct inhibition involves the suppression of local principal cells or inhibitory neurons by long-range GABAergic projections from remote brain regions.

D. Disinhibition of principal cells occurs when their source of inhibitory inputs is suppressed by another population of inhibitory neurons. Figure adapted from (Roux and Buzsáki, 2015)

et al., 2012; Kato et al., 2012; Wachowiak et al., 2013). The innovative use of head-restrained mice has greatly eased recordings in awake animals, sometimes engaged in goal-directed behavior or during learning.

Activity of inhibitory neurons is greatly influenced by behavior. For instance, activity of PV+ neurons in the hippocampus substantially varies with oscillation regimes. In the absence of oscillatory activity, PV firing is low ($6.5Hz$), and it increases during theta oscillations ($21Hz$). During sharp wave ripples, PV firing augment by an order of magnitude ($> 120Hz$, Hu et al. (2014)). In the sensory cortex, Carl Petersen's group found that barrel cortex SOM+ cells hyperpolarized during whisker deflection (Gentet et al., 2012) and PV+ cells fired at lower rates in hit versus miss trials in an associative learning task (Sachidhanandam et al., 2016). In the medial prefrontal cortex (involved in complex cognitive tasks), SOM+ neurons are suppressed when mice entered the reward zone in a reward foraging task, while PV+ activity increased as animals left the reward zone (Kvitsiani et al., 2013).

1.2.3 "Balanced" inhibition and excitation

It follows from the strong interconnections between inhibitory and excitatory neurons that neuronal network dynamics can only be maintained if the excitatory drive is counterbalanced by inhibition. Through feedforward and/or feedback inhibition, excitatory afferents are somehow scaled, or "balanced" by inhibition (Isaacson and Scanziani, 2011; Roux et al., 2014). These changes in excitation and inhibition strength, which are temporally close, have been observed in multiple cortical regions, such as the auditory (Wehr and Zador, 2003), somatosensory (Wilent and Contreras, 2004), visual (Xue et al., 2014), and olfactory cortex (Poo and Isaacson, 2009). Similarly, in the medial prefrontal cortex, disruption of the excitatory/inhibitory balance by tonic depolarization of excitation disrupted social exploration behavior. Interestingly enough, this phenotype was rescued by selective activation of PV+ neurons. In addition, individual layer 2/3 pyramidal cells in the visual cortex receive inhibition that scales with the excitation they receive (Xue et al., 2014). When excitatory drive was genetically manipulated, inhibition from PV-, but not SOM-, expressing cells varied with excitation (Xue et al., 2014), suggesting that PV-containing neurons are the inhibitory neurons responsible for balancing inhibition in mouse visual cortex. In addition to scaling individual cell's excitatory input, the group of Scanziani showed that in hippocampal gamma oscillations, inhibition can rapidly follow excitation, in a cycle-to-cycle basis, inducing modulation of gamma oscillation over a wide band of frequencies (Atallah and Scanziani, 2009). Excitation and inhibition do not balance strictly in space and time, but rather, a ratio between excitatory and inhibitory conductances seems to be overall maintained. Inhibition and excitation are spatially distributed along the dendrites, somas

and axon's initial segments of neurons and are temporally shifted upon appropriate stimulation, such that they do not cancel each other out.

1.2.4 Inhibition narrows opportunity window for input integration

Temporally precise disruption of excitation and inhibition occurs in the presence of external or internal stimulation. Afferent inputs or firing of local principal neurons recruit feedforward or feedback inhibition, respectively and therefore excitation on principal cells precedes inhibition with a monosynaptic delay (Pouille and Scanziani, 2001; Stokes and Isaacson, 2010). In circuit engaging PV cells, this synaptic delay can be as brief as 1 ms (Pouille and Scanziani, 2001). In the olfactory cortex, feedforward inhibition does not recruit PV cells, rather it recruits horizontal and NG cells (Stokes and Isaacson, 2010; Suzuki and Bekkers, 2010, 2012). Although feedforward inhibition occurs at the dendrites of principal neurons in this example, afferent input stimulation also elicit short-latency inhibition of principal cells ($< 2ms$) (Stokes and Isaacson, 2010).

1.2.5 Inhibition shapes tuning properties of excitatory neurons

A basic property of cortical neurons is that specific features of the environment differentially drive the spike output of individual cells. For example, different bar orientations differentially drive different neuron in the visual cortex, different odors differentially drive neurons in the olfactory cortex, etc. Preferential tuning of a cell corresponds to maximum activity (as assessed by cell firing or membrane depolarization; see Figure 1.4,A, black traces). Inhibition plays a clear role in selective tuning. For instance, GABA_AR pharmacological blockade broadens tuning of principal cells in a variety of cortices (Isaacson and Scanziani, 2011), and notably in the APC (Poo and Isaacson, 2009). Inhibitory neurons are more broadly tuned than excitatory neurons in auditory, visual and olfactory cortex (Isaacson and Scanziani, 2011; Poo and Isaacson, 2009). Consistently, inhibitory current in principal cells were found to be more broadly tuned than their excitatory counterpart (Poo and Isaacson, 2009). Therefore, non-preferred stimuli elicit an excitation/inhibition ratio in principal cells in favor of inhibition, while preferred excitation evokes a ratio permitting further spike output. Stimuli eliciting the best overall responses ("preferred" stimuli) are stimuli eliciting the biggest excitatory/inhibitory conductance ratio. Interestingly, tuning of inhibitory neurons (and notably PV neurons) is correlated with the extent of the dendritic arborization. The more developed the arborization, the broader the tuning (Tremblay et al., 2016). In addition, timing of excitation compared to inhibition can also generate selective tuning. In response to a

sensory stimuli in auditory (Wehr and Zador, 2003), somatosensory (Wilent and Contreras, 2005) and visual cortex (Liu et al., 2010) inhibition will follow excitation with a few ms delay (with a feedforward inhibition mechanism, as seen before). This lag was greater for preferred stimulus compared to non-preferred stimuli (Wilent and Contreras, 2005), allowing more time for synaptic integration.

In the olfactory cortex, GABA_BRs were found to preferentially depress intracortical inputs, with minimal impact on afferent fiber synapses (Poo and Isaacson, 2011). Odor stimulation strongly drives intracortical activity, and GABA_BRs agonist baclofen was shown to have stronger effect on broadly-tuned neurons (Poo and Isaacson, 2011), suggesting a role for GABA_BRs in shaping olfactory cortical neuron tuning properties. Thus, in sensory systems, the spatio-temporal between excitation and inhibition depend on stimulus features, such as odor identity in the olfactory cortex (Poo and Isaacson, 2009). Inhibition can sharpen tuning of cortical neurons without being itself tuned to the opposite direction. Because neighboring cortical neurons have different excitation/inhibition ratios (Xue et al., 2014), neighboring neurons are not tuned to the same stimuli, which shapes the population response to a stimulus (e.g, olfactory cortex neurons respond sparsely to odor stimulation (Stettler and Axel, 2009)).

1.2.6 Inhibition controls the gain of neurons

As a stimulus increases (either in intensity or frequency), a given neuron typically responds with an increase in action potentials emitted, until it eventually reaches an asymptotic firing rate. The relationship between input and cell output is the transfer function of a neuron, also called gain of the neuron (Figure 1.4,A). Therefore, the gain of a neuron determines its ability to respond over a range of input dynamics, with weak inputs eliciting a minimal response, increasing inputs inducing higher responses, with a certain slope in the input/output response, and finally strong inputs saturate cell output. The minimal to maximal response that a given neuron is capable of is known as its dynamic range. Through a mechanism called gain control, a neuron can undergo changes in its threshold, slope or saturation level, thus revealing that a neuron's gain is not fixed. This is thought to be important in order for a sensor to have an optimal response to inputs that can vary strength. Below, I first review the different types of gain control that shape neuronal activity and then finish by discussing studies that report gain control in brain circuits.

Often, neuronal gain takes the form of a sigmoidal curve (with a log scale used to describe input strength). Gain control can affect the sigmoidal curve in at least three ways: it can shift the curve on the x axis, y axis, or change the slope without necessarily affecting the threshold or the saturation. 1) A shift on the x axis results in a modification to the threshold of the cell to

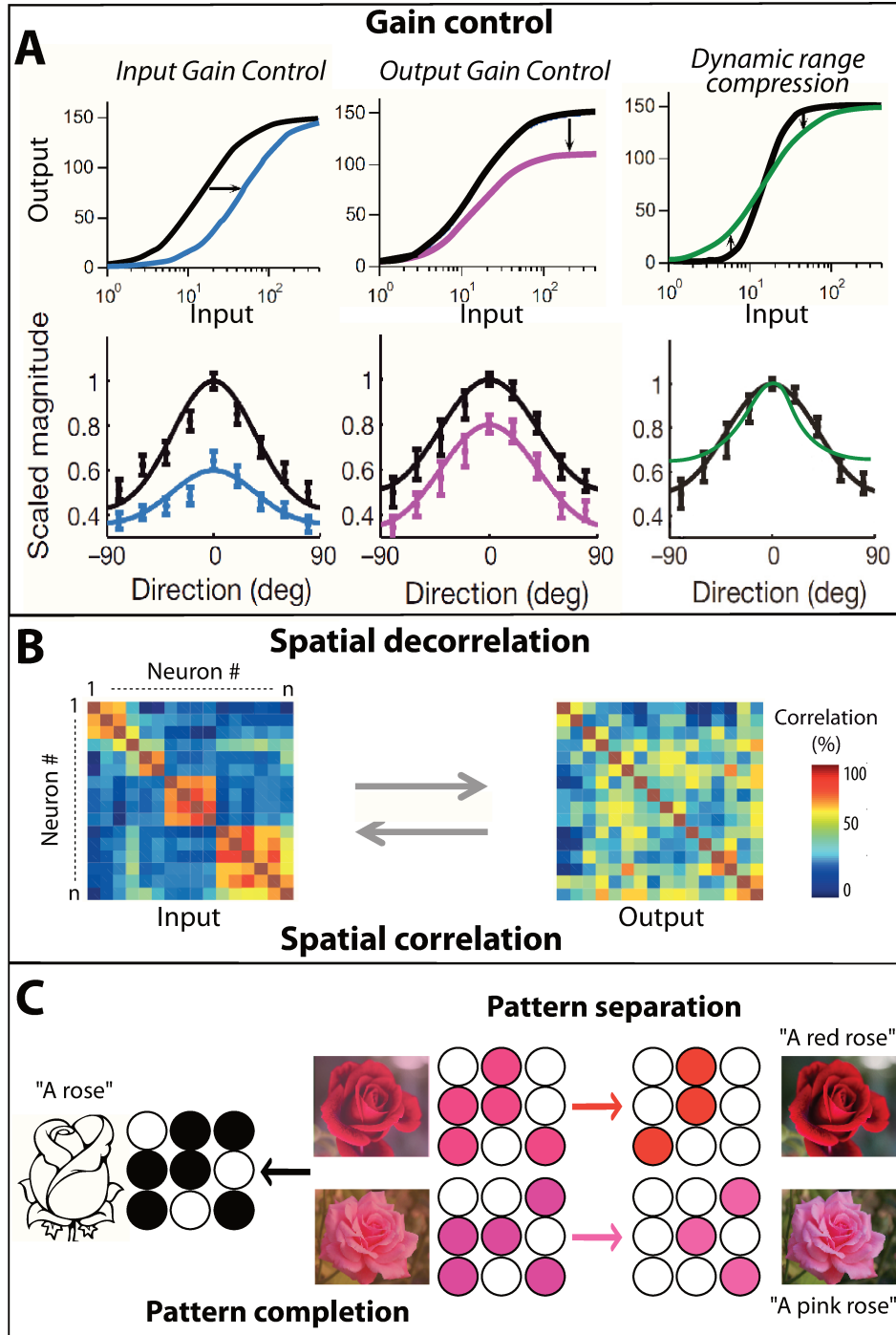


Figure 1.4 – Main functions of inhibition in the brain.

Figure 1.4 (Continued) – A. Gain control. Input-output functions before (black) and after (color) gain control. Input gain control (left) divides the received input by a given factor, in a non-linearly fashion. Output gain control (middle) divides the produced output by a given factor and thus preserves the shape of the curve. Dynamic range compression (right) transforms the gain in a more complex fashion. It controls a neuron’s dynamic range by altering the response to weak and strong input in a different manner. It also sharpen or broaden a neuron’s tuning curve. Top line is adapted from (Uchida et al., 2013a), bottom line is original data (left, middle) or based on original data from (Wilson et al., 2012).

B. Spatial transformations. Each neuron is represented in a line and in the corresponding row. Correlation between the activity of the neuron x and neuron y is represented in the pixel row x and the column y . Red indicates high correlations and blue low correlations. Spatial decorrelation separates the activity of correlated neurons while spatial correlation renders the activity of uncorrelated neurons more similar.

C. Pattern separation and generalization. Circles represent neurons. White circles are non-activated neurons and black or colored circle are activated neurons. Pattern separation is the transformation that separates the neuronal representation of two similar objects, as illustrated by the images of the red and pink roses and the schematic representation of neuronal activity for the two inputs before, and after, pattern separation. In contrast, pattern completion is the transformation that recruits similar neuronal assemblies with slightly different inputs. Slightly different inputs initially recruit slightly different cell assemblies, but generalization might occur to lead to the activation of the same cell assembly for the two stimuli. This is thought to allow integrated representation, such as the concept of a rose generalized from the red and pink roses illustrated here. Another form of pattern completion occurs when degraded inputs are presented. Reconstruction of the full pattern is mediated through pattern completion mechanisms.

be activated by incoming inputs (Figure 1.4,A, top left). This alters weak stimulation more compared to stronger inputs, since cell firing saturation remains unchanged. This shift on the x axis is implemented by a divisive or multiplicative effect on the strength of the stimulus itself. Therefore, this type of gain control is often named "input gain control". In the case where the gain of the neuron does not follow a sigmoidal curve but peaks at a given input value and decreases for lower and higher values – as is the case for tuning curves – input gain normalization will result in **divisive** or **multiplicative** gain control (Figure 1.4,A, bottom left). This sharpens or broadens the neuron's tuning curve. 2) A shift on the y axis results in a modification of the saturation level (Figure 1.4,A, top middle). In that scenario, the response itself is shifted, for all input strengths. It is therefore usually called output or response gain control. In the case of a tuning curve, the operation implemented on the gain is **additive** or **subtractive** (Figure 1.4,A, bottom middle). It increases or decreases the response without affecting the shape of the tuning. Lastly, a shift in the slope of the gain results in a change in neuron sensitivity to the input dynamic (Figure 1.4,A, right), thus preserving the neuron's dynamic range. In the case of a tuning curve, this operation sharpens or broadens the neuron's tuning curve.

Gain control is probably the signal transformation where specific neuronal population contribution has been the most extensively studied. Both feedforward and feedback inhibition can support such a computation. For instance, Pouille and Scanziani (2009), showed that feedforward inhibition tracks the increase in incoming excitatory drive through PV neurons and thus preventing principal cell saturation. By this mean, inhibition normalization extend the dynamic range of principal neurons. In the olfactory bulb (OB), PV+ cells are mediating broad feedback to principal cells (Miyamichi et al., 2013). Silencing these PV+ cells with pharmacogenetic tools indicates that they have a divisive gain control on the principal cell output, yet principal cells tuning properties remained unaffected (Kato et al., 2013). Selective optogenetic inhibition of SOM+ neurons in the olfactory cortex revealed that although SOM+ neurons provide subtractive inhibition on principal cells, they too did not affect tuning properties (Sturgill and Isaacson, 2015). SOM cells were found to inhibit both principal cells and PV+ inhibitory neurons, suggesting that the resulting subtractive effect on principal cells is generated by the interplay of a distinct class of GABAergic neurons. In the visual cortex, recent work nicely demonstrated different roles for PV and SOM neurons on principal cell gain control, either divisive or subtractive (Atallah et al., 2012; Wilson et al., 2012; Zhang et al., 2014). However, because of discrepancies between studies, it is not clear which type of neuron mediates what function. In fact, it rather seems that the computation performed by the distinct types of GABAergic neurons is flexible and depends on their pattern of activation by sensory stimuli and brain states (see Tremblay et al., 2016 for a review). However, these studies were probably the first demon-

strations showing that a specific aspect of signal processing can be attributed to distinct cell types.

Membrane potential and resistance of a neuron is likely to determine whether the dominant contribution of inhibition is a conductance change (in high-resistance regions, shunting inhibition) or current flow (in depolarized zones, hyperpolarizing inhibition). In essence, shunting inhibition tends to be divisive while hyperpolarization is subtractive.

1.2.7 Inhibition of inhibition

As we saw in the subsection "1.1", certain GABAergic neurons specialize in inhibiting other GABAergic neurons. VIP-expressing neurons are known to preferentially target SOM neurons for instance. In the auditory cortex, VIP+ neurons were shown to disinhibit principal neurons *via* inhibition of both SOM and PV inhibitory neurons (Pi et al., 2013). In addition, Letzkus et al. (2011) show that a disinhibitory mechanism mediates associative fear learning in auditory cortex. Interestingly, this disinhibitory circuit was mediated by layer 1 inhibitory neurons, where VIP+ neurons are found. Moreover, Pi and colleagues (2013) determined that disinhibition on principal cells resulted in an additive effect on the cell tuning curves, while inhibition onto GABAergic neurons was divisive. This is another example showing that a GABAergic population can not be restricted to a single function in cortical network but its function should rather be considered in light of its input connectivity and output targets.

1.2.8 Cell assembly recruitment

The brain has the ability to discriminate two similar stimuli, but also to generalize over different inputs (Figure 1.4,B,C). For example, roses of similar color (red and pink) generate similar neuronal patterns, that can be learned to be dissociated with experience. Alternatively, repeated experiences allow generalization (or pattern completion), such that the two objects are recognized as roses despite their singularities.

The ability of the brain to decorrelate inputs is thought to be accomplished by pattern separation, which dissociates overlapping population activity. Generalization, however is thought to happen *via* a phenomenon called pattern completion, where dissimilar activity patterns become more similar (Figure 1.4,B). Lateral inhibition is thought to help pattern separation by implementation of "winner takes all" circuit mechanism, in which the more active cell triggers inhibition of the less active ones *via* highly interconnected network. This mechanism contributes to sparsification and activity decorrelation is thought to be necessary for pattern separation (Figure 1.4,B,C).

In contrast, repeated stimuli, with similar network activation and behavioral relevance, can be associated through recurrent connectivity and form more correlated responses and recruit a more similar ensemble of neurons through spatial correlation and pattern completion (Figure 1.4,B,C). In addition, when an input is degraded, distributed activity and highly connected excitatory network permits the recruitment of unactivated neurons to engage the full neuronal ensemble. Formation of cell assembly can be generated through plasticity phenomena upon repetitive activation of a cell population. This highly recurrent connectivity matrix is a hallmark of the olfactory cortex and might be the circuit basis for the remarkable pattern completion occurring in the olfactory system (Haberly, 2001).

Other kinds of spatial transformation are performed by inhibitory mechanism. Center-surround inhibition is a mechanism by which mostly active cells inhibit surrounding, less activated cells *via* lateral inhibition. In the visual cortex, targeted recording of SOM+ neurons in awake, head-restrained mice reported that SOM+ neurons attenuate surround suppression in V1 (Adesnik et al., 2012).

In addition GABAergic neurons, and notably PV-expressing neurons participate in grid (Buetfering et al., 2014) and place cell (Wilson and McNaughton, 1993) formation in the hippocampus.

1.2.9 Oscillations

Brain oscillations play an important role in the communication between brain areas, sensory processing and cognitive processes. During oscillatory periods, populations of neurons fire in synchrony, thereby allowing them to cooperate in the depolarization of a common downstream structure. Through this mechanism, oscillations are thought to bind neuronal assemblies.

Oscillatory rhythms occur at different time scales in the brain, from slow ($< 1Hz$, "Up" and "Down" states) to fast cycles ($> 200Hz$ during ripple events). Oscillatory mechanisms are thought to be supported either by principal neuron-to principal neuron interaction, or by an interplay between inhibitory and excitatory neurons. In the latter case, activity in principal cells triggers feedback inhibition that terminates firing of principal neurons. Substantial reciprocal, and notably electrical coupling between inhibitory neurons is thought to support fast oscillations. Fast-spiking properties of PV cells place them in a good position to regulate fast oscillations. Inhibitory neurons can generate and pace the rhythm of oscillations. Both theta and gamma rhythms have been shown to be modulated by PV+ neurons (Hu et al., 2014). Indeed, stimulation of PV+ cells at theta frequency induces theta spike resonance in CA1 pyramidal cells, and stimulation at gamma frequency increases gamma oscillations in the local field potential (LFP) (for a review of the role of GABAergic neurons on hippocampal oscillations see Allen and Monyer, 2014). Conversely, inhibition of PV activity reduces

gamma oscillations. In the OB, reciprocal interactions between granule cells and principal cells are responsible for gamma rhythm generation (40–100Hz in the OB; Lepousez et al., 2013), while Fukunaga and coworkers (2014) confirmed that granule cells are involved in gamma oscillations and extended the above findings by showing that glomerular layer GABAergic neurons regulate theta oscillations (1–10Hz in the OB). Therefore, in the OB, distinct classes of neurons participate in different oscillatory activity. It is important to note that neuronal activity can also be coordinated without oscillations, as long as an external input provides a necessary time reference.

1.2.10 Inhibition in plasticity and learning

Circuit interactions are not fixed and are subject to adaptation in order to better encode relevant stimuli. In the brain, plasticity is a mechanism by which structure and function adapt to the ongoing activity. Plasticity is notably necessary for learning. For a long time, plasticity of brain circuits was thought to mainly rely on glutamatergic synapses, while GABAergic transmission was assumed to be relatively invariant. However, it has been demonstrated that inhibitory synapses undergo several forms of plasticity, thus providing an additional source for adapting circuits to incoming inputs.

Dendrites of granule cells (GCs) of the OB exhibit high structural plasticity, notably in the context of odor learning (Lepousez et al., 2014; Sailor et al., 2016). In addition, retrograde messengers modulate GABA release, notably through the cannabinoid signaling system (Iremonger et al., 2013; Younts and Castillo, 2014), and protein synthesis has been shown to be necessary for presynaptic long-term plasticity (Younts et al., 2016). Plasticity also occurs at the postsynaptic site. Changes in subunit composition of GABA_ARs (Succol et al., 2012), phosphorylation (Hirano and Kawaguchi, 2014), associated or scaffolding proteins (Zacchi et al., 2014), or changes in Cl⁻ driving force (Raimondo et al., 2012; Woodin et al., 2003) alter the conductance associated with single GABA_AR. On the other hand, the number of available GABA_ARs (Hirano and Kawaguchi, 2014) as well as regulation of GABA concentration by changes in GAT activity (Scimemi, 2014) modify the total amount of current elicited by a given amount of GABA molecules released. Recent evidence suggests that tonic inhibition is also plastic, with variations in expression of δ -GABA_ARs at hippocampal neurons with the ovary cycle (Barth et al., 2014). Finally, postsynaptic GABA_BRs expressed on GABAergic neurons were found to mediate disinhibition in hippocampal GCs, and this GABA_B-mediated disinhibition was required for induction of long-term potentiation (LTP) induced in the frequency range of physiological stimulation (Mott and Lewis, 1991). Similarly, GABA_BRs were shown to modulate long-term potentiation in Purkinje cells of the cerebellum (Gao et al., 2014).

Finally, multiple examples demonstrate that plasticity at GABAergic

synapses modifies network function and allows learning. For instance, adult-born neurons in the olfactory bulb were shown to facilitate learning in an odor-reward association task (Alonso et al., 2012). PV-containing neurons of the visual cortex are transiently down-regulated during monocular deprivation, which appears to be necessary for ocular dominance plasticity. Furthermore, auditory fear-conditioning or olfactory learning induce plastic changes in PV+ neurons of the hippocampus (Donato et al., 2013; Letzkus et al., 2011) or in adult-born neurons of the olfactory bulb, respectively (Lepousez et al., 2014).

In conclusion, significant advances have been made in the last decade in understanding the function of inhibition in brain circuits, and notably with regards to GABAergic neuron diversity. Distinct types of GABAergic neurons are embedded differentially in microcircuits (and provide canonic inhibition schemes, such as feedforward and feedback inhibition), they are recruited differentially by specific behavioral epochs and brain states, and they have distinct influence on local or distant neuronal networks. As a result, they allow different circuit computations in specific network contexts. Computations executed by GABAergic neurons include arithmetic operations on a neuron gain, influence on spike timing and oscillations, tuning properties of neurons and influences on cell assembly recruitment. Furthermore, plasticity permits GABAergic neurons to adapt to their environment and strongly influences behavior. Interestingly, tonic GABA_AR-dependent inhibition has also been reported to be plastic (Barth et al., 2014). This suggests that, although extrasynaptic GABA receptors induce persistent inhibition, the magnitude of this tonic current is not constant over time and is likely dynamically regulated. In the next section, I will review some functions mediated by the extrasynaptic GABA_BRs. I will particularly insist on the fact that these receptors are more than just sensors of GABA spill-over and can play a role in inducing or regulating fast network activity in the brain.

1.3 Functional role GABA_BR-mediated inhibition

GABA_BRs are receptors with slow kinetics, and are classically thought to be activated in context of synchronized and repeated GABA release, which will lead to accumulation of GABA and spilling-over outside the synaptic cleft to bind extrasynaptic GABA_BRs (Scanziani, 2000). However, emerging evidence suggests a more spatially and temporally constrained mode of GABA_BR activation, both pre- and postsynaptically. In this section, I review a few of the currently accumulating examples arguing in favor of a spatially or temporally restricted activation of GABA_BRs.

Function according to GABA_BR subunit composition. Subunit composition is associated with different subcellular locations. Elegant studies by the group of Bettler (Vigot et al., 2006) and Larkum (Pérez-Garci et al., 2006) demonstrated the subunit composition-dependent localization of GABA_BRs and investigated their differential functions. Vigot and colleagues (2006) generated two specific knock-in mice, lacking either GABA_B1a or 1b subunit specifically to show, within the hippocampus, that GABA_B1a was localized at CA3 axon terminals while GABA_B1b were confined on postsynaptic CA1 neurons. In mice lacking GABA_B1a, object recognition was disrupted, while no change was observed in mice lacking the 1b subunit (Vigot et al., 2006). In the neocortex, layer 5 pyramidal cells are unusual in having both axonal and dendritic sites for action potential generation (Larkum et al., 2001, see "1.1"). Using the mice generated by Vigot et al. (2006), Perez-Garci and coworkers (2006; 2013) found that GABA release activates GABA_B1b to generate a long-lasting inhibition of layer 5 pyramidal cells. Furthermore, GABA_A-mediated IPSPs on pyramidal neurons were blocked by GABA_B1a-containing GABA_BR activation, therefore showing that GABA_{B(1a,2)}Rs act as presynaptic autoreceptors on inhibitory neurons (Pérez-Garci et al., 2006). In addition, GABA_BRs containing either the 1a or 1b isoform of the R1 subunit have been associated with different functions during sleep network dynamics. During sleep, cortical networks alternate between synchronized periods of depolarization and burst firing (Up states), and periods of hyperpolarization (Down states). Up states are involved in memory consolidation and Down states may play a role in regulating neuronal homeostasis. In mice lacking GABA_B1a, layer 1a stimulation terminates Up states but blocking the remaining GABA_B1b failed to prolong Up states as found with wild-type mice. In contrast, in GABA_B1b-lacking mice, layer 1a stimulation did not terminate Up states but blocking of the remaining GABA_B1a did prolong Up states (Craig et al., 2013). Thus, these studies collectively show that pre- and postsynaptic GABA_BRs vary in subunit composition and play different roles in network dynamics.

GABA_BRs mediate confined shunting inhibition. In the example above, Perez-Garci and coworkers (2006; 2013) show that postsynaptic GABA_BRs produce inhibition on layer 5 pyramidal cells. Interestingly, they further demonstrate that GABA_BRs induce a long-lasting inhibition of Ca²⁺ spikes, but not back-propagating Na⁺ spikes, by directly inhibiting Ca²⁺ channels (Pérez-Garci et al., 2013). A similar study dissecting a circuit mediating GABA_BR-dependent inhibition onto these layer 5 pyramidal cells came to similar conclusions Palmer et al. (2012). In this study, hindpaw stimulation induced a disynaptic inhibition of ipsilateral layer 5 pyramidal neurons. Disynaptic inhibition is mediated by interhemispheric connections from contralateral principal cells relaying onto NG cells (Palmer et al., 2012).

The resulting feedforward inhibition could be induced by GABA_BR activation (Palmer et al., 2012). Importantly, hyperpolarization evoked on these neuron somas was minimal, rather GABA_BR-dependent inhibition was mediated by blockade of Ca²⁺ channels (Palmer et al., 2012). Taken together, these results show that GABA_BRs can mediate shunting inhibition to principal cell, which is restricted to the dendritic tree.

Restricted spatial recruitment of pre- and postsynaptic GABA_BRs.

GABA_BRs are not necessarily activated by non-specific volume transmission. Indeed, in the somatosensory cortex, NG cell stimulation activate postsynaptic GABA_BRs on layer 4 fast-spiking GABAergic neurons but not presynaptic GABA_BRs at thalamic axons (Chittajallu et al., 2013). Similarly, Booker et al. (2013) showed that postsynaptic GABA_BRs inhibit perisomatic-, but not dendritic tuft-, targeting PV neurons in hippocampus (Booker et al., 2013). Furthermore, in substantia nigra dopaminergic neurons, subcellular enrichment in postsynaptic GABA_BRs associated with different inputs lead to qualitatively different recruitment of GABA_BRs in responses to striatal, pallidal or nigral GABAergic afferent stimulation *in vivo* (Brazhnik et al., 2008). Taken together, these results suggest that differential recruitment of GABA_BRs, can shift the balance between incoming inputs, and between somatic and dendritic inhibition onto principal cells, thus leading to a shift in information encoded by these principal neurons.

GABA_BRs activated by temporally sparse activity.

GABA_BR-mediated IPSPs can arrive from unitary events in cortical network. In somatosensory cortex and hippocampal slices, single action potential in NG cells was sufficient to activate GABA_BRs on postsynaptic pyramidal neurons (Price et al., 2008; Tamas, 2003). Solitary spikes in a single neurogliaform cell might replace the concerted action of several GABAergic neuron in activating GABA_BRs. However, it should be noted that NG cell-mediated inhibition might be particular in that high amounts of GABA might be released simultaneously by many NG cell axonal boutons targeting principal cells dendrites, and GABA_BRs activation might occur in the vast majority of nearby neurons (Oláh et al., 2009). Thus, two modes of GABA_BR activation might co-exist: 1) local, spatially restricted activation that require repetitive and/or synchronous synaptic release of GABA, or 2) broad spatial activation that require only a single action potential. These two modes of activation are in agreement with classic views on GABA_BR recruitment mechanisms, but specific manipulation of GABAergic neuron subtypes suggest that they could be supported by different mechanisms.

GABA_BRs and fast rhythmic activity Although GABA_BRs are classically described as receptor for coincident and repetitive activation of in-

hibitory neurons (Scanziani, 2000), they are in good position to play a role in network oscillations. Various cognitive processes are thought to be supported by synchronized network activity, such as sensory processing, motor control, working memory, or consolidation of memory. Disruption of oscillations can lead to brain disorders such as epilepsy or schizophrenia. We already saw the role of GABA_BRs in generating slow oscillations such as Up and Down states during sleep, and emerging evidence suggests a role for GABA_BRs in modulating fast oscillations such as γ oscillations. Both in the hippocampus and the neocortex, reciprocally connected fast-spiking inhibitory neurons and principal cells are thought to generate gamma oscillations. In hippocampal slices, GABA_BRs were found to suppress re-emergence of oscillations (Brown et al., 2007), while GABA_BRs mediate stronger inhibition in distant, non-reciprocally connected inhibitory-excitatory pairs in the neocortex (Oswald et al., 2009). These heavier GABA_BR-mediated currents result in suppression of self-emergent γ oscillation (Oswald et al., 2009). Disruption of normal oscillations eventually lead to epileptiform activity. GABA_BRs have notably been shown to play a role in absence epilepsy, and GABA_BR knock-out mice are prone to develop seizures (Craig and McBain, 2014; Kohl and Paulsen, 2010).

Conclusion on the role of GABA_BRs in brain networks In conclusion, GABA_BRs are extrasynaptic receptors with slow kinetics, and were classically thought to be activated in context of synchronized and repeated GABA release (Scanziani, 2000). However, emerging evidence suggests a more spatially and temporally constrained mode of GABA_BR activation: they play a role in fast network dynamics (Craig and McBain, 2014), NG cells do not need rhythmic depolarization to activate post-synaptic GABA_BRs (Oláh et al., 2009), single action potentials can trigger GABA_BR activation (Tamas, 2003), and GABA_BRs can be activated in a synapse-specific manner (Chittajallu et al., 2013). GABA_BRs form large complexes (Pin and Bettler, 2016), whose composition, and notably in GABA_B1 isoform, influences receptor localization (Pérez-Garci et al., 2006; Vigot et al., 2006), kinetics, desensitization, and eventually function (Gassmann and Bettler, 2012). Therefore, GABA_BRs can have a profound effect on the state of a network and on how it processes and encodes incoming information and GABA_BR activation might well depend on the local "brain state" to influence circuit function. Notably, manipulation on GABA_BRs induced impairment at the behavior level, as demonstrated in a object recognition task (Vigot et al., 2006). Furthermore, GABA_BR loss of function has been associated with brain function deficits, for instance presynaptic GABA_B1a receptor impairment leads to generalized fear responses (reviewed in Jasnow et al., 2012) and persistent weakening of GABA_BR-associated GIRK currents induced by a foot-shock exposure participate in depression-like syndromes (Lecca

et al., 2016). Gain of function alterations are also associated with altered brain function, for example genetic knock-in mice with enhanced postsynaptic GABA_BR activity showed decreased spatial memory consolidation (Terunuma et al., 2014). Therefore, it is not surprising that GABA_BRs are involved in a myriad of cognitive and neurological functions (such as depression, epilepsy and drug addiction; Cryan and Slattery, 2010; Heaney and Kinney, 2016; Kasten and Boehm, 2015; Kohl and Paulsen, 2010). Lack of selective ligand for pre- and postsynaptic GABA_BRs had precluded detailed studies on GABA_BRs function for decades, but recent advances in knowledge about receptor structural organization (Pin and Bettler, 2016) and mouse genetics (Haller et al., 2004; Vigot et al., 2006), together with technological advances in circuit manipulation and activity monitoring, permit the investigation of defined receptor function. Although the clinical use of GABA_BR modulators is currently limited of somatic diseases such as neuropathic pain and dystonia, there is now high expectations for GABA_BRs modulators in clinical applications.

1.4 Long-range GABAergic projections in the brain

Studies on GABAergic neurons focused almost entirely on locally projecting inhibitory neurons (which gave rise to the use of the word interneurons to refer to inhibitory neurons), rather than inhibitory neurons projecting to different brain areas. Projecting GABAergic neurons are known for a long time, with the example of medium spiny neurons of the striatum or Purkinje cells of the cerebellum, however these examples represent exceptions as they constitute the sole output of their brain region. Brainstem nuclei and the hypothalamus also contain a variety of projecting GABAergic neurons, notably implicated in sleep regulation and anxiety behavior. In cortical areas and in the basal forebrain, several long-range GABAergic projections have been described early in parallel to the main output projections (glutamatergic in cortical areas, cholinergic in the septum and basal forebrain, cholinergic in the ventral tegmental area, etc). However, these parallel GABAergic fibers received little attention. In addition, the same axon may co-release glutamate and GABA, as it was recently shown in mesohabenular axons (Root et al., 2014b).

Early studies of GABAergic projecting neurons in areas where they do not constitute the sole output was technically challenging, but recent advances in mouse genetics, optogenetics and large-scale reconstruction of brain tissue now permit specific investigation of GABAergic projections. Tackling the GABAergic projection system brings conceptual questions to the forefront: what is the need for having long-range inhibitory projections to distant networks? To gain insight into this issue, I review here some fundamental work on GABAergic projections. In this work, I adopted the definition

of "long-range" projections stated by Caputi et al. (2013): "we consider a GABAergic cell as being 'long-range' when it connects brain areas associated with distinct functions. At least in this context we do not consider lateral inhibition or interlaminar connectivity within one sensory modality as 'long-range' connectivity".

Diversity of the GABAergic projections in the brain. Long-range GABAergic projections were first detected *via* unspecific retrograde (such as horse radish peroxidase, fast blue, fluorogold or cholera toxin subunit B) or anterograde markers (such as *Phaseolus vulgaris*), combined with immunohistochemistry of GAD, VGAT or GABA. However, sensitivity of the immunolabeling is suboptimal. To improve the efficacy of the technique, more recent studies took advantage of a genetically engineered mouse line expressing GFP under the promoter of GAD67 to report dually-labeled cells. Characterization of the GABAergic neuron subtypes (such as SOM, PV or 5HT3aR) was performed by immunohistochemistry. Later, cell-specific Cre-lines were developed, allowing direct characterization of the GABAergic projecting neuron population.

Long-range GABAergic projections are not as rare as initially thought, since they are estimated to represent 0.5% of the GABAergic cells in the neocortex and are distributed throughout it, and GABAergic projections have been reported between distinct areas of the neocortex and between contralateral cortices (Tomioka et al., 2005). A variety of subcortical areas were found to project GABAergic axons to the neocortex or hippocampus (corticopetal projections, from zona incerta (Lin et al., 1990), hypothalamus (Vincent et al., 1983), basal forebrain (Freund and Meskenaite, 1992) or the septum (Freund and Antal, 1988), to the basal ganglia (Brown et al., 2012) or to the olfactory bulb (Zaborszky et al., 1986). The neocortex was also found to connect subcortical areas with inhibitory axons (corticofugal projections, to the basal forebrain (Jinno and Kosaka, 2004; Tomioka et al., 2015), and amygdala (Lee et al., 2014)). Finally, reciprocal connections between the entorhinal cortex and hippocampus (Basu et al., 2016; Melzer et al., 2012), and between the medial septum and hippocampus (Jinno and Kosaka, 2002; Takács et al., 2008) have also been reported (for reviews on long-range GABAergic projections, see Caputi et al., 2013 and Tamamaki and Tomioka, 2010). Multiple resources are now online for rapid scanning of long-range projections in the brain, notably with some being cell-type specific (from The Allen Institute for Brain Science: <http://connectivity.brain-map.org/>, or founded by the National Institute of Health: <http://www.mouseconnectome.org/>).

Broadcasting inhibition. Hippocampal GABAergic neurons not only project to the entorhinal cortex or the septum, but also to the subiculum, presubiculum and other extrahippocampal areas (Jinno, 2009; Jinno et al.,

2007). Similarly, neocortex GABAergic projection neurons connect other cortical areas and a wide variety of basal ganglia structures, such as the caudate putamen, globus pallidus, nucleus accumbens and olfactory tubercle (Tomioka et al., 2005, 2015). In addition, projecting GABAergic cells also emit locally arborizing axons (Jinno and Kosaka, 2002; Picardo et al., 2011; Tomioka et al., 2005, 2015).

Diversity of the projecting cells. Data from the literature report a vast diversity of the cell population sending GABAergic projections. Taking one look at molecular marker expression for instance, hippocampo-septal projections were found to mainly express SOM and CB, while septo-hippocampal inhibitory neurons contain mainly PV. Cortico-cortical projection neurons were found to express mainly neuronal NO synthase (nNOS), but also SOM and NPY for example (Caputi et al., 2013; Tamamaki and Tomioka, 2010). Within the hippocampal system (Jinno, 2009) or neocortex (Lee et al., 2014; Tomioka et al., 2015), long-range projecting GABAergic neurons also appear to be heterogeneous .

It remains unknown whether distinct classes of GABAergic projection neurons are born from different niches and at different times during embryogenesis, like the local interneurons counterpart. One study reported that early-born, pioneer GABAergic cells born before embryonic day 10 ("hub" cells) produce long-range projecting GABAergic neurons of the hippocampus (Picardo et al., 2011) and other brain structures.

Postsynaptic targets. Optogenetic tools allowed to further investigate the nature of the target cells, i.e the postsynaptic cells contacted by long-range GABAergic axons. It seems that cortico-cortical GABAergic projections mainly target non-GABAergic cells, while centripetal and centrifugal projections, as well as basal to olfactory bulb projections and septo-hippocampal and hippocampo-enthorinal GABAergic loops preferentially target inhibitory neurons (Basu et al., 2016; Caputi et al., 2013; Freund and Antal, 1988; Gracia-Llanes et al., 2010b; Melzer et al., 2012; Tamamaki and Tomioka, 2010). In the latter case, long-range projecting GABAergic neurons induce disinhibition of principal cells in the target region (Basu et al., 2016).

Function of long-distance inhibition. Technical challenges in rapid scanning of GABAergic specific connectome (however laboratories such as the Allen Institute for Brain Science are making considerable progress), and fast large-scale tissue reconstruction, as well as limitation in the availability of cell-type specific Cre mouse lines precludes quantitative studies, appreciation of the full extent of the long-range projecting GABAergic cells in the brain, and study of their function. However, because of their long-range

nature, one can hypothesize that projecting GABAergic axons would play an important role in synchronizing distant brain structures, and therefore would be involved in the emergence or modulation of synchronized, coherent brain oscillations (Caputi et al., 2013; Jinno, 2009; Tamamaki and Tomioka, 2010). Indeed, activation of GABAergic projections from the medial entorhinal cortex enhances theta oscillation in the target structure, namely CA1 region of the hippocampus (Melzer et al., 2012) and inactivation of the septo-hippocampal GABAergic projection greatly reduce theta oscillations in the hippocampus (Brandon et al., 2014). Only a handful of studies tackled the function of these long-range inhibitory projections on behavior. When stimulated during a real-time place preference task, long-range GABAergic projections from the medial prefrontal cortex to the nucleus accumbens was shown to elicit acute avoidance behavior, suggesting that these projections can transmit aversive signals (Lee et al., 2014). Furthermore, using electron microscopy, and optogenetic tools with electrophysiological recordings and behavior, Brown et al. (2012) showed that ventral tegmental area GABAergic neurons specifically project onto a cholinergic interneurons, but not medium spiny neurons, of the nucleus accumbens. This is remarkable since cholinergic neurons represent only a very small fraction of the neurons in the targeted nucleus. When activated using channelrhodopsin-2 (ChR2), projecting GABAergic neurons paused cholinergic neurons and this led to enhanced discrimination between two stimuli in a fear conditioning paradigm (Brown et al., 2012). In another study, Basu et al. (2016) found that the lateral entorhinal cortex, similarly to the medial entorhinal cortex (Melzer et al., 2012), sends GABAergic inputs to the hippocampal region CA1. These GABAergic inputs target a subclass of cholecystokinin-expressing (CCK+) inhibitory neurons. In response to CA3 stimulation, these CCK+ neurons normally mediate feedforward inhibition onto principal neurons. As a result, when transiently activating lateral entorhinal cortex GABAergic projections, CA3 inputs onto CA1 principal cells were enhanced. Then, the authors showed, using Ca^{2+} imaging, that lateral entorhinal cortex GABAergic axons were responsive to various sensory stimuli. Finally, Basu and colleagues (2016) found that inactivating lateral entorhinal GABAergic inputs using pharmacogenetics altered both fear conditioning and novel object recognition. These three recent works show that both subcortical and corticofugal long-range GABAergic projections are engaged in cognitive tasks.

In conclusion, it seems that:

1. long-range projecting GABAergic neurons are more common than initially thought,
2. they have largely diverse expression of molecular markers and morphology,
3. their axon arborizes locally in addition to a usually wide (but rather

sparsely) innervation pattern of brain regions.

However, little remains known about their function. Undoubtedly, this issue will significantly benefit from the development of mouse genetic, optogenetic and calcium imaging, as well as large-scale morphological reconstruction.

1.5 Conclusion on the role of inhibition in brain circuits

In this chapter, we saw that inhibition and excitation are tightly regulated in space and time. Inhibition fluctuates with excitation and create window for signal integration. GABAergic neuron dynamics are crucial for maintaining normal brain function since several neurological and psychiatric diseases (including epilepsy, schizophrenia, depression and autism) have been associated with altered inhibition (Marín, 2012).

In this first chapter, we saw that GABAergic neurons are extremely diverse in terms of morphology, intrinsic properties as well synaptic connectivity. In addition, GABAergic neurons are not restricted to an interneuron population, as often simplified. Long-range projecting GABAergic neurons are somewhat common in the brainstem or hypothalamus, but accumulating evidences now points towards a more ubiquitous long-distance inhibitory system connecting the cortex to subcortical regions or different cortical areas. These projecting GABAergic fibers might not be very numerous compared to their glutamatergic counterpart, but they could regulate important functions, such as synchronization across brain regions.

The great diversity of brain function is supported by the great diversity in inhibitory neuron populations and their variety in firing activity and connectivity within the networks they are embedded in. Feedforward and feedback inhibition, but also disinhibitory mechanisms, allow GABAergic neurons to control the gain and the selective tuning of individual neurons, and permit control of the dynamic range of the population, spatial recruitment of cell assemblies through pattern separation and completion, as well synchronization of neuronal activity. Extrasynaptic inhibition is also important for regulating network dynamics, comprising fast rhythmic activities. Notably, GABA_BRs have been implicated in a variety of non-classical functions for such slow receptors: GABA_BRs control the relative influences of different inputs within a circuit, and therefore refine circuits recruited by long-range feedforward and feedback inhibition. GABA_BRs can further be activated by GABA released from a single action potential and in addition to hyperpolarizing inhibition, GABA_BRs can mediate shunting inhibition localized onto a specific subcellular compartment. GABA_BR subunit composition influence its location and its role in brain circuits.

GABAergic transmission is more plastic than initially assumed, and this

adaptation of activity to ongoing inputs reflects plasticity at glutamatergic transmission to allow learning and memory at the behavioral level.

I will now review the organization of the main olfactory system, with a focus on the olfactory bulb. We will see that such inhibitory motifs and functions are commonly found in the olfactory system.

Chapter 2

Introduction to the olfactory system

The olfactory system is composed of several different subsystems, namely the main olfactory system, the accessory olfactory system, the trigeminal system, the septal organ of Maser and the Gruenberg Ganglion. The main olfactory system allows perception of odors, while the accessory olfactory system is thought to be more suited to detect pheromones in many species (excluding humans). The functional distinction between the main and accessory olfactory system is not entirely clear: a large degree of overlap exists in the stimuli they detect. The trigeminal system is involved in chemical and mechanical sensation such as warmth, cooling and irritation. It is thought to mediate avoidance of potentially harmful substances. The Septal Organ of Maser and the Gruenberg Ganglion systems are present in the main olfactory epithelium and their function remains unknown.

Throughout the manuscript, I will focus on the the main olfactory system of rodents, and particularly on the olfactory bulb (OB). In this chapter, I start with an anatomical and synaptic description of the early olfactory system –from the nose to the olfactory cortex– to better encompass the intricate network the OB is embedded in.

2.1 Signal transduction: from the nose to the brain

Olfaction starts with inhalation of odorants in the nasal cavity and ends with the perception of an odor. Strictly speaking, odors are the mental representations resulting from the inhalation of small volatile molecules. Odor objects can be composed of a single odorant, or many hundreds of them (for example, coffee contains > 800 odorants). In the nasal cavity, odorants are sensed by a family of olfactory receptors (ORs) present in olfactory sensory neurons (OSNs), located in the olfactory epithelium. ORs transduce odor molecule binding into electrical activity in the OSNs. A large array of ORs

(Buck and Axel, 1991) allow the detection of extremely diverse molecular inputs. The number of functional ORs varies across species and has been estimated to be over 1200 in rodents (Zhang and Firestein, 2002), ~ 400 in humans, and $\sim 60 - 350$ in insects. In addition to this, ORs generally exhibit relatively loose tuning to odorant chemical features. As a result, a given odorant activates a combination of OSNs in the nasal epithelium and the identity of an odorant can therefore be described by a "combinatorial code". The extreme diversity of codes that can be generated with several hundreds to thousands of ORs enables animals to perceive and discriminate an outstanding diversity of odors. Recently, it has been suggested that humans can discriminate more than one trillion of odors (Bushdid et al., 2014). Although the number stated in this article might have been overestimated due to the calculation pitfalls, it was nevertheless a lower limit estimated with mixtures of 128 odorants "only", well below the thousands of odorants detectable by humans. Indeed, many more odorants can be detected by humans. In any case, the strategy adopted by the olfactory system is in marked contrast with those employed by other sensory systems. Color vision, for example, uses only 3 different photoreceptors and allow discrimination of $\sim 2.3 - 7.5$ millions colors. Similarly to color vision that can discriminate different color intensities, olfaction can detect odors across a wide range of concentrations. A distinct odor concentration elicits differential OR recruitment patterns, based on the affinity of the ORs for the molecule.

A typical mammalian genome encodes hundreds of OR genes, but a given OSN expresses only a single type of OR. Sensory neurons expressing the same OR are widely distributed across the olfactory epithelium, although some broad expression domains exist. OSNs in the nose send their axons to the first brain relay for olfactory information – the olfactory bulb (OB) – and OSN axon terminals form anatomical units on the surface of the OB: the glomeruli (Figure 2.1, Figure 2.2,A,B).

Each glomerulus receives inputs from OSNs that express the same OR (Figure 2.1). Conversely, OSNs expressing a particular OR project to (usually) two glomeruli in the ipsilateral OB (Mombaerts, 1996). As such, each odor activates a specific pattern of glomeruli distributed across the surface of the OB, and this pattern is conserved from animal to animal. Besides, the pattern of glomerular activation evolves across time, in part due to dynamical interaction between ORs and odor molecules. Odor recognition or discrimination is thus transferred from the olfactory epithelium to the OB, where the brain has to decipher the spatiotemporal activity map across the two-dimensional sheet of glomeruli in the OB. Odor recognition is a pattern-recognition problem defined by $\sim 1,000$ input channels (ORs or glomeruli, in rodents).

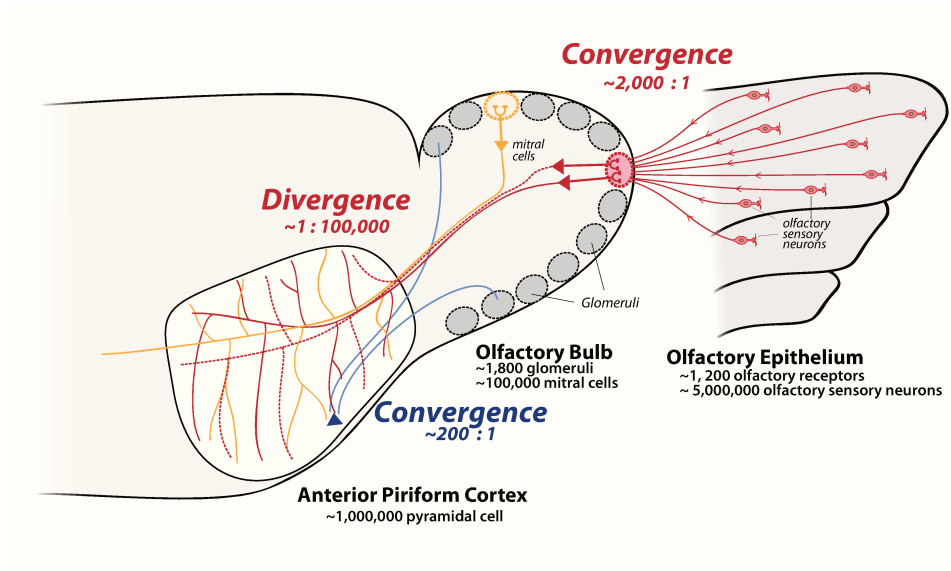


Figure 2.1 – Connectivity in the early olfactory system. Olfactory sensory neurons in the olfactory epithelium project to the olfactory bulb, the first brain relay for olfaction. Sensory neurons expressing the same olfactory receptor project usually to two glomeruli at the olfactory bulb surface, with a ratio of $\sim 2,000$ sensory neurons for 1 olfactory bulb principal cell (mitral cell). There is therefore a high degree of convergence in the transmission of olfactory information to the brain. In turn, mitral cells broadcast the information to the olfactory cortex, and notably the anterior olfactory nucleus and the anterior piriform cortex. A mitral cell project to about 100,000 pyramidal cells in the piriform cortex (divergence). In contrast, a given pyramidal cell in the anterior olfactory cortex receives input from ~ 200 glomeruli (convergence). Thus, both convergence and divergence appear at the connectivity between the olfactory bulb and the anterior piriform cortex. This figure also illustrates the spatial divergence of mitral cell projections to the anterior piriform cortex: two mitral cell receiving inputs from the same glomerulus (in red) innervate cortical regions as diverse as two mitral cells receiving inputs from different glomerulus (red and yellow). Number of glomeruli, mitral cells and pyramidal cells are from (Shepherd GM, 2004). The upper limit of convergence between the glomeruli and pyramidal cells was estimated by Davison and Ehlers (2011), while the convergence was calculated from the number of pyramidal cells, the convergence ratio and the total number of glomeruli. Adapted from (Lepousez and Gheusi, 2011).

Glomerular "maps" The stereotyped nature of OSN axon projections into the OB leads to a surprisingly high level of repeatability of glomerular position, both between hemispheres and across individuals. The position of the glomeruli targeted by a genetically tagged OR was found to be highly conserved. Functional studies also reported that roughly similar activation patterns were evoked by the same odorants across mice. Recently, a work using a large set of odorants to image ~ 200 glomeruli in mice and rats at high resolution determined that the average error in the relative position of dorsal glomeruli was on the order of a single glomerular diameter (Soucy et al., 2009). Despite this reproducibility in the arrangement of glomeruli, no clear topography has yet been found in the pattern of glomerulus activation. This type of topography, called chemotopy, refers to a spatial and systematic representation of odorant features (such as, for example, chemical "class", length of the carbon chain, number of aromatic cycles, etc) on the glomerular layer (GL) of the OB.

2.2 Synaptic organization in the Olfactory Bulb

2.2.1 Microcircuits in the Glomerular Layer

OSN axons synaptically terminate on the dendrites of several neuronal populations in the GL of the OB (Figure 2.2,C). This consists in the first step of information processing in the brain and shapes odor responses in OB output neurons, namely mitral and tufted cells (MCs and TCs, respectively, and collectively referred as M/T cells). In this section, I will briefly review the synaptic organization between OSN axons and OB cells, and in between OB neurons. Discussion on how different OB microcircuits shape sensory-evoked inputs will be addressed later, once the global connectivity picture has been described.

Classic electron microscopic studies (Pinching and Powell, 1971a) described at least three different types of juxtglomerular (JG) neurons: the GABAergic periglomerular (PG) cells and superficial short axon cells (sSACs), and the glutamatergic external tufted cells (eTC; Figure 2.2,C). All these JG cell types can be further divided into subtypes.

Periglomerular cells. PG cells are the most numerous neurons surrounding the glomerulus and are the main source of GABAergic inhibition in the glomerular layer. Both type-I and type-II PG cells are axonless neurons, which extend their dendrites in a single glomerulus (Figure 2.2,C and Figure 2.3). In addition to GABA, type-I, but not type-II, PG cells produce the neuromodulator dopamine. They receive direct inputs from the OSN and from other JG cells, but also from MCs and TCs and centrifugal fibers (Figure 2.2,C; see below). They contact in turn MCs and TCs apical dendrites, thereby forming a reciprocal dendrodendritic synapse (Figure 2.2,C).

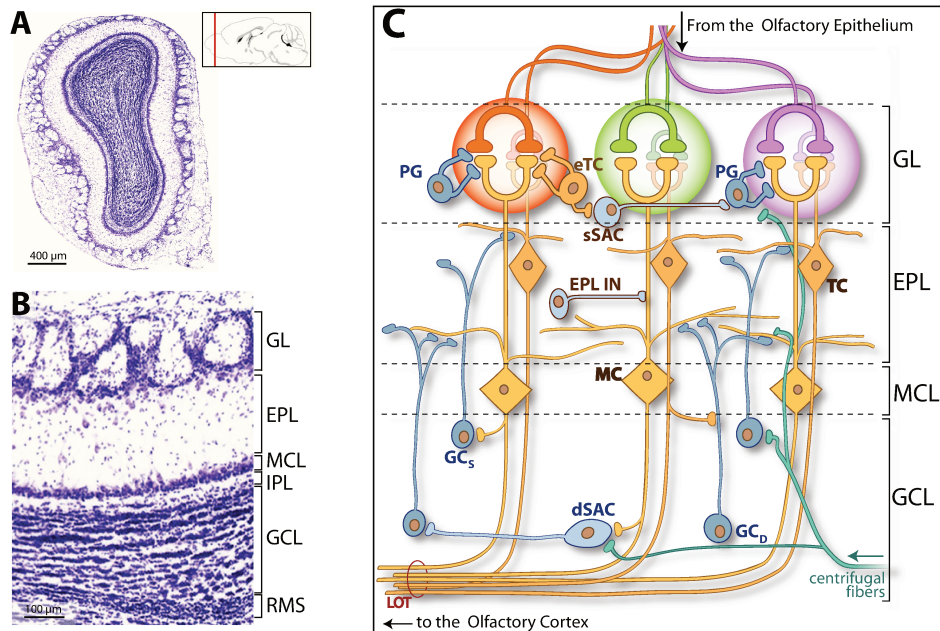


Figure 2.2 – Cytoarchitecture and Circuits of the Olfactory Bulb.

A. Coronal section through the olfactory bulb showing the macroscopic organization (creyl violet staining). Inset: section level.

B. Zoom of the section in A., showing the laminar organization of the olfactory bulb. From superficial to deep: the glomerular layer (GL) is the olfactory bulb input layer containing the sensory axon terminals and the juxtglomerular cells arranged in glomeruli. The external plexiform layer (EPL) contains dendrites and a few somas. The mitral cell layer (MCL) is the thin layer containing mitral cell (MC) somas. The internal plexiform layer (IPL) sits superficial to the granule cell layer (GCL), which consist in densely packed inhibitory granule cells (GCs). At the core of the GCL is situated the rostral migratory stream (RMS), which brings new neurons to the olfactory bulb throughout life.

C. Olfactory bulb network and synaptic organization of its main cell types. Glutamatergic neurons are in orange and inhibitory cells in dark blue. See main text for details. Sensory axon terminals (dark orange, green and purple) synapse onto periglomerular (PG) cells, external tufted cells (eTCs) and superficial short axon cells (sSACs) in the GL. Information is then transmitted to mitral cells (MCs) and tufted cells (TCs). Mitral and tufted cell lateral dendrites make synapses with granule cells (GCs) in the EPL. Other GABAergic interneurons of the EPL (EPL IN) are also making synapse with mitral and tufted cells. Deep short axon cells (dSACs) synapse on granule cells in the GCL. Axons from mitral and tufted cells bundle to exit the olfactory bulb, forming the lateral olfactory tract (LOT). Centrifugal fibers (light blue) mainly originate from the olfactory cortex and neuromodulatory brain regions and innervate virtually every elements of the OB. At first glance, cortical centrifugal fibers mainly innervate the GCL while centrifugal fibers from neuromodulatory regions mainly innervate the GL. See Chapter "3" for more details. C is adapted from (Lepousez et al., 2013).

Therefore, they provide feedforward inhibition to M/T cells following sensory stimulation (Najac et al., 2015). In addition, PG cells can release GABA that activates presynaptic GABA_B heteroreceptors at OSN axon terminals and depresses further glutamate release (Aroniadou-Anderjaska et al., 2000). Notably, single activation of OSNs seems to be sufficient to activate GABA_BRs at OSN axon terminals (Aroniadou-Anderjaska et al., 2000). Lastly, PG cells can also inhibit each other (Murphy et al., 2005). In conclusion, PG cells are well-suited to gate sensory information within a glomerulus.

Superficial Short Axon Cells. sSACs are GABAergic neurons, which can be divided into "classic" sSACs, and more recently described tyrosine hydroxylase+ (TH+) sSACs. Classic sSAC extend their dendrites in the interglomerular space, while TH+ sSAC dendritic arborization spans multiple glomeruli. sSAC axons appear to have axons projecting across multiple glomeruli (Figure 2.2,C). TH+ sSACs have been identified on the basis of their immunoreactivity and therefore produce dopamine (in contrast to classic sSAC). In addition, it seems that sSACs can release glutamate as well. Indeed, a study reported that focal stimulation of the isolated GL induced excitatory synaptic responses hundreds of microns away from the stimulation site (Aungst et al., 2003) and a very low fraction of glutamatergic cells is produced through adult neurogenesis (Brill et al., 2009). Therefore, a third type of sSAC might exist. Classical sSAC receive inputs from PG cells, eTCs and other sSACs and centrifugal fibers. In contrast, TH+ sSACs have been shown to receive inputs from eTCs from the same glomerulus only. Classic sSAC are reciprocally connected to PG cells and other classic sSAC, but also input onto MCs. TH+ sSACs however are connected to eTCs belonging to other glomeruli. Glutamatergic sSAC however were reported to input onto both PG cells and eTCs from other glomeruli (Aungst et al., 2003). In conclusion these cells are in a good position for coordinating the output of multiple glomeruli across the OB.

External Tufted Cells. Lastly, eTCs are local (non-projecting) glutamatergic neurons of the GL (Figure 2.2,C). They are also segregated into two groups, depending on whether or not they bear secondary dendrites. Apical dendrites extend into a single glomerulus, while the secondary dendrite branches in the superficial external plexiform layer. eTCs receive direct inputs from the OSNs (De Saint Jan et al., 2009; Hayar et al., 2004) and are reciprocally connected through GAP junctions. They relay excitation to MCs and TCs (De Saint Jan et al., 2009) as well as to other JG cells. eTCs seem to be the main source of excitation to PG cells and sSACs (Hayar et al., 2004). Indeed, eTCs are the main target of OSN axons, while only a fraction of PG cell was found to exhibit monosynaptic response to OSN stimulation (Hayar et al., 2004). Therefore, it was suggested that eTCs participate in

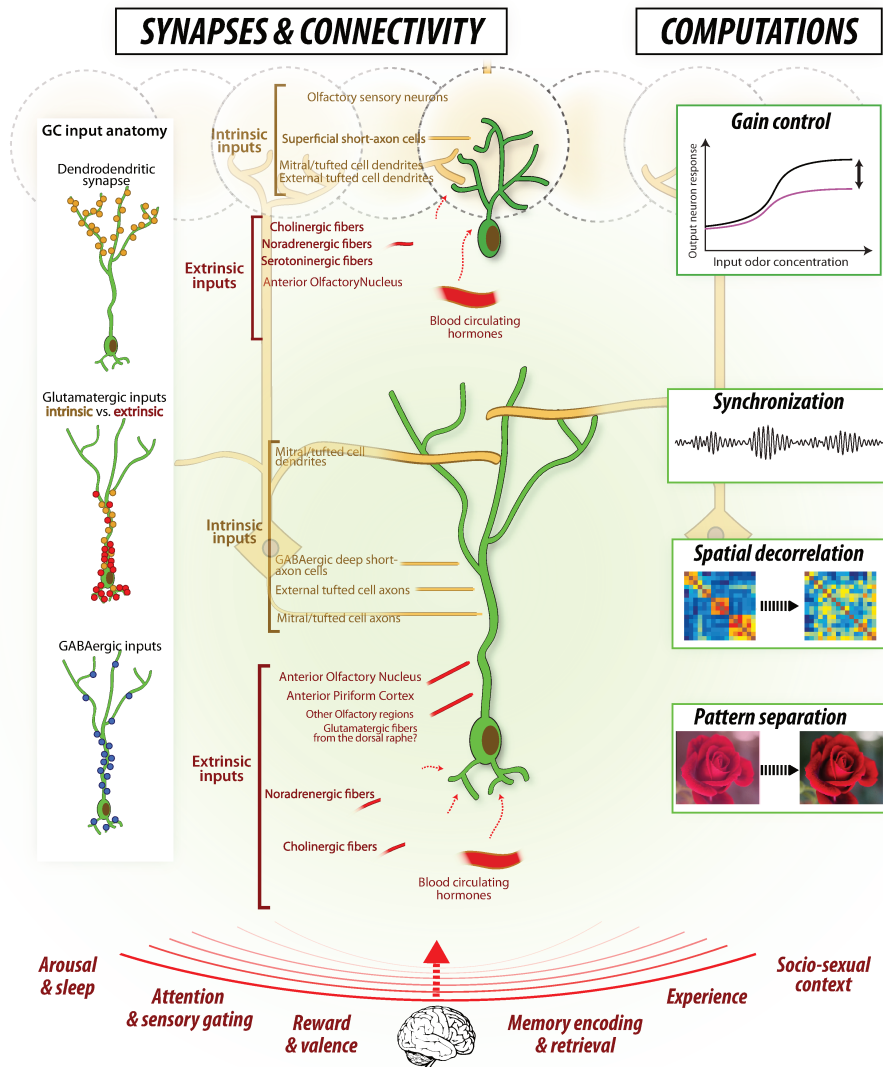


Figure 2.3 – Periglomerular and Granule cells structures and functions. (Left) Granule cell (GC) input anatomy. Dendrodendritic inputs are restricted to the apical part of GC dendritic tree, whereas glutamatergic and GABAergic axodendritic inputs are mainly found in the proximal parts. Most GABAergic inputs onto GCs are thought to originate from deep short-axon cells. (Middle) Periglomerular (PG) cells and GCs are targeted and influenced by different local neurons of the olfactory bulb network (intrinsic inputs; yellow), as well as by centrifugal fibers originating from remote brain regions and by blood-circulating hormones (extrinsic inputs; red). (Right) Main computations performed by PG cells (gain control) and GCs (synchronization, spatial decorrelation and pattern separation) in the olfactory bulb. GCs,d: superficial and deep GCs. Adapted from (Lepousez et al., 2013).

the amplification of sensory input and coordination of glomerular output.

Relay of Olfactory information to Mitral and Tufted cells. With the exception of sSACs, all JG cell types extend their dendritic arbors within a single glomerulus. MCs and TCs also extend their apical dendrites in a single glomerulus (Figure 2.2,C). Neurons elaborating their dendrites in the same glomerulus are called sister cells. As such, sister MCs are MCs that send their apical dendrites to the same glomerulus. However, it is still debated whether OSNs can drive direct excitation onto M/T cells or M/T excitation arises from a multistep pathway. A single electrical stimulation of OSN evokes an initial fast EPSC followed by a long-lasting depolarization in MCs (De Saint Jan et al., 2009; De Saint Jan and Westbrook, 2007; Schoppa and Westbrook, 2001). If it seems admitted in the field that the slow component of that long-lasting depolarization originates from a multistep pathway driven by eTCs (De Saint Jan et al., 2009; De Saint Jan and Westbrook, 2007; Hayar et al., 2004; Schoppa and Westbrook, 2001), evidence showed that M/T cells can respond to OSN stimulation with a long-lasting depolarization lacking the monosynaptic component (Gire and Schoppa, 2009) and one can argue that the initial fast EPSCs might be elicited by direct activation of MC apical dendrites and lateral excitation between sister MCs (Pimentel and Margrie, 2008; Schoppa and Westbrook, 2002; Urban and Sakmann, 2002; see below). Weaker electrical stimulation, as well as specific optogenetic activation of OSNs indeed suggest that MCs receive "negligible" direct inputs, and excitation arises mainly from a polysynaptic pathway involving eTCs (Gire et al., 2012; Gire and Schoppa, 2009). It remains unclear whether this multistep pathway is mediated by a synaptic relay or through volume transmission of glutamate onto MC extrasynaptic receptors (Gire et al., 2012).

Because of their morphology, neurochemistry and synaptic organization, the different JG cells are likely to play a different role in shaping MCs and TCs activity, and thus in odor information processing. In the last chapter of this introduction, we will see how this microcircuit, influenced by centrifugal inputs, shapes odor coding in the OB.

2.2.2 Olfactory bulb output neurons: routing the information to the olfactory cortex

In the previous section, we saw that OSN input is first shaped by the GL microcircuit and transmitted to MC and TCs apical dendrites. The signal then propagates to MCs and TCs somas in the mitral cell or external plexiform layer, respectively (MCL and EPL; Figure 2.2,C). It then back-propagates in MC and TCs lateral dendrites, that extend horizontally in the EPL, covering up to a third of the circumference of the EPL (Figure 2.2,C; Orona

et al., 1984). In that layer, MCs and TCs lateral dendrites make reciprocal synapses with GCs (Figure 2.4). This will be the focus of the next section, in which I will review the synaptic organization of MCs and TCs.

Mitral and Tufted cells morphological organization. MC and TCs share many morphological properties. For example, they both extend a single primary dendrite to one of several thousand glomeruli. Thus, each projection neuron receives information originating from only one type of olfactory receptor type. However, we saw in this section that local networks heavily shape M/T cells activity. For instance, hyperpolarization-activated currents (I_h or "sag" potentials) are more similar in sister M/T cells than in non-sister pairs (Angelo et al., 2012) and sister M/T cells are connected with gap junctions (Schoppa and Urban, 2003). Nevertheless, if odor-stimulation was found to elicit similar responses in terms of firing rate change in sister M/T cells, distinct spike timing in relation to the respiratory cycle were also observed (Dhawale et al., 2010; Fukunaga et al., 2012; Igarashi et al., 2012). Additionally, sister cells were found to exhibit variable odor-tuning properties, depending on odor concentration and their relative location to the activated glomerulus (Kikuta et al., 2013). When investigating the differences between MCs and TCs, Fukunaga and colleagues (2012; 2014) showed that local inhibition functionally separates MC and TC firing activity. Indeed, TC voltage membrane potential and firing activity locks to earlier phases of the respiratory cycle compared to MCs, and this shift is established by local inhibitory neurons in the GL –presumably PG cells– that selectively delay MCs (Fukunaga et al., 2012, 2014).

Mitral and tufted cells also both send lateral dendrites in the EPL and project their axons to olfactory cortical regions. However, fine morphological features vary between mitral and tufted cells. For instance, TCs extend their lateral dendrites in the superficial EPL, while MC lateral dendrites are found in the deeper EPL (Figure 2.2,C). In addition, cell bodies of TCs are sparsely found in the EPL, and those of MCs are more densely packed and located in the MCL. Axonal targets of MCs and TCs also differ. TCs project their axons in the anterior part of the olfactory cortex, including the anterior olfactory nucleus (AON), APC and olfactory tubercle, but apparently not in the *tenia tecta*. By contrast, MCs projects widely throughout the olfactory cortex (AON, olfactory tubercle, anterior and posterior piriform cortex, lateral enthorinal cortex, cortical amygdala; see Figure 2.5, left side).

In addition, mitral and tufted cells are generating at different stages during development: whereas most MCs are born between embryonic days 10 and 13, TCs are born during a later period (embryonic days 13–16; (Imamura et al., 2011; Imamura and Greer, 2015)). The distinction in the timing of genesis between mitral and tufted cells may affect the differential locations of their somas, extension patterns of secondary dendrites, axon projections,

and terminal locations (Imamura et al., 2011; Imamura and Greer, 2015; Inaki et al., 2004).

Functionally, TCs have lower threshold to spike upon electrical or odor stimulation (Igarashi et al., 2012; Kikuta et al., 2013), and accordingly, TCs show a higher spontaneous firing rate and a broader tuning compared to MCs (Kikuta et al., 2013). Recent reports also indicate that odor stimulation elicits an earlier response in relation to the respiratory cycle in TCs compared to MCs (Fukunaga et al., 2012; Igarashi et al., 2012).

As for the other cell types, MCs and TCs can further be divided into subgroups, mainly depending on their soma location or lateral dendritic arborization (Nagayama et al., 2014). That is, TCs with soma residing in the intermediate EPL are called middle TCs, while those whose soma is in the deep EPL are named internal TCs. Likewise, Type-I and type-II MCs are MCs whose lateral dendrites innervate the deep or intermediate EPL, respectively.

Lateral and self-excitation. In addition to receiving feedforward excitation from eTCs, M/T cells can excite themselves or each other. Glutamate release from mitral or tufted cell apical dendrite tuft is known to induce AMPA and NMDA receptor-mediated current in the same cell or a sister cell, resulting in self or lateral excitation (Margrie et al., 2001; Schoppa and Westbrook, 2001; Urban and Sakmann, 2002). This self or lateral excitation is presumably mediated by glutamate spill over. The compartmentalized anatomy of glomeruli may provide a chemical compartment for glutamate pooling. However, a study reported that a single spike is sufficient to evoke a current in postsynaptic sister cells, which is consistent with synaptic, and not spill-over, transmission (Pimentel and Margrie, 2008). This current was AMPA, but not NMDA, receptor-dependent. Although weak, it was produced in absence of drugs promoting glutamate release or binding (Pimentel and Margrie, 2008). In addition, GAP junctions between M/T cell dendritic tufts are also connecting sister cells.

Another form of lateral excitation was reported to happen in the EPL. Indeed, although M/T cells dendrites do not directly synapse onto one another in the EPL (Pinching and Powell, 1971b; Price and Powell, 1970b), neighboring M/T cell might excite each other or themselves *via* spillover of glutamate that binds high-affinity NMDAR (Christie and Westbrook, 2006; Isaacson, 1999; Salin et al., 2001). However, these interactions are substantially smaller than those reported in the same glomerulus (Carlson et al., 2000; Schoppa and Westbrook, 2001; Urban and Sakmann, 2002), and necessitate the presence of drugs promoting glutamate release or reception (e.g., glutamate reuptake blockers, increase NMDAR open probability)

2.2.3 Reciprocal connection with Granule cells

Sensory inputs are first shaped by the GL microcircuit before being transmitted to M/T cells. Stimulation then propagates to M/T cells somas and lateral dendrites in the EPL, where their reciprocal connection with GC apical dendrites further refined M/T cell activity.

Granule cells synaptic organization GCs are the most prominent type of cells in the OB, they have been estimated to be $\sim 3,100,000$ in the rat (Eyre et al., 2009) and are two orders of magnitude more numerous than M/T cells. It has been estimated that a single M/T cell connects to approximately 2,000 GCs and a single GC contacts about 100 M/T cells (Lepousez et al., 2013). GCs are axonless GABAergic neurons, whose apical dendrites usually extend in the EPL and the less profuse basal dendrites are confined in the granule cell layer (GCL; see Figure 2.2 and 4.1,A). GC apical dendrites form reciprocal synapses with M/T cell lateral dendrites in the EPL (see below, 2.2.3 and Figures 2.4, and 2.3). In addition to receiving inputs from M/T cells in the EPL, GCs are postsynaptic targets in the GCL of eTC axon and M/T cell axon collaterals en route to the olfactory cortex, as well as the target from another type of GABAergic neurons, namely deep short axon cells (Figure 2.3). GCs are also the major target of a variety of top-down inputs (Figure 2.2 and Figure 2.3). Because inputs in the GCL are deeply intricate, it has been difficult to study M/T axon inputs to GC soma or proximal dendrites. Centrifugal inputs and their relation to OB neurons will be the focus of the next chapter.

In addition to PG cells, adult neurogenesis produces GCs throughout the life of the animal. GCs are the main cell type produced in the OB of adult rodents (95% *vs.* 5% of PGCs Hack et al., 2005; Lois and Alvarez-Buylla, 1994). Newborn GCs in the OB are more excitable compared to pre-existing GCs (Lepousez et al., 2013) and young adult-born neurons uniquely exhibit spike timing-dependent plasticity (STDP) and long-term potentiation, which is thought to be critical for their survival (Nissant et al., 2009). Loss-of-function experiments lead to long-term memory impairment (Lazarini et al., 2009; Sultan et al., 2010) and gain-of-function manipulation was able to increase learning speed (Alonso et al., 2012), suggesting an importance for adult neurogenesis in OB function and notably memory and discrimination. However, the mechanism by which these effects are mediated are still debated. Adult neurogenesis is thought to facilitate M/T cell odor response decorrelation and olfactory memory formation, but it is not clear how adding new plastic neurons to the pre-existing circuits can help perform such computations. This is particularly puzzling since early postnatally-born neurons have been shown to exhibit structural spine plasticity as dynamic as adult-born neurons, and much higher than in the cortical regions (Livneh et al., 2014; Sailor et al., 2016). Adult neurogenesis functions and implications for

computation are an active domain of which further description can be found elsewhere (for a review on that matter, see Cleland, 2010; Lepousez et al., 2013).

GCs can be broadly classified in 3 main subtypes based on their soma location and apical dendritic extension (Nagayama et al., 2014). Type-II GCs have their soma situated in the deep GCL, their basal and apical dendrites branch in the internal EPL. In contrast, type-III GCs have their soma situated in the superficial GCL or up to the MCL, they also have basal dendrites and their apical dendrites branch in the superficial EPL. Therefore, it is commonly assumed that deep GCs form synapses in the deep EPL with MC lateral dendrites, whereas superficial GCs contact TC lateral dendrites in the superficial EPL. This is not necessarily always the case, since type-I GC ramify dendrites throughout the EPL independently of their soma location. All these GC types form reciprocal synapses with M/T cells and are produced by adult neurogenesis. In addition to these three classical GC subtypes, three non-conventional subtypes also seem to exist. Type IV GCs ramify their dendrites in the GCL, while type-V GCs have their soma in the MCL, lack basal dendrites, and branch their dendrites in the deep EPL (Merkle et al., 2014). These two cell types appear to also be generated throughout life (Merkle et al., 2014). Finally, type-S GCs extend their dendrites in the MCL and might provide perisomatic inhibition to MCs.

In the following paragraph, I will detail the reciprocal connectivity between M/T cells and GCs in the EPL.

The M/T cell-GC dendrodendritic synapse Apical dendrites of inhibitory GCs make reciprocal dendrodendritic synapses with lateral dendrites of M/T cells in the EPL (Figure 2.4,A-B).

Both synaptic partners contribute to the pre- and postsynaptic elements and the physiology of MC-GC dendrodendritic synapse has been greatly studied (Figure 2.4,C). Action potentials back-propagate from M/T cell somas into lateral dendrites, open voltage-gated Ca^{2+} channels, trigger vesicular fusion and release of glutamate from M/T cell dendrites (Isaacson and Strowbridge, 1998). Glutamate binds ionotropic receptor (AMPA, but mainly NMDAR) at GC membrane surface that 1) lead to Ca^{2+} influx through NMDAR and 2) depolarizes the dendrite and recruit voltage-dependent Ca^{2+} channels. Ca^{2+} transients then directly trigger GABA release back onto M/T cell dendrites. This reciprocal synapse can mediate inhibition between pairs of M/T cells (lateral inhibition) or onto itself (self inhibition).

Ca^{2+} transients induced in GCs can either be local or global (Egger et al., 2005). They can be confined inside a dendritic spine head because the spine neck has a high electrical resistance and can isolate the spine head from

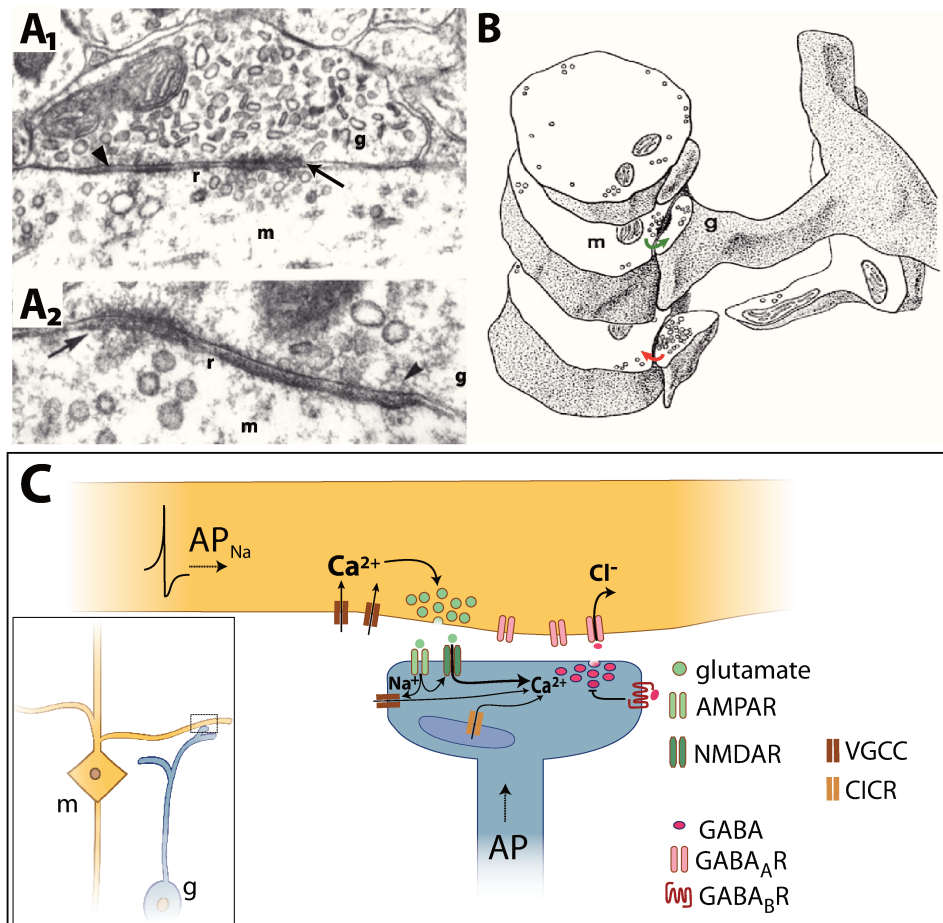


Figure 2.4 – The MC-GC dendrodendritic synapse.

A. Structure of the reciprocal synapse (r) examined through electron microscopy. Arrows show asymmetric synapses while arrowhead show symmetric synapses between a mitral cell (m) and a granule cell (g). Asymmetric synapses have round presynaptic vesicles and a thick postsynaptic density. In contrast, symmetric synapses have flattened presynaptic vesicles and more symmetric densities. Note also the presence of a mitochondrion in the granule cell spine head. From Price and Powell (1970a)

B. Schematic of the 3D organization of the mitral cell (m)-granule cell (g) dendrodendritic synapse in the EPL. The green arrow illustrates the glutamatergic transmission from mitral cells to granule cells. The red arrow depicts reciprocal, GABAergic transmission from granule cells to mitral cells. From Shepherd GM (2004)

C. Signaling pathways at the MC-GC dendrodendritic synapse. Action potential back-propagation in MC lateral dendrites induces local calcium influx, which in turn triggers glutamate release and activates mainly NMDAR at GC spine heads. NMDAR activation can lead to sufficient Ca^{2+} concentration increase to directly evoke Ca^{2+} -dependent GABA release back onto MC dendrites. Alternatively, glutamate release from MCs can activate AMPAR and depolarize GC spine, which in turn activates voltage-gated calcium channels (VGCCs). Ca^{2+} influx then leads to Ca^{2+} -induced calcium release (CICR) from internal stock in mitochondria, thereby triggering GABA release. GABA release from GCs can also be evoked by action potential-dependent recruitment of VGCCs. C. is adapted from Lepousez et al. (2013).

the dendritic shaft (Bywalez et al., 2015). In addition, dendritic voltage-gated Na^+ channels might boost postsynaptic Ca^{2+} entry through the activation of high threshold voltage-gated Ca^{2+} channels (Figure 2.4,C). In this scenario, GABA is therefore released from the reciprocal spine head only. Alternatively, back-propagating somatic Na^+ spikes, or Ca^{2+} spikes initiated by high-voltage gated channels at GC dendrites, can propagate to the entire GC dendritic tree and evoke global GABA release (Figure 2.4,C). These two modes of Ca^{2+} propagation -local or global- support either local, graded inhibition or global inhibition. The kinetics of these two forms of inhibition are distinct. Indeed local inhibition is dependent on the slow kinetics of NMDARs, thereby extending the window of Ca^{2+} accumulation and vesicle exocytosis. This inhibition takes the form of a barrage of IPSCs lasting hundred of ms (Isaacson and Strowbridge, 1998). In contrast, spikes produce fast Ca^{2+} entry and lead to faster inhibition onto M/T cells.

In addition to mediating inhibition onto M/T cells *via* GABA_A receptor activation, GABA can activate GABA_B receptor at GC dendrites. GABA_B activation prevents further GABA release by inhibition of high threshold voltage-gated Ca^{2+} channels, but not through activation of GIRK channels (Figure 2.4,C; Isaacson and Vitten, 2003). Interestingly, GABA_B -mediated inhibition of GABA release 1) was independent of action potentials triggered by Na^+ channels, 2) reduces during repetitive GABA release and 3) decreased upon enhanced dendrodendritic inhibition (Isaacson and Vitten, 2003). Activation of GABA_B receptors has functional consequences on M/T cells. First, it shapes the short-term plasticity of the synapse. Indeed, upon repeated stimulation of M/T cells, the magnitude of the IPSC barrage increases and eventually saturates, perhaps reflecting the activation of GABA_B receptors at GC spines. Furthermore, GABA_B activation shapes the spatial extent of depolarization, and with it, the spatial extent of lateral interactions between M/T cells. Recently, we showed that adult-born GCs are not regulated by GABA_B receptors (Valley et al., 2013), therefore conferring unique plasticity properties at the M/T cells-newborn GC synapse. As such, addition of newborn GCs has a unique consequence in terms of GABA release onto M/T cells lateral dendrites, excitation propagation and lateral inhibition.

2.2.4 Additional microcircuits

So far, we have seen that sensory inputs drive M/T cell activity, which is itself actively shaped by two layers of inhibition: the first one is mediated by the GL microcircuits as early as the input layer, the second one is largely mediated by GCs in the EPL and controls the spread of excitation in M/T cells. This section sheds light onto other microcircuits that further refine the activity of OB neurons and particularly M/T cells.

Inhibition from External Plexiform Layer Neurons A tremendous body of research has focused on the M/T cells-GC synapse, yet the EPL contains an additional form of inhibition onto M/T cells (Figure 2.2,C). Distinct classes of GABAergic neurons are located in the EPL, namely Van Gehuchten and multipolar cells. These cell types can be further subdivided according to molecular markers, soma or dendritic morphology. Like PG cells and GCs, all EPL GABAergic neurons but a subtype of multipolar cells -large SACs- are axonless neurons and their multipolar dendrites are thought to make reciprocal synaptic contacts with the somas and dendrites of M/T cells (Nagayama et al., 2014). Recent studies investigated the reciprocal connectivity between MCs and EPL neurons, compared to the MC-GC connectivity. Both Corticotropin Releasing Hormone⁺ (CRH⁺) (Huang et al., 2013, 2016) and PV⁺ EPL neurons (Kato et al., 2013; Miyamichi et al., 2013) were shown to be reciprocally connected with M/T cells. CRH- and PV-expressing EPL neurons were also shown to be more broadly connected to M/T cells than GCs. However, following associative olfactory learning, CRH⁺ EPL-MC connectivity was found to be less plastic than the MC-GC connection (Huang et al., 2016).

Inhibition mediated by deep Short Axon Cells GCs are not the only cell type that one can find in the layer they gave their name to, the GCL (Figure 2.2). On the basis of shape, size and location of the soma, orientation of the dendritic tree and the presence of dendritic spines or not, as visualized by Golgi staining techniques, different non-GC types have been described and collectively named deep short axon cells (dSACs). Their population has been estimated to $\sim 13,500$ in the rat (Eyre et al., 2009), therefore GCs are about 200 times more numerous than dSACs. Four main types emerged: Blanes, Golgi, vertical Cajal, and horizontal cells. Smaller subpopulations have also been revealed, such as stellate cells in the monkey, giant cells in the rat. These cells were found to express a variety of markers for GABAergic neurons (NPY, VIP, SOM, CB, PV, CR), receptors and enzymes, but none of these markers are uniquely expressed in dSACs. Moreover, they were found to label only small subpopulation of dSACs. However, a more recent study (Eyre et al., 2008) performed intracellular injection of dyes and could observe the axonal arborization in addition to other morphological parameters. It revealed that cells with very different morphologies can have similar axonal arborization patterns and that cells with similar morphologies can have very different axonal patterns. Thus, the authors performed unsupervised clustering of their reconstructed cells and distinguished 3 main subtypes, based on the axonal morphology of the cells: GL-dSACs that project axons up to the GL but extend very few axons in the GCL or EPL, EPL-dSACs that extend their axons in the EPL and in the superficial GCL and GCL-dSACs whose axons are restricted to the GCL (Burton et al., 2017; Eyre et al., 2008). This

new classification comprises cells from different classical cell subtypes. For example, EPL-dSACs comprises both Cajal and Blanes cells. In addition, using intracellular labeling of dSACs, Eyre and colleagues (2008) reported that dSACs can extend their axons in olfactory regions, like in the AON, APC or OT, and in a basal forebrain area (HDB), although these projections were found to be very infrequent compared to M/T cells (Eyre et al., 2008, 2009). In the following paragraph, I will review the synaptic organization of dSACs.

Taken as a whole, dSACs receive inputs from M/T cell axon collaterals (Eyre et al., 2008) and from top-down axons (Boyd et al., 2012; Markopoulos et al., 2012), and are thought to inhibit GCs, but not M/T cells (Figure 2.2; Burton and Urban, 2015; Eyre et al., 2008). However, it seems that different dSAC types are embedded in different microcircuits in the OB. The comprehensive function remains elusive because different studies used different classifications of dSACs. Blanes cells for instance were shown to inhibit GCs (Pressler and Strowbridge, 2006). Notably, electrical stimulation in the GL triggers persistent firing in Blanes cells, thus inducing a barrage of IPSCs on GCs (Pressler and Strowbridge, 2006). In a following study, Pressler et al. (2013) characterized another dSAC subpopulation, namely Golgi cells. Golgi cells were found to respond to depolarizing stimuli with two different modes: phasic or tonic firing. The authors did not characterize the potential synaptic targets of these cells. However, morphology-reconstruction studies suggest that Golgi cells synapse onto GCs as well (Eyre et al., 2008; Gracia-Llanes et al., 2003; Kosaka and Kosaka, 2010; Price and Powell, 1970b). In contrast to the studies performed by Pressler and colleagues (2006, 2013), Gracia-Llanes et al. (2003) reported a subpopulation of VIP-expressing dSACs that selectively synapse onto other VIP-positive dSACs, but not GCs. Moreover, Burton et al. (2017) reported that a subpopulation of GL-dSAC, expressing the $\alpha 2$ -subunit of the nicotinic receptor, are reciprocally connected to eTCs and TCs, but not to MCs, and provide inhibition to GCs. Taken together, these studies report a diversity of interglomerular microcircuits dSACs are embedded in. In particular, Blanes and Golgi cells seem to be well-positioned for regulating GC excitability, while nicotinic receptor-expressing GL-dSACs seem to be fitted to regulate GL microcircuits. In both cases, dSACs are in good position to regulate the level of inhibition on M/T cells.

Lack of systematical classification of these different types of non-GCs rendered their study difficult. Thus, for the sake of clarity, we will collectively refer to these cells as dSAC in this manuscript, otherwise stated.

2.3 From the Olfactory Bulb to the Olfactory Cortex

A given OB principal cell sends its apical dendrite to a single glomerulus, while the populations of M/T cells multiplex odor information to a variety of olfactory cortical areas. Sensory inputs highly converge in the OB (from 5,000,000 sensory neurons to $\sim 1,800$ glomeruli). In turn, the $\sim 100,000$ OB output neurons send divergent information to roughly 1,000,000 pyramidal cells in the primary olfactory cortex. From the cortical neuron point of view, olfactory information is convergent since a single neuron receives inputs from about 200 OB neurons (see Figure 2.1)

In contrast to other sensory systems, the OB sends direct projections to the olfactory cortex, without a thalamic relay. Therefore, the OB has been poised to implement computations similar to the ones performed in the thalamus (Kay and Sherman, 2007). Indeed both the OB and sensory thalamus are the last stage of sensory processing before the primary sensory cortices and represent an anatomical bottleneck before the cortex. In addition, as we will see in the following section, they both receive massive glutamatergic top-down inputs from sensory cortices and neuromodulatory influences of the same nature from the same brainstem centers and from the basal forebrain (Figure 2.5). At the circuit level, both OB and sensory thalamus output cells receive direct glutamatergic inputs from sensory axons and are highly reciprocally connected with GABAergic neurons (although the GABAergic source to thalamic principal cells comes from an external nucleus, the GABAergic feedback remains relatively local). Besides, principal cells and the GABAergic neurons they are connected with receive feedback inputs from sensory cortices in both systems. At the computational level, both the OB and sensory thalamus perform gain control of sensory inputs, both pre- and postsynaptically (with GABA_B or dopamine receptor-mediated neurotransmitter release modulation, and microcircuit gating sensory inputs to principal cells; Figure 2.3). Contrast enhancement through spatial decorrelation is another computation performed in the OB as well as in the thalamus (through GC-mediated lateral inhibition or interglomerular inhibition, for instance; Figure 2.3). Fast oscillations are also a hallmark of both brain structures (Figure 2.3), although it remains unclear what function it serves in the thalamus. The olfactory bulb and cortex are telencephalic structures while thalamus and other sensory cortices are diencephalic. Thus, one can speculate that through convergent evolution, the olfactory system and other sensory systems developed similar strategies to serve similar functions. In addition, it is worth noting that an olfactory thalamus does exist. It receives inputs from various olfactory structures but how this olfactory thalamus contributes to olfactory perception remains poorly understood (Courtiol and Wilson, 2014). Recipient of M/T cell axons are olfactory areas such as the AON, tenia tecta,

APC, olfactory tubercle, posterior piriform cortex, nucleus of the lateral olfactory tract, cortical amygdala, and lateral enthorinal cortex (Ghosh et al., 2011; Igarashi et al., 2012; Miyamichi et al., 2011; Sosulski et al., 2011).

As seen above, a chemotopic map is established in the OB GL but no map has been found in the different olfactory regions, raising the question: why does the olfactory cortex disrupt the map established before? Each area of the OC is thought to be involved in different attributes of information processing. Different areas of the OC may read the OB code in distinct manners. Notably, studies investigating the OC innervation pattern by M/T cells axons in a spatially restricted fashion or using rabbiies virus techniques to label cells projecting only to a restricted target region revealed that AON, APC and cortical amygdala are differentially innervated by M/T cells: the OB to AON connections show a broad dorso-ventral topography, while connections to the APC are dispersed and homogeneous, and connections to CoA are broad but spatially segregated (Ghosh et al., 2011; Miyamichi et al., 2011; Sosulski et al., 2011). In this manuscript, I focus on the interaction between the OB and its main output regions and main source of feedback, namely the AON and APC.

Organization of the Anterior Olfactory Nucleus The AON is the anterior-most olfactory cortical region. It is located in the olfactory peduncle, between the OB and APC. The AON was historically thought to be a nucleus but it is clearly cortical in organization. It can be divided in two sub-regions: AON *pars externa* (AONpE), a thin ring of dense cells surrounding the rostral end of the AON, and AON *pars principalis* (AONpP). AONpP is further subdivided in the *pars medialis* (AONpm), *pars dorsalis* (AONpd), *pars lateralis* (AONpl) and *pars ventroposterior* (AONvp). AONpP is a two-layered cortex with the deepest layer, layer 2, containing pyramidal-shaped neurons as well as inhibitory neurons. Superficial and deep pyramidal cells in layer 2 exhibit different electrical properties, and some morphological parameters also vary between neurons from distinct AONpP subdivisions (Kay, 2014). In addition to pyramidal cells in layer 2, the literature suggest considerable heterogeneity in cell morphologies (Brunjes et al., 2005). AONpP contains at least five distinct classes of inhibitory neurons, identified based on a combination of molecular markers, morphology and electrical properties, which are reminiscent of interneuron types of the neocortex (Kay, 2014). If the circuitry of the APC has been well characterized (see below), AON synaptic organization received less attention. The AON receives direct input from M/T cells in layer 1a and from the APC or contralateral AON in layer 1b. Layer 1 also contains apical dendrites of neurons in layer 2. Projections from M/T cell axons are topographic in the AONpE, with regards to dorso-medial axis and antero-posterior axis (Brunjes et al., 2005), and recent evidence suggest a broad topography along the same axis in

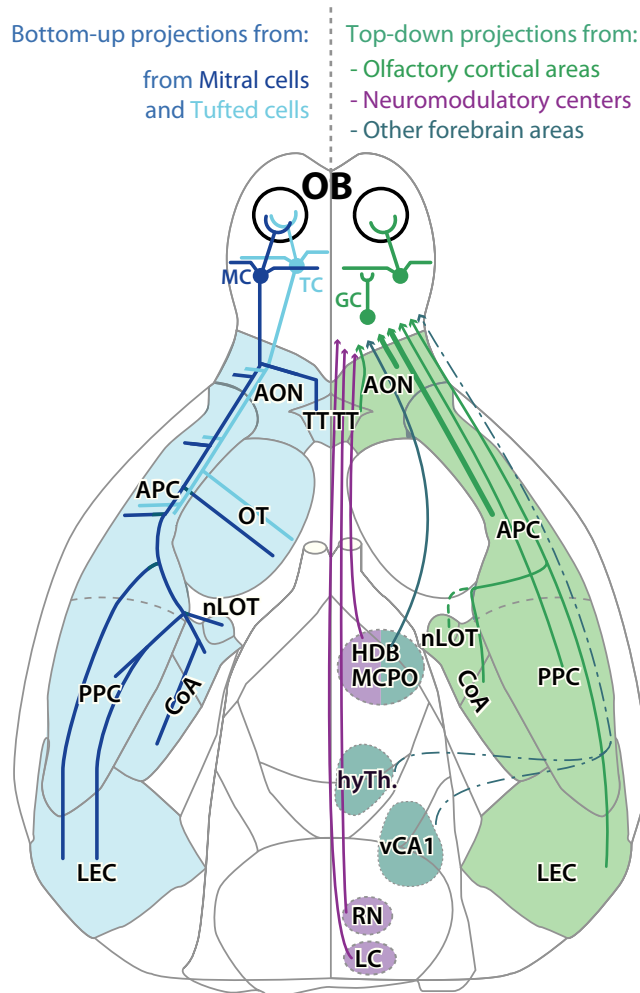


Figure 2.5 – Outputs and inputs to the Olfactory Bulb.

(Left) Diagram showing the axonal projections of MCs and TCs. MCs project axons to nearly all areas of the olfactory cortex, whereas TCs project axons to anterior areas of the olfactory cortex, but apparently spare the tenia tecta (TT). (Right) Diagram showing the origin and the diversity of the inputs to the olfactory bulb. Olfactory cortical areas are reciprocally connected to the olfactory bulb, with the exception of the olfactory tubercle (OT). Neuromodulatory brain regions also project to the olfactory bulb. Other forebrain regions were occasionally reported to send a few projections to the olfactory bulb. Note that the basal forebrain region HDB/MCPO sends GABAergic projections in addition to neuromodulatory projections.

AON: Anterior olfactory nucleus; TT: Tenia tecta; APC: Anterior piriform cortex; OT: Olfactory tubercle; PPC: posterior piriform cortex; nLOT: nucleus of the lateral olfactory tract; CoA: Cortical amygdala; LEC: Lateral entorhinal cortex; HDB/MCPO: Nucleus of the horizontal limb of the diagonal band of Broca / Magnocellular preoptic nucleus; RN: Raphe nuclei; LC: Locus coeruleus; hyTh.: hypothalamus; vCA1: ventral *cornu ammonis* region 1.

the AONpP (Ghosh et al., 2011; Miyamichi et al., 2011). AONpP, but not pE, is also involved in feedforward projections to the APC (Brunjes et al., 2005; Hagiwara et al., 2012) with projections following a broad topography: AONpd, pl and vp project mainly to dorsolateral, central and ventromedial APC, respectively (Brunjes et al., 2005; Luskin and Price, 1983). The AON is also implicated in feedback regulations to the OB, as we will see in further details below. In addition to feedback projections to the OB, the AON projects to, and receive projection from, non-olfactory brain regions, and particularly hippocampal or peri-hippocampal regions (Aqrabawi et al., 2016, see also the connectivity studies performed by the Allen Institute for Brain Science: <http://connectivity.brain-map.org/>). Finally, regions of the AON project to the contralateral OB, AON and APC *via* the anterior commissure. To my knowledge, there is no consensus role proposed for the AON in olfactory information processing, although its great bilateral connectivity makes it a good candidate in coordinating activity between left and right sides.

Organization of the Anterior Piriform Cortex The APC is the largest region of primary olfactory cortex, situated on the ventral side of the brain, behind the AON. The APC is a paleocortex, composed of three layers. From superficial to deep: layer 1 is the input layer with inputs from M/T cell axons forming layer 1a (as for the AON) and recurrent or inputs from AON arriving in layer 1b. Layer 2 contains densely packed principal cells, and layer 3 comprises a combination of principal cells and GABAergic neurons (Figure 2.6).

Deep to layer 3 is the endopiriform cortex (EndoP), mainly populated with glutamatergic multipolar neurons. Furthermore, layer 2 can be divided into two sublayers, 2a being roughly the superficial half of layer 2, and 2b the deeper half. Afferent inputs from the OB form synapses mainly with the distal dendrites of layer 2 principal cells. However, the strength and connectivity of these first synapses appear to be cell-type specific: the semilunar (SL) cells in L2a receive stronger inputs while the superficial pyramidal (SP) cells in L2b receive weaker sensory inputs (Figure 2.6,A; Suzuki and Bekkers, 2006, 2011). Recurrent network activity and connectivity in the APC is well-described (Franks et al., 2011; Haberly, 2001; Poo and Isaacson, 2011; Suzuki and Bekkers, 2011). Particularly, recurrent connections are highly distributed over several mm, while recurrent connections in classical primary sensory cortices decrease rapidly over a few hundred of microns (Franks et al., 2011). Recent work has demonstrated that connectivity scheme is also cell-type specific. SL cells make synapses onto layer 2b SP cells without forming recurrent synapses onto themselves, while SP cells are recurrently connected (2.6,A; Choy et al., 2015; Suzuki and Bekkers, 2011; Wiegand et al., 2011). Interestingly, Isaacson's group showed that recurrent

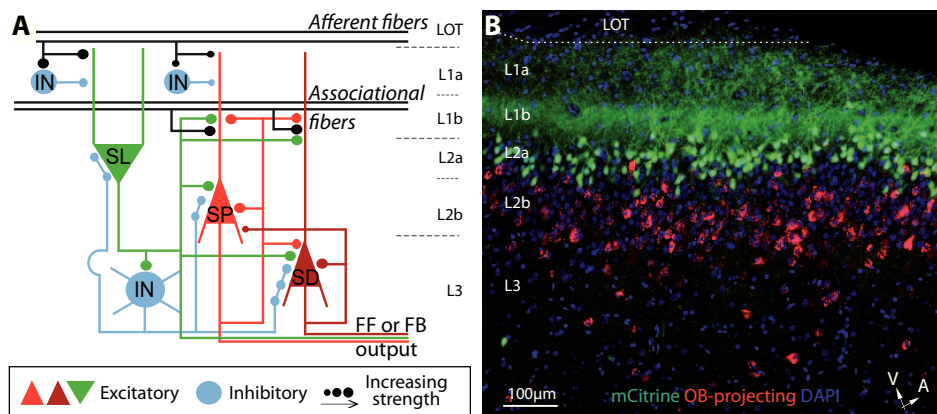


Figure 2.6 – Cytoarchitecture and Circuits of the Anterior Piriform Cortex.

A. Afferent fibers from the LOT mainly synapse onto SL cell dendrites and inhibitory neurons from layer 1a, thus driving feedforward inhibition to SL cells in layer 2a. In the piriform cortex, feedforward inhibition is mediated by dendrite-targeting, PV- neurons. SL cells relay the information to SP and DP cells in layer 2b and 3, respectively. SP and DP are heavily recurrently connected through associational fibers in layer 1b and 3. Layer 3 inhibitory neurons (PV+) heavily control principal cells excitation *via* feedback inhibition. Finally SP and DP cells, but also SL cells project axons to downstream and upstream olfactory regions, and to non-olfactory brain regions. See text for references. Green and red triangles indicate principal cells, blue circles are inhibitory neurons. Sizes of the circle at synapses correspond to synapse strength. IN: inhibitory neurons; SL: Semi-lunar cells; SP and DP: superficial and deep pyramidal cells; LOT: lateral olfactory tract.

B. Sagittal section through the anterior piriform cortex. mCitrine genetically labels SL cells in layer 2a (48L mouse) and red labels neurons projecting to the olfactory bulb, mainly SP and DP cells of layer 2b and 3, respectively. From Mazo et al., 2017.

connections, but not afferent inputs from the OB, are sensitive to GABA_BRs modulation (Franks and Isaacson, 2005; Poo and Isaacson, 2009). Therefore, layer 2 is populated with a mix of principal cells, namely SL and SP cells (Suzuki and Bekkers, 2006), playing different roles in the synaptic processing of olfactory information (Suzuki and Bekkers, 2011).

Single piriform neurons receive convergent inputs from multiple glomeruli (Apicella et al., 2010), and at the population level, odor information in the APC is sparse, distributed, and lacks evident topographic organization (Ghosh et al., 2011; Illig and Haberly, 2003; Miyamichi et al., 2011; Poo and Isaacson, 2009; Rennaker et al., 2007; Sosulski et al., 2011; Stettler and Axel, 2009). Odor information encoded by assemblies of APC cells is then transmitted to a variety of olfactory regions such as the AON, the posterior piriform cortex, cortical amygdala, lateral entorhinal cortex, or back to the OB (Diodato et al., 2016; Haberly, 2001; Haberly and Price, 1978a; Padmanabhan et al., 2016; Quraish et al., 2004; Yang et al., 2004). This information is also sent to non-olfactory brain regions such as the orbitofrontal cortex (Chen et al., 2014). Recent works using modern tracing techniques are now deciphering the organization of APC projection channels according to their targets (Chen et al., 2014; Diodato et al., 2016; Padmanabhan et al., 2016), Mazo et al., *submitted*).

Therefore, 1) the lack of obvious topographic input from the OB to the AOC, 2) the sparse and distributed recruitment of APC neurons to sensory stimulation, 3) the widely distributed internal connections and external projections and 4) the fact that APC also projects to areas thought to play a role in complex functions related to integrating sensory cues with behavior (such as the prefrontal cortex or hypothalamus), assessing the emotional or motivational significance of sensory cues (such as the amygdala or orbitofrontal cortex), and multisensory association and memory (such as the entorhinal cortex), suggest that the APC is more functionally analogous to "higher order" or "association" cortex than a classical primary cortex would be. In line with this, in addition to classical functions of primary sensory cortex such as odor identity and concentration invariance, the APC is poised to serve as a storage unit and an integrating center for pattern detection and feature combination (Davison and Ehlers, 2011; Haberly, 2001; Wilson and Sullivan, 2011).

Chapter 3

Top-down to the Olfactory Bulb

Sensory perception does not emerge from a series of feedforward stages, each extracting progressively more complex features of the external stimuli. Rather, sensing the external world requires the confluence of bottom-up and top-down inputs. "Top-down", or centrifugal, refers to cognitive influences and higher-order representations that impinge on earlier steps in information processing. This idea is in stark contrast with the classical notion of a cortical hierarchy in sensory processing, where information is conveyed in a feedforward manner to higher levels in the hierarchy. This view emerged from classical work in vision, where retinal input are transmitted forward to the thalamus, and from the thalamus to visual cortex area 1 (V1). In primates, V1 then sent projection to V2, V2 to V3 and V3 to V4. However, inputs with opposite direction have latter been reported. In particular, V1 top-down inputs to the thalamus were found more numerous than feedforward inputs from the thalamus to V1. In addition, top-down inputs also target very early stages in sensory processing, such as the superior colliculus in the visual system (Collins et al., 2005).

Top-down signal carries a rich amount of information that shapes sensory perception. For instance, cingulate cortex-to-V1 top-down input stimulation increased the gain of V1 neurons and enhanced the discrimination performance of the animal (Zhang et al., 2014). In addition, top-down inputs are thought to convey information relative to the internal state (or brain state) of the animal, and/or might convey messages based on the animal's previous experience and its expectations that would act as a prediction signal –or a prior– to the expected stimulus. Top-down influences would be the neuronal support of selective attention (when an animal has to focus on a given stimulus in a perceptual task while discarding background or distractors).

In olfaction, the OB –although positioned at the earliest brain region for odor information coding– receives substantial number of projection fibers from various brain regions (Figure 2.5, right part). The abundance of such

centrifugal fibers indicates that the OB is under extensive control by other brain areas. Although top-down inputs are known for a century (Cajal, 1911), knowledge on their function has only grown recently. Indeed, understanding of bottom-up pathways has grown rapidly thanks to early development of molecular biology techniques, while top-down inputs functional investigation took advantage of recent development of genetic tools, such as optogenetic and functional calcium imaging.

Centrifugal fibers diversity falls into two groups according to their origin. One group consists of projections arising from the brain regions receiving inputs from the OB (the olfactory cortex), the other group is the projections arising from areas that do not (Figure 2.5). The origins of the former are subdivisions of the olfactory cortex, sending glutamatergic feedback inputs, while the latter is composed of neuromodulatory centers. A couple of studies also reported that a handful of cells from other brain regions (such as the ventral hippocampus and hypothalamus) send projections to the OB as well (Carson, 1984; Shipley and Adamek, 1984) but this matter still needs further exploration. Here, while 'centrifugal' or 'top-down' will refer to a brain region innervating the OB or its axons, I will restrict the use of 'feedback' to a brain region innervating and being innervated by the OB, thus forming a loop between the two regions.

In this chapter, I review the diversity of the centrifugal fibers innervating the OB, according to their origin and their neurochemical content. Fine and detail features might vary across species, but the general organization usually remains invariant. In this work, I will focus my description of top-down inputs in mice.

3.1 Glutamatergic feedback from the olfactory cortex

Glutamatergic fibers innervating the OB are mainly originating in the olfactory cortex. Pioneer work using antero- and retro-grade labeling tools in a variety of animal species (the shrew, cat, rabbit, rat and mouse) discovered that the AON, APC, posterior piriform cortex, cortical amygdala and the nucleus of the olfactory tract are projecting back to the OB (Carson, 1984; Davis and Macrides, 1981; de Olmos et al., 1978; Haberly and Price, 1978a,b; Luskin and Price, 1983; Shipley and Adamek, 1984). In contrast, the olfactory tubercle seems not to send feedback projections to the OB and tenia tecta appears to send a very few, or none.

Centrifugal projection from the OC is often referred to as a "feedback" connection because macroscopic examination revealed a reciprocal connection between the OB and OC. However, this reciprocity might not be point-to-point, i.e the OC neuronal population activated by upstream OB neuron

axon collaterals might not send in return inputs to the same population in the OB. Within the olfactory cortex, the AOC is the region sending the vast majority of axons to the OB ($\sim 90\%$; Carson, 1984).

3.1.1 Projections originating from the anterior olfactory nucleus

Distribution of axon terminals. About half of the neurons back-projecting to the OB originate from the AON (Carson, 1984). They seem to be evenly distributed across AON layers (de Olmos et al., 1978), and AON neurons as a whole project both ipsi- and contralaterally (Davis and Macrides, 1981; Haberly and Price, 1978b; Luskin and Price, 1983; Shipley and Adamek, 1984). The different AON subregions have distinct projection patterns to the OB, but axons from all these regions terminate in the GCL. In the mouse, retrograde labeling studies confirmed the origin of ipsi- and contralateral fibers according to the AON subdivisions (Carson, 1984; Shipley and Adamek, 1984), but to date no anterograde study analyzed systematically the layer-wise distribution of the projections emanating from the different AON subdivisions. Therefore, my review here is based on data from different species, with some subtle differences in the innervation patterns (see Figure 3.1,A).

AON *pars dorsalis*, *lateralis* and *ventralis* (respectively AONpd, AONpl and AONpv) send bilateral axonal projections via the AC, with lighter projections in the contralateral side (Davis and Macrides, 1981; Luskin and Price, 1983). Ipsilateral as well as contralateral projections from AONpv have been predominantly found in the superficial GCL and the deep GL (Davis and Macrides, 1981; Luskin and Price, 1983). Light labeling is also found across all the OB layer, notably in the EPL (Davis and Macrides, 1981; Luskin and Price, 1983). In contrast, while AONpd and AONpl ipsilateral projections predominantly terminate in the superficial GCL and in the deepest third of the GL, the main contralateral projections have only been found in the superficial GCL, with no labeling in the GL (Davis and Macrides, 1981). However, a report came to slightly different conclusions in rats (Luskin and Price, 1983). In particular, the authors found that AONpd and AONpl project symmetrically to both OBs, and do not include fibers in the GL. AON *par medialis* (AONpm) mainly sends axonal projections to ipsilateral OB, with minimal labeling in the contralateral side (Davis and Macrides, 1981; Luskin and Price, 1983; Shipley and Adamek, 1984). Terminals were predominantly found in the deep GCL and only faint labeling was observed in superficial GCL or across the other OB layers (Davis and Macrides, 1981; Luskin and Price, 1983). In sharp contrast, AON *pars externa* (AONpE) exclusively extend heavy axonal arborization in the contralateral OB (Davis and Macrides, 1981; Haberly and Price, 1978b; Shipley and Adamek, 1984) and axons terminate in the superficial GCL (Davis and Macrides, 1981;

Luskin and Price, 1983). Finally, AONpE projections to the contralateral OB seem arranged in a topographic manner, along the dorsoventral axis, i.e. fibers originating from the dorsal portion of AONpE mainly innervate the dorsal GCL, and fibers from the ventral portion mainly innervate the ventral GCL (Davis and Macrides, 1981; Luskin and Price, 1983).

In conclusion, most of the detailed papers have similar general findings: all subdivisions but AONpE have ipsilateral projections and all regions but AONpm have contralateral projections. In addition, the GCL is always innervated by top-down fibers. Several conclusions can be drawn from these studies:

1. The heavy and widespread innervation across OB layers indicates that the AON is capable of interacting on the odor processing by the OB, at nearly every step.
2. There are substantial regional differences in the projection patterns of the different AON subdivisions indicating that they might serve different functions. Notably AONpE exclusively sends contralateral projection while AONpm mostly sends ipsilateral inputs to the OB.
3. The variations in data studying a connection known for a century calls for more precise techniques and quantifications to understand the organization of this feedback.

In addition to the different projection patterns within the OB, AON sub-region inputs to other brain regions also differ. For example, AONpd and AONpl, that have similar bilateral and symmetrical projections to the OB, differ in their connections with other parts of the olfactory system. The heaviest projection from AONpl is bilaterally to the APC, while AONpd heaviest projection is toward contralateral AON, and notably AONpl (Haberly and Price, 1978b).

Postsynaptic targets. The classical anatomical studies mentioned above have described a robust feedback loop from the AON to the OB, but the functional connectivity between AON axons and OB cells has been more difficult to address until the recent development of optogenetic tools.

To my knowledge, a single work addressed the functional connectivity of AON top-down inputs to the OB (Markopoulos et al., 2012). In this study, the authors introduced ChR2 in the AON of rats to manipulate top-down axon activity. In acute OB slices, the authors found that GCs in the GCL and sSAC, PGs and eTCs in the GL receive direct inputs, consistent with anatomical observation of OB innervation pattern by AON axons. They also reported disynaptic inhibition following AON axons light stimulation onto MCs. By slicing the GL in the recorded tissue, Markopoulos and colleagues discovered that at least a third of the inhibition onto MCs is originating in

the GL. GCs are the probable other source of inhibition driven by AON axon stimulation. Then, the authors investigated the impact of AON axon terminals stimulation on M/T cells firing activity in anesthetized animals *in vivo*. AON axon light stimulation depressed both spontaneous and odor-evoked firing activity. It is worth noting here that recording in anesthetized animals biased M/T cells response to excitation in response to odor stimulation. Surprisingly, in addition to disynaptic inhibition, the authors revealed that light stimulation of AON axons elicits excitatory responses in MCs both *in vitro* and *on vivo*. However, these currents were weak, but frequent (recorded in > 90% of the MCs) and with fast onset. In conditions isolating glutamate release by ChR2-containing axons (Petreanu et al., 2007), MCs receive similar excitatory current, with comparable connectivity frequency. Pharmacological characterization further showed that excitation in MCs was not evoked by glutamate spill-over. These features suggest that MCs receive direct, but weak, synaptic excitation from AON axon terminals.

Functional impact of AON fibers to the OB. In a recent study, Aqrabawi et al. (2016) aimed to manipulate the activity of AONpm using pharmacogenetic tools. However, the use of intraperitoneal ligand injection precluded selective investigation of the descending fibers to the OB, rather the whole AONpm activity was altered. Inhibition or activation of AONpm activity induced enhancement or impairment of olfaction-dependent behaviors, respectively (Aqrabawi et al., 2016). Interestingly, the authors found topographically-organized inputs from the CA1 region of the ventral hippocampus (such that labeling along an antero-posterior axis in the ventral CA1 led to axonal innervation along a medio-lateral axis in the AONpm). Upon selective stimulation of the ventral CA1 axon terminals in the AONpm, olfactory-guided behavior was impaired, showing that ventral CA1 inputs to AONpm can recapitulate the effects observed by manipulating the whole AONpm activity (Aqrabawi et al., 2016).

Besides, a recent elegant paper from Oettl et al. (2016) showed that oxytocin, a system critical for social behaviors, influences AON activity and thereby its top-down projections to the OB. GCs were found to be excited by oxytocin application in the AON, and M/T cells received more spontaneous inhibition. On odor-evoked activity, it resulted in an increase in signal-to-noise ratio. At a behavioral level, optogenetic stimulation of oxytocin release enhanced olfactory exploration of conspecific and social recognition while having no effect on non-social odor discrimination. Conversely, deletion of oxytocin receptors in the AON impaired memory of social recognition (Oettl et al., 2016).

3.1.2 Projections originating from the anterior piriform cortex

Laminar distribution of the projecting neurons. The APC has long been known to receive projections from the OB, but whether or not it projects back to the OB had been initially debated (Davis and Macrides, 1981). The use of more sensitive HRP protocols and autoradiography finally demonstrated that the APC is reciprocally connected to the OB in several species. Quantitative analysis of the number of cells contributing to top-down projections to the OB suggests that more than a third of the OB-projecting cells originate in the piriform cortex (Carson, 1984). Further works using retrograde HRP tracing reported an uneven distribution of OB-projecting neurons across APC layers (Haberly and Price, 1978a,b; Shipley and Adamek, 1984, to name just a few). Layer 2b and 3 cells are the predominant source of cortical feedback while layer 2a cell population is minimally back-projecting (Haberly and Price, 1978a; Shipley and Adamek, 1984). A recent study confirmed and quantified these findings using injection of specific retrograde tracers such as cholera toxin B subunit (Diodato et al., 2016), or fluorophore-coated latex beads, combined with transgenic animal-based labeling (Mazo et al., *submitted* Figure 2.6,B). Between 40 – 50% of the cells were found in layer 2b and 21 – 45% in layer 3 according to these studies. Along the rostral-caudal (or antero-posterior) axis, the number of retrogradely labeled cells in the APC falls off at approximately the rostral end of the olfactory tubercle (de Olmos et al., 1978; Haberly and Price, 1978b; Shipley and Adamek, 1984). However, this qualitative observation might be somewhat exaggerated since APC cells are more densely packed in its rostral part than it is in its caudal region.

In addition to projecting back to the OB, layer 2b and 3 cells were found to project to the subdivisions of the orbitofrontal and medial prefrontal cortices (Chen et al., 2014; Diodato et al., 2016). In contrast, layer 2a cells were found to project back to the AON or forward to the cortical amygdala or lateral entorhinal cortex (Diodato et al., 2016, Mazo et al., *submitted*). Interestingly, neuron projecting to either the mediodorsal or submedial orbitofrontal cortex were segregated along the antero-posterior and dorso-ventral axis of the APC (Chen et al., 2014). In contrast, we observed that layer 2b neurons projecting either to the OB or PPC were intermingled and overlapping populations (Mazo et al., *submitted*). Therefore, the APC-to-orbitofrontal cortex topography matches the orbitofrontal-to-APC one.

In conclusion from all these works, the APC is projecting to a diversity of brain regions, olfactory or not, but it is not clear how the output channels are organized according to their target regions. With the exception of the decreasing gradient of projecting cells when going caudally, no obvious organization has been seen in the distribution of the APC OB-projecting cells. Superficial and deep pyramidal cells (SP and DP cells) from layer 2b and 3

respectively, send back projections to the OB from the entire length of the APC, thereby forming the cortico-bulbar loop.

Axon terminals laminar distribution In contrast to the AON, very few or no APC cells are sending contralateral projections (Boyd et al., 2012; Davis and Macrides, 1981; Luskin and Price, 1983; Figure 3.1,A). Although labeling has always been reported in the GCL, the projection pattern of APC fibers in the OB seems to differ between experiments. This might be due to the use of different species as animal models, but also the targeting of different parts of the APC, and sometimes targeting of the APC and posterior piriform cortex in non-specific manners. To give some examples, in the hamster Davis and Macrides (1981) reported labeling in superficial GCL but no labeling in the GL. The authors also noticed a gradual shift from superficial to deep parts of the GCL in fibers originating from rostral to caudal APC. In contrast, in rats, Luskin and Price (1983) observed a labeling in the deep GCL and did not find any evidence of a gradient. In recent studies in mice, investigators observed an innervation of both the GCL and the GL (Boyd et al., 2012; Otazu et al., 2015).

Single-cell tracing technique demonstrates that individual APC feedback axon can innervate the contralateral OB and can arborize in the GL in rats (Matsutani, 2010). Finally, work mapping the projection patterns from the APC in the OB also noticed a superficial to deep gradient of innervation as injections were performed more caudally in the APC (Hintiryan et al., 2012). Since deep GCs appeared to be preferentially connected to MCs and superficial GCs to TCs, feedback fibers might have distinct function based on their origin.

APC feedback activity Corticobulbar feedback activity and function remain unclear, nevertheless increasing number of investigations are now addressing these issues. Using 2-photon imaging, the authors investigated Ca^{2+} transients in APC axons during spontaneous and odor-evoked activity. Imaging studies comparing Ca^{2+} activity in the GL and GCL did not find substantial differences in either type of activity, therefore I review here the data for the two layers indiscriminately. Spontaneously, a fraction (25%) of GCaMP-expressing boutons show brief and diverse activity in awake animals (Otazu et al., 2015). Boutons belonging to the same axons displayed higher activity correlation than boutons that were not assigned to the same axonal branch (Otazu et al., 2015). This activity reflects ongoing activity of APC pyramidal neurons. Odor stimulation evoked activity in about a third of the imaged boutons (Boyd et al., 2015; Otazu et al., 2015), which is consistent with an APC imaging study that found 35% of layer 2 neurons are odor responsive (Stettler and Axel, 2009). Sensory-evoked activity was diverse, with boutons showing either excitatory or inhibitory responses. Boutons exhibit-

ing both excitatory and inhibitory responses were rare (Boyd et al., 2015; Otazu et al., 2015). Interestingly, upon odor-reward associative learning, the number of inhibitory responses to odor stimulation in APC axons increased (Garcia DaSilva et al., personal communication). With variations of odor concentrations, responses of individual boutons rarely shifted from excitatory response and *vice versa* (Otazu et al., 2015). In addition, individual boutons were found to be highly odor-selective and other more promiscuous, and adjacent boutons could have divergent tuning properties (Boyd et al., 2015; Otazu et al., 2015). Temporal dynamics of odor-evoked responses were diverse, with phasic or transient responses to odorant onset or offset, ramping activity or long-lasting responses lasting several seconds (Boyd et al., 2015; Otazu et al., 2015). Anesthesia/wake comparison revealed reduction in spontaneous events during anesthesia (Boyd et al., 2015; Otazu et al., 2015). Odor-evoked inhibition of Ca^{2+} transients was reduced under anesthesia, while the effect on excitatory responses is more controversial, with one study reporting less boutons showing excitatory responses and weaker strength of the responses (Boyd et al., 2015), the other reporting stronger and more robust responses on average under anesthesia (Otazu et al., 2015). Next, the two studies investigated the functional organization of cortical projections within the OB. There was no obvious spatial arrangement in the distribution of feedback boutons regarding their response profile (Boyd et al., 2015; Otazu et al., 2015). Similarly, cortical feedback is not co-tuned with the glomerulus they target (Boyd et al., 2015). A similar study aimed at recording AON feedback axon activity in the OB (Rothermel and Wachowiak, 2014). However, it seems that in this study the authors failed to restrict their injections to the AON as dense soma labeling is observed in the GCL, and fewer somas could even be observed in the MCL. Dense labeling is also evident in the EPL, which suggests again that GCs were labeling using the author's injection protocol. Therefore, results from this study should be taken with caution. Nevertheless, the authors report similar findings for AON bouton transients as what was later found in APC axons. Using larger-scale imaging, Rothermel and Wachowiak (2014) found that AON axons are excited by odor, and more active and with more diverse dynamics in the wake state. Interestingly, the authors could also record odor-evoked activity on contralateral side, consistent with the contralateral projections of the AON (moreover, contralateral labeling is more likely to come from axons).

To summarize, these studies found that

1. Cortical axon activity in the OB is dependent on the brain state of the animal (anesthetized *vs.* awake).
2. Diverse responses are elicited in cortical axons following odor stimulation. Excitatory as well as inhibitory responses were recorded, with diverse temporal dynamics. Axon boutons were sharply tuned or more

promiscuous, but interestingly enough, single boutons very rarely display both excitatory and inhibitory responses. Odor-excited and odor-inhibited boutons activity seem to not be correlated, therefore they might reflect different APC output channels.

3. There is no obvious functional topographic organization of cortical feedback to the olfactory bulb regarding odor response co-segregation, co-tuning of spatially clustered boutons or co-tuning between glomeruli and feedback axon boutons.

Postsynaptic targets Before the development of optogenetic tools, functional properties of cortical feedback connections have been described only in a handful of *in vitro* studies using stimulating electrodes (Balu et al., 2007; Laaris et al., 2007; Nissant et al., 2009). Because the primary recipient for fibers originating in the APC is the GCL, the authors focused on inputs to GCs. They found that GCs are heavily functionally connected to APC inputs and thus, that cortical feedback stimulation provides a strong source of feedforward inhibition onto MCs (Balu et al., 2007; Nissant et al., 2009). Only recently has the connectivity matrix between cortical feedback and OB neurons been further studied. By introducing ChR2 in Nstr1+ cells of the APC (using transgenic animals), the authors gained control over cortical axons while recording putative postsynaptic cells in the OB. Light stimulation of ChR2+ axons in acute OB slices confirmed that GCs were densely connected to both cortical structures and further revealed that APC axons are directly synapsing onto PG cells, sSACs and dSACs (Boyd et al., 2012). In addition to these AMPA receptor-dependent strong and fast inputs, and similarly to AON axons, APC feedback inputs were found to form unconventional synapses with MCs: excitatory inputs were weak and had slow kinetics (rise time $\sim 6.7ms$, decay time $\sim 36.3ms$), were barely insensitive to membrane potential, had very small trial-to-trial variability and failed to elicit MC spiking (Boyd et al., 2012). This type of event was frequently observed in slices. In addition to this weak direct excitatory current, cortico-bulbar axons optogenetic stimulation produced disynaptic inhibition onto MCs (Boyd et al., 2012). In anesthetized animals, APC axon light stimulation had no impact on MC spontaneous activity but was able to decrease odor-evoked activity of both excitatory and inhibitory responses.

Therefore:

1. Both the APC and AON send direct inputs to GCs, PG cells and sSACs. Additionally, the AON is connected to eTCs while the APC make synapse with dSACs. However, these differences are likely due to different focuses from the different studies.
2. Both the APC and AON form weak synapses on MCs

3. *In vivo*, both APC and AON axon stimulation produce feedforward inhibition of MC odor-evoked activity.

In vivo, whole-cell patch clamp examined subthreshold activity of GCs in awake, head-restrained mice (Youngstrom and Strowbridge, 2015). In this study, the authors found that GCs receive highly variable inputs, that they divide into two subpopulations: fast, large EPSPs on the one hand and slow, small EPSPs on the other hand. The latter likely originates from a distant site while the former likely originates from a proximal site (presumably dendrodendritic vs. top-down inputs; Balu et al., 2007; Laaris et al., 2007; Nissant et al., 2009). Therefore, by recording spontaneous EPSPs in GCs, the authors found a likely signature of cortical activity on GCs. The faster and larger fraction of the EPSPs ($\sim 10\%$ of the all the EPSPs) showed robust phase modulation to the respiratory cycle (Figure 4.1,B; Youngstrom and Strowbridge, 2015), consistent with a phase-locking of olfactory cortex neurons to the respiration. These results suggest cortical feedback will modulate GC temporal spiking activity.

Loss-of-function experiments have recently been performed with muscimol injection in the APC while imaging M/T cells, using genetically-encoded GCaMP indicator (Tbet-Cre mice; Otazu et al., 2015). In these conditions, odor stimulation triggered a response in a greater number of MCs, and these responses were stronger and less selective. At the population level, MC responses to odor become more similar after pharmacological inactivation of the APC. By contrast, TCs were less impacted by muscimol injection (Otazu et al., 2015).

Finally, top-down inputs from the olfactory cortex are subject to neuromodulation. Indeed, type 1 receptors to cannabinoids are expressed at cortico-bulbar axon terminals and their activation induces a reduction of synaptic transmission, at least to GCs (Soria-Gómez et al., 2014). As a result, feedforward inhibition onto M/T cells is reduced *in vivo*. Furthermore, endocannabinoids production was enhanced following a 24h fasting in rodents, and specific deletion of cannabinoid type 1 receptors at cortico-bulbar axons is sufficient to suppress the fasting-induced hyperphagia observed in control animals (Soria-Gómez et al., 2014). Cannabinoid type 1 receptor signaling was then shown to reduce olfactory detection threshold in fasting mice (Soria-Gómez et al., 2014). Therefore, by selectively inhibiting the top-down input-to-GC synaptic transmission, cannabinoid system activation causes odor detection to be enhanced and induces hyperphagia in fasted animals. This study demonstrates the importance of investigating the relevance of top-down inputs regulation on OB function, notably with regards to the animal's brain state, and shows the importance of neuromodulation on behavior.

3.1.3 Topography of cortical feedback projections

When considering antero-posterior or dorso-ventral OB organization, no clear topography in feedback fibers seems to exist. Feedback fibers originating both from the AON and APC, with the notable exception of contralateral projections from AONpE, seem to be distributed diffusely throughout the bulb (see for example, Luskin and Price, 1983). Therefore, the coarse topography in bottom-up inputs (dorso-ventral organization of OB-to-AON inputs) seems to be lost in feedback projections. However, it is interesting to raise the observation that topographic organization at the macroscopic level might exist if one considers the laminar organization of the OB, rather than organization along arbitrary axis (Figure 3.1,A).

At a finer level, single neuron axons were found to form patches of boutons (Matsutani, 2010), and injection of two different dyes $500\mu\text{m}$ apart in the OB leads to little overlap in retrogradely labeled cells within the APC (while consecutive injections in the same place led to high degree of overlap, Mazo et al., *submitted*). Additionally, utilizing rabies virus injection in the OB GCL and 3D reconstruction of feedback-projecting neurons in the olfactory cortex, it was shown that APC, but not AON, projecting cells have a non-random organization. Indeed, APC neurons close to each other are more likely to project to similar OB regions (Padmanabhan et al., 2016). This findings contrast the random structure of feedforward inputs described previously (Ghosh et al., 2011; Miyamichi et al., 2011; Sosulski et al., 2011) and argue for some degree of organization in top-down fibers.

Lastly, topography might appear in the organization of APC output channels. Indeed, recent studies looking at the APC projection channels to different brain areas revealed that 1) APC cells projecting to distinct subdivisions of the orbitofrontal cortex were spatially segregated (Chen et al., 2014), and 2) although macroscopically intermingled, APC cells projecting to the cortical amygdala, lateral entorhinal or medial prefrontal cortex were segregated in different layers (Diodato et al., 2016). In contrast OB and PPC-projecting cell distributions overlapped within layer 2b (Mazo et al., *submitted*).

3.1.4 Conclusion on glutamatergic cortical feedback

In this section, we saw that the OB is heavily reciprocally connected to the olfactory cortex. Figure 3.1,A recapitulates the laminar distribution of the ipsi- and contralateral top-down inputs originating from both the AON and APC. The function this feedback supports remains speculative, but it is evident that it heavily shapes OB neuron activity and behavior. In this section, I did not review the literature on feedback organization from the tectum, posterior piriform cortex, cortical amygdala and lateral entorhinal cortex. These feedback inputs represent much less numerous projection and knowledge about their connectivity to OB neurons and their impact on

OB odor coding is scarce or null. Although $\sim 90\%$ of the cells projecting to the OB originate in the olfactory cortex, the OB also receives glutamatergic projections from other cortical brain regions such as the hippocampus or hypothalamus (and the dorsal raphe, see below; Carson, 1984; Shipley and Adamek, 1984). The extent to which hippocampal and hypothalamic projections contribute to information processing and odor-guided behavior is not known.

In addition to these excitatory top-down inputs, the OB receives inputs from neuromodulatory centers. This will be the focus of the next section.

3.2 Top-down inputs from neuromodulatory regions

Projections that do not originate in the olfactory cortex are emanating from neuromodulatory centers, in the brainstem and basal forebrain (Shipley and Adamek, 1984), with the former being the second most important source of retrogradely labeled cells from the OB ($\sim 4\%$; Carson, 1984). Basal forebrain innervates the OB with cholinergic and GABAergic fibers, while the brainstem sends noradrenergic and serotonergic (but also glutamatergic) fibers to the OB. These neuromodulators are thought to be released in a state-dependent manner and to alter the function of neuronal circuits by acting on the properties of neurons and synapses. In contrast to their diffuse and widespread innervation of brain regions, neurons containing such neuromodulators are found in distinct and relatively small nuclei. Until the development of optogenetics, these neuromodulatory fibers were studied much more frequently than neurotransmitter fibers, probably because they could easily be labeled by immunohistochemistry and specifically manipulated *via* local pharmacology.

3.2.1 Serotonergic neuromodulation

The serotonergic pathway innervates a wide variety of brain areas and is thought to modulate sensory perception, including that of the olfactory system (Lottem et al., 2016; Petzold et al., 2009). Serotonin (5-hydroxytryptamine or 5-HT) is mainly released by neurons whose somas are located in the raphe nuclei in the brainstem. The OB is a major recipient of serotonergic innervation (McLean and Shipley, 1987; Steinfeld et al., 2015).

Anatomy of fibers from the dorsal raphe to the OB. Immunohistochemistry studies against 5-HT reported heavy labeling in the GL, and weaker immunoreactivity in deeper layers of the OB (McLean and Shipley, 1987; Steinfeld et al., 2015). Steinfeld and colleagues (2015) did not visualize somas in the OB, indicating a purely extrinsic source of 5-HT fibers in the OB. Similarly, anterograde tracer injection in the raphe nuclei led to

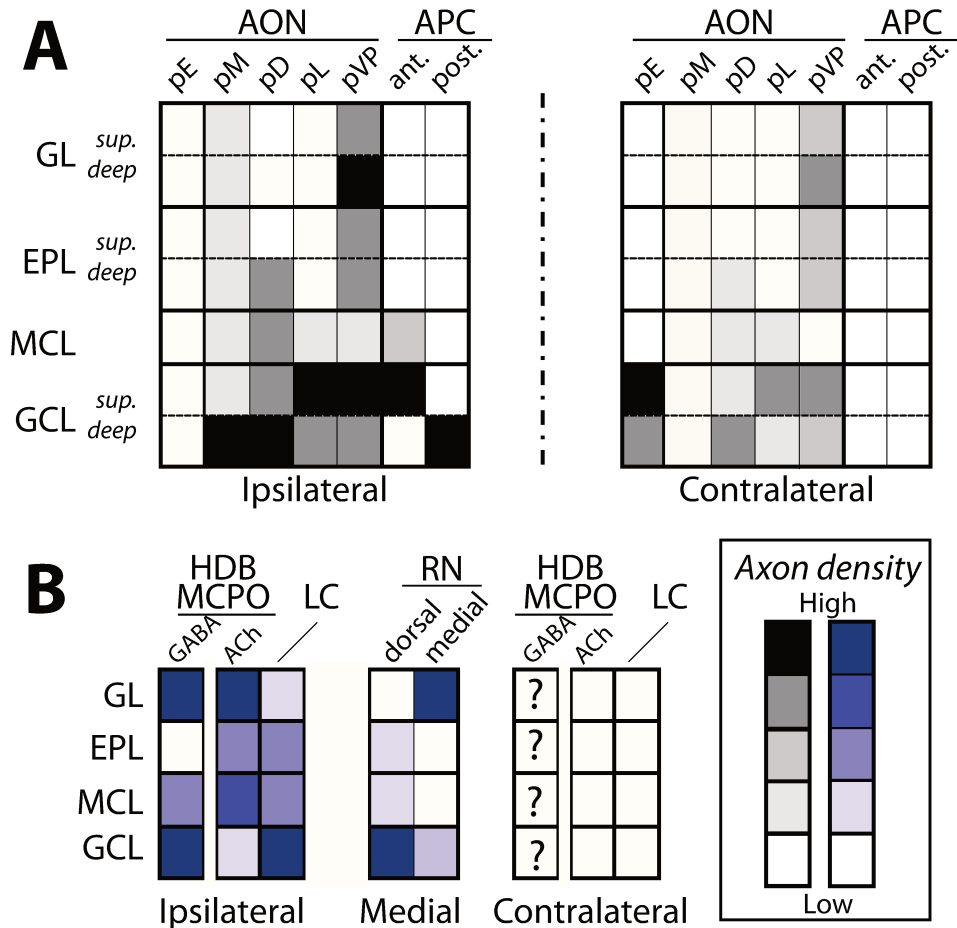


Figure 3.1 – Relative densities of centrifugal fibers across olfactory bulb layers.

Fibers originating from the different subdivisions of the anterior olfactory cortex (A) or from neuromodulatory brain regions (B). Densities are coded in shades of black or purple and should be compared across layers and between ipsi- and contralateral sides, but not between structures. Dark colors represent high labeling and white colors absence of labeling. For example, *pars ventro-posterioralis* has dense ipsilateral axonal projection to the deepest part of the GL and superficial GCL. Lighter projections are found across the other OB layers, with lowest density in the MCL. Projection pattern in the contralateral is similar, but the density of fibers is lower.

AON: Anterior olfactory nucleus; pE: *pars externalis*; pM: *pars medialis*; pD: *pars dorsalis*; pL: *pars lateralis*; pVP: *pars ventro-posterioralis*; APC: anterior piriform cortex; ant., post.: anterior and posterior parts of the APC, respectively; HDB/MCPO: nucleus of the horizontal limb of the diagonal band of Broca/ Magnocellular preoptic nucleus; LC: Locus coeruleus; RN: raphe nuclei.

high fiber density in the GL, while other OB layers were only weakly labeled (McLean and Shipley, 1987).

Raphe nuclei are divided in median raphe nucleus (MRN) and dorsal raphe nucleus (DRN), both of which were found to project to the OB (McLean and Shipley, 1987). However, since MRN and DRN are known to be distinct in terms of projection patterns in other brain regions, Steinfeld and coworkers (2015) used viral injections in one or the other nucleus to revisit this question in the OB. Injections mainly targeting the MRN resulted in similar projection pattern as observed in earlier studies, that is heavy labeling in the GL and weak labeling in other layers (Steinfeld et al., 2015). However, targeted injections in the DRN produced high labeling in the GCL and only modest fluorescence in other OB layers, and notably the GL (Steinfeld et al., 2015, but see also Suzuki et al., 2015). If labeling in the GL colocalized well with 5-HT staining, it seemed to not colocalize with serotonergic immunodetection in the GCL of DRN-injected mice (Steinfeld et al., 2015). Therefore, it appears possible that DRN uses another neurotransmitter than 5-HT to innervate the GCL. Notably, neuron expressing GABA, glutamate, dopamine, substance-P as well as CCK have been identified in the DRN.

5-HT receptors are metabotropic receptors (with the exception of 5-HT₃ being a ligand-gated ion channel) comprising six family members, from 5-HT₁ to 5-HT₆. 5-HT_{1A} and 2 have been found to be expressed by M/T cells and JG cells in the OB. It seems that 5-HT_{1A} are also expressed at GC membrane, although *in vitro* experiments demonstrate a lack of direct effect on GC by serotonin (Schmidt and Strowbridge, 2014). Anatomical studies showed that 5-HT expressing fibers impinge onto both GABAergic and non-GABAergic fibers in the GL (Gracia-Llanes et al., 2010a), and notably sSAC (Suzuki et al., 2015).

Impact of serotonergic modulation on the OB network. *In vitro*, 5-HT can excite eTCs *via* 5-HT_{2A} receptors (Liu et al., 2012), and mediate both inhibition and excitation on MCs and TCs (Hardy et al., 2005; Huang et al., 2017). Recently, 5-HT was also demonstrated to depolarize sSACs through binding of 5-HT_{2C} receptors, without affecting spike output (Brill et al., 2015). However, Brill and colleagues' data (2015) suggest that 5-HT increased GABA release from sSAC in a spike-independent manner. The authors did not report any effect of 5-HT on PG cells (Brill et al., 2015). Furthermore, Petzold et al. (2009) showed that 5-HT inhibit OSN presynaptic terminals in a GABA_BR-dependent manner, likely via increasing GABA release from local GABAergic neurons. In conclusion, 5-HT release has several effects on the OB circuit: 1) it increases eTC-mediated feedforward excitation onto sSAC, PG cells and MCs, 2) it directly increases inhibition mediated by sSAC and 3) these network effects increase spontaneous MC

firing without enhancing responses to suprathreshold sensory input (Brill et al., 2015).

In addition, brief stimulation of raphe nuclei has also been shown to elicit serotonergic-independent responses in OB neurons. Indeed, eTCs were found to be excited by brief raphe nuclei stimulation (Kapoor et al., 2016; Liu et al., 2012). Surprisingly, eTC excitation was direct but mediated by glutamatergic transmission, thereby demonstrating that raphe nuclei can co-release 5-HT and glutamate, even in the GL. In addition, an *in vivo* study showed that both GABAergic PG cells and dopaminergic sSAC spontaneous activity, but not odor-response, is enhanced by brief activation of fibers originating in the DRN (Brunert et al., 2016). This effect was also likely mediated by glutamate transmission. *In vitro*, raphe nuclei fiber stimulation elicited opposing effect on both mitral and tufted cells (Kapoor et al., 2016). Indeed, excitation was followed by inhibition. Excitation was delayed and asynchronous, suggesting a polysynaptic mechanism, possibly involving recurrent excitation from eTCs. Inhibition arrived even later onto MCs and TCs and was blocked by glutamate receptor antagonist. A scenario involving direct excitation of eTCs, which drives a feedforward inhibition mediated by GL GABAergic neurons onto MC and TCs could explain these observations. In addition, Kapoor and colleagues (2016) found a 5-HT receptor-sensitive component in light-evoked inhibition onto M/T cells. It remains unclear whether this inhibitory action of 5-HT is mediated by direct activation of 5-HT receptors at M/T cell membrane or indirect activation of serotonergic receptors on inhibitory neurons.

In vivo, brief stimulation of the DRN induced heterogeneous responses on M/T cells, with an overall increased on odor-evoked responses, but not on spontaneous activity (Brunert et al., 2016; Kapoor et al., 2016). Two-photon analysis of Ca^{2+} transients in MCs and TCs separately revealed that raphe nuclei brief stimulation enhances odor-driven activity in TCs, while MCs odor response was bidirectionally modulated and resulted in increased MC decorrelation of odor responses (Kapoor et al., 2016).

Interestingly, accessory OB and main OB neurons are differentially modulated by serotonergic fiber afferents (Huang et al., 2017), showing how activation of the same system can provoke distinct responses in similar target regions. DRN stimulation was also found to suppress spontaneous activity of APC neurons, but the diminution of odor-evoked firing could be explained solely by the subtractive effect of light on baseline activity (Lottem et al., 2016). The effect of the dorsal raphe on the APC could affect feedback projections to the OB. Therefore, as for the oxytocin system influencing the AON, the serotonergic system is in good position to influence OB activity and olfactory processing at multiple steps, and by multiple pathways in the olfactory system. Finally, DR neurons activation was able to drive reward behavior, mainly through its glutamatergic component, but also partially through a serotonergic component (Liu et al., 2014). Rat pups with sero-

toninergic fiber depletion failed to develop an odor preference triggered by odor-tactile stimuli association, and 5-HT_{2A/2C} receptors were found to be necessary for the acquisition phase of learning (Matsutani and Yamamoto, 2008).

Therefore most studies on the serotonergic system have focused on slow timescales, but recently, rapid modulation of downstream activity and sensory processing as well as dynamic impact on ongoing behavior has started to receive more attention.

3.2.2 Inputs from the locus cœruleus

The OB receives projections from another brainstem nucleus: the locus cœruleus (Macrides et al., 1981; McLean et al., 1989; Shipley and Adamek, 1984; Shipley et al., 1985). In sensory systems, noradrenaline (NA) inputs have been associated with experience-dependent plasticity. The locus cœruleus is a noradrenergic center that sends highly divergent axons to a wide variety of brain structures (Schwarz et al., 2015). Indeed, using viral-genetic based tracing techniques, the authors recently confirmed that the locus cœruleus neurons projecting to a specific brain region also project to the other investigated areas (namely the OB, hippocampus, auditory cortex and medulla). This high divergence of locus cœruleus outputs supports an output broadcast model rather than a discrete output model. In particular, OB-projecting neurons also project to all the aforementioned areas. Reciprocally, individual locus cœruleus neurons receive inputs from multiple brain regions (neocortex, medulla, cerebellum, hypothalamus among many others), regardless of their projection pattern, therefore locus cœruleus neurons receive highly integrative inputs.

Anatomy of locus cœruleus fibers to the OB. Even though retrograde labeling labeled contralateral cells in the LC (Macrides et al., 1981; Shipley and Adamek, 1984), anterograde labeling from LC reported no or few fibers in the contralateral OB (McLean et al., 1989; Shipley et al., 1985). Within the OB, NA fibers contain numerous varicosities, densely distributed along the entire length of each axon. Across OB layers, axon terminals are distributed in a graduate fashion, with heaviest labeling in the IPL and GCL, fewer staining in the MCL and EPL and minimal staining in the GL (Gómez et al., 2005; McLean et al., 1989; Shipley et al., 1985).

Impact of noradrenergic modulation on the OB network. Both α isoforms ($\alpha 1$ and $\alpha 2$) and β receptors for NA are expressed across all layers of the bulb, with expression patterns varying between studies. A general trend leans toward a deep expression of alpha receptor and more distributed expression for beta (see for example Nicholas et al., 1993a,b; Woo and Leon, 1995). Individual OB neurons appear to express multiple adrenergic receptor

subtypes. For example, MCs express all three receptors subtypes ($\alpha 1$, $\alpha 2$ and β) while GCs express $\alpha 1$ and $\alpha 2$ receptors.

In vitro studies showed that $\alpha 1$ and $\alpha 2$ receptors have opposing effect on GC activity. While activation of $\alpha 1$ increased GC activity and thus inhibition on MCs, $\alpha 2$ activation suppressed GC excitability and therefore diminished inhibition on MCs (Nai et al., 2010, 2009). Since $\alpha 2$ receptors have a higher affinity for NA than $\alpha 1$ receptors, $\alpha 2$ effects of NA dominates at low concentration (decreased MC inhibition) whereas $\alpha 1$ effects supplant $\alpha 2$ at increasing NA concentration (increased MC inhibition). NA seems also to directly excite MCs (Hayar et al., 2001).

In vivo, LC activation renders M/T cells more responsive to weak olfactory nerve stimulation, while having no effect on stronger olfactory nerve stimulation (Devore et al., 2012). In sharp contrast, pairing of odor and LC stimulation produced suppression of M/T cell odor responses (Shea et al., 2008). This effect could be mediated by an action of NA at the OSN terminals. Indeed, although an *in vitro* study did not report any effect of NA in glomerulus signaling (Hayar et al., 2001), a recent work utilizing pharmacology and GCaMP2 to image glomerular responses when stimulating the LC showed that NA triggers a reduction in the gain of the presynaptic inputs to the glomeruli (Eckmeier and Shea, 2014). In addition, β receptor activation was recently shown to increase the frequency and strength of eTC rhythmic bursting (Zhou et al., 2016). This might be to date the first convincing data on the impact of β receptor activation in the OB of adult rodents.

Overall, transection of the NA pathway to the OB decreased odor-induced *cfos* expression (a gene whose expression immediately increases in response to an augmentation in cell activity), and NA depletion in ewes prevented the memory formation of their own lambs (Matsutani and Yamamoto, 2008). Daily pairing of odor and tactile stimuli induces NA-dependent odor preference in rat pups and the same pairing protocol has been shown to increase NA levels in the OB (Matsutani and Yamamoto, 2008).

Although it is clear that NA plays an important role for olfactory processing in the OB, but also in odor learning, the mechanisms by which these effects are mediated remain unclear and debated. Different affinities for NA of the different receptors, combined with a pleiotropic distribution among OB neurons precluded target- and receptor-specific investigation of NA effects. To date, no study has investigated the specific contribution of NA fibers on OB network, without stimulating the whole LC. Furthermore, NA putative action on other OB neurons (such as dSAC, eTCs, etc) remains unknown.

3.2.3 Cholinergic inputs from the basal forebrain

Within the basal forebrain, projections originate from the nucleus of horizontal limb of the diagonal band of Broca (HDB), magnocellular preoptic nucleus (MCPO) or from a transition zone between the two structures. Fewer projecting cells are also found in the nucleus of the vertical limb of the band of Broca. Anatomical distinction between these regions are not clear, and boundaries differ significantly between species. That is why, for the sake of clarity, we will collectively refer to these projecting regions as HDB/MCPO.

HDB/MCPO is the main source of acetylcholine (ACh) in the brain. The cholinergic system is thought to act as a global activating system since cholinergic neurons fire higher during wakefulness than during slow-wave sleep. The basal forebrain sends widespread axon collaterals innervating the whole neocortex and the OB.

Anatomy of HDB/MCPO fibers in the OB. As in the neocortex, cholinergic fibers exhibit a high number of small varicosities throughout the volume of the OB. Thus, cholinergic neuromodulation is likely to happen in a wide area within the OB. Across OB layers, fibers are distributed with highest density in the GL, and lower innervation was found in the GCL (Ichikawa and Hirata, 1986; Rothermel et al., 2014).

Impact of cholinergic modulation on the OB network. ACh activates fast ionotropic (nicotinic) and slow metabotropic (muscarinic) receptors expressed at the neuron membrane. In the OB, expression of the two types is well segregated, although recent functional studies demonstrated that muscarinic receptors are expressed at sSACs surface (Pignatelli and Belluzzi, 2008) and GL-dSACs express nicotinic receptor subunit $\alpha 2$ (Burton et al., 2017). Nicotinic receptors are distributed in outer bulbar layers, from the GL to the MCL while muscarinic receptors are expressed in the GCL. ACh activates PGs and MCs through nicotinic receptors (Castillo et al., 1999), but nicotinic receptor-mediated GABA release also attenuates MC reponse to OSN stimulation (D'Souza and Vijayaraghavan, 2012). Effect of muscarinic receptor activation is less clear. Castillo and coworkers (1999) observed that GCs are inhibited by muscarinic receptors at the soma, while muscarinic receptor activation at GC dendrite enhances GABAergic transmission. Furthermore, Pressler and colleagues (2007) showed that muscarinic receptor activation alters GC electrical properties following spike discharge (afterhyperpolarization is blocked and afterdepolarization is recruited). When rhythmic stimulation is applied to GCs, this lead to potentiation of GCs and inhibition of MCs (Pressler et al., 2007), consistently with results from Castillo et al. (1999). In addition, recent studies suggest that activation of muscarinic receptors inhibits sSAC (Pignatelli and Belluzzi, 2008) and activation of nicotinic receptors triggers two distinct effects

on eTCs: direct excitation, and increase in polysynaptic inhibition. Inconsistency exists among *in vivo* studies. First, it should be noted that in the HDB/MCPO, cholinergic and GABAergic somas and axons are intermingled, which restricts the interpretation of the data acquired by early studies using electrical stimulation. Nevertheless, more recent studies using pharmacology or optogenetic tools to selectively manipulate cholinergic activity also came to inconsistent observations. Pharmacological manipulation of ACh pathway either produced inhibition of putative M/T cells or had no effect on their excitability. Optogenetic activation of HDB/MCPO led to M/T cell spontaneous activity inhibition and to sharpening of their odor tuning properties (Ma and Luo, 2012), while optogenetic activation of cholinergic axon terminals induced increase in M/T cell spontaneous and odor activities, with no effect on odor tuning (Rothermel and Wachowiak, 2014). In these two latter studies, the experimenters used distinct light protocols to investigate functional impact onto M/T cells *in vivo*. Ma and colleagues (2012) used light stimulation of the somas while Rothermel and Wachowiak (2014) restricted light illumination onto the fiber terminals. Because cholinergic fibers from the HDB/MCPO innervate a wide diversity of brain regions, and notably the AON and APC (which in turn provide massive feedback to the OB), stimulating the cholinergic somas in the HDB/MCPO may not be well-suited for specific investigation of the impact of cholinergic terminals onto the OB. Interestingly, when Rothermel and coworkers (2014) stimulated HDB/MCPO somas directly to compare their data with those from Ma and Luo (2012), the authors observed mixed modulation of M/T cells. Therefore, it appears that engaging only the axonal fibers reaching the OB is different from bulk stimulating HDB/MCPO cholinergic neurons. This is not surprising, but it is an interesting comparison since the cholinergic system is thought to behave as an generalized attention system in the brain.

While detailed investigation on cholinergic impact on OB neurons and network is still in progress, behavioral studies have shown an association with plasticity. Indeed, short-term retention of olfactory memory was impaired by blockade of muscarinic transmission while nicotinic transmission alteration depressed discrimination between similar odorants (Matsutani and Yamamoto, 2008).

3.2.4 Conclusion on neuromodulatory top-down

The number of projecting cells do not systematically correlate with fiber density and functional impact. Therefore, although very few cells in neuromodulatory regions project to the OB compared to olfactory cortex neurons (Carson, 1984), it does not mean that this descending pathway has negligible impact on OB function. Figure 3.1,B recapitulates the projection patterns originating from neuromodulatory centers.

Manipulation of the neuromodulatory pathways in the OB has been as-

sociated with an impact on behavior. Neuromodulatory fibers have a high density of release sites, inducing a wide release of transmitters in the OB. These neuromodulators then act on multiple OB targets and bind a variety of receptors. Affinity and kinetics of the receptors vary, rendering the interpretation of the data complex. Different concentrations or regimes of activity of these neuromodulatory fibers might produce opposite effects on the OB network. The pathways through which the different neuromodulators are acting in different contexts are still unclear, as well as the contributions of each individual receptors. As a result, the consequences of neuromodulator system activation remain elusive, although noradrenergic, serotonergic and cholinergic systems are known to have profound effects on the OB network, olfactory-driven behavior, and learning.

3.3 GABAergic top-down

Inputs from the basal forebrain. We have seen earlier that the HDB/MCPO is the major source for cholinergic inputs to the OB. Macroscopically, the HDB/MCPO contains cholinergic neurons in its medial half, while GABAergic neurons are located on the caudal half, and especially the lateral part (also labeled as MCPO). However, at the cellular level GABAergic and cholinergic are intermingled in the HDB/MCPO. Importantly, only 10–20% of the OB-projecting neurons in the HDB were found to colocalize with ChAT immunostaining. Using retrograde tracer and immunolabeling for both ChAT and GAD (the fact that GAD actually exists under two distinct isoforms was unknown at that time), Zaborsky and coworkers (1986) found that HDB/MCPO contains both cholinergic and GABAergic projection neurons. Surprisingly, the authors found that within the HDB/MCPO, the OB-projecting cell population is composed of a larger number of GABAergic cells than cholinergic ones.

Using electrical stimulation, the group of McKenzie showed that lateral HDB elicits inhibition in OB granule cells, resulting in the depolarization of M/T cells (Kunze et al., 1992a,b). However, due to the lack of specificity in using electrical stimulation, the observed effect on M/T cells is likely to emerge from a mix of the GABAergic and cholinergic influences from the HDB. In contrast to their cholinergic counterpart, the issue of laminar distribution in the OB of GABAergic fibers originating in the HDB/MCPO has remained unaddressed for decades. This is due to the fact that cholinergic elements in the OB have an exclusive external source while intrinsic GABAergic elements are abundant. Recently, Gracia-Llanes et al. (2010b) combined anterograde tracer injection with immunogold postembedding detection for GABA, in order to tackle the distribution of the GABAergic fibers emanating from the HDB/MCPO. They first observed that GABAergic fibers are morphologically well distinguishable from cholinergic fibers (different num-

ber of en passant boutons, different thickness of the axon shaft). Then they remarked that GABAergic fibers are distributed in the GL, IPL and GCL, and rarely in other OB layers (see Figure 3.1,B). Symmetrical synapses were observed onto GCs dendrites –but only rarely on somas– and onto type 1 PG cells. Furthermore, Nunez-Para and coworkers (2013) took advantage of transgenic mice to selectively express ChR2 in GABAergic HDB/MCPO neurons. The authors reported the presence of ChR-expressing fibers in the GCL, and to a lower extent in the GL and EPL. HDB/MCPO GABAergic fibers were found to innervate both the main OB and the accessory OB. When light-stimulating the fibers in acute OB slices, GCs decreased their firing rate and exhibited robust IPSCs that were blocked by GABAzine. In addition, dSACs, PG cells and MCs seem to be connected to GABAergic fibers from the HDB/MCPO (Sanz Diez, SfN Poster, 2016). Selective pharmacogenetical silencing of the GABA fibers induced a reduction in the ability of mice to discriminate between odors in a novel odor discrimination test (Nunez-Parra et al., 2013). However, the interpretation suffers from the fact that the exogenous receptor’s ligand was injected systematically, and therefore inhibited the whole HDB/MCPO, rather than HDB/MCPO projections to the OB specifically.

Controverted evidence of GABAergic inputs from the olfactory cortex. Retrograde labeling studies occasionally found some GABAergic OB-projecting neurons in the layer 3 of the APC, or in the hypothalamus (Zaborszky et al., 1986). In addition, a recent study also reported the presence of GABAergic OB-projecting neurons from the APC using retrograde tracer injection in the OB, and genetic labeling for GAD2 (Diodato et al., 2016), although the genetic labeling of GABAergic neurons reported in this study is somewhat different from that reported in the literature (see for instance Haberly, 2001; Suzuki and Bekkers, 2010). Other studies selectively expressing viruses in APC GABAergic neurons failed to label fibers in the OB (Otazu et al., 2015) and GABAergic APC neuron stimulation was not successful in triggering direct inhibition on OB cells (Boyd et al., 2012).

3.4 Conclusion on top-down inputs to the olfactory bulb

From this section, it seems obvious that olfactory perception results from the integration of confluent bottom-up and top-down pathways. Indeed in olfaction, the first brain relay for odor information processing is massively innervated by a variety of neurotransmitters or neuromodulators, such as glutamate released from cortical feedback fibers and from the dorsal raphe nucleus, serotonin and noradrenaline released from fibers originating from the brainstem, and acetylcholine and GABA from fibers emanating from

the basal forebrain. The way these brain regions (or their axon terminals) interact with each other is unknown, as well as the conditions in which they are recruited during appropriate behavior.

Chapter 4

Olfactory Coding in the Olfactory Bulb

Neurons transmit information in a discrete manner through action potentials. Therefore, a fundamental question in neuroscience is to understand how spike trains convey meaningful information to downstream brain regions. That is, what is the neuronal code used to communicate information? As stated by Uchida and coworkers (2013b), there are three main constraints for a code. 1) Neuronal activity should vary with a stimulus. Thus, one should examine how neuronal activity varies with different parameters of that stimulus and which aspect of this neuronal activity may carry reliable information about the stimulus. 2) For a neuronal response to serve as a code it must be readable by a downstream brain region. Eventually, information decoding should be read out by animals to guide their behavior. Therefore, one can use either level of information integration to address whether or not a change in neuronal activity could be used as a code or not. 3) A code is only relevant if it allows powerful information processing. Hence, investigators should address why a code is used, i.e what are the computational advantages of that code.

Olfactory information is transmitted to the OB *via* OSN inputs to the GL. An odor molecule dynamically activates a determined set of glomeruli, thereby creating a spatiotemporal map at the OB surface. Notably, mice can discriminate a single odorant in a variable odor background composed of mixtures of up to 16 odorants (Rokni et al., 2014). In addition, they have the amazing ability to discriminate odors with high accuracy in a few hundreds of milliseconds (Abraham et al., 2004; Uchida and Mainen, 2003). However, the exact code used by the OB to transmit olfactory information remains unknown.

In this last chapter of the introduction, I first review the oscillatory

rhythms, prominent in the OB, before detailing the odor responses of the different neuronal elements of the OB. I then review how the output channels of the OB, M/T cells, respond to odor stimulation. Next, I expose current views on the code that might be used by M/T cells. Finally, I describe centrifugal influences on OB odor coding and behavior.

4.1 Large scale temporal coding in the olfactory bulb

Oscillatory rhythms are prominent in the mammalian OB, especially in awake animals. They are generated across a wide range of frequency bands, detected during electroencephalograms or from the local field potential (LFP). The LFP corresponds to the extracellular sum of the activity of many neurons (from 100 to 10,000; Kay, 2014). Neurons can be considered as electrical dipoles when stimulated, with a sink of current at the depolarizing site, counterbalanced by a distal source of current. This current flow generates potential differences, and thus a change in the extracellular voltage compared to the reference electrode. If cells are spatially arranged in a similar fashion (i.e, they exhibit a current sink and source in the same respective layers), and if a sufficient number of cells are recruited synchronously, this voltage change relative to the reference electrode can be big enough to be detected by a recording electrode. This requires the brain tissue to be arranged in a laminar fashion, as it is the case for the cortex and the OB. As such, the change in voltage detected in the extracellular space, i.e the sign of the deflection in the LFP, depends on the localization of the recording electrode relative to the sink and the source of current. For instance, an electrode going deeper across the layers of a tissue will record a negative deflection in the layers superficial to the current sink, and a positive deflection once the electrode has passed the current sink. If the potential does not reverse, the depolarization is probably generated by a distant source of current. A more detailed analysis is sometimes necessary to address questions involving the source of an LFP event: the current source density analysis. This method uses spatial derivatives of voltage signals across different layers to identify the current source and sink (Pettersen et al., 2011).

Oscillatory rhythms in the OB. In the OB, GCs are mainly contributing to the LFP. Indeed, their parallel geometry, their density and their morphological organization (somas in the GCL, dendrites exclusively in the EPL, no axon) place them in the best condition to generate current flow between their dendrites in the EPL and their somas in the GCL (Rall and Shepherd, 1968). However, under certain particular conditions, other neuronal types can largely contribute to the LFP. For example, stimulation of the LOT provokes back-propagating action potentials in M/T cell axons, which

generates brief, transient oscillatory activity mainly evoked by M/T cells depolarization (Rall and Shepherd, 1968). In conclusion, LFP signals give a different information than unit recordings (recordings of neuronal spike activity). Spike events can not be assessed using LFP recordings, and therefore spike timing information is lost, however the activity of a population of neurons can be questioned at once. It is therefore possible to address the level of synchrony and cooperativity between cells in the network. A major pitfall of LFP recording is however the lack of specificity. Because neuronal activity is highly intricated, it is sometimes hard to assign a LFP event to a specific cell type.

Three major bands have been identified in the OB as having functional relevance: the theta band (1-10 Hz), beta band (15-40 Hz) and gamma band (40-100 Hz). These bands are associated with distinct network events and emerge from different neuronal interactions. These oscillatory rhythms are mutually interdependent.

Theta rhythms. Inputs from the periphery in the OB are transmitted through the OSN in the nasal epithelium. As respiration is a cyclic phenomenon, inputs to the OB are also rhythmic. Sensory inputs are thought to be the source of the theta band activity (1-10 Hz, Gray and Skinner (1988); Kay (2014)). Theta oscillations in the OB are highly correlated with the respiration cycle, at least for the lowest frequencies. Consistently, M/T cell membrane potential (Margrie and Schaefer, 2003; Youngstrom and Strowbridge, 2015) and firing activity (Buonviso et al., 1992; Fukunaga et al., 2012; Lepousez and Lledo, 2013) are rhythmic and phase-locked to the breathing activity (also somewhat weakly). Similar observations were recently obtained from GCs: GCs membrane potential (Youngstrom and Strowbridge, 2015) as well as firing activity (Czakoff et al., 2014) are modulated by the phase of the respiration. Both M/T cells (Cury and Uchida, 2010; Gschwend et al., 2012; Kay and Laurent, 1999; Rinberg and Gelperin, 2006) and GCs (Czakoff et al., 2014) phase modulations of firing activities were much weaker in awake compared to anesthetized state. OSN inputs are thought to drive these M/T cell rhythmic activity (Cang and Isaacson, 2003; Margrie and Schaefer, 2003; Phillips et al., 2012). In tracheotomized animals, the establishment of an artificial nasal air flow is sufficient to induce phase modulated spikes in M/T cells (Courtiol et al., 2011; Phillips et al., 2012). At the population level, M/T cells lock to heterogeneous phases of the respiratory cycle (Buonviso et al., 1992; Fukunaga et al., 2012; Lepousez et al., 2013). When the sniff frequency increases, the locking of individual neurons decreases (Kay and Laurent, 1999). However, recent intracellular recordings suggest that voltage membrane phase tuning of both M/T cells and GCs is little sensitive to high frequency sniffing ($> 3.5Hz$) or locomotion (Youngstrom and Strowbridge, 2015). Further deciphering of the mecha-

nism inducing MCs and TCs phase-locking to the respiratory cycle showed that TCs are locked to earlier phases of the inspiration period, with little phase change when odor concentration increases, whereas MCs are coupled to later periods of the inspiration and show greater phase advance when odor concentration increases (Fukunaga et al., 2012, but see also Phillips et al., 2012). It is thought that theta oscillations are both driven by OSN inputs and shaped by glomerular microcircuits (Kay, 2014). Glomerular layer circuitry is poised to facilitate theta frequency oscillations by reciprocal excitation between chemically or electrically coupled M/T cells or by action of excitatory eTCs. Besides, further olfactory structures are modulated by respiratory inputs. Indeed, the olfactory cortex displays theta oscillation partially coherent to the respiration cycle (Chabaud et al., 2000; Wilson, 1998), and APC cell firing activity is also modulated by the respiratory rhythm (Gire et al., 2013). Therefore, theta rhythms may be back-propagated to the OB through cortico-bulbar retroprojections. Recently, *in vivo* patch recording of OB GCs in awake, head-restrained animals demonstrated that they receive fast and large rhythmic ESPCs at the theta frequency (Figure 4.1,B; Youngstrom and Strowbridge, 2015), likely arising from the olfactory cortex (Balu and Strowbridge, 2007; Nissant et al., 2009). Intracellular recording in anesthetized mice failed to detect a significant contribution of centrifugal inputs to M/T cells phase-locking (Phillips et al., 2012), but cortical feedback activity is depressed under anesthesia (Boyd et al., 2015; Otazu et al., 2015). This discrepancy between the influences of cortical feedback on GCs and M/T cells might well arise from the different brain states (awake vs. anesthetized) during which the data were obtained.

Gamma rhythms. In awake mice, gamma oscillations (40-100 Hz) are an additional spontaneous cyclic activity. Gamma oscillations are nested on theta oscillations, in the peak and descending phase of the inhalation. Work in the laboratory and others, dissecting the circuit underlying gamma oscillations in slices, in awake mice, and using computational models demonstrated that both spontaneous and odor-evoked gamma rhythms are generated by the reciprocal synapses between M/T cells and GCs (Bathellier, 2005; Fukunaga et al., 2014; Lagier et al., 2004; Lepousez and Lledo, 2013; Neville and Haberly, 2003). Many decades of work have contributed to the knowledge of the microcircuit supporting gamma oscillations, which was already theorized by Rall and Shepherd early work (1968). Furthermore, gamma oscillations are supported by NMDAR activation on GCs (Lepousez and Lledo, 2013). Gamma oscillations can be further divided into two distinct subbands: high gamma (60-100 Hz) and low gamma (40-60 Hz), respectively appearing at the beginning and second half of the gamma cycle. High gamma oscillations may be more spatially restricted than low gamma ones, while low gamma subband may reflect, or be generated by, a synchronization between distant

M/T cells sending their apical dendrites in distinct glomeruli (Lepousez and Lledo, 2013). Another possible scenario is that high gamma oscillation would originate from TC-GC interactions, while low gamma ones would be generated by MC-GC interactions (Manabe and Mori, 2013), in accordance with faster kinetics of TC action potentials (Burton and Urban, 2014) and their earlier coupling to the respiratory cycle (Fukunaga et al., 2012). These two scenarios are not mutually exclusive. Finally, despite the local origin of gamma oscillations, this rhythm is under the influence of top-down inputs. Non-selective blockade of centrifugal afferents caused gamma oscillations to increase dramatically in the OB (Gray and Skinner, 1988; Martin et al., 2006).

Beta rhythms. Lastly, rhythms with an intermediate frequency can be observed in the OB (15-40 Hz). The beta regime power increases upon repetition of presentation of the same odor or when an odor is associated with a valence through associative learning (Kay, 2014; Kay et al., 2009). A very small number of odors also appear to generate beta oscillations in the OB without repetitive exposure (Neville and Haberly, 2003). Odor-evoked beta oscillations span several cycles of the respiratory rhythm, suggesting that beta oscillations are not driven by sensory inputs. In contrast, beta oscillations are likely to be driven by interactions between the olfactory cortex and the OB, since centrifugal feedback blockade completely abolishes beta regimes (Gray and Skinner, 1988; Martin et al., 2006; Neville and Haberly, 2003). However, it is not clear whether beta oscillations are generated in the olfactory cortex and back-propagate to the OB, if they rely on the bulbo-cortical loop activity, or if feedback fibers simply act as an obligatory drive of a local circuit within the OB able to generate such oscillations. What can be assured, is that beta frequencies are highly coherent across olfactory areas and are likely to be important for coordinating networks from different olfactory regions. Gamma and beta rhythms seem to have different pharmacological profiles (beta rhythms are not affected by a NMDAR blockade; Lepousez and Lledo, 2013), but centrifugal input blockade leads to opposite effects in the gamma and beta band (Gray and Skinner, 1988; Martin et al., 2006; Neville and Haberly, 2003), suggesting that these two regimes use the same circuits, but are recruited in different contexts.

In conclusion, the OB generates discrete rhythms underlied by different microcircuits, that are engaged in different contexts. For instance, by selectively manipulating GL or GCL inhibition, Fukunaga and coworkers (2014) elegantly showed that GL inhibition regulates MCs odor response latency to the theta cycle while GCL inhibition controls OB gamma frequencies and alters the fast rhythmic firing activity (in the gamma range) of OB principal cells, evoked by odor stimulation. Theta oscillations are largely related to sensory inputs, but can also be associated with higher cognition processes.

Indeed, coherence magnitude between theta oscillations in the OB and hippocampus was positively related to the learning level during an odor discrimination task (Kay, 2014). Beta oscillations are thought to be important for coordinating information processing across several brain regions working together, but beta power has also been shown to be modulated by the strength of sensory inputs (Kay, 2014). Finally, gamma oscillations are generated by the MC-GC reciprocal synapse activity and are behaviorally associated with sensory processes. Indeed, in mice with disinhibited GCs (lacking functional GABA receptors on GCs using a knock-out for the GABA_AR subunit $\beta 3$), gamma oscillations were increased (Nusser et al., 2001) and mice were faster at discriminating odors (Nunes and Kuner, 2015). However, the synaptic and cellular mechanisms involved in such deficits remain unclear. Oscillatory rhythms can generate an internal clock for a temporal code to be read out by downstream brain structures (Laurent, 2002), and as M/T cell spike timing conveys meaningful information to the olfactory cortex (Cury and Uchida, 2010; Dhawale et al., 2010; Margrie and Schaefer, 2003; Shusterman et al., 2011), OB oscillations are likely to play a key role in proper transmission of olfactory information.

In the sections below, I will detail the response evoked by different types of OB neurons, embedded in different microcircuits. This will allow a better understanding of how M/T cell responses are shaped by the OB network.

4.2 Transformation in the Glomerular Layer

It remains unclear how OSN activity is modulated by odors and sniffing behavior in awake mice. Indeed, a recent report shows that intrinsic optical imaging, widely used as an indirect measure of OSN terminal activity, appears to not be correlated with either OSN neurotransmitter release, postsynaptic activity or neurovascular coupling (Vincis et al., 2015). Rather, OB intrinsic optical imaging seems to reflect solute and water movement in OSN axon terminals, whose correlation with neuronal activity is not known (Vincis et al., 2015). In this section, I focus on odor coding by postsynaptic JG cells in the GL, namely sSACs, PGs and eTCs.

Odor coding at the mesoscale level. At the GL level, odor stimulation induces intermingled excitation and inhibition of individual glomerulus (Homma et al., 2013). Because inhibition in OSN axons has never been observed, the authors conclude that inhibition recorded in glomeruli emerges from inhibition of the postsynaptic compartment, and thus postsynaptic activity can dominate presynaptic activity. Excited and inhibited cells are organized as clusters, respectively around the excited and inhibited glomeruli (Homma et al., 2013). Deeper cells in the GL have been reported to be more

broadly tuned than superficial JG cells, and tuning properties of these deeper cells overlap the activity of distinct glomeruli (Kikuta et al., 2013). It is worth noting that M/T cells were found to be more narrowly tuned than the glomerulus they are projecting to (Kikuta et al., 2013). From these broad-scale recordings, it appears that inhibition is triggered by odor application in a spatially selective manner, and does likely not emerge from a center-surround mechanism. Selective inhibition in a subset of glomeruli might generate contrast enhancement in downstream M/T cells. Notably, this contrast enhancement mechanism is poised to be better suited for fragmented map processing than a center-surround inhibition mechanism (Cleland and Sethupathy, 2006).

Odor coding by JG cells. The first *in vivo* study of JG cells dates back from the 90's and recorded the activity of a small number of cells. Recent studies more systematically investigated the contribution of JG cells to M/T cells inhibition and odor coding, but knowledge about their contribution remains sparse, partly because *in vivo* preparation often considered JG population as whole. JG cells exhibit a wide diversity of spontaneous activities and odor responses, but often strongly phase-locked to the respiration in anesthetized animals (Homma et al., 2013; Wachowiak et al., 2013). Odor stimulation was dominated by excitatory responses but could induce both excitatory and inhibitory responses in individual neurons. JG also showed a diversity of odor response kinetics, such as response to the onset or offset of the odor (Homma et al., 2013), but this was less pronounced compared to GC kinetics variations (Wachowiak et al., 2013). Increase in odor concentration increases the number of responsive cells at the population level and the response strength at the individual neuron level. Interestingly, some neurons change their response polarity with high concentration and in an odor-specific fashion, suggesting that odor-evoked response is not determined by intrinsic properties, neither is it hard-wired. As a population, JGs show a wide dynamic range with regards to odor concentration (spanning two or three order of magnitude), in line with the data obtained from M/T cells (Homma et al., 2013).

Impact of GL network activity on M/T cell odor responses. To investigate the contribution of GL inhibition at the M/T cells level, Economo et al. (2016) expressed the calcium indicator GCaMP in M/T cells and compared Ca^{2+} transients in the somas to the transients in the apical dendrites. The authors found that M/T cells apical dendrites are excited and inhibited in a glomerulus and odor-specific manner, corroborating previous results (Homma et al., 2013) at the M/T cell level, and in awake animals (Economo et al., 2016). This was not trivial given that anesthesia reduces sSACs and PG cells odor response (Wachowiak et al., 2013). However, increases in odor

concentrations altered M/T cell apical dendrite responses in a largely non-linear fashion, with changes in polarity upon increasing odor concentrations, for instance. Similarly to JG cells, M/T cell apical dendrite odor responses showed intermingled patterns of excitation and inhibition. Furthermore, mixture of two odorants, one of which eliciting inhibitory responses, could induce a global inhibitory response (Economo et al., 2016). Again, selectivity of inhibitory patterns, domination of inhibition in binary mixtures of odorants, together with an only weak scaling between inhibition and total excitation argue against a global and center-surround mode of inhibition in M/T cell apical dendrites. Because GCs were found to only weakly impact slow (hundreds of ms) odor-evoked inhibition of M/T cell membrane potential or spike output (Fukunaga et al., 2014), they rather unlikely substantially contribute to the observation made in this imaging study.

In addition, a specific PG cell subpopulation expressing the potassium channel Kv3.1 presumably mediates potent intraglomerular feedforward inhibition, indiscriminately onto MCs, TCs and eTCs (Najac et al., 2015). This type of inhibition was even recruited by weak OSN stimulation (Najac et al., 2015).

Computation performed in the GL. Besides contrast enhancement, GL circuit is thought to play an important role in selectively gating M/T cell odor response at low concentration. Indeed, PG neurons have a lower activation threshold than eTCs and can prevent OSN-induced firing of M/T cells. Feedforward inhibition can therefore mediate a gain control mechanism over M/T cells (Gire and Schoppa, 2009; Najac et al., 2015). Alternatively, interglomerular inhibition could support input normalization. Given the spatially distributed activation of glomeruli at the surface of the OB, microcircuits are thought to mediate crosstalks across coactive glomeruli to perform computation such as normalization and pattern correlation/decorrelation. Notably, increase in odor concentration not only increases some glomeruli response and recruits additional glomeruli, but it also inhibits others. sSAC extend axons across several glomeruli, up to $1.5mm$ away (Aungst et al., 2003; Pinching and Powell, 1971a) and are thought to support interglomerular signaling in acute slices (Aungst et al., 2003). Taking advantage of the fact that a subpopulation of sSAC are both dopaminergic and GABAergic GL neurons, Banerjee et al. (2015) labeled and manipulated DAT^+ cells in the GL to ask this question *in vivo*. They found that odor responses of DAT^+ cells scale with concentration, and these neurons convey far-reaching divisive inhibition onto M/T cells, mediated through inhibition of eTCs. Moreover, a recent study showed that DAT^+ sSACs are also capable of gating sensory information –and thereby M/T cell output– at the level of OSN axons by activating presynaptic $GABA_B$ Rs and dopamine type 2 receptors (Vaaga et al., 2017). Interestingly enough, as a consequence of this normalization

mechanism, M/T cell odor responses were found to be more dissimilar at the population level (Banerjee et al., 2015). Therefore, it seems that sSACs, through their wide glomeruli innervation, permit computations in the GL such as odor response decorrelation and gain control in M/T cells population.

In addition, GL inhibition can shape M/T cell temporal activity. Indeed, by optogenetically manipulating GL GABAergic neurons selectively, Fukunaga and coworkers (2014) showed that GL inhibition regulates the temporal aspect of MC firing with regard to theta oscillations. Furthermore, the intraglomerular inhibition described by Najac et al. (2015) was found to promote spike timing variability of sister MCs.

In conclusion, despite the easy access to JG cells due to their superficial localization, the function of GL microcircuit has been addressed only recently. This is partly due to a historical focus on GC-MC interaction and partly to the great diversity of GL neurons that precluded cell-type specific investigations for a while (although this issue starts to be addressed *in vivo* as well, see Banerjee et al. (2015); Wachowiak et al. (2013)). Nevertheless, GL microcircuits are thought to gate sensory information transmitted to OB output cells, and to constrain spatial recruitment of M/T cell population.

4.3 Transformation by Granule cells

GCs are heavily reciprocally connected with M/T cells at the population level. Therefore, they are in good position to shape sensory representation by OB output cells. Multiple works demonstrated that alteration of GC activity influences sensory perception, and especially odor discrimination in mice (Abraham et al., 2010; Alonso et al., 2012; Nunes and Kuner, 2015; Nusser et al., 2001, to name just a few). It seems reasonable to suggest that GC's ability to accelerate or reduce odor discrimination learning involves pattern decorrelation and completion, respectively. Indeed, a recent study revealed a causal link between GC activity and pattern separation by M/T cells. By optogenetically activating or pharmacologically inhibiting GCs, Gschwend et al. (2015) showed that GC activity bilaterally alters similarity in M/T cell odor responses as well as behavioral performances. Interestingly, speed of discrimination learning, rather than odor discrimination *per se*, is often altered when GC activity is altered. In line with this observation, an *in vitro* imaging study reported odor responses kinetics in GCs with a time scale similar to odor discrimination (Kapoor and Urban, 2006). However, assessing GC synaptic impact on M/T cell activity is difficult because it can release GABA in response to somatic antidromic Na⁺ spikes, dendritic Ca²⁺ spikes, or in a local, spike-independent manner (see above, Egger et al., 2003, 2005).

Suprathreshold odor responses. Numerous preliminary studies have been limited to GC recordings in anesthetized mice (Cang and Isaacson, 2003; Labarrera et al., 2013; Margrie and Schaefer, 2003), but more recent studies investigated odor coding by GCs in awake mice. Electrophysiological recordings showed that GC spontaneous firing activity is low in anesthetized mice (Cang and Isaacson, 2003; Labarrera et al., 2013; Margrie and Schaefer, 2003) and is enhanced, and more broadly distributed across frequencies in the awake state (Figure 4.1,C; Fukunaga et al., 2014). For a direct comparison see Cazakoff et al. (2014); Kato et al. (2012). GC odor responses are sparse and excitatory in anesthetized mice (Cazakoff et al., 2014; Fukunaga et al., 2014; Labarrera et al., 2013) and were found somewhat more frequent and diverse in awake mice (Figure 4.1,D; Cazakoff et al., 2014; Kato et al., 2012; Wienisch and Murthy, 2016).

A recent two-photon imaging study by Wienisch and Murthy (2016) observed important additional properties of the GC response to odor stimulation. However, it is worth noting that these results were acquired in anesthetized animals and need to be confirmed in the awake state. First, GC responses were not linearly correlated to increasing odor concentration, and this property was due to inhibition on GCs (Wienisch and Murthy, 2016). Second, population response of GCs was correlated to the number of activated glomeruli and odors that sparsely activate glomeruli tended to activate non-random clusters of GCs (probably because they are activated by sister M/T cells). Finally, odor stimulation could elicit local Ca^{2+} transients in GC dendrites without affecting the soma (Wienisch and Murthy, 2016), supporting the notion that GC dendrites can release GABA in a somatic spike-independent manner, thereby inhibiting a restricted number of M/T cells. GC activity was increased in the awake mouse and can be responsible for the sparse representation of odor responses in M/T cells (Koulakov and Rinberg, 2011).

Infrathreshold odor responses. Intracellular recordings demonstrated that subthreshold excitatory responses (both "spikelets" and EPSCs) to odor stimulation are predominant and more frequent than spike emission (detected in $\sim 70\%$ of the cells; Figure 4.1,B; Labarrera et al., 2013), suggesting that GCs are broadly tuned to infrathreshold activity. Interestingly, odor presentation also triggered inhibitory responses in GCs, although much more sparsely, as observed by intracellular electrophysiological recordings (IPSCs, in $\sim 20\%$ of the cells, Cang and Isaacson, 2003; Labarrera et al., 2013) or two-photon imaging (Wienisch and Murthy, 2016). *In vitro*, GABAergic inhibition does not only regulate GC spike output but also shunts depolarization locally in the dendrites (Burton and Urban, 2015). This result suggests that inhibition can directly regulate subcellular calcium dynamics in GC dendrites and thereby recurrent or lateral inhibition onto M/T cells.

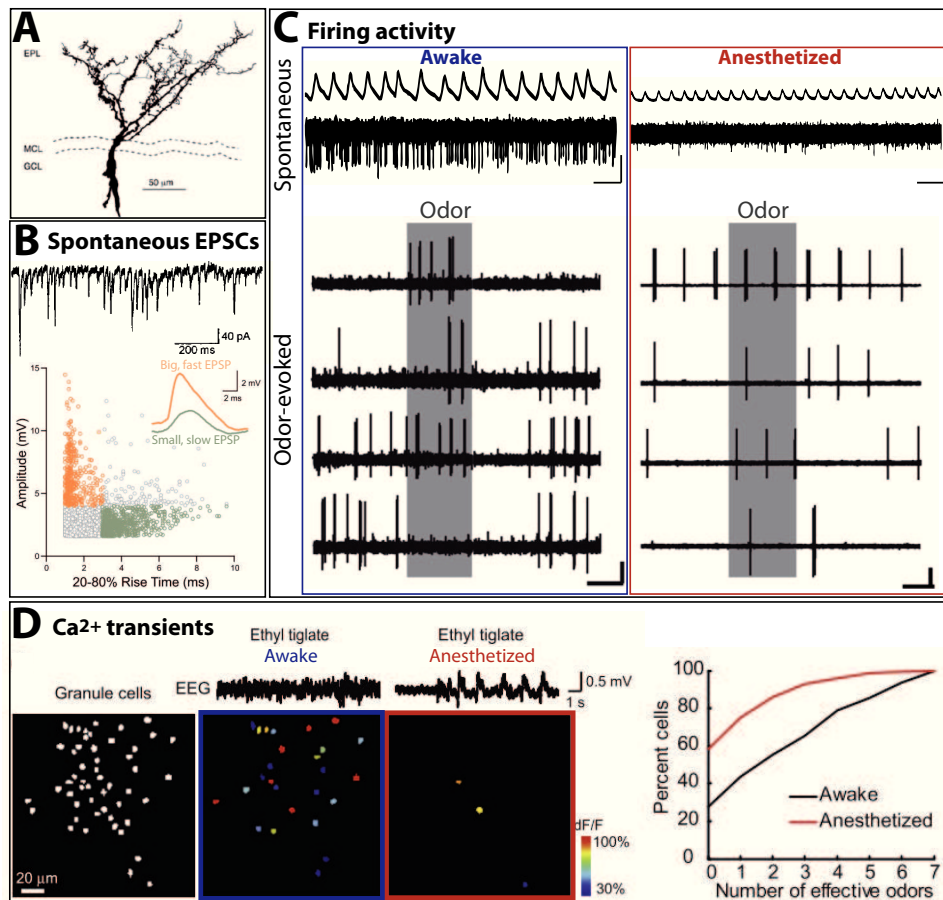


Figure 4.1 – Spontaneous and Odor-evoked activity in Granule Cells.

A. Reconstruction of a GC recorded *in vivo*. From Margrie and Schaefer, 2003

B. Spontaneous EPSCs in GC *in vivo*. (Top) Example trace from Cang and Isaacson, 2003. (Bottom) Two populations of EPSPs can be determined: fast, large EPSPs (orange) and slow, small EPSPs (green). Fast, large EPSPs are rhythmic and likely driven by cortical feedback inputs. From Youngstrom and Strowbridge, 2015.

C. Firing activity of GCs in the awake (left, blue box) and anesthetized (right, red box) states. (Up) Respiratory traces show the changes in sniffing activity during anesthesia. Spontaneous firing activity is higher in awake compared to anesthetized state. Scale bars are 1s and 1 mV. (Bottom) Odor-evoked activity is more heterogeneous in the awake state. In contrast to the anesthetized-state, GCs in awake mice variably responded to odor stimulation (gray box) with activation (awake trace 1), delayed onset activation (awake trace 2) and inhibition (awake trace 4) in response to different odors (gray shading shows time of odor presentation). Scale bars, 5mV and 1s (anesthetized), and 2mV and 1s (awake). From Cazakoff et al., 2014.

D. Ca^{2+} activity imaging demonstrates that odor stimulation evokes denser responses in the GC population of awake animals. (Left panels) Heatmap of an example population response to stimulation with ethyl tiglate in both the awake and anesthetized states. (Right) Summary data for the 336 granule cells recorded. The cumulative distribution of the number of GCs responding to an increasing number of odors (out of seven) confirms that GCs are more responsive to odors in the awake state (Kato et al., 2012).

Inhibition can arise from local dSACs (Boyd et al., 2012; Eyre et al., 2008; Pressler and Strowbridge, 2006) and/or from an external source (see the subsection 3.3).

In conclusion, *in vivo* GC recordings recently contributed to a good body of knowledge on different aspects: 1) GC activity is low in basal conditions and sparse following odor stimulation (although higher than in the anesthetized state), 2) Ca^{2+} transients can be local in dendritic spine or global in the entire tree, and 3) GC spines exhibit high structural plasticity. The main functions associated with GCs are the synchronization of M/T cells activity in the gamma range and the decorrelation of similar M/T cell population activity, that eventually leads to patterns separation (Figure 2.3).

4.4 Transformation by other Olfactory Bulb neurons

Odor coding by dSACs. To my knowledge, a single *in vivo* study recorded from putative dSACs. These extracellular recordings suggest that dSACs respond reliably, with short latency and with long-lasting spike trains to odor presentation (Labarrera et al., 2013), as suggested *in vitro* (Burton and Urban, 2015).

A class of external plexiform neurons implements gain control of M/T cell odor responses. Recent advances in molecular genetics and imaging permitted the investigation of odor coding by a class of GABAergic interneurons that received little attention so far: the PV-expressing neurons of the EPL.

Using rabies-based labeling of M/T cells presynaptic partners, Miyamichi et al. (2013) identified a prominent neuronal population in the EPL expressing the Ca^{2+} -buffer protein PV. Another study independently tackled the issue of odor coding by EPL PV+ neurons and its impact on M/T cells (Kato et al., 2013). The M/T cell-EPL PV+ neuron synaptic organization was found to be spatially broader than M/T cell-GC organization (Kato et al., 2013; Miyamichi et al., 2013), and their reciprocal connectivity was greater than the M/T cell-GC one (Kato et al., 2013). Using targeted electrophysiological or optical recordings, the two studies further found that PV-expressing neurons in the EPL are broadly tuned to odor stimulation (more than M/T cells and GCs; Kato et al., 2013; Miyamichi et al., 2013), and preferentially respond with an increase in their firing rate (Miyamichi et al., 2013). Interestingly, Kato and coworkers (2013) showed that pharmacological suppression of EPL PV+ neuron activity enhances M/T cells odor-evoked activity, without affecting the tuning curve. Indeed, EPL PV+ neurons have a divisive effect on M/T cell odor tuning both at the individual and at the population levels (Kato et al., 2013). Although gain control is

largely thought to emerge from GC-to-M/T cell interaction (Soucy et al., 2009), these two studies shed light on an additional microcircuit, located in the EPL, able to tweak M/T cell odor tuning properties.

Now that we saw how different elements of the OB respond to olfactory stimulation, I will describe below how M/T cells, the OB output channels, respond to odor stimulation.

4.5 Odor responses in M/T cells

In anesthetized animals, odor stimulation induces both excitatory and inhibitory responses in M/T cells. The responses were observed at the firing level as well as at the voltage membrane potential level (Figure 4.2,A; (Bathellier et al., 2008; Cang and Isaacson, 2003; Davison and Katz, 2007; Economo et al., 2016; Fukunaga et al., 2012; Rinberg et al., 2006). As in anesthetized animals, odor stimulation evokes both inhibitory and excitatory events in M/T cells in the awake mouse (Shusterman et al., 2011; Yamada et al., 2017). However, firing rate changes were found to be weak and sparse (Figure 4.2,B; Cury and Uchida, 2010; Gschwend et al., 2012; Otazu et al., 2015; Rinberg et al., 2006; Shusterman et al., 2011, but see also Gschwend et al., 2016, suggesting that natural odors activate a denser array of M/T cells than observed with monomolecular odors). These results are in agreement with an early study by Kay and Laurent (1999) showing that only 11% of M/T cells responded to odor stimulation in freely behaving rats. Direct comparison between anesthetized and awake states came to similar conclusions, both using calcium imaging (Kato et al., 2012) and electrophysiology (Davison and Katz, 2007; Kollo et al., 2014; Rinberg et al., 2006). Although sparse coding can be an effective way to encode information in the OB (see Koulakov and Rinberg, 2011), this observation raises the question whether or not odor information can be solely coded by a change in firing rate in M/T cells (rate coding).

In contrast, response patterns and kinetics were found to be more diverse in the awake state compared to anesthetized animals (Cury and Uchida, 2010; Davison and Katz, 2007; Gschwend et al., 2015; Shusterman et al., 2011). Notably, M/T cells can respond to odor stimulation with an increase or decrease in activity during or after stimulation, or with a more persistent change in firing activity that lasts beyond odor exposure (Bathellier et al., 2008). Therefore, data obtained from awake animals ask whether M/T cell temporal dynamics could be used for coding odor information in downstream regions. M/T cell odor responses can be investigated in relation to several temporal scales.

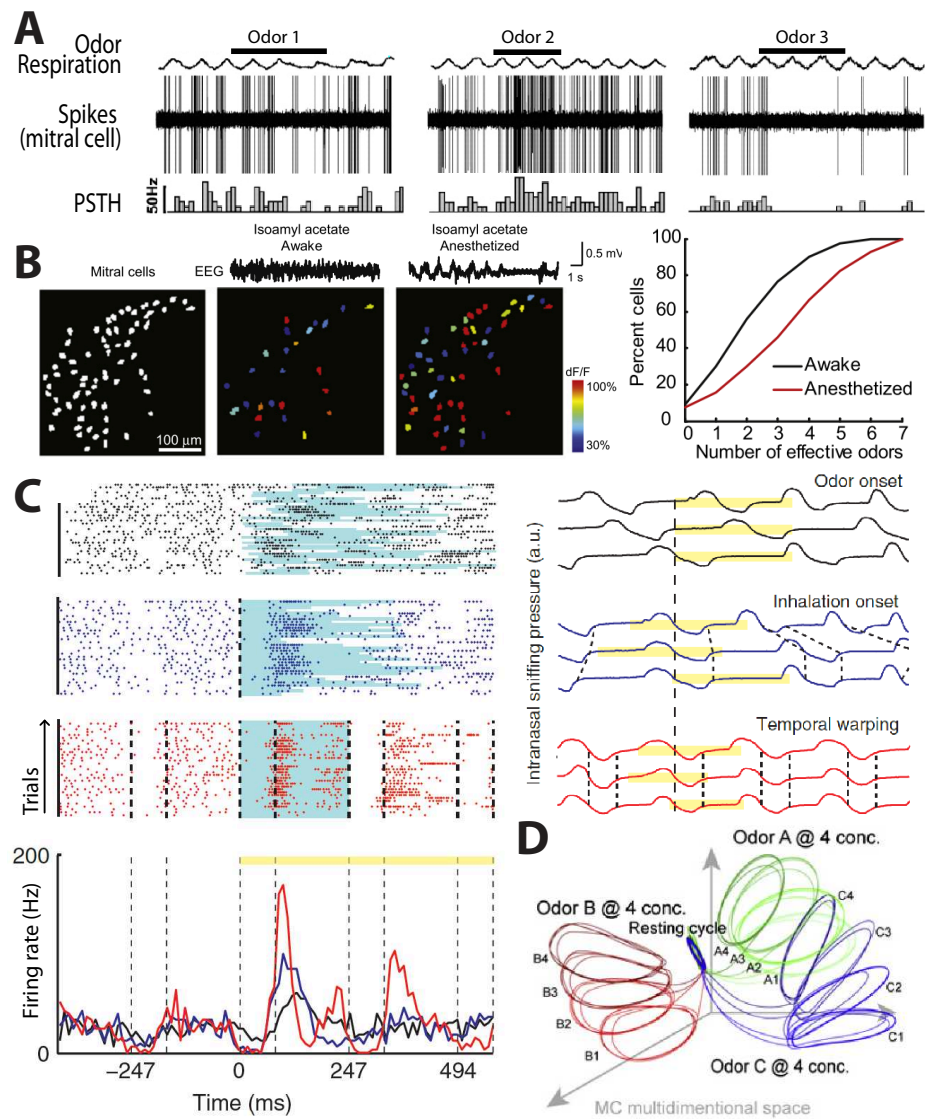


Figure 4.2 – Multiple Odor response properties in Mitral and Tufted cells.

A. Firing rate coding in anesthetized animals. Up: odor stimulation (dark bar) and respiration trace. Middle: MC spikes (each vertical bar is a spike). Bottom: Peri-stimulus time histogram (PSTH): averaged firing rate around the odor presentation time across multiple repetitions. The example cell shown does not responding to odor 1 (left), responds with an increase in firing rate to odor 2 (middle), and a decrease in firing rate to odor 3 (right). From Nagayama et al., 2004.

B. Ca^{2+} activity imaging showing that MC population response to odor is sparser in the awake state, consistent with broader tuning of GCs. Left: example MC population response. Right: summary data from 340 MCs. From Kato et al., 2012.

Figure 4.2 (Continued) – C. Temporal coding with the respiratory cycle. Responses to odor stimulation are either aligned to odor onset (black), inhalation onset (blue) or "temporally warped", in order to normalize the duration of the respiratory cycle (red; see right panel). Raster plot (each line represents a trial and each tick is a spike) and PSTH plots for a mitral/tufted cell in response to an odor stimulus, synchronized by odor onset (black), inhalation onset (blue) and temporally warped (red). The light blue lines underlying the raster plots indicate the duration of the first sniff after odor onset. Yellow bars indicate the stimulus duration. Dashed lines indicate the beginning and the end of the inhalation intervals. From Shusterman et al., 2011

D. M/T cell population dynamics over slow, non-oscillatory time scale. MC responses to odors are complex and vary over time, even after odor offset. To represent the population response over time, firing responses of a large number of recorded neurons can be simultaneously considered by putting them together in a population vector. Each row represents an individual neuron activity over time, and every column represents a snapshot of the neuronal population activity in a defined time bin. It is important to note the difference with the averaged population firing, as population vectors preserve the specificity of individual neural responses. The population activity over time is then plotted as a trajectory in a multidimensional space (the space of all recorded neurons). In the example depicted here, three odors were tested (A, green; B, red; C, blue), at four different concentrations each (1, 2, 3, 4). MC population activity describes a circle at resting state and evolves to another cyclic activity following odor presentation (in $\sim 1s$). After odor offset, MC population activity goes back to resting state. Repeated odor presentation evokes a reproducible activity pattern and changes in odor concentration evoke similar cyclic trajectories. However, odor cycles can be more different between two different concentrations of the same odor than between different odors. From Bathellier et al., 2008.

M/T cell odor responses are locked to sniffing. M/T cells spontaneous activity is weakly phase-locked in awake compared to anesthetized animals (compare Fukunaga et al., 2012, 2014; Markopoulos et al., 2012; Phillips et al., 2012 and Cury and Uchida, 2010; Fukunaga et al., 2012; Lepousez and Lledo, 2013; Shusterman et al., 2011, for example). Notably, M/T cell voltage membrane potential is also phase-locked to the respiratory cycle (Fukunaga et al., 2012, 2014; Margrie and Schaefer, 2003; Youngstrom and Strowbridge, 2015).

In anesthetized animals, odor stimulation leads to phase-locked theta burst-spiking activity in M/T cells (Cang and Isaacson, 2003; Margrie and Schaefer, 2003). Sniff-locked theta bursts in M/T cells are reliable across respiration cycles, but present a progressive decrease in action potential latencies (Cang and Isaacson, 2003; Margrie and Schaefer, 2003). Sniffing is actively modulated in awake animals, notably during odor presentation (Kepecs et al., 2007; Uchida and Mainen, 2003). Nevertheless, when M/T cell odor responses are aligned to the inhalation onset (Cury and Uchida, 2010) or temporally warped (such that sniff cycles are aligned to the same phase and theta durations are normalized to the average value; Figure 4.2,C; Shusterman et al., 2011; Smear et al., 2011), phase-locked responses were also observed in awake mice. In addition, spike timing was found to depend on odor identity (Cury and Uchida, 2010; Gschwend et al., 2012; Shuster-

man et al., 2011). These transient changes in firing rate within a respiratory cycle are often obscured in analyses examining averaged firing rate independently of the respiratory cycle. Synchronization of sister M/T cells that fire at similar phases of the sniff cycle diverges in response to odor stimulation (Dhawale et al., 2010). At the population level, odor-evoked responses are not so sparse in the OB of awake animal when taking into account the temporal changes in M/T cell firing activity, (15 – 60% of M/T cells respond to an odor; Cury and Uchida, 2010; Gschwend et al., 2012; Shusterman et al., 2011).

M/T cell odor responses in relation to fast oscillatory rhythms.

Fast oscillatory cycles are prominent in awake animals, but not in anesthetized preparations. In awake mice, M/T cell spiking activity is also modulated by gamma (Buonviso et al., 2003; Lepousez et al., 2013). Furthermore, it seems that any neurons in the network fire in synchrony during gamma episodes (Friedrich et al., 2004; Laurent and Davidowitz, 1994). However, a synchronized neuron does not necessarily fire at every gamma cycle and can skip several oscillatory cycles (Bathellier et al., 2006; Friedrich et al., 2004; Lagier et al., 2004). The power of gamma oscillations increases in animals when they have to perform a difficult discrimination task (Beshel et al., 2007), gamma oscillations respond differently to odors, and spike phase synchronization of a subset of M/T cells in the gamma band differs between odors (Li et al., 2015). In addition, manipulation on gamma oscillations often altered behavior (see for example: Lepousez and Lledo, 2013; Nunes and Kuner, 2015). Therefore, gamma band oscillations are presumed important for odor processing, but it is not clear through what mechanism.

M/T cell dynamics at slower, non-oscillatory time scales.

When odors are presented to an animal, responses usually exhibit complex activities, with delayed or long-lasting activation, or responses at odor offset, etc. (see for example Bathellier et al., 2008). To overcome individual responses diversity, investigators performed population activity analyses. To do so, the firing response of a large number of neurons is considered using a population vector. It is important to note here that the population vector is different from the averaged population firing since population vectors preserve the specificity of individual neuronal responses. Indeed, the dimension of a population vector is equal to the number of neurons composing this vector.

These slow patterns of principal neurons were first found in the fish OB (Friedrich and Laurent, 2001) and antennal lobe of insects (thought to be the functional equivalent to the OB; Laurent and Davidowitz, 1994). They have later been reported in the OB of the anesthetized mouse (Figure 4.2,D; Bathellier et al., 2008). Initially, M/T cell population activity is in a resting state, but following odor stimulation, trajectories start to transition to an

odor steady-state, reached within a second or so. This odor steady-state lasts until the odor offset, and then evolves back to the resting state (Bathellier et al., 2008; Friedrich and Laurent, 2001; Mazor and Laurent, 2005). Interestingly, these patterns become less similar (decreasing in population correlation) within seconds after stimulus onset, as it has been observed in the mammalian OB (Bathellier et al., 2008), fish OB (Friedrich and Laurent, 2001) and insect antennal lobe (Brown et al., 2005; Stopfer et al., 2003). This observation raises the possibility that slow mechanisms can serve as a contrast enhancement mechanism. To date, no study has investigated whether slow, non-oscillatory population dynamics also exists in awake mice and whether it could decorrelate population firing activity.

4.6 Olfactory code in the Olfactory Bulb

Detailed knowledge about the underlying physiology enables studying the function of the OB, which consists in transformation and transmission of the sensory inputs to the rest of the brain. After having described how OB neurons respond to odor stimulation, I will now expose current opinions regarding the way OB output neurons might encode olfactory information. It is worth noting here that M/T cell activity changes with odor stimulation should be considered as a code only if it can be read out by downstream neurons. Precise data on APC organization – for instance – is currently available, but detailed information about how it could decode information from M/T cells is still lacking. Nevertheless, information decoding by cortical structures is an active field of research (see for example Bolding and Franks, 2017) and the coming years should provide more knowledge on that issue.

Time constraints for the olfactory code. A code is only relevant if the timescale needed to build it is smaller than the animal’s behavioral response. To investigate the time needed for rodents to discriminate between odorants, experimenters used operant conditioning odor-reward association tasks. Mice can discriminate odor pairs with high accuracy in less than 200ms (Abraham et al., 2004; Uchida and Mainen, 2003), which is only a fraction of a sniff. In a task where mice are free to lick at any time following odor onset, performance were not dependent on whether mice took only a single sniff or more (Cury and Uchida, 2010). This data suggests that a single sniff contains enough information for high accuracy discrimination. In contrast, when mice were challenged with more difficult discrimination, the time the animal took to perform with high accuracy increased significantly (an additional 70-100 ms, Abraham et al., 2004). In a more recent study, the authors presented the odors for short and controlled durations and observed that accuracy not only depends on the difficulty of the task but also on the sampling time (Rinberg and Gelperin, 2006). High accuracy was obtained for

difficult tasks with discrimination time about $600ms$. These studies introduce the notion of speed-accuracy tradeoff in olfactory discrimination, where temporal integration of M/T cell spiking activity over wider time scales is necessary for fine odor discrimination.

However in these behavioral experiments, timing is not purely constraint by olfactory mechanisms but also comprises the decision time and motor output. In this view, Wesson and colleagues took a different approach: they directly imaged Ca^{2+} transients in head-restraint rats performing an odor-discrimination task (Wesson et al., 2008a,b). Doing so, they found that the delay between the first sniff and the first odor-evoked calcium response was $\sim 100 - 150ms$. Therefore, the total time for olfactory perception, decision making and motor command could be compressed in less than $100ms$ in easy discrimination tasks. In a similar two-alternative choice discrimination task, head-restraint mice were found to reach 75% accuracy in less than $150ms$, using low concentration and non-trigeminal odorants (Resulaj and Rinberg, 2015). Therefore, it appears that olfactory discrimination *per se* can be achieved in a fraction of a sniff. It would be interesting to record M/T cell activity in an odor discrimination task and to calculate when population odor response significantly diverges, in order to ask what is the timescale for encoding odors purely at the OB level. However, this might not be difficult to address since broad-scale imaging achieved by Ca^{2+} imaging might be too slow to detect such rapid changes in activity.

In addition, one should keep in mind that the discrimination tasks widely used to address the speed of olfactory perception are relatively simple from a computational point of view (discrimination between two odors, even if they are hard to distinguish) and therefore might involve a different –and faster?– code than computationally more difficult tasks. Besides, operant conditioning might bias the animals to use an olfactory code that it learned, in order to be more efficient for performing the task. Different codes might be used in naive animals. Indeed, it was recently shown that the level of difficulty in a discrimination task profoundly impacts M/T cell odor representation and population decorrelation (Chu et al., 2016).

Because olfaction is highly dependent on rhythmic activities, temporal patterning of emitted spikes has been proposed to encode odor information. The broad definition of a temporal code I will use here is as follows: any neuronal response where spike timing carries information to a downstream decoder.

Coding with the sniff cycle. Spike timing related to the sniff cycle has been proposed to encode odor information. Indeed, M/T cells first spike latency has been demonstrated to depend on odor identity and intensity (Margrie and Schaefer, 2003) and theta oscillations were later shown to enhance spike precision (Schaefer et al., 2006). The authors then built computational

models showing that a latency-based coding 1) has a larger capacity (i.e. number of odors that can be encoded) than a spike-count or an instantaneous firing rate-based coding (Margrie and Schaefer, 2003) and 2) permits a high level of stimulus discrimination (Schaefer et al., 2006). However, M/T cell firing in awake animals is higher and therefore it introduces noise in the onset of the odor-driven activity. In a more recent study investigating the odor code in awake animals, decoding using the first spike latency performed poorly compared to decoding with subsniff patterns (see below; Cury and Uchida, 2010). However, it is important to note that odor stimulation evokes similar responses in MCs and TCs, as assessed by two-photon imaging (Yamada et al., 2017), but induces a phase-shift in the temporal coding of MC, but not TC, toward spiking at earlier phases of the respiratory cycle (Fukunaga et al., 2012). This shift was found to be more pronounced at higher odor concentrations (Fukunaga et al., 2012). Therefore, a subset of neurons might still be able to code odor properties with latency to the first spike.

In a study looking at the information contained in finer timescales, the authors found that subsniff response patterns allowed better discrimination between odorants than total spike count from the entire respiration cycle, and were best predictive of the behavioral performance of the animal (Cury and Uchida, 2010). Furthermore, the authors found that most of the information was contained within the first 100ms after inhalation onset. Interestingly, the subsniff pattern of the odor-evoked response was conserved between slow and high-frequency respiratory activity. However, it is not clear what could be encoded during subsniff patterns.

Coding with gamma oscillations. Gamma rhythm emerges from the synchronous activity of M/T cells and GCs in the OB. Synchronously active neurons are more likely to drive suprathreshold activity in a common downstream neuron than asynchronous inputs. Since M/T cells neurons are not equally synchronized to gamma oscillations (see for example Lepousez et al., 2013), increasing synchrony in an ensemble of M/T cells could strongly increase its impact onto downstream cortical neurons. This requires downstream neurons to be embedded into an appropriate bandpass filtering network, which was shown to be the case for APC neurons due to the delayed feedforward inhibition they receive (Stokes and Isaacson, 2010). In the insect antennal lobe, a projection neuron spike was proved more likely to have a significant impact on the downstream neuron if it fires in phase with fast oscillations (Perez-Orive et al., 2002). In the zebrafish in contrast, dorsal telencephalon neurons – the functional analog of the olfactory cortex – were found to act as a lowpass filter and as such, render neurons largely insensitive to M/T cell synchronous activity (Blumhagen et al., 2011).

By this means, M/T cell assemblies could encode odor information without changing their firing rate. Phase-locked spikes might also be used in ad-

dition to non phase-locked spikes to carry a different type of information. For instance, when mice were engaged in discrimination tasks, it was found that coherence between M/T cell spikes and gamma oscillations increased, and this could convey relevant information to discriminate the odors, regardless of their associated value (Li et al., 2015). Conversely, overall spike firing and sniff-locked responses progressively diverged with learning of the outcome associated with the odors (Li et al., 2015), and M/T cells can change their response polarity with change in the odor-reward association (Doucette and Restrepo, 2008). According to this scenario, overall spike firing rate or sniff-locked responses seem to code for odor values, while gamma-locked spikes would rather code for odor identity. Interestingly, the use of a combination of olfactory codes was also found in the fish, but in this case phase-locked spikes were coding for odor categorization while non phase-locked spikes were coding for odor identity (Friedrich et al., 2004).

At the behavioral level, the power of gamma oscillations was enhanced in rats performing a difficult discrimination task (Beshel et al., 2007), and enhancing odor-evoked gamma oscillation as well as increasing synchronization of M/T cells to that cycle led to a decrease in odor mixture discrimination and an increase in odor sampling time (Lepousez and Lledo, 2013). Finally, a study analyzing odorant information conveyed by M/T cells suggests that gamma oscillations can provide the optimal temporal clock for spike integration (Gschwend et al., 2012). Therefore, proper gamma oscillations seem to be important for odor coding, either by synchronizing M/T cell activity and thus enhancing their impact on downstream neurons, or/and by setting a clock that downstream neurons can read for input integration.

Coding with slow timescale. We have seen before that odor stimulation evokes slow pattern at the population level, which evolves over time to reach a steady-state at around 1s after odor onset. Odor discriminability increases in time (Friedrich and Laurent, 2001; Mazor and Laurent, 2005). However 1) maximum decorrelation was reached at the steady-state in fish OB (Friedrich and Laurent, 2001) while it was highest at the time of maximum velocity of the population vector in insect antennal lobe (Mazor and Laurent, 2005) and 2) available data in mice suggest that discriminability of odor representation over the slow time scale does not improve over time (Bathellier et al., 2008). However, data in mice were acquired from anesthetized mice and it is not known how ensemble dynamics behave in awake rodents.

Coding with summed firing rate. A computational model has shown that rate coding is sufficient for accurate odor classification (Bathellier et al., 2008). However, this model was based on data from anesthetized animals, where basal firing rate are lower and odor-evoked responses are more prominent and greater than in the awake state. Nevertheless, sparseness of neu-

ronal responses (both in terms of number of responding M/T cells, but also in term of temporal sparseness, i.e, transient activity) might be efficient enough for robust olfactory coding (Koulakov and Rinberg, 2011). In addition, studies from the group of Restrepo suggest that firing rate changes might still code odor information, and notably odor quality (value) rather than identity. Indeed, M/T cell population tended to increase firing rate to the rewarded odor but not to the unrewarded one. This association switched when odor contingencies were switched (reversal learning; Doucette and Restrepo, 2008). Furthermore, overall firing rate diverged when learning the odor-reward association task, and this was no true when the animals were passively exposed to the same odors (Li et al., 2015)

Conclusion. To conclude, M/T cell activity is influenced in many ways by odor stimulation at different time scales. At the population level, M/T cells sparsely change their overall firing rate during odor presentation, but finer changes in temporal activity, recruiting a greater number of cells, can be detected in addition (such as subsniff patterns, latency to the first spike with regard to sniff oscillations, gamma band synchrony, or integration using the gamma band as a clock). In contrast, slow population trajectories might also serve to decorrelate odor-evoked neuronal activity. Importantly, studies by Smear and colleagues (2013; 2011) used light-activation of OSN to test several coding hypotheses. They show that mice can behaviorally read temporal patterns of OSN axon activity when multiple glomeruli were activated (Smear et al., 2011), or when activating a single glomerulus, but at different phases of the sniff cycle (Smear et al., 2013). This time code was shown to be readable by olfactory cortex neurons (Haddad et al., 2013). Furthermore, stimulation of a glomerulus which was not recruited by an odor led to the perception of a different odor object. This suggests that the precise glomerular map activated by odors also carry meaningful information and exact spatial patterns are important for odor perception (Smear et al., 2013). This raises the problem of odor mixture segmentation, i.e, the ability to identify individual odorants against a background of odors. Recently, it was shown that mice can identify a single odor in a mix of up to sixteen background odors (Rokni et al., 2014). However, the way the "olfactory cocktail party" problem (by analogy with the cocktail party in audition) is solved is not known, especially since non-linearity phenomena arise between odorants in the olfactory system (notably at the GL level, see Homma et al., 2013; Wachowiak et al., 2013).

Apart from the APC, little is known about the decoding capacities of OB downstream areas. Because different regions of the olfactory cortex receive parallel inputs directly from the OB, one can hypothesized that different olfactory cortical regions process different types of olfactory information. Optogenetic studies support this idea. Indeed, inactivation of OB-to-Cortical

amygdala, but not OB-to-APC or OB-to-Olfactory Tubercle, projections abolished innate behavioral responses (Root et al., 2014a). Furthermore, M/T cell synchronous activity in fish was ineffective in driving dorsal telencephalon neurons as mentioned before, but LFP recordings show that it might well be processed in another area of the telencephalon (Blumhagen et al., 2011). Therefore, the olfactory cortices could function as parallel associational cortices (with different regions integrating different odor properties such as odor identity, odor quality, or innate behavior), rather than functioning as a hierarchically-organized cortex like the visual cortex (where higher hierarchical areas process more complex features of the visual field). Thus, it will be interesting to address whether different OB downstream brain regions read different codes or if they read the same code differently.

Through multiple examples, we saw in this section that the animal internal or brain state heavily influences M/T cell basal and odor-evoked activity. Indeed, M/T cells spontaneous activity is higher (Kollo et al., 2014) and more weakly phase-locked in awake compared to anesthetized animals (compare Fukunaga et al., 2012, 2014; Markopoulos et al., 2012 and Cury and Uchida, 2010; Lepousez and Lledo, 2013; Shusterman et al., 2011, for example). Fast oscillations such as beta and gamma regimes are also largely dependent on the brain state. Gamma oscillations emerge in awake animals while beta oscillations are associated with learned odor-reward associations (Kay, 2014). Thus, the overall OB network is sensitive to the animal brain state. Notably, GC spontaneous activity was lower in anesthetized mice compared to awake ones (Cazakoff et al., 2014; Kato et al., 2012), and the strength of the dendrodendritic synaptic inhibition was modulated by waking and distinct rhythms during anesthesia (slow and fast waves anesthesia, thought to recapitulate slow and fast waves sleep; Tsuno et al., 2008). The effect on the dendrodendritic synapse is mediated by cholinergic transmission, likely arising from the basal forebrain (Tsuno et al., 2008) and since GCs are heavily innervated by top-down fibers, centrifugal inputs are in good position to mediate such brain state-dependent changes in olfactory responses. Centrifugal influences onto olfactory coding and behavior will be reviewed in the following section.

4.7 Cortical influences on olfactory coding and behavior

The OB receives centrifugal projections from its output regions and neuromodulatory brain centers and these top-down inputs strongly impact OB neurons and M/T cell odor responses *in vivo* (See chapter 3). These inputs were proven crucial for maintaining OB oscillations (Gray and Skinner, 1988; Martin et al., 2006; Neville and Haberly, 2003). Centrifugal inputs manipulation, and notably neuromodulatory fibers, has been associated with

a variety of behavioral deficits, yet, their precise influence on odor coding remains highly debated. In this section, I focus on the description of glutamatergic feedback influences on olfactory coding. For a review of the impact of cholinergic and noradrenergic impact on OB sensory coding, see Devore and Linster (2012).

OB odor responses are modulated by centrifugal inputs. In a previous chapter (Chapter 3), we have seen that centrifugal inputs profoundly impact OB neuron and network activity. Notably, functional dissociation between the centrifugal inputs and the OB altered bulbar oscillations (Gray and Skinner, 1988; Martin et al., 2006; Neville and Haberly, 2003) and resulted in impaired formation of odor-reward memories, but not spontaneous odor discrimination (Kiselycznyk et al., 2006).

In addition, previous exposure to an odor decreases OB responses to that odor only, but anesthetized animals did not show that adaptation, even if the animal was awake during the initial exposures, suggesting that adaptation is an active strategy (Kato et al., 2012). Furthermore, an early study by Kay and Laurent (1999) showed that only $\sim 10\%$ of M/T cells were responding to odorants, but $> 90\%$ exhibited some modulation by the task contingencies. Similarly, Pager (1983) found that various internal states related to nutrition influence M/T cell responses to food odors. Recently, our collaborators and us showed that fasting induces cannabinoid release in the OB of rodents, which binds cannabinoid type 1 receptors at the cortical axon-to-GC synapse and depresses glutamate release (Soria-Gómez et al., 2014). We further showed that genetic deletion of cannabinoid type 1 receptors selectively at cortical axons is sufficient to suppress fasting-induced hyperphagia (Soria-Gómez et al., 2014). To my knowledge, this is the first study tackling the important role of modulation of feedback axon activity.

Centrifugal fibers also affect learning. Indeed, during odor discrimination learning, M/T cell responses to the rewarded and to the unrewarded odors synchronize and diverge, respectively (and these changes switched during reversal learning; Doucette et al., 2011; Doucette and Restrepo, 2008). Synchronization between M/T cells during odor learning was shown to be partially dependent on noradrenergic signaling (Doucette et al., 2011). Similarly, MC odor response population patterns to the rewarded and unrewarded odors were found to decorrelate across days during an odor discrimination learning, and cortical top-down inputs could participate in this phenomenon, as assessed by computation (Yamada et al., 2017). Finally, odor learning, but not passive odor exposure, induced an increase in the average density of spines on GC proximal dendrites, presumably due to increase activity at the AOC-to-GC synapse (Lepousez et al., 2014). Remarkably, AOC stimulation evoked stronger EPSCs onto GCs in the odor learning condition (Lepousez et al., 2014). Odor discrimination learning decorrelated MC, but not TC,

population activity evoked by both the rewarded and unrewarded odors, and dissimilarity in MC population activity was more predictive of the animal performance than dissimilarity in TC population activity (Yamada et al., 2017). Thus, pattern separation in OB output neurons was correlated with behavioral performance (Gschwend et al., 2015; Yamada et al., 2017). Consistently, pharmacological inactivation of the APC increases M/T cell odor responsiveness (Otazu et al., 2015). Interestingly MC odor responses were more affected than TC odor responses during APC inactivation (Otazu et al., 2015).

Centrifugal inputs influence OB computations. Therefore, it appears from these studies that cortical feedback allows task- and context dependent control of OB responses. A recent article put into perspective a computational model of the cortico-bulbar loop, and this model could reproduce several experimental results (Zhaoping, 2016). Notably, the cortico-bulbar loop could be used to unspecifically increase discrimination sensitivity of OB neurons by a population gain control. This enhances high-frequency responses of modeled M/T cells. In reality, mice could learn the ideal level of cortical feedback to increase their sensitivity to the right level in a task- and context-dependent manner. For example, it was reported in mice that neuronal representations diverged during a difficult task, but not for an easy task (Chu et al., 2016), suggesting that feedback control is engaged during the difficult, but not the easy, task. Another application of Zhaoping’s model is related to the “olfactory cocktail party” problem. The model predicts that in order to identify a target odor in a mixture of many (Rokni et al., 2014), centrifugal feedback is engaged to specifically enhance sensitivity to the targeted odor (Zhaoping, 2016). To answer the same theoretical question of odor mixture segmentation in a world composed of an extremely large set of odors, Grabska-Barwinska and colleagues (2017) used a different approach. The authors used a Bayesian approach to model the early olfactory system (OB and olfactory cortex, dynamically and reciprocally connected): neuronal activity evoked by an odor was transformed into a probability distribution of a set of odors. This model was able to reproduce the data obtained experimentally by Rokni et al. (2014). Moreover, this model makes some experimentally addressable predictions (Grabska-Barwińska et al., 2017). First, inhibition from GC to MC should be divisive. However, testing this prediction requires to understand the neuronal code used by M/T cells and their input/output relationship. Second, the model predicts that when an unknown odor is presented, many granule cells should fire, but at low rates. In contrast, when a known odor is presented, a small fraction of granule cells should fire, but at relatively high rate. In addition to having the capacity to demix odors, this probabilistic way of coding information for the brain might explain how we develop the amazing ability to segment stimuli of the external world.

Centrifugal fibers have a tremendous impact on odor coding by the OB. In fact, the code used by OB neurons might only make sense when refined by top-down inputs. In other words, OB neurons might code odor information in a task- or context-dependent manner. Therefore, finding the code used in the olfactory system might not be as straightforward as finding the code used in the different regions involved in olfactory perception until the odor object is eventually recognized. Rather, it might need considering centrifugal activity, which impacts odor encoding.

Part II
Results

Results

This thesis work focuses on the study of the regulation and function of cortical feedback inputs to the OB. Existence of these cortical feedback innervating the OB has been suggested by Ramon y Cajal anatomical work, more than a century ago (1911). Following this discovery, a great amount of work has focus on exploring the localization of the brain centers emitting these top-down fibers and the distribution of the cells within the identified structure. Distribution of the descending fibers across the OB layers, and originating from the different brain regions, has also been extensively studied. However, study on the physiology of cortical feedback inputs has been poorly investigated until recently and their function remains largely unknown. In addition to initial technical challenges, there are at least two important reasons why cortical feedback function is poorly understood. First, regulation of feedback activity has been documented in a single study to my knowledge (Soria-Gómez et al., 2014). Second, the diversity of the cortical feedback is largely underestimated, both in regards to the cortical subdivisions and in regard of their neurochemical content.

Development of genetically encoded proteins to selectively manipulate or monitor the activity of cortical axons *in vivo* now permit selective investigation of their contribution to sensory processing and the establishment of causal relationship between their activity and behavior. In this work, I investigated the regulation of the well-known glutamatergic cortical feedback inputs in the OB, and the functional impact of this regulation (Section "1"). In a parallel study, I discovered and investigated a new class of cortical feedback: an inhibitory feedback originating in the anterior olfactory cortex. The connectivity of these long-distance GABAergic connections, as well as their natural regime of activity and their functional impact on OB neurons and mouse behavior are then explored (Section "2").

Chapter 1

Cortical top-down inputs to the olfactory bulb are regulated by GABA_BRs (Article 1)

1.1 Results from the article

The OB is the first brain region for olfactory information processing, only one synapse away from sensory neurons. However, it is massively innervated by a diversity of brain regions, such as the olfactory cortex and neuromodulatory centers in the brainstem and the basal forebrain. These descending inputs are diverse in terms of chemicals they release and the brain regions they originate from are thought to play distinct roles in sensory processing and behavior (ACh from the basal forebrain is thought to be involved in attention and arousal, serotonin from raphe nuclei in learning-associated behavior, glutamatergic inputs from the olfactory cortex in discrimination and memory, etc). Because all the regions targeting the OB widely innervate other brain regions (and this also true for the olfactory cortex), a local regulation of centrifugal axon terminals would be efficient in altering synaptic transmission to the OB while leaving transmission to other targeted regions unaffected.

Immunohistochemical labeling directed against the subunit 1 of the GABA_BR produces dense labeling in the GL, weak labeling in the EPL, but also moderate labeling in the GCL. Labeling in the GL and EPL have already been associated with presynaptic GABA_BR expression at OSN terminals and GC apical dendrites, respectively (Aroniadou-Anderjaska et al., 2000; Isaacson and Vitten, 2003; Valley et al., 2013). However, no functional expression was reported in the GCL. Because the main synaptic element in the GCL in the synapse between top-down axons and GCs, we examined this synaptic transmission in presence of drug modulating GABA_BR activation.

To gain control over cortical top-down axons, we injected the light-gated ion channel channelrhodopsin 2 (ChR2) in the primary or anterior olfactory cortex (AOC, which comprises both the AON and APC). Light-stimulation of cortical ChR2⁺ axons in the OB produced monosynaptic excitation as well as disynaptic inhibition in GCs. Both of them were blocked by the GABA_BR agonist baclofen and restored with the GABA_BR antagonist CGP 52432 (here named CGP for clarity; Figure 1). Thus, both direct (excitatory) and indirect (inhibitory) cortical axon-to-GC pathways were found to be modulated by GABA_BRs. Similarly *in vivo*, light-stimulation of cortical axon terminals elicit a GABA_BR-modulated field EPSP (fEPSP), which reflect GC depolarization (Figure 2A-D). Together, these results show that functional GABA_BRs are expressed at the cortical axon-to-GC synapse. To investigate whether GABA_BRs are expressed presynaptically at cortical axon terminals, we utilize a genetically engineered mouse with a "floxed" GABA_{B1} gene (Haller et al., 2004). In these mice, Cre expression recombine the GABA_{B1} gene, leading to non-functional GABA_BRs. We thus co-injected AAVs expressing the Cre recombinase or a Cre-dependent version of ChR2 in the AOC of these mice and showed that immunoreactivity in the GCL was selectively decreased compared to wild-type animals (Figure 2G). Thus, GABA_BRs are expressed at least at presynaptic cortical axons. In mice lacking GABA_BRs in the AOC and their cortical axons (AOC^{GABA_B-/-} mice), we found no effect of baclofen on the fEPSP (Figure 2E). Therefore, functional GABA_BRs are expressed mainly at presynaptic cortical axons to the OB and depress transmitter release to GC upon activation. Next, we addressed the functional consequence of this regulation on the OB output cells: M/T cells. Consistent with a depression of the cortical drive to GCs, baclofen depressed the light-evoked feedforward inhibition onto M/T cells. This was true for both spontaneous (Figure 3) and odor-evoked activity (Figure 6 and 7). At the level of a single light pulse, baclofen was able to reduce the pronounced light-evoked inhibition (Figure 4A,B). In addition, in about a third of the recorded M/T cells, single light pulse evoked increase in M/T cell firing (Figure 4C). Surprisingly however, direct excitation was unaffected by baclofen application (Figure 4D). As a result of the differential modulation by baclofen of feedforward inhibition and direct excitation, M/T cells were more likely to follow the patterned stimulation from the AOC (up to 50Hz; Figure 4E). At the network activity level, specific activation of GABA_BRs at cortical-axons depressed spontaneous beta oscillations, while baclofen-mediated decrease in gamma oscillation was more likely due to GABA_BR activation at GC apical dendrites.

GABA_B Receptors Tune Cortical Feedback to the Olfactory Bulb

 Camille Mazo, Gabriel Lepousez, Antoine Nissant, Matthew T. Valley, and Pierre-Marie Lledo

Laboratory for Perception and Memory, Institut Pasteur, F-75015 Paris, France, and Centre National de la Recherche Scientifique, Unité Mixte de Recherche 3571, F-75015 Paris, France

Sensory perception emerges from the confluence of sensory inputs that encode the composition of external environment and top-down feedback that conveys information from higher brain centers. In olfaction, sensory input activity is initially processed in the olfactory bulb (OB), serving as the first central relay before being transferred to the olfactory cortex. In addition, the OB receives dense connectivity from feedback projections, so the OB has the capacity to implement a wide array of sensory neuronal computation. However, little is known about the impact and the regulation of this cortical feedback. Here, we describe a novel mechanism to gate glutamatergic feedback selectively from the anterior olfactory cortex (AOC) to the OB. Combining *in vitro* and *in vivo* electrophysiological recordings, optogenetics, and fiber-photometry-based calcium imaging applied to wild-type and conditional transgenic mice, we explore the functional consequences of circuit-specific GABA type-B receptor (GABA_BR) manipulation. We found that activation of presynaptic GABA_BRs specifically depresses synaptic transmission from the AOC to OB inhibitory interneurons, but spares direct excitation to principal neurons. As a consequence, feedforward inhibition of spontaneous and odor-evoked activity of principal neurons is diminished. We also show that tunable cortico-bulbar feedback is critical for generating beta, but not gamma, OB oscillations. Together, these results show that GABA_BRs on cortico-bulbar afferents gate excitatory transmission in a target-specific manner and thus shape how the OB integrates sensory inputs and top-down information.

Key words: feedforward inhibition; olfaction; oscillations; sensory circuits; synapse; top-down

Significance Statement

The olfactory bulb (OB) receives top-down inputs from the olfactory cortex that produce direct excitation and feedforward inhibition onto mitral and tufted cells, the principal neurons. The functional role of this feedback and the mechanisms regulating the balance of feedback excitation and inhibition remain unknown. We found that GABA_B receptors are expressed in cortico-bulbar axons that synapse on granule cells and receptor activation reduces the feedforward inhibition of spontaneous and odor-driven mitral and tufted cells' firing activity. In contrast, direct excitatory inputs to these principal neurons remain unchanged. This study demonstrates that activation of GABA_B receptors biases the excitation/inhibition balance provided by cortical inputs to the OB, leading to profound effects on early stages of sensory information processing.

Introduction

Sensory systems use prior experience and expectation to interpret the outside world. The integration of external information re-

quires combining the bottom-up flow of sensory information with top-down signals from higher brain areas. In the olfactory system, odorant information from sensory neurons are first integrated in the main olfactory bulb (OB) before broadcasting to the olfactory cortex through OB principal cells, the so-called mitral and tufted (M/T) cells (Poo and Isaacson, 2009; Franks et al., 2011). In turn, the olfactory cortex, and mainly the anterior piriform cortex and anterior olfactory nucleus (respectively APC and AON, collectively called the anterior olfactory cortex, AOC),

Received Oct. 20, 2015; revised June 4, 2016; accepted June 9, 2016.

Author contributions: C.M., G.L., M.T.V., and P.-M.L. designed research; C.M., G.L., A.N., and M.T.V. performed research; C.M., A.N., and M.T.V. analyzed data; C.M., G.L., and P.-M.L. wrote the paper.

This work was supported by the life insurance company AG2R-La-Mondiale, the Agence Nationale de la Recherche (ANR-15-CE37-0004), and the Laboratoire d'Excellence Revive (Investissement d'Avenir, ANR-10-LABX-73). Our laboratory is part of the Ecole des Neurosciences de Paris (ENP) Ile-de-France network and is affiliated with the Bio-Psy Laboratory of Excellence. C.M. is a recipient of a fellowship from the French Ministère de l'Éducation Nationale et de la Recherche. We thank Carine Moigneu and Laurent Cotter for viral injections; all members of the Lledo laboratory for their insights during the course of these experiments; Kurt Sailor for editing the manuscript; Manuel Mamelì for helpful discussions; Bernhard Bettler for providing GABAB^{fllox/lox} mice; Anne Lanjuin and Catherine Dulac for the Tbet-Cre mice; Karl Deisseroth and Edward Boyden for optogenetic tools; Gaël Moneron for help in setting up the fiber photometry path and the Genetically-Encoded Neuronal Indicator and Effector (GENIE) Project; and the Janelia Farm Research Campus of the Howard Hughes Medical Institute for sharing GCaMP6f constructs.

The authors declare no competing financial interests.

M.T. Valley's present address: Allen Institute for Brain Science, 601 Westlake Ave. N, Seattle, WA 98109.

Correspondence should be addressed to Pierre-Marie Lledo, Laboratory for Perception and Memory, Institut Pasteur and CNRS, 25 rue du Dr. Roux, 75 724 Paris Cedex 15, France. E-mail: pmllledo@pasteur.fr.

DOI:10.1523/JNEUROSCI.3823-15.2016

Copyright © 2016 the authors 0270-6474/16/368289-16\$15.00/0

projects back to the OB (Haberly and Price, 1978a, 1978b; Davis and Macrides, 1981). Cortico-bulbar projections mostly synapse with axonless OB interneuron granule cells (GCs) and, to a lesser extent, with M/T cells. This glutamatergic input onto GC proximal dendrites initiates action potentials and mediates feedforward inhibition onto M/T cells (Balu et al., 2007). In addition, GCs receive glutamatergic input from M/T cells on their apical dendrites, triggering locally reciprocal GABA release back onto M/T cells, thereby producing recurrent or lateral inhibition (Isaacson and Strowbridge, 1998).

In addition to the great number of glutamatergic cortico-bulbar inputs from the AOC, the OB also receives top-down inputs from neuromodulatory centers, including serotonergic fibers from the raphe, noradrenergic fibers from the locus coeruleus, and cholinergic and GABAergic fibers from the basal forebrain (Matsutani and Yamamoto, 2008; Linster and Fontanini, 2014). Given the abundance and diversity of top-down inputs to the OB and their strong impact on OB functions (Shea et al., 2008; Petzold et al., 2009; Boyd et al., 2012; Ma and Luo, 2012; Markopoulos et al., 2012; Soria-Gómez et al., 2014), deciphering how these inputs are modulated is essential to understanding their physiological role and how they regulate the OB network.

In this study, we demonstrate that GABA_B receptors (GABA_BRs), G-protein-coupled receptors of GABA, regulate specific cortico-bulbar excitatory synaptic transmission. Using conditional genetics to selectively knock out GABA_BR expression in the AOC, together with a combination of *in vitro* and *in vivo* electrophysiology, optogenetics, and fiber-photometry-based calcium imaging, we characterized the functional role of GABA_BR modulation at cortico-bulbar terminals. We show that presynaptic activation of GABA_BRs strongly depresses the AOC-to-GC synapse, resulting in diminished feedforward inhibition onto M/T cells' spontaneous and odor-evoked activity. However, the direct AOC-to-M/T cell excitation remains unchanged. In addition, activation of GABA_BRs also reduces OB spontaneous beta oscillations (15–40 Hz). Collectively, these data uncover a mechanism by which the cortical top-down influence to the OB can be refined precisely.

Materials and Methods

Animals

Adult wild-type (WT) C57BL/6RJ, GABA_B(1)^{fl/fl} (Haller et al., 2004), and Tbet-Cre (Haddad et al., 2013) male mice (maintained on a C57BL/6RJ background; 2–5 months old at the time of injection) were used in the study. This work was performed in compliance with the French application of the European Communities Council Directive of September 22, 2010 (2010/63/EEC) and approved by the local ethics committee (CETEA 89, project #01126.02).

Viral injection

Adeno-associated virus [AAV; capsid serotype 2/9 for Channelrhodopsin-2 (ChR2), ChRimson, and Cre viruses, and 2/1 for GCaMP6f] were generated by the Penn Vector Core or produced by the Institut National de la Santé et de la Recherche Médicale (INSERM, UMR 1089, IRT1 Vector platform Nantes, www.atlantic-gene-therapies.fr) from ChR2- (K. Deisseroth; catalog #26969 and #20297; Addgene), ChRimson- (E. Boyden; catalog #62723; Addgene), Cre recombinase-, or GCaMP6f (Penn Vector Core)-encoding plasmids. For electrophysiology experiments, high-titer stock of AAV containing the CaMKIIa-hChR2(H134R)-eYFP-WPRE construct (viral titer, 9.4×10^{12} genome copies per milliliter, $n = 14$ mice for *in vitro* recordings, $n = 15$ for *in vivo* recordings) or a 1:6 mixture of an AAV containing CaMKII-Cre-WPRE (viral titer, 1.1×10^{14}) and an AAV containing EF1a-DIO-hChR2(H134R)-mCherry-WPRE (viral titer, 1.4×10^{13}) were injected in WT ($n = 5$) and age-matched GABA_B(1)^{fl/fl} mice ($n = 4$). A separate cohort of animals were also injected with an AAV containing hSyn-

hChR2(H134R)-mCherry-WPRE [$n = 3$ for *in vitro* recordings, $n = 5$ for *in vivo* field EPSP (fEPSP) characterization solely]. No significant difference between using the Syn or CaMKIIa promoter was seen and results were pooled. For photometry experiments, high-titer stock of AAV containing the hSyn-ChRimson-TdTomato-WPRE (viral titer, 2.2×10^{13}) or hSyn-DIO-GCaMP6f-WPRE construct (viral titer: 1.1×10^{13}) were injected in Tbet-Cre mice ($n = 15$ odor-recording pairs from 2 mice). For viral injections, mice were deeply anesthetized with a ketamine and xylazine mixture (150 mg/kg Imalgene and 5 mg/kg Rompun, respectively, i.p.) and placed in a stereotaxic apparatus. A small craniotomy was performed and viral solution was injected into the AOC (stereotaxic coordinates: 2.1 mm anterior from bregma, 1.9 mm lateral, and at a depth of 3.3 and 3.7 mm from the brain surface; 150–200 nl/site, 300–400 nl total), allowing virus diffusion in the anterior APC and latero-posterior AON, or into the OB (AP: 5 mm, ML: 1.7 mm, DV: 0.7–1.5 mm, 300 nL total) through a glass micropipette attached to a Nanoinjector system (Nanoject II).

Electrophysiology

Slice recording. Tissue preparation was performed as described in Valley et al. (2013). Briefly, tissue was dissected in artificial CSF (ACSF) and 300- μ m-thick slices were vibrosectioned. Recordings were made with borosilicate glass pipettes with a tip resistance between 3 and 6 M Ω . Recordings were discarded if the access resistance exceeded half the input resistance of the cell or if the access resistance varied by $\sim 30\%$ during the experiment. Data were digitized at 10 kHz (EPC9double; HEKA). ChR2 stimulation used a 470 nm light-emitting diode array (Bridgelux). Light duration was controlled using a digital Sequencer (Master-8; A.M.P.I.) and all stimulations were given with an interstimulus interval of 20 s.

In vivo recording. Awake recordings were performed as described previously (Lepousez and Lledo, 2013; Soria-Gómez et al., 2014). Mice were anesthetized and an L-shaped metal bar and a silver reference electrode were fixed to the caudal part of the skull. Optic fibers [multimode, 430 μ m diameter, numerical aperture (NA) 0.39, Thorlabs] were bilaterally implanted above the anterior commissure (400 μ m posterior to the sinus of the olfactory bulb, 0.9 mm lateral, and at a depth of 2.3 mm from the brain surface with an angle of $\sim 30^\circ$). After 1 week of recovery, mice were slowly and progressively trained for head restraint habituation and a 5% sucrose solution was given as a reward. The craniotomy was performed the day before recording and protected with silicone sealant (KwikCast). An array of 4 tungsten electrodes (~ 3 M Ω ; FHC) glued to one or two miniature cannulas (polyimide tubing, 0.0035 inch, Neuralynx; positioned 100–200 μ m above the electrode tips, connected to a 10 μ l Hamilton syringe) was slowly lowered into the OB and a drop of silicone sealant was applied to the brain surface to increase recording stability. Both LFP and spiking signals were continuously recorded 40 min before and 60 min after local drug microinjection through the miniature cannula (injection speed: 0.05 μ l/min; 0.15–0.3 μ l total). Signals were pre-amplified (HS-18; Neuralynx), amplified (1000 \times ; Lynx8, Neuralynx) and digitized at 20 kHz (Power 1401 A/D interface; CED). The identity of M/T cells units were established on the basis of several criteria: (1) stereotaxic coordinates of the mitral cell layer; (2) decrease in both gamma oscillation amplitude and light-evoked fEPSP in the mitral cell layer compared with the LFP recorded in the GC layer (GCL) or external plexiform layer (EPL), where the current sources/sinks are localized (Neville and Haberly, 2003); (3) increase in background spiking activity in a narrow band of 100–150 μ m; (4) typical spontaneous activity patterns coarsely time locked to the respiration rhythm; and (5) odor-evoked responses. Light stimulation of AOC axons was performed using either an optic fiber placed on the OB brain surface or with implanted optic fibers coupled to a DPSS laser (473 nm, 150 mW; CNI Lasers; output fiber intensity, 20 mW) via a custom-built fiber launcher and controlled by a PS-H-LED laser driver connected to the CED interface. Light stimulation consisted in single, paired (40 Hz), or train stimulation (10–100 Hz) of 5-ms-long light pulses. The respiration signal was recorded using a thermocouple (0.005 inch Teflon-coated thermocouple, 5TC-TT-JI-40-1M; Omega) placed in front of the animal's nostril, amplified (10,000 \times), and band-pass filtered (0–10 Hz). The craniotomy

was cleaned and covered with Kwik-Cast between sessions. Four recording sessions per mouse (2 per hemisphere) were made at least 1–2 d apart.

Characterization of the light-evoked fEPSP (see Fig. 2*B,C*) was performed in anesthetized mice. Animals were anesthetized using ketamine/xylazine and positioned in a stereotaxic frame. The animal's body temperature was maintained at 37.5°C by a heating pad and the respiration was monitored to control the anesthesia. LFP recordings were then performed as described above.

Odor presentation. We used a custom-built flow-dilution olfactometer controlled by the CED interface. Pure monomolecular odorants (Sigma-Aldrich) were diluted in mineral oil (10%) in odorless glass vial. Saturated odor vapor was further diluted with humidified clean air (1:10) by means of computer-controlled solenoid pinch valves. Odor presentation dynamics were monitored and calibrated using a mini-photoionization detector (mini-PID, Aurora). Cycles of odor, light, and odor + light presentations were repeated at least seven times for each condition. Stimuli were applied for 1 s and a given odorant was presented every 50 s to reduce sensory adaptation. The odorants used in the final dataset were as follows: valeraldehyde ($n = 11$ responses), acetophenone ($n = 5$), butyric acid ($n = 3$), 2-hexanone ($n = 3$), (S)-limonene ($n = 3$), ethyl tiglate ($n = 2$), ethyl butyrate ($n = 1$), ethyl valerate ($n = 1$), and 1,4 cineole ($n = 1$) and a binary (1:1) mixture of 1-pentanol and 1,4 cineole ($n = 4$), ethyl butyrate and ethyl valerate ($n = 4$), valeraldehyde and ethyl tiglate ($n = 1$), (S)-limonene and 2-hexanone ($n = 1$).

Calcium imaging using fiber photometry

A fiber photometry system adapted from Gunaydin et al. (2014) was used (see Fig. 7*A*). Immediately after GCaMP6f virus injection in the OB, optic fibers (multimode, 430 μm diameter, NA 0.48, LC zirconia ferrule) were implanted bilaterally in the dorsolateral part of the OB above the virus injection site. Three weeks after injection, GCaMP6f was excited continuously using a 473 nm DPSS laser (output fiber intensity, 0.4–0.5 mW; CNI Lasers) reflected on a dichroic mirror (452–490 nm/505–800 nm) and collimated into a 400 μm multimode optic fiber (NA 0.48) with a convergent lens ($f = 30$ mm). The emitted fluorescence was collected in the same fiber and transmitted by the dichroic mirror, filtered (525 ± 19 nm), and focused on a NewFocus 2151 femtowatt photoreceptor (Newport; DC mode). Reflected blue light along the light path was also measured with a second amplifying photodetector (PDA36A; Thorlabs) to monitor light excitation and fiber coupling. Signals from both photodetectors were digitized by a digital-to-analog converter (Power 1401; CED) at 5000 Hz and recorded using Spike2 software. For AOC stimulation using ChRimson, an optic fiber (multimode, 430 μm diameter, NA 0.39, with LC zirconia ferrule; Thorlabs; 5–10 mW output fiber intensity) were implanted bilaterally above the AOC and connected to a DPSS laser (589 nm, 200 mW; CNI Lasers) via a custom-built fiber launcher. For drug injection, bilateral acute intrabulbar injections were done through implanted guide cannulas (injection volume, 0.5 μl ; speed, 0.1 $\mu\text{l}/\text{min}$ via a 33-gauge cannula connected to a 10 μl Hamilton syringe). For odor presentation, mice were placed in a small, ventilated cage (~0.5 L). Pure monomolecular odorants (Sigma-Aldrich) were diluted in mineral oil (1%) in an odorless glass vial and saturated odor vapor was delivered directly into the ventilated cage at a flow rate of 3 L/min. Odors were presented every 30 s and odor presentation dynamics in the cage were monitored constantly using a mini-PID (Aurora). The odorants used in the final dataset were as follows: valeraldehyde ($n = 3$), ethyl tiglate ($n = 3$), pentyl acetate ($n = 3$), ethyl valerate ($n = 2$), 2-hexanone ($n = 1$), ethyl butyrate ($n = 1$), linalool ($n = 1$), and pentanol ($n = 1$).

Pharmacology

Lidocaine (2-diethylamino-*N*-(2,6-dimethylphenyl)acetamide, 2% *in vivo*), NBQX (2,3-dioxo-6-nitro-1,2,3,4-tetrahydrobenzo[*f*]quinoxaline-7-sulfonamide; 1 mM *in vivo*), baclofen ((*RS*)-4-Amino-3-(4-chlorophenyl)butanoic acid; 250 μM in slice and 2.5 mM for *in vivo* experiments), and CGP 52432 ([3-[[[3,4-dichlorophenyl)methyl]amino]propyl] (diethoxymethyl)phosphinic acid; 10 μM for slice and 100 μM for *in vivo* recording) were obtained from Sigma-Aldrich or Tocris Bioscience and dissolved at a final concentration in either sterile saline for *in vivo* experiments or ACSF for slice experiments. Analyzing the changes in fEPSPs at different depths in the GCL

after baclofen injections allowed an estimation of the drug diffusion to be <500–600 μm (see “Results” section).

Histology

For postrecording histological analysis of electrode positioning and ChR2 expression, animals were intracardially perfused [4% paraformaldehyde (PFA) in 0.1 M phosphate buffer] and the brains were removed and postfixed in the same fixative overnight. Sixty-micrometer-thick brain sections were cut on a vibratome, rinsed in PBS, counterstained with the nuclear dye 4,6-diamidino-2-phenylindole (DAPI), and mounted on slides. Viral expression at the injection site was confirmed and OB sections were inspected to check for proper axonal expression, absence of virus diffusion into the OB, and the absence of significant somatic labeling in the OB. To amplify the eYFP fluorescent signal, immunohistochemistry was performed with a chicken anti-GFP primary antibody (1:4000, 06-896, Millipore Bioscience) and rabbit anti-chicken secondary antibody conjugated to Alexa Fluor-488 (1:1000, 1-11039; Life Technologies). In some experiments, the position of the recording electrode was confirmed using a fluorescent DiI (Life Technologies).

GABA_BR1 immunohistochemistry was performed as described in Valley et al. (2013) with minor modifications. Live brain tissue sections were cut (300 μm), allowed to recover for 15 min in ACSF, and then quickly transfer to ice-cold 4% PFA for 30 min. Slices were then cryoprotected in 30% sucrose overnight and 12- μm -thick sections were cut using a cryostat the next day. Immunohistochemistry against GABA_BR1 was performed the same or following day. Slices were rinsed, blocked in normal goat serum for 2 h, and incubated in primary antibody (guinea pig anti-GABA_BR1, 1:3000, AB2256; Millipore Bioscience) for 48 h at 4°C. The secondary antibody (anti-guinea pig conjugated to A647, 1:1000; Life Technologies) was incubated for 2 h. Slices were then rinsed, counterstained with DAPI, mounted with Mowiol, and imaged with a confocal microscope (LSM 700; Zeiss). Quantification of the GABA_BR1 immunoreactivity was reported as the fluorescence optical density in an optical plane where GL staining was maximal using ImageJ software.

Data analysis

For light-evoked field potentials, a 10 min time window before and 10 min after drug injection was used to average evoked signals. For the fEPSP characterization, the steepest slope calculated in a 1 ms window was measured to avoid contamination by the fiber volley component. Similar results were found when measuring the slope between 20% and 80% of the descending phase of the peak. When discernable, the amplitude of the fiber volley was also measured.

For measurements of M/T cell-spiking activity, a minimal 10 min time window before and 10 min after drug injection were used for the analysis (up to 40 min before and after drug application). Signals were high-pass filtered (0.3–9 kHz) and spike detection, sorting, clustering, and spike waveform analysis were performed using Spike2 software (CED) followed by manual cluster adjustment. For single-unit validation, all sorted cells displaying >1% of their interspike intervals below a 3.5 ms refractory period were discarded from the analysis. Careful attention was taken to discard any unit that showed some significant change in spike amplitude or waveform caused by the local infusion of drugs.

We determined whether a cell receives significant inhibition or excitation by extracting individual trials and comparing the firing rate during light to the basal firing rate using a Wilcoxon matched-pairs rank-sum test. A 1 s time window was used to detect whether the cell receives significant inhibition after repeated light stimulation. A 15 ms sliding time window after light stimulation and a 5 ms sliding window, respectively, were used to detect inhibition and excitation elicited by a single light pulse.

The change in firing rate to repeated light stimulation (see Fig. 3) was calculated as follows:

M/T cell firing rate change

$$= \frac{\text{firing rate (stimulus, 1 s)} - \text{basal firing rate (1 s)}}{\text{basal firing rate (1 s)}} \times 100$$

With the firing rate (stimulus, 1 s) being the M/T cell's firing rate during the stimulation (light, odor, or both) and the basal firing rate the averaged cell's firing rate during the second before the light stimulation.

In Figure 4B, the normalized firing rate in response to a single light pulse was calculated as follows:

Normalized M/T cell firing rate (t)

$$= \frac{\text{firing rate (light, 2 ms)} - \text{basal firing rate (2 ms)}}{\text{firing rate (light, 2 ms)} + \text{basal firing rate (2 ms)}}$$

With the firing rate (light, 2 ms) being the M/T cell's firing rate over a 2 ms period during the light stimulation and the basal firing rate (2 ms) being the cell's firing rate during the 20 ms preceding light stimulation reported to a 2 ms time period.

For the analysis of direct excitation in Figure 4D, the M/T cell's firing activity was normalized as follows:

M/T cell firing rate change (t)

$$= \frac{\text{firing rate (light, 1 ms)} - \text{basal firing rate (1 ms)}}{\text{basal firing rate (1 ms)}}$$

With firing rate (light, 1 ms) being the M/T cell's firing rate over a 1 ms period during the light stimulation and basal firing rate (1 ms) being the cell's firing rate during the 20 ms preceding light stimulation reported to a 1 ms time period. To analyze the coupling between AOC stimuli and M/T cell firing (see Fig. 4E), light pulses from the same stimulation train were pooled and the same calculation as above was performed, with the firing rate (light, 10 ms) being the average number of spikes in a 10 ms time window starting 1 ms after light onset and the basal firing rate being the average number of spikes in the 10 ms time window directly preceding light stimulation.

For phase modulation analysis, the thermocouple signal was down-sampled (0.5 kHz) and filtered (0–10 Hz) to extract the sniffing signal. Oscillation peaks (exhalation end) were identified using an automatic threshold algorithm and a phase histogram (72 bins) of M/T cell spikes relative to the identified peak was computed to measure the phase preference and length of the normalized vector as a measure of modulation strength.

For spontaneous oscillations, signals were down-sampled (5 kHz) and low-pass filtered (0–300 Hz), and 10-min-long epochs excluding 1.5 s after onset of light stimulation (0.5 s after the end of the stimulation) were extracted and subjected to a fast Fourier transformation (Hanning window, 2.44 Hz resolution) to obtain the power spectrum and the spectral power in each frequency band of interest.

For photometry experiments, signals were smoothed (0.02 s window) and down-sampled to 500 Hz. For each trial, the signal was normalized to the averaged fluorescence of the trial using the $\Delta F/F$ ratio as follows:

$$\frac{\Delta F}{F}(t) = \frac{F(t) - F_0}{F_0}$$

With F_0 being the average fluorescence over the trial. Sessions with significant averaged changes in the reflected blue light ($>1\%$ $\Delta F/F$) were discarded from the analysis.

Statistics

All reported variances are SEM. In all graphs, excluding the box-and-whiskers plots, the mean is represented. In box-and-whiskers plots, the line in the middle of the box represents the median, the box edges represent the 25th to 75th percentiles and the whiskers represent the minimum and the maximum. All two-tailed Wilcoxon signed-rank tests, Mann-Whitney tests, ANOVAs, and curve fit were performed using commercial analysis software (GraphPad Prism) with $p < 0.05$ considered significant. For circular data, Hotelling paired test (significance $p < 0.05$) was performed with Oriana (Kovac Computing Services).

Results

Activation of presynaptic GABA_BRs depresses cortical synaptic transmission onto granule cells

Because AOC projections to the OB predominantly innervate the GCL (Haberly and Price, 1978a, 1978b; Davis and Macrides, 1981) and, because previous immunohistochemical studies reported the presence of GABA_BR subunits in that layer (Margeta-Mitrovic et al., 1999), we investigated the presence and the functional role of GABA_BRs at AOC-to-OB synapses. We injected the AOC of adult mice with AAV to express ChR2 in cortico-bulbar axons (Fig. 1A–C). As reported previously, ChR2-eYFP expression was confined mainly to the GCL and found to a minor extent in the mitral cell and glomerular layers (see also Haberly and Price, 1978a, 1978b; Davis and Macrides, 1981; Boyd et al., 2012; Markopoulos et al., 2012). No labeled somas were seen across bulbar layers (Fig. 1B, D) as already reported (Lepousez et al., 2014). Light stimulation of ChR2⁺ axons in horizontal OB slices (Fig. 1E) evoked monosynaptic EPSCs in voltage-clamped GCs that were abolished upon GABA_BR agonist R/S-baclofen treatment (hereafter referred as baclofen, 250 μM) and subsequent application of GABA_BR antagonist CGP-52432 (hereafter referred to as CGP, 10 μM) partially restored the EPSC amplitude ($-79.9 \pm 3.8\%$ in baclofen and $-20.2 \pm 15.2\%$ in CGP, one-way ANOVA: $p = 0.0009$, Dunn's *post hoc* test: $p < 0.05$ for baseline vs baclofen and $p < 0.01$ for baclofen vs CGP; $n = 8$; Fig. 1F). Previous slice studies showed that baclofen application did not affect GC resting membrane potential, input resistance, or threshold to spike (Isaacson and Vitten, 2003; Valley et al., 2013), suggesting no direct postsynaptic action of baclofen onto GCs. In addition to direct excitatory inputs, cortico-bulbar axons light stimulation produced disynaptic inhibition onto GCs, presumably originating from deep short axon cells (Boyd et al., 2012; Markopoulos et al., 2012). NBQX-sensitive IPSCs were recorded in 8 of the 35 recorded GCs and these IPSCs were blocked by baclofen and restored with CGP application ($-80.1 \pm 4.3\%$ in baclofen, $-20.1 \pm 9.7\%$ in CGP and $-89.5 \pm 2.4\%$; in NBQX, one-way ANOVA: $p = 0.0005$, $p < 0.01$ for baseline vs baclofen and $p < 0.05$ for baseline vs NBQX and baclofen vs CGP; $n = 7$; Fig. 1G).

We next evaluated the *in vivo* functional impact of GABA_BR modulation on the OB circuit activity. We recorded LFP *in vivo* and induced light stimulation of ChR2⁺ axon terminals with an optic fiber positioned at the OB surface (Fig. 2A). A field response composed of an early (N1) and late (N2) component was observed (Fig. 2B, C). Although the voltage depth profile of N1 (peaking at ~ 2 ms) was monotonic across OB layers, N2 reversed polarity at the mitral cell layer (Fig. 2B), indicating that N2 encompassed a current sink in the GCL and a current source in the EPL, as reported in studies using electrical stimulation in the APC (Neville and Haberly, 2003; Manabe et al., 2011). These signals were generated mainly by GC depolarization because these cells and their dendrites occupy the vast majority of the space in the GCL and in the EPL and are morphologically organized as a dipole between these two layers (Rall and Shepherd, 1968). Pharmacological characterization in anesthetized animals showed that local microinfusion of AMPA receptor antagonist NBQX (1 mM) into the GCL strongly reduced the N2 slope, with no significant effect on the N1 amplitude (N2: $-69.5 \pm 10.9\%$; N1: $-8.9 \pm 4.9\%$, $n = 3$; Fig. 2C). In contrast, local infusion of lidocaine (2%), a voltage-gated Na⁺ channel blocker, strongly decreased both N1 and N2 (N2: $-60.4 \pm 1.7\%$; N1: $-79.8 \pm 5.9\%$, $n = 4$; Fig. 2C; two-way ANOVA: drug effect: $F_{(2,19)} = 54.6$,

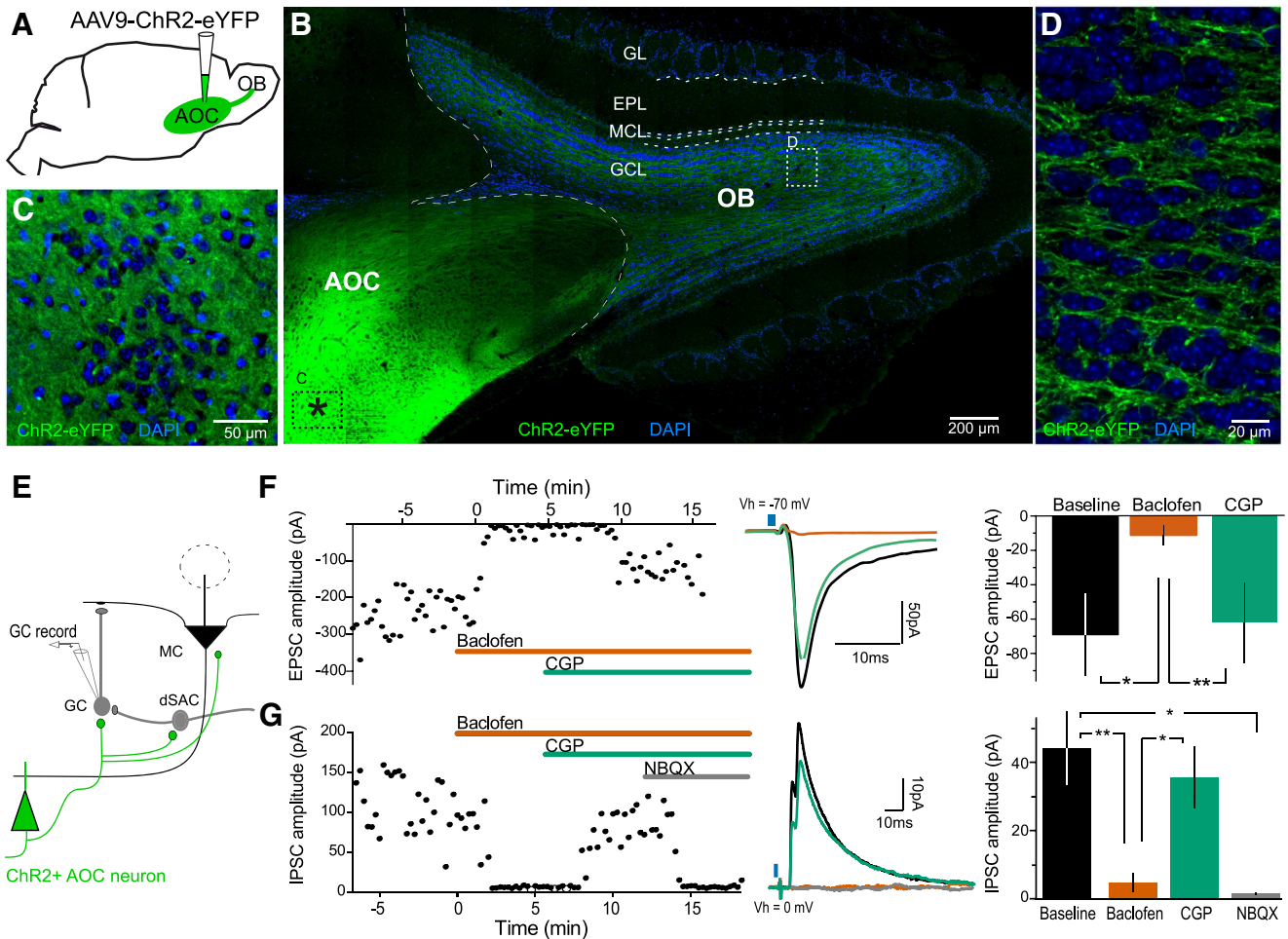


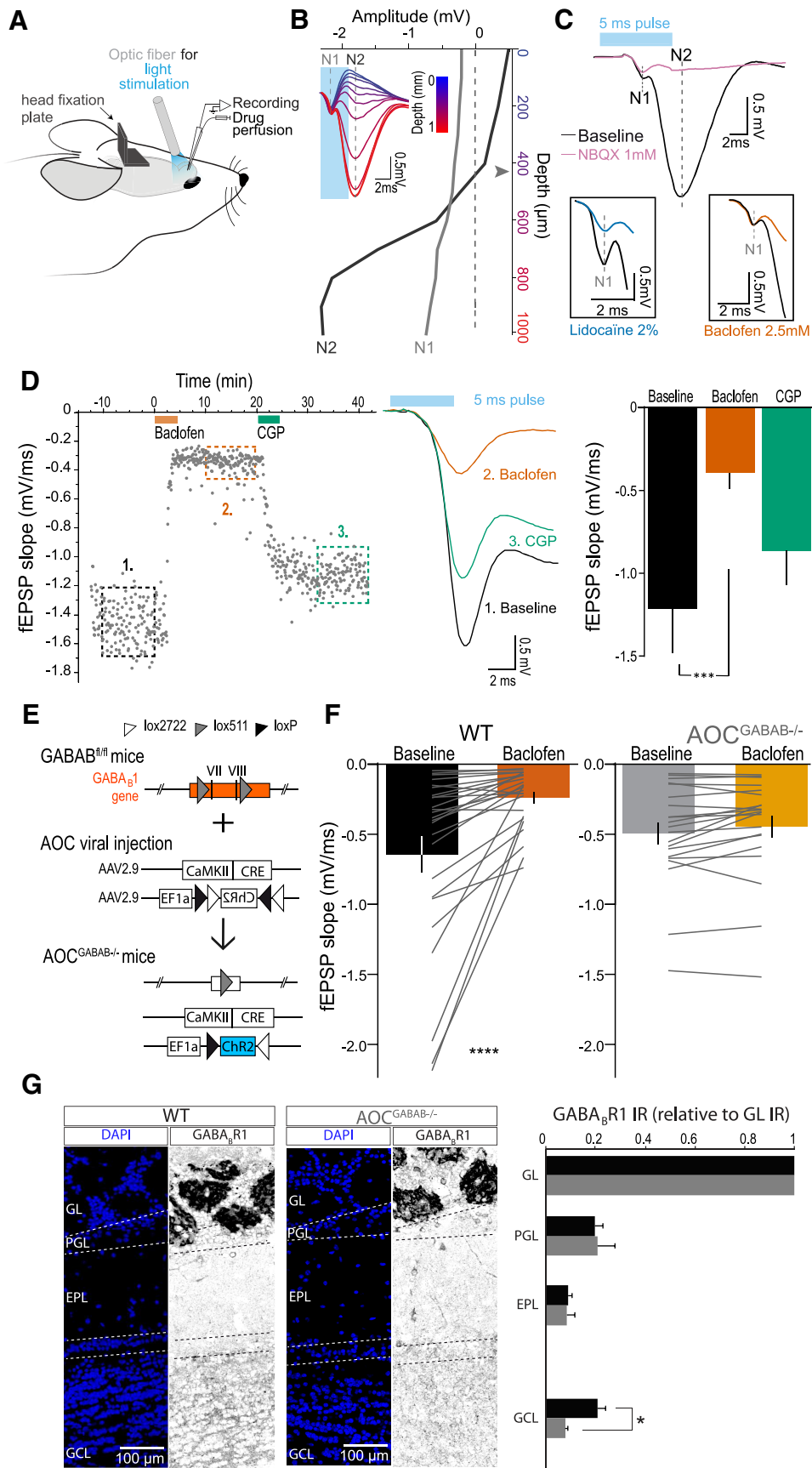
Figure 1. GABA_B activation depresses the glutamatergic AOC-to-GC synapse *in vitro*. **A**, Schematic representing AAV2/9-ChR2-eYFP injection into the AOC and cortico-bulbar ChR2⁺ axons targeting the OB. **B**, Horizontal section showing the injection site (*) in the AOC and ChR2 expression along the OB layers. ChR2-eYFP expression was mainly confined to the GCL. **C**, Higher magnification of region “C” in **B** indicating ChR2 expression in the AOC. **D**, Higher magnification of region “D” in **B** showing the dense ChR2-eYFP expression in the OB GCL and the absence of ChR2⁺ soma. **E**, Recording schematic. GCs were patched and cortico-bulbar axons were light stimulated. **F**, AOC axon light stimulation evoked GABA_B-sensitive excitation in GCs. Left, EPSC amplitude time course in basal, baclofen (250 μM), and CGP 52432 (10 μM) conditions. Middle, Representative averaged traces. Right, Averaged EPSC amplitudes. **G**, AOC axon light stimulation evoked GABA_B-sensitive disinhibition in GCs. Left, IPSC amplitude time course in basal, baclofen (250 μM), CGP 52432 (10 μM), and NBQX (10 μM) conditions. Middle, Representative averaged traces. Right, Average IPSC amplitudes. GL, Glomerular layer; EPL, external plexiform layer; MCL, mitral cell layer; GCL, granule cell layer. MC, mitral cell; GC, granule cell; dSAC, deep short axon cell. **p* < 0.05, ***p* < 0.01 with a Dunn’s multiple-comparisons test after one-way ANOVA.

p < 0.0001 and drug × negativity: $F_{(2,19)} = 6.8$, *p* = 0.006, Holm–Sidak’s multiple-comparisons *post hoc* test: N1: *p* = 0.48 for NBQX and *p* < 0.0001 for lidocaine, N2: *p* < 0.0001 for both drugs compared with vehicle); vehicle injection had no effect on N1 or N2 (*p* = 0.32, *n* = 4; *p* = 0.94, *n* = 7; respectively). Both N1 and N2 amplitude increased with the power of photostimulation and disappeared in the absence of ChR2. Together with recent studies reporting that light stimulation of cortico-bulbar axon terminals drives direct excitation of GCs (Boyd et al., 2012; Markopoulos et al., 2012), our data strongly suggest that N1 is a ChR2⁺-induced Na⁺-spike-dependent fiber volley invading AOC axon terminals, while N2 is a fEPSP generated by AMPAR-dependent depolarization, specific to GCs.

In anesthetized and awake head-restrained mice, local micro-infusion of baclofen (2.5 mM) in the GCL did not alter the fiber volley ($-3.2 \pm 2.7\%$, *n* = 4, Wilcoxon matched-pairs signed-rank test: *p* = 0.63; Fig. 2C), but produced a 2-fold decrease in amplitude and slope of the light-evoked fEPSP. This effect was reversed by subsequent application of CGP (100 μM; fEPSP slope: $-65.5 \pm 8.6\%$ in baclofen and $-32.5 \pm 8.5\%$ in CGP; fEPSP

amplitude: $-56.18 \pm 7.3\%$ in baclofen and $-20.0 \pm 11.5\%$ in CGP; one-way ANOVA: *p* < 0.0003 for both slope and amplitude, Dunn’s multiple-comparisons *post hoc* test: baseline vs baclofen: *p* < 0.001 for slope and amplitude, baclofen vs CGP *p* < 0.05 for amplitude and *p* = 0.074 for slope; *n* = 8; Fig. 2D).

To estimate the diffusion of baclofen in the OB, we first validated that, after a first baclofen injection, the second injection at the same site did not depress further the fEPSP amplitude and slope, which is compatible with local saturation of GABA_BRs. However when baclofen was injected a second time ~500–600 μm below we observed a strong reduction of the fEPSP, comparable to the reduction observed after the first dorsal injection ($-63.3 \pm 7.8\%$, *p* = 0.23 with Wilcoxon signed-rank test, *n* = 5). This suggests that the first injection did not reach the second site located ~500–600 μm deeper in the GCL. To confirm this observation, we injected the same volume and concentration of the nuclear dye DAPI and *post hoc* histological analysis permitted us to estimate the dye diffusion to be <500 μm. We concluded that, using our injection protocol, baclofen cannot diffuse in an area >600 μm within the OB and therefore cannot significantly dif-



fuse to the AOC. Furthermore, we did not observe any significant difference between anesthetized and awake mice in the structure of the light-evoked fEPSP or in the effect of baclofen ($-48.5 \pm 4.5\%$ in anesthetized vs $-47.0 \pm 5.7\%$ in awake mice, $n = 8$ and 25 , respectively, $p = 0.98$), and data were therefore pooled. However, because cortico-bulbar top-down inputs are sensitive to wakefulness (Boyd et al., 2015; Otazu et al., 2015), the ensuing *in vivo* experiments were performed solely in awake animals.

To strengthen our *in vitro* results suggesting a presynaptic localization of GABA_BRs at the AOC-to-GC synapse (Fig. 1F), we designed a conditional knock-out approach to delete GABA_BRs in a region-specific manner. A transgenic mouse line that possesses critical exons VII and VIII of the GABA_B(1) gene flanked with lox sites (GABAB^{fl/fl} mice; Haller et al., 2004) was used. To knock-out the expression of GABA_BRs and express Chr2 in the same population of cortico-bulbar fibers, two AAVs expressing either Cre recombinase (AAV-CaMKIIa-Cre) and a Cre-dependent Chr2 (AAV-EF1a-DIO-Chr2-mCherry) were co-injected in the AOC of age-matched WT ($n = 5$) and GABAB^{fl/fl} mice ($n = 4$). Using this strategy, Chr2-eYFP was a reporter for Cre expression and thus identified the population of cells in which GABA_BRs were conditionally knocked out in GABAB^{fl/fl} mice (hereafter named AOC^{GABAB^{-/-}}) (Fig. 2E). As a control, we injected AAV directly expressing Chr2 under the control of the CaMKIIa promoter in WT mice (AAV-CaMKIIa-Chr2-EYFP; $n = 7$). Three months after viral injection, Cre expression led to Chr2-mCherry labeling of cortico-bulbar axons. In awake animals, baclofen caused a 2-fold decrease in the light-evoked fEPSP slope and amplitude in WT mice, but had no significant effect in AOC^{GABAB^{-/-}} mice (WT: slope: $-49.4 \pm 6.1\%$, amplitude: $-47.0 \pm 5.6\%$, $n = 25$ and AOC^{GABAB^{-/-}}: slope: $-6.3 \pm 5\%$, amplitude: $-7.3 \pm 3.2\%$, $n = 21$; Two-way ANOVA on slope: baclofen \times genotype: $F_{(1,44)} = 9.26$, $p = 0.004$; Fisher's *post hoc* test: $p < 0.0001$ in WT animals and $p = 0.57$ in AOC^{GABAB^{-/-}} mice; on amplitude: $F_{(1,44)} = 9.37$, $p = 0.004$; Fisher's *post hoc* test: $p < 0.0001$ in WT and $p = 0.58$ in AOC^{GABAB^{-/-}}; saline in WT: $-4.8 \pm 7.5\%$, $n = 7$, Wilcoxon matched-pairs signed-rank test: $p = 0.94$; Fig. 2F). To confirm that GABA_BR expression was indeed diminished in cortico-bulbar axons, we performed immunohistochemical labeling for the GABA_BR1 subunit in OB slices. The immunoreactivity was decreased selectively in the

GCL of AOC^{GABAB^{-/-}} mice, but not in the GCL of WT animals (interaction genotype \times OB layer: $F_{(2,14)} = 4.41$, $p = 0.033$, $p = 0.049$ for the GCL and $p > 0.05$ for the other layers, $n = 5$ WT and $n = 4$ AOC^{GABAB^{-/-}}; Fig. 2G). Together, these data demonstrate that the expression of presynaptic GABA_BRs in cortico-bulbar axons allows depression of excitatory feedback onto GCs.

Activation of presynaptic GABA_BRs depresses cortico-bulbar feedforward inhibition onto M/T cells

We next examined the effect of GABA_BR activation in cortical fibers on M/T cell spontaneous firing activity. Extracellular recordings of M/T cells (see Materials and Methods section for identification criteria) were performed in awake, head-restrained mice and the same cells were recorded before and after local perfusion of baclofen within the vicinity of the electrode (Fig. 3A). In WT and AOC^{GABAB^{-/-}} mice, baclofen did not alter the M/T cell spontaneous firing rate ($-8.3 \pm 4.0\%$ in WT, $n = 42$; $-0.3 \pm 4.5\%$ in AOC^{GABAB^{-/-}}, $n = 29$; two-way ANOVA: $F_{(1,69)} = 2.75$, $p = 0.10$), consistent with an *in vitro* study reporting no postsynaptic effect of baclofen on M/T cells (Isaacson and Vitten, 2003). We also investigated whether baclofen changes the temporal relationship between M/T cell firing and the sniff cycle. At the population level, M/T cell phase preference to the sniff cycle did not significantly shift with baclofen application ($+40.8 \pm 34.7^\circ$ in WT, $n = 17$, and $-28.9 \pm 45.4^\circ$ in AOC^{GABAB^{-/-}} animals, $n = 16$, $p = 0.33$ and $p = 0.15$ with a paired Hotelling test), whereas it induced a small increase in the strength of the sniffing modulation of M/T cell firing activity in WT, but not AOC^{GABAB^{-/-}} mice (mean vector length: baseline: 0.07 ± 0.01 ; baclofen: 0.11 ± 0.01 ; baclofen: $F_{(1,39)} = 5.93$, $p = 0.02$; however, baclofen \times genotype interaction: $F_{(1,39)} = 3.64$, $p = 0.064$; Fisher's LSD *post hoc* test: WT: $p = 0.0013$, $n = 25$, AOC^{GABAB^{-/-}}: $p = 0.74$, $n = 16$).

Previous OB slice experiments showed that cortico-bulbar stimulation drives disynaptic inhibition onto M/T cells, mainly mediated by GCs, which is abolished by glutamatergic blockers (Balu et al., 2007; Boyd et al., 2012; Markopoulos et al., 2012). Here, we applied a 1 s light train stimulation on cortico-bulbar axons while recording M/T cell activity using an optic fiber positioned either on top of the OB surface or implanted above the anterior commissure. Because the olfactory cortex send back information to the OB at various regimes (beta, 15–40 Hz, by Gray and Skinner, 1988; Neville and Haberly, 2003; Martin et al., 2006; gamma frequencies, 40–100 Hz, by Boyd et al., 2012; theta, 1–10 Hz, by Youngstrom and Strowbridge, 2015), we decided to span the whole spectrum of cortical axon activity with stimulation frequencies ranging from 10 to 100 Hz. Figure 3B shows the response of an example M/T cell to three frequencies of light stimulation (10, 33, and 67 Hz) and Figure 3C illustrates the inhibition triggered by the different light stimulation patterns on each individual recorded M/T cells. The percentage of change in firing rate is color coded (blue represents inhibition and red excitation). 21/22 of the recorded M/T cells ($\sim 95\%$) showed reduced firing activity upon cortical stimulation (Wilcoxon matched-pairs rank-sum test for each cell, light stimulation vs prestimulation, $p < 0.05$; Fig. 3C, left), as reported previously (Markopoulos et al., 2012; Soria-Gómez et al., 2014). The percentage of inhibition was not related to the cell's spontaneous firing rate ($y = 0.0041x - 0.73$, $R^2 = 0.012$, slope not different from 0: $p = 0.63$, $n = 21$), and maximum inhibition was distributed from 33 to 50 Hz (Fig. 3D). Figure 3E represents the effect of 33 Hz light stimulation on individual M/T cells. At the M/T cell population level, firing inhibition as a function of stimulation

←

Figure 2. Presynaptic GABA_BR activation depresses the glutamatergic AOC-to-GC synapse *in vivo*. **A**, Schematic drawing of the recording configuration. In head-restrained mice, Chr2⁺ axons were optogenetically stimulated by delivering light through an optic fiber. Drugs were perfused using a miniature cannula in the vicinity of the electrode tips. **B**, Light-evoked field recordings across the different OB layers (color-coded, inset). Depth profile of events N1 and N2 is reported. Arrowhead indicates the depth at which N2 reversed polarity. **C**, Pharmacological characterization of N1 and N2. N1 was depressed by 2% lidocaine but remained unaffected by NBQX (1 mM), baclofen (2.5 mM), or vehicle application. N2 was decreased by lidocaine and NBQX, but not vehicle. **D**, Light-evoked fEPSP was modulated by GABA_BR. Left, fEPSP slope time course in basal, baclofen (25 mM), and CGP 52432 (100 μM) condition. Middle, Representative averaged traces. Right, Average fEPSP slope. **E**, Schematic of the conditional knock-out approach. In GABAB^{fl/fl} mice, co-injection of AAV2/9-CaMKII-Cre and AAV2/9-EF1a-DIO-Chr2 viruses in the AOC led to a nonfunctional GABA_BR1 gene in the neuronal population excitable with light. **F**, Baclofen depressed the fEPSP slope in WT, but not in AOC^{GABAB^{-/-}} mice. **G**, Immunohistochemical staining against GABA_BR1. Left, Horizontal OB sections showing the distribution of GABA_BR1 expression across the layers in a WT and a AOC^{GABAB^{-/-}} mouse (inverted grayscale). Quantifications (right; GL immunoreactivity set to 1) revealed a specific reduction of GABA_BR1 immunoreactivity in the GCL of AOC^{GABAB^{-/-}} mice. PGL, periglomerular layer. *** $p < 0.001$ with a Dunn's multiple-comparisons test after one-way ANOVA * $p < 0.05$, **** $p < 0.0001$ with a Fisher's LSD test after two-way ANOVA.

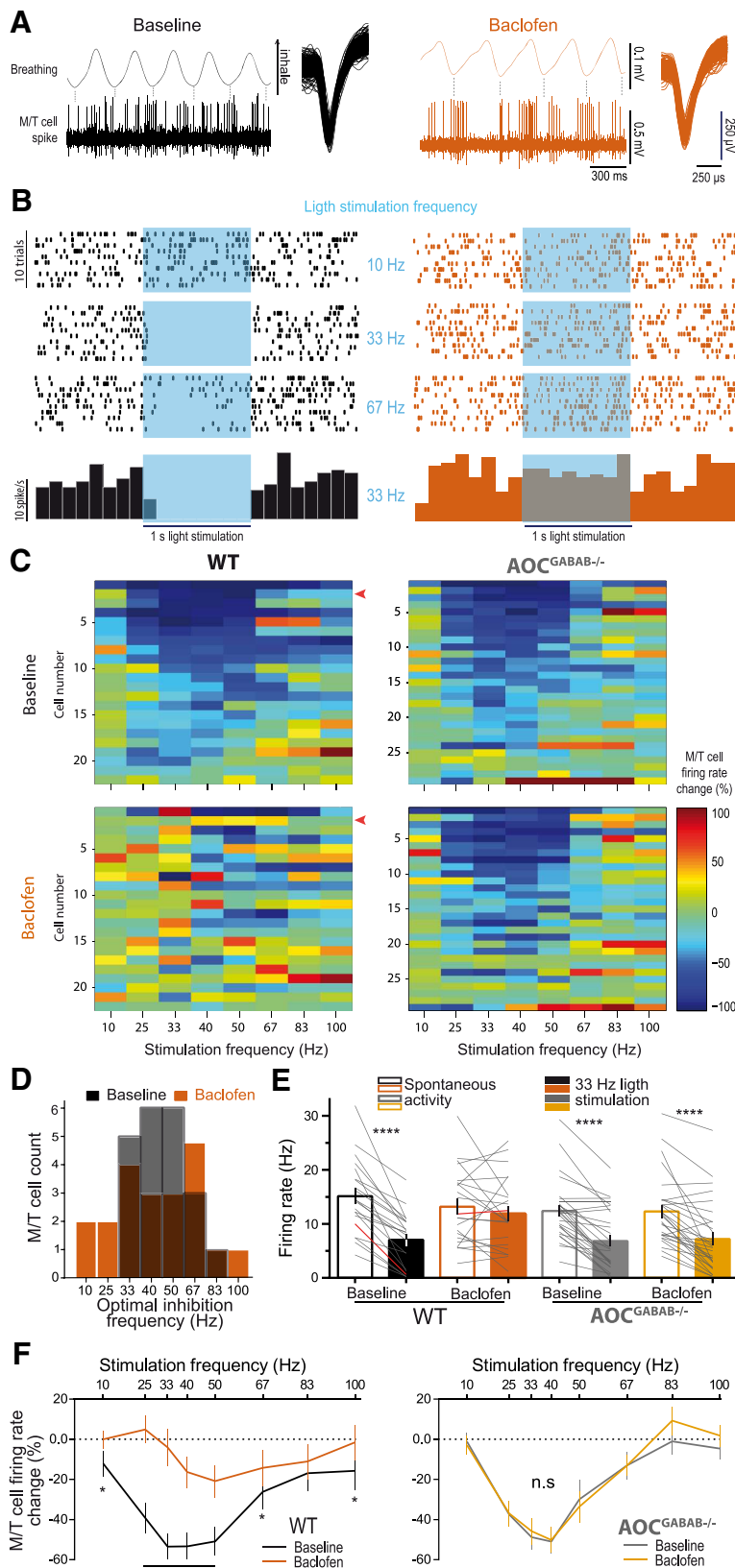


Figure 3. GABA_BR activation at AOC axon terminals suppresses inhibition onto M/T cells. **A**, Example of M/T cell awake spontaneous spiking activity associated with breathing signal during basal and baclofen (2.5 mM) conditions. **B**, Top, Raster plot of a cell's response to patterned light stimulation (10, 33 and 100 Hz, 1 s) of AOC axons before (left) and after baclofen application (right). Bottom, PSTH of the neuron's response to 40 Hz light stimulation. **C**, Heat map of individual neuron's response in WT ($n = 22$, left) and AOC^{GABAB-/-} mice ($n = 29$, right) to the different light stimulation frequencies in baseline (top) and baclofen

frequency followed a bell-shaped curve with 33–50 Hz driving maximum inhibition (from $-13.0 \pm 6.7\%$ at 10 Hz to $-55.9 \pm 6.4\%$ at 33 Hz; $n = 21$ cells; Fig. 3F, left). When the same cells were recorded in the presence of baclofen, the magnitude of the light-evoked inhibition of M/T cells decreased significantly. For example, the powerful inhibition induced by 33 Hz light delivery in baseline conditions was abolished in presence of baclofen ($-53.2 \pm 6.8\%$ in basal condition and $-1.3 \pm 12\%$ in baclofen; baclofen: $F_{(1,20)} = 24.92$, $p < 0.0001$; baclofen \times light interaction: $F_{(1,20)} = 20.31$, $p = 0.0002$, Fisher's LSD *post hoc* test: $p < 0.0001$ in basal condition and $p = 0.23$ in baclofen; Figure 3E). CGP application partially restored the light-induced inhibition (e.g., M/T cell firing change at 33 Hz: $-92.4 \pm 4.7\%$ in baseline, $-8.0 \pm 20.1\%$ in baclofen and $-47.0 \pm 12.3\%$ in CGP, $n = 2$). Across all frequencies, baclofen blocked the light-induced inhibition of M/T cells (baclofen and baclofen \times light frequency interaction: $F_{(1,21)} = 20.31$, $p = 0.0002$ and $F_{(7,147)} = 8.41$, $p < 0.0001$, respectively; Fisher's LSD *post hoc* test, $p < 0.05$ except for 83 Hz light stimulation, where $p = 0.31$, $n = 21$; Fig. 3C,F), whereas vehicle application had no effect ($F_{(1,7)} = 0.80$, $p = 0.40$, $n = 8$).

Because M/T cell inhibition could also be blocked by GABA_BR action at the GC dendrodendritic synapse (Isaacson and Vitten, 2003; Valley et al., 2013), the same experiments were performed in AOC^{GABAB-/-} mice. In these transgenic animals, light stimulation delivered at various frequencies decreased M/T cell firing with a similar bell-shaped relationship ($n = 29$ cells; Fig. 3F, right) and individual M/T cells displayed light-evoked inhibition comparable to WT mice (e.g., for 33 Hz stimulation: $-48.8 \pm 6.1\%$ in M/T cell firing rate, $n = 29$ cells; Fig. 3C,E). However, baclofen did not alter the light-evoked inhibition of M/T cell in

(bottom) conditions. Blue represents inhibition and red excitation. Red arrow indicates the example cell in **B**. **D**, Distribution of the frequencies driving maximum inhibition across M/T cell population. **E**, Effect of 33 Hz light stimulation on individual M/T cell firing rate before and after baclofen application in WT and AOC^{GABAB-/-} animals. Red lines represent the example cell shown in **B**. Note that baclofen did not affect the M/T cell spontaneous firing rate. **F**, Percentage of firing rate change before and after baclofen application as a function of stimulation frequency. AOC axon stimulation produces a similar tuning curve to light frequencies in WT and AOC^{GABAB-/-} mice. * $p < 0.05$, **** $p < 0.0001$ with a Fisher's LSD test after two-way ANOVA.

these animals ($F_{(1,28)} = 0.46, p = 0.50, n = 29$; Fig. 3C,F). Therefore, these results demonstrate that presynaptic GABA_BR activation at cortico-bulbar axon terminals blocks M/T cell feedforward inhibition.

During these experiments, the influence of cortical inputs on the OB activity was revealed using long-lasting and repeated light stimulation. To examine M/T cell responses to transiently active AOC inputs, we analyzed M/T cell firing activity in response to a single, 5-ms-brief light pulse. In WT mice, 18/22 M/T cells (~82%) showed a transient suppression of their firing after such a brief light stimulation (Wilcoxon matched-pairs rank-sum test for each cell, $p < 0.05$). Figure 4A shows a representative cell responding to a single 5 ms light pulse before and after baclofen treatment (top and bottom, respectively). This rapid, transient inhibition of M/T cell firing peaked at 10 ms and lasted ~30 ms (Fig. 4A,B). Baclofen treatment decreased this inhibition (two-way ANOVA: $F_{(1,17)} = 12.39, p = 0.003$; baclofen \times time interaction, $F_{(34,578)} = 9.55, p < 0.0001$, Sidak's multiple-comparisons test: $0.0001 < p < 0.05$ between 4 and 14 ms after light onset; $n = 18$; Fig. 4A,B) and dampened the peak amplitude ($-20.7 \pm 8.1\%$ in baclofen; Wilcoxon match-pairs rank-sum test: $p = 0.009, n = 18$), resulting in only 13 of 22 recorded cells still showing significant inhibition after baclofen treatment. This feedforward inhibition decayed with a time constant of 17.3 ms in basal conditions and 20.9 ms with baclofen application ($r^2 = 0.96$ and 0.65 , respectively; not significantly different, $p = 0.29, n = 18$) and recovered after CGP infusion ($n = 2$). In AOC^{GABAB^{-/-}} animals, the light-evoked inhibition was observed in all M/T cells recorded under basal conditions (29/29) and in 28 of 29 recorded cells with baclofen treatment. Baclofen application did not change the time course of inhibition ($F_{(1,28)} = 0.612, p = 0.44, n = 29$) or the peak amplitude ($-2.4 \pm 4.3\%, p = 0.49, n = 29$) (Fig. 4B). These results demonstrate that brief light stimulation of AOC axons is sufficient to elicit feedforward inhibition onto M/T cells and GABA_BR activation can depress this disinaptic inhibition driven by single cortical inputs.

Cortical feedback excitation to M/T cells is insensitive to presynaptic GABA_BR modulation

Because AOC glutamatergic afferents to the OB also excite M/T cells directly (Markopoulos et al., 2012; Fig. 1E), we next examined direct excitation from AOC axons in the same M/T cell population. Figure 4C shows an example M/T cell responding with a rapid and precise increase of firing activity in response to a single 5-ms-long light pulse in both basal and baclofen conditions. We found that 7/22 (~32%) of M/T cell cells received significant direct excitatory input in basal conditions (Wilcoxon match-pairs rank-sum test for each cell). In the 7 M/T cells exhibiting direct excitation before and after baclofen treatment, we observed a slightly prolonged excitation in baclofen conditions, although not significant (two-way ANOVA: interaction time \times baclofen: $F_{(29,174)} = 1.01, p = 0.46$; baclofen: $F_{(1,6)} = 5.12, p = 0.064; n = 7$; Fig. 4D). No difference was observed in the peak amplitude or in the latency to peak (peak amplitude: $+4.6 \pm 4.3\%$ in baclofen, $p > 0.99$; peak latency: 3.0 ± 0.6 ms in baseline vs 2.9 ± 0.5 ms in baclofen, $p > 0.99$, Wilcoxon match-pairs tests; $n = 7$; Fig. 4D). We also observed that 2/14 cells showed direct excitation with baclofen treatment, but not in basal conditions. In AOC^{GABAB^{-/-}} mice, we detected a significant direct excitation in 17/29 (~59%) of the recorded M/T cells. After baclofen administration, 20/29 (~70%) M/T cells received significant excitation, but baclofen treatment had no effect on this excitation (time \times baclofen interaction: $F_{(29,464)} = 0.73, p = 0.85$; peak

amplitude: $-11.4 \pm 15.9\%$ in baclofen, $p = 0.0984$; and peak latency: 4.35 ± 0.56 ms in baseline and 4.59 ± 0.54 ms in baclofen, $p = 0.47; n = 17$; Fig. 4D).

In vitro, light activation of AOC axons failed to reveal fast excitatory synaptic responses on M/T cells, which would have supported the fast evoked firing activity observed *in vivo*. Instead, we observed small, slow inward currents (average amplitude -9.3 ± 0.9 pA, $V_h = -70$ mV; $n = 9$) blocked by NBQX ($-89.5 \pm 2.4\%; p = 0.0003; n = 6$), as described previously (Boyd et al., 2012; Markopoulos et al., 2012). Moreover, these evoked currents were frequent *in vitro* (18/24) and were blocked by baclofen ($-78.5 \pm 3.1\%$ in baclofen and $-23.8 \pm 6.7\%$ in CGP; $F_{(1,356,10.85)} = 36.31, p < 0.0001$, one-way ANOVA, $p < 0.05$ for all Holm–Sidak's *post hoc* test; $n = 9$). Conversely, light-triggered M/T cell spiking *in vivo* was rare (7/22) and insensitive to baclofen (Fig. 4D). Furthermore, the slow kinetics of the *in vitro* EPSCs (time to peak from light onset: 5.4 ± 0.5 ms) are incompatible with the *in vivo* sharp light-evoked spiking (time to peak from light onset: 3.0 ± 0.6 ms). In addition, these slow EPSCs were shown to be unable to trigger M/T cell spiking in slices (Boyd et al., 2012). Collectively, these discrepant observations suggest that these slow currents recorded *in vitro* do not underlie the fast spiking that we observed *in vivo*. The recorded EPSCs *in vitro* could reflect glutamate receptor activation in electrophysiologically remote regions of M/T cell lateral dendrites or gap junctionally coupling with cells receiving direct synaptic inputs.

In vivo, because the efficiency of cortical inhibition of M/T cells is dependent on the stimulation frequency (Fig. 3F), we investigated whether GABA_BR differentially influenced M/T cell excitatory/inhibitory biphasic response driven at different frequencies. In baseline conditions, M/T cell spiking activity after cortical stimulation decreased at frequencies >10 Hz (Fig. 4E). Baclofen extended the increase in spiking activity after cortical stimulation to higher frequencies (up to 50 Hz) in WT, but not in AOC^{GABAB^{-/-}} animals (WT: frequency \times baclofen: $F_{(7,42)} = 5.87, p < 0.0001$, Fisher's *post hoc* test: $p < 0.01$ for 10 to 50 Hz; $n = 7$; AOC^{GABAB^{-/-}}: $F_{(7,91)} = 0.68, p = 0.69; n = 14$; Fig. 4E). This result indicates that GABA_BR activation extends the functional coupling between cortical excitation and M/T cells response in the 10–50 Hz activity band. In summary, activation of cortical feedback triggers both fast direct excitation and feedforward inhibition onto M/T cells, but GABA_BR activation selectively depresses the inhibitory tone while sparing excitation, thereby reformatting the ratio between excitation and feedforward inhibition received by M/T cells.

Activation of presynaptic GABA_BRs modulates OB oscillatory activity

Previous studies showed that oscillations and temporal activity might be under the control of extrinsic top-down inputs (Engel et al., 2001). Oscillatory rhythms are prominent in the OB of awake mice (Fig. 5A,B). On the top of breathing-related theta oscillations (1–10 Hz), which are largely driven by olfactory sensory inputs, gamma oscillations (40–100 Hz) are generated by the dendrodendritic synapse (Rall and Shepherd, 1968; Gray and Skinner, 1988; Neville and Haberly, 2003; Kay et al., 2009; Lepousez and Lledo, 2013), whereas beta oscillations (15–40 Hz) are thought to be driven by interactions between the olfactory cortex and the OB (Gray and Skinner, 1988; Neville and Haberly, 2003; Martin et al., 2006). In light of this circuit segregation, we sought to determine whether GABA_BR-mediated depression of AOC inputs to the OB would alter specific oscillatory frequencies. We found no change in theta power in presence of baclofen in WT or

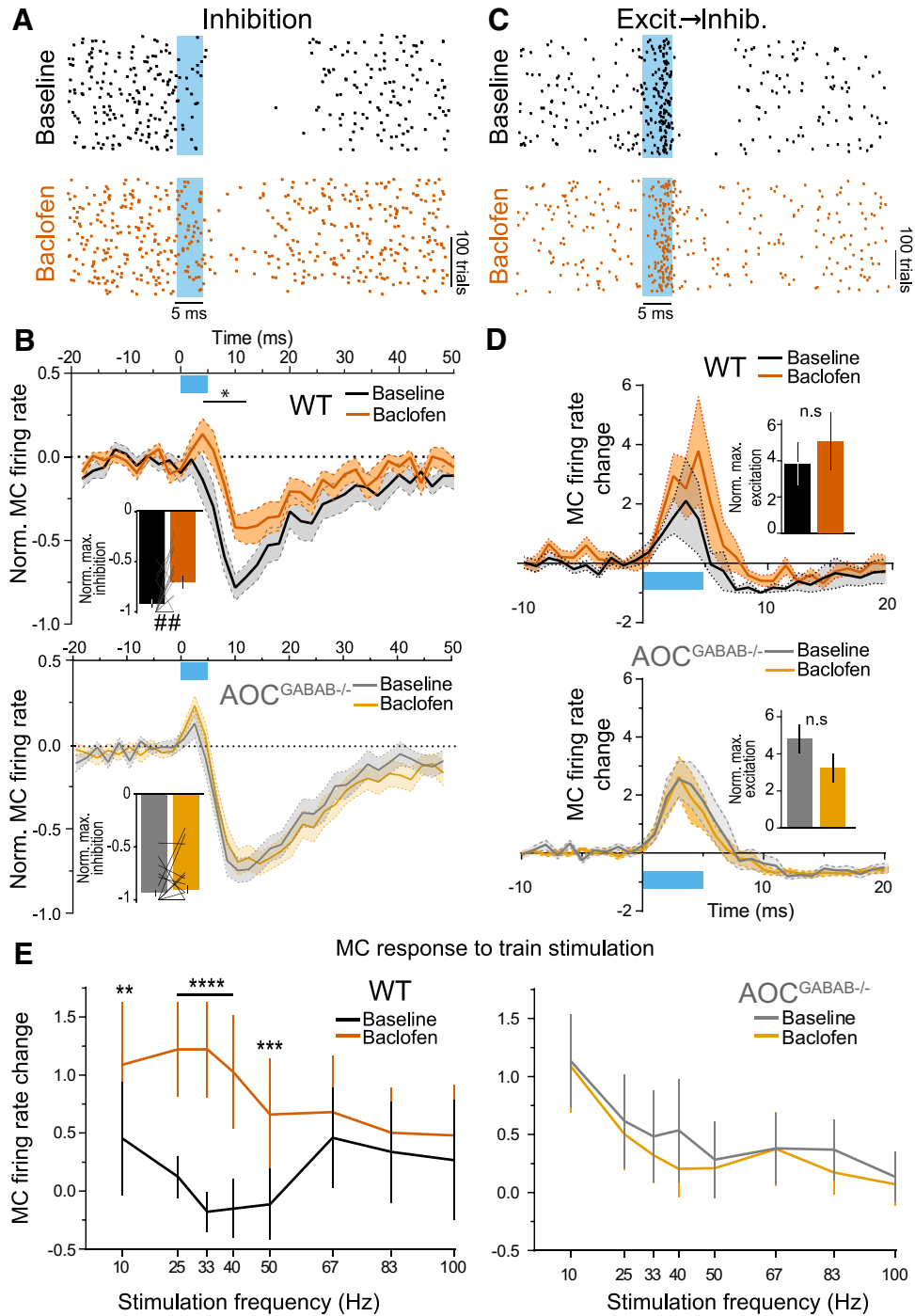


Figure 4. Single light pulse analysis reveals target-specific GABA_B modulation of cortical inputs to the OB. **A**, Raster plot of a cell inhibited by a single light pulse (5 ms), before (top) and after (bottom) baclofen (2.5 mM) application. **B**, Normalized PSTH of M/T cell population after a single light pulse delivery in WT (top), $n = 18$ and AOC^{GABAB^{-/-}} mice (bottom, $n = 29$) before and after baclofen application. Inset, Normalized firing rate trough in basal and baclofen conditions. **C**, Raster plot of a cell displaying a brief excitation followed by a prolonged inhibitory response after light stimulation and before (top) and after (bottom) baclofen application. **D**, Normalized PSTH of the M/T cell receiving direct excitation to a single light pulse in WT (top, $n = 7$) and AOC^{GABAB^{-/-}} animals (bottom, $n = 14$) before and after baclofen application. Inset, Normalized firing rate peak. **E**, M/T cell mixed excitatory/inhibitory response to AOC train light stimulation. Normalized change in M/T cell firing rate during 10 ms after light stimulation for the same neurons as in **D**. In baclofen conditions, WT M/T cell displayed a higher excitatory response to light at 10–50 Hz stimulation. $\#\#p < 0.05$ with a Wilcoxon matched-pairs rank-sum test; $*p < 0.05$ to $p < 0.0001$ with a Sidak's multiple-comparisons test after two-way ANOVA, $**p < 0.01$, $***p < 0.001$, $****p < 0.0001$ with a Fisher's LSD test after two-way ANOVA.

in AOC^{GABAB^{-/-}} animals (WT: $-0.8 \pm 15.4\%$, $n = 21$; AOC^{GABAB^{-/-}}: $-17.6 \pm 7.0\%$, $n = 29$; Two-way ANOVA, $F_{(1,48)} = 5.59$, $p < 0.02$, but Fisher's LSD *post hoc* test: $p = 0.11$ and 0.09 in WT and AOC^{GABAB^{-/-}} animals, respectively; vehicle injection in WT: $p = 0.55$, Wilcoxon matched-pairs rank-sum test, $n = 9$; Fig. 5B,C). Together with the absence of a significant

effect of baclofen on M/T cell spontaneous activity, these results suggest that local baclofen application in the GCL did not permit baclofen diffusion superficially to the GL. In contrast, baclofen strongly decreased gamma oscillations in a similar fashion in WT and AOC^{GABAB^{-/-}} animals (WT: $-42.8 \pm 5.6\%$, $n = 21$ and AOC^{GABAB^{-/-}}: $-44.0 \pm 4.3\%$, $n = 29$, $F_{(1,48)} = 20.18$, $p <$

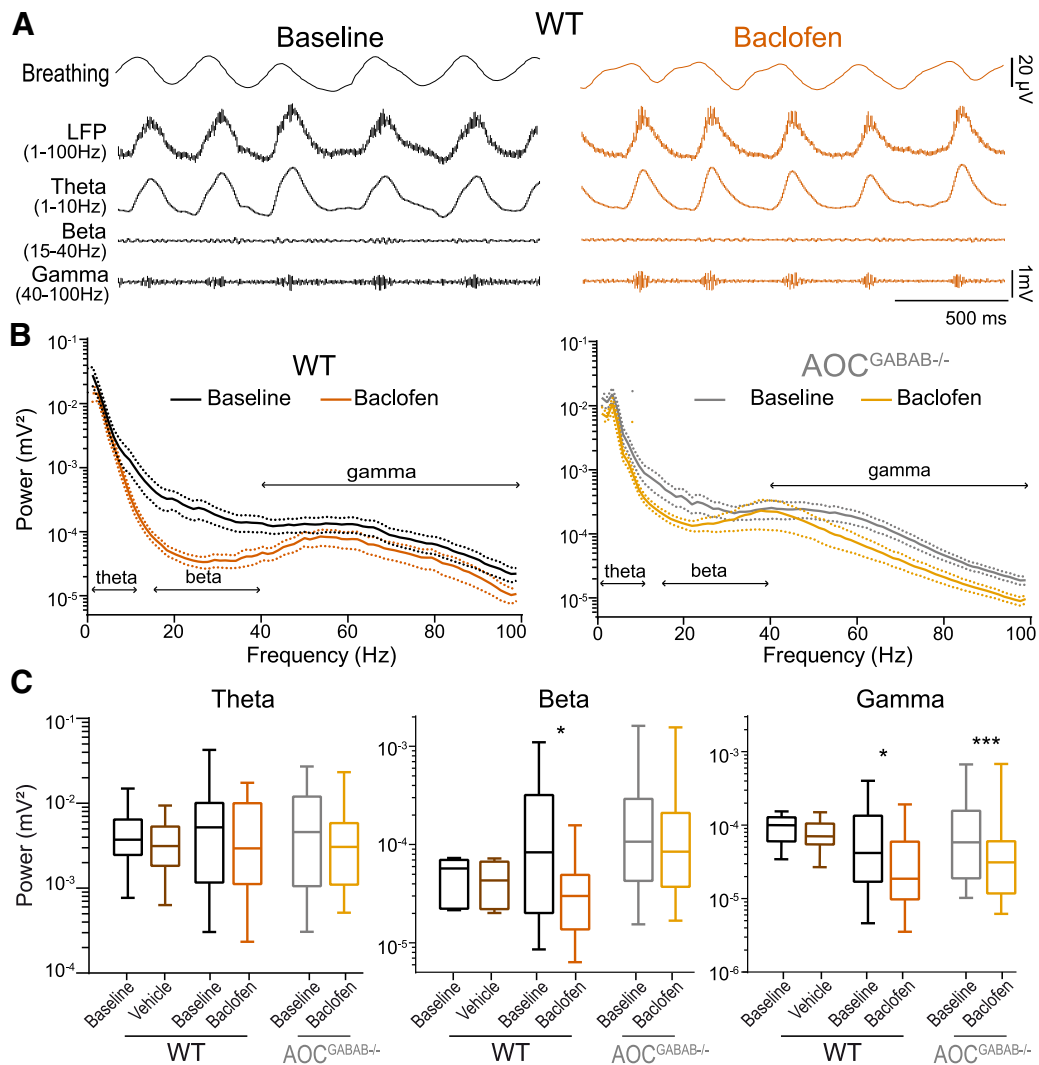


Figure 5. Activation of GABA_BRs on cortical feedback projections depresses beta OB oscillations. **A**, Example recordings of awake LFP and filtered signals showing spontaneous theta (1–10 Hz), beta (20–40), and gamma (40–100 Hz) band before (left) and after (right) baclofen (2.5 mM) injection. **B**, Whole power spectrum of spontaneous LFP before and after baclofen application in WT (left) and AOC^{GABAB-/-} (right) mice. **C**, Spontaneous theta, beta, and gamma oscillation power before and after baclofen application in WT and AOC^{GABAB-/-} animals. * $p < 0.05$, *** $p < 0.001$ with a Fisher's LSD test after two-way ANOVA.

0.0001; Fisher's LSD *post hoc* test: $p = 0.017$ in WT and $p = 0.0002$ in AOC^{GABAB-/-}, vehicle in WT: $-12.2 \pm 10.4\%$, $p = 0.50$; $n = 9$; Fig. 5B,C). Therefore, the reduction of gamma rhythms likely reflects GABA_BR activation at GC-to-MC synapses (Isaacson and Vitten, 2003; Valley et al., 2013) that are unaltered by our conditional knock-out approach (Fig. 2G). In contrast to gamma oscillations, baclofen strongly decreased spontaneous beta oscillations in WT animals, but not in AOC^{GABAB-/-} mice (respectively, $-54.0 \pm 6.9\%$, $n = 21$ and $-17.8 \pm 7.0\%$, $n = 29$, $F_{(1,48)} = 9.60$, $p < 0.005$, Fisher LSD *post hoc* test: $p < 0.05$ in WT and $p = 0.08$ in AOC^{GABAB-/-}; vehicle in WT: $-7.2 \pm 3.6\%$, $p = 0.50$, $n = 9$; Fig. 5B,C). Therefore, presynaptic GABA_BR activation on cortico-bulbar inputs regulates spontaneous beta but not gamma oscillations in the OB.

AOC feedforward inhibition of odor-evoked M/T activity is depressed by GABA_BR activation

We next investigated the impact of GABA_BR activation at AOC axons on sensory-evoked activity in M/T cells. By stimulating AOC axons during odor presentation, we analyzed the effects of

light stimuli on odor-evoked responses (Fig. 6A). We used frequencies of 10, 33, and 67 Hz to deliver light pulses because these frequencies recruit distinct degree of inhibition (Fig. 3F) and correspond to different regimes of cortical activities (respectively theta, beta, and gamma). Figure 6B shows an example M/T cell response to odor and simultaneous odor + light stimulation at baseline or in the presence of baclofen.

Across the population of M/T cells, odor stimulation resulted in either excitation or inhibition in awake mice ($n = 16$ and $n = 24$ odor-unit pairs, respectively, six mice; Fig. 6C,D). Baclofen application had no effect on the population response ($-1.76 \pm 4.19\%$; two-way ANOVA: baclofen \times stimulation: $F_{(3,117)} = 12.92$, $p < 0.0001$; Sidak's multiple-comparisons test: $p = 0.99$; $n = 40$; Fig. 6E). Simultaneous odor + light stimulation produced a significant decrease in odor-evoked M/T cell firing activity at light frequencies of 33 and 67 Hz, whereas 10 Hz light stimulation did not alter the neuron's evoked activity (one-way ANOVA: $F_{(3,72,144.9)} = 22.4$, $p < 0.0001$; Holm-Sidak's multiple-comparisons test: $p = 0.061$ for 10 Hz, $p < 0.0001$ for 33 and 67 Hz stimulation; $n = 40$; Fig. 6Di,Dii,Diii), regardless of whether the odor was excitatory or inhibitory ($p > 0.05$ at 10 Hz and $p <$

0.0001 at 33 and 67 Hz for both odor responses, $n = 16$ and $n = 24$, respectively; Fig. 6E). The light-induced inhibition of M/T cell odor-evoked activity was diminished with baclofen for both 33 and 67 Hz stimulation, whereas baclofen had no effect on 10 Hz light stimulation (baclofen-induced diminution of light inhibition: 10 Hz: $-3.1 \pm 4.2\%$, 33 Hz: $-34.4 \pm 5.4\%$, 67 Hz: $-12.3 \pm 6.2\%$; baclofen $F_{(1,39)} = 4.38$, $p < 0.043$, baclofen \times stimulation: $F_{(3,117)} = 12.92$, $p < 0.0001$; $p = 0.92$, $p < 0.0001$ and $p < 0.05$ at 10, 33 and 67 Hz; $n = 40$; Fig. 6E). When separately analyzing odor-inhibited and odor-excited neurons, we observed that, for odor-inhibited responses, baclofen depressed the inhibition of M/T cell activity induced by simultaneous odor and light application at 33 or 67 Hz. For odor-excited responses, baclofen produced a significant decrease in M/T cell inhibition only when odor stimulation was paired with 33 Hz light (odor-inhibited neurons: $F_{(1,23)} = 29.0$, $p < 0.0001$, baclofen \times stimulation: $F_{(3,69)} = 27.9$, $p < 0.0001$; $p < 0.0001$ for 33 and 67 Hz, $n = 24$; odor-excited neurons: $F_{(1,15)} = 0.67$, $p = 0.043$, baclofen \times stimulation: $F_{(3,45)} = 36.1$, $p < 0.0001$; $p < 0.01$ for 33 Hz and $p = 0.49$ for 67 Hz, $n = 16$). Therefore, in the context of odor-evoked M/T cell activity, GABA_BR activation at AOC axon terminals depresses the cortico-bulbar inhibition on M/T cells.

To confirm the impact of cortical GABA_BR presynaptic activation on odor-evoked activity of the M/T cell population, we performed calcium imaging in freely behaving animals using fiber photometry (Fig. 7A). To specifically record M/T cell Ca²⁺ transients, we injected a Cre-dependent AAV expressing GCaMP6f (Chen et al., 2013) in the dorsolateral region of Tbet-Cre mice OBs (Haddad et al., 2013). GCaMP6f was excited continuously at low intensity (0.4–0.5 mW) and the volume fluorescence was collected using an optic fiber implanted above the injection site, spectrally separated using a dichroic mirror, and emission intensity was measured with a femtowatt photodetector (Fig. 7A,B). To gain independent light control of AOC axons and to avoid cross-excitation between GCaMP6f and ChR2, we injected the red-shifted channelrhodopsin ChRimson (Klapoetke et al., 2014) into the AOC and targeted red light stimulation above the AOC, which was connected to a 589 nm laser (Fig. 7A,B). Using this technique, AOC light stimulation at 10, 33, or

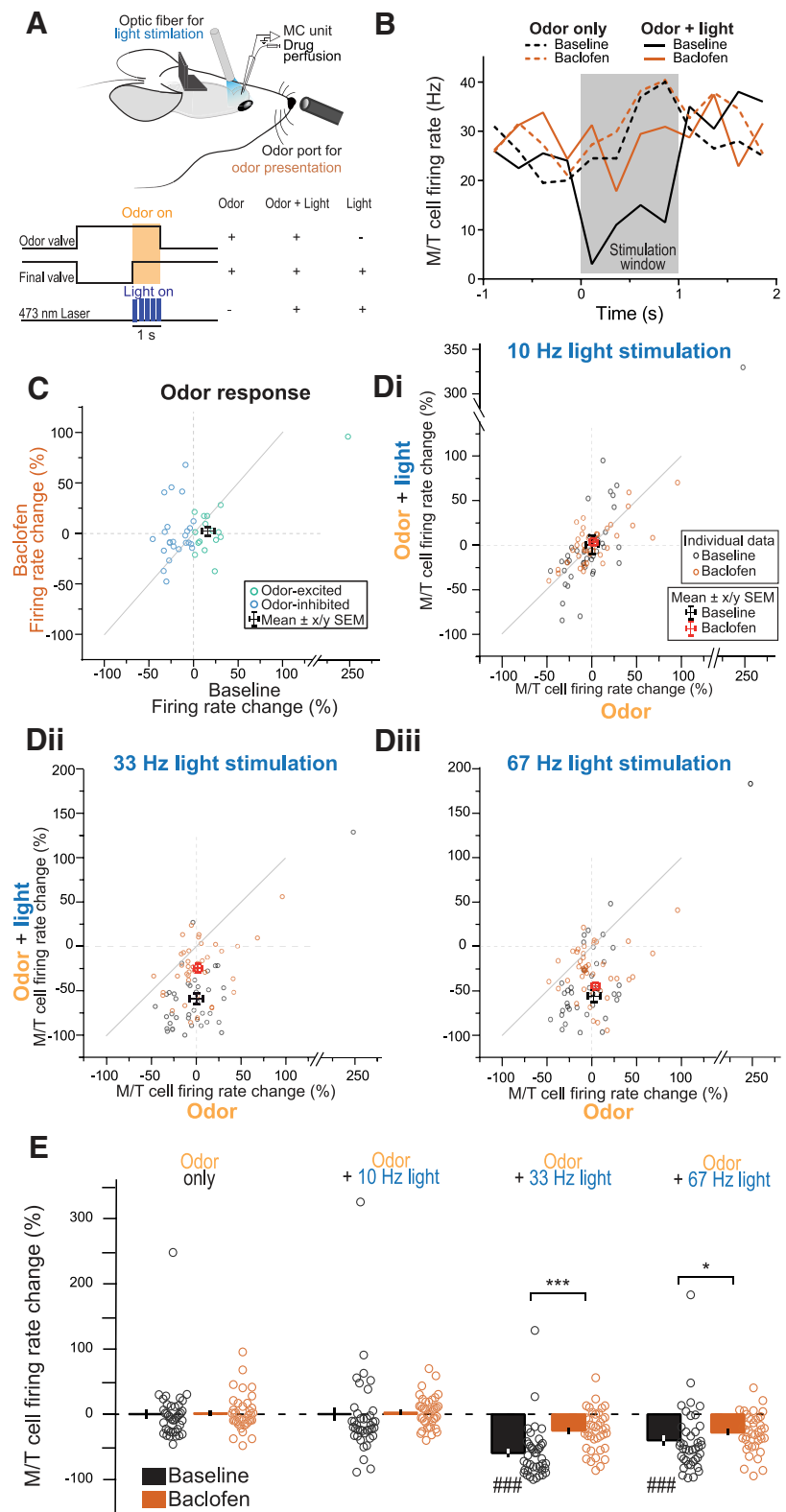


Figure 6. GABA_BR activation at AOC axons diminishes the light-induced inhibition of M/T cell odor-evoked activity. **A**, Top, Schematic drawing showing light delivery and odor presentation to the animal's nose while recording M/T cell activity in awake mice. Bottom, Timing of the stimuli presentation. Light and/or odor were alternatively presented for 1 s. The final valve always opened at the onset of stimulation even in light-only trials. **B**, Example cell's response to odor or simultaneous odor and light presentation in baseline and baclofen conditions. **C**, Odor response of individual neuron–odor pair ($n = 40$) in baseline and baclofen conditions. **D**, Firing rate change of neuron–odor pairs ($n = 40$) to odor only or simultaneous odor and light presentation at 10 (**Di**), 33 (**Dii**), or 67 Hz (**Diii**). **E**, Summary of the impact of 10, 33, or 67 Hz light stimulation on odor-evoked activity of individual neuron–odor pair in baseline and baclofen conditions. Black and red crosses represent the mean \pm x and y SEM. ### $p < 0.0001$ with a Holm–Sidak's multiple-comparisons test after one-way ANOVA; * $p < 0.05$ and *** $p < 0.001$ with a Sidak's multiple-comparisons test after two-way ANOVA.

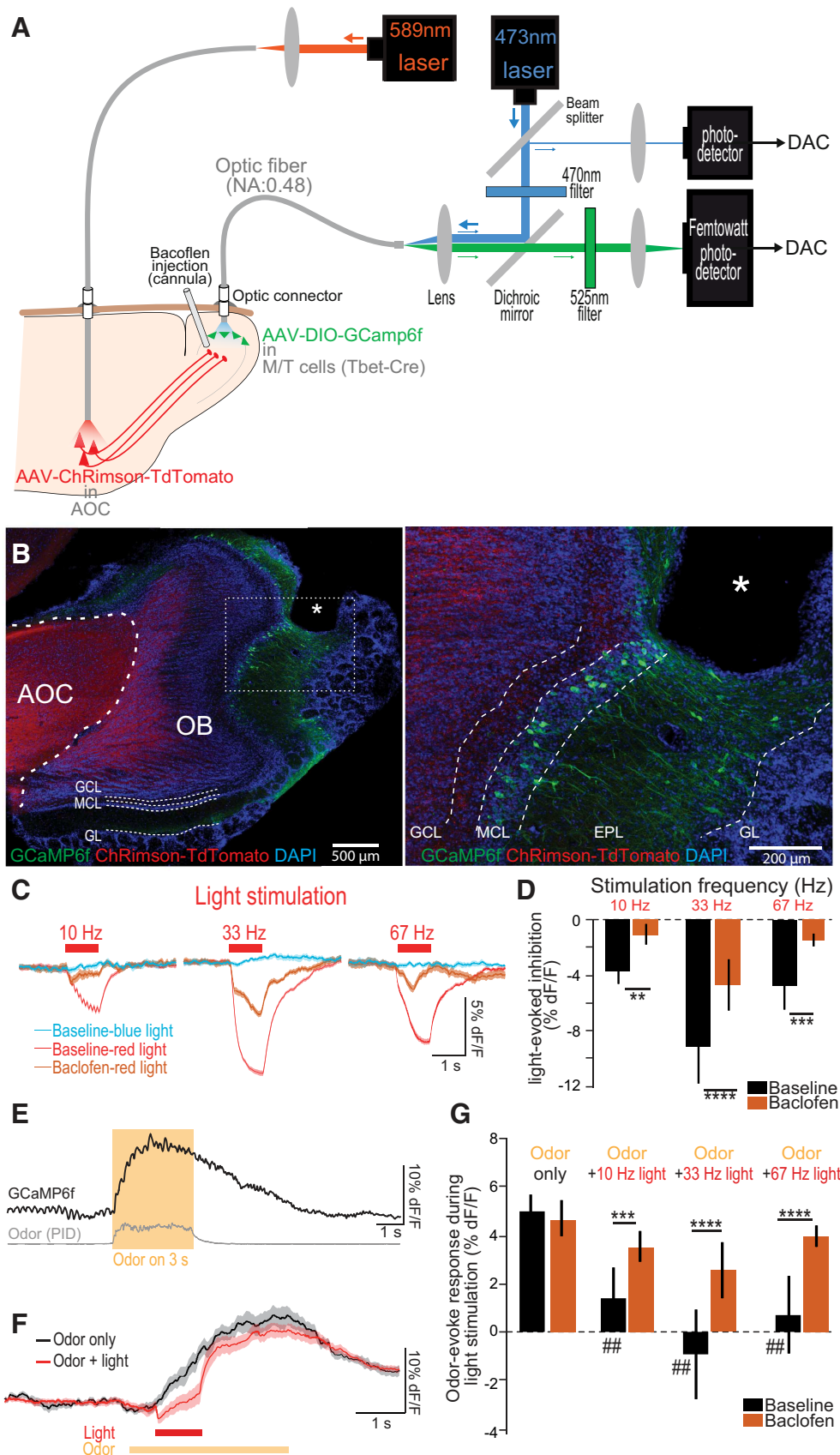


Figure 7. Fiber photometry of Ca^{2+} dynamics reveals that light-induced inhibition of M/T cell odor-evoked activity is reduced by $GABA_B$ activation. **A**, Schematic of the experimental paradigm using fiber photometry. Conditional $GCaMP6f$ expression in $Tbet-Cre$ mice was restricted to M/T cells. Light path for $GCaMP6f$ fluorescence excitation and emission was through a single $400 \mu m$ fiber optic (NA 0.48) connected to an implanted optic fiber targeting the dorsolateral part of the OB. The red-shifted channelrhodopsin $ChRimson$ was expressed in AOC neurons and light activated using an optic fiber implanted above the injection site and connected to a 589 nm laser. **B**, Confocal images showing $ChRimson$ expression in AOC axons and $GCaMP6f$ (Figure legend continues.)

67 Hz with red light (589 nm, 5–10 mW) produced a global reduction of spontaneous fluorescence at the recording site ($\Delta F/F$: $-3.7 \pm 0.9\%$ at 10 Hz, $-9.2 \pm 2.7\%$ at 33 Hz, and $-4.8 \pm 0.7\%$ at 67 Hz, $n = 6$; Fig. 7C), confirming the sensitivity of fiber photometry to detect a population decrease in Ca^{2+} transients during spontaneous activity in freely behaving mice. These effects were not observed when using blue light (473 nm) at the intensity used for GCaMP6f excitation (0.4–0.5 mW), validating the absence of cross-excitation between ChR2 and GCaMP6f (Fig. 7C). With local OB infusion of baclofen, this inhibition was reduced (two-way ANOVA: baclofen $F_{(1,5)} = 13.05$, $p = 0.015$, Holm–Sidak’s multiple-comparisons test: $p < 0.01$ for all light frequencies; Fig. 7C,D). Upon odor presentation, M/T cell responses were characterized by a strong elevation in fluorescence superimposed on a robust breathing modulation of the signal (Fig. 7E). We observed an increase in the GCaMP6f signal in all the odor-recording site pairs in basal conditions (Fig. 7F) and these odor-evoked transients remained unchanged in presence of baclofen (baseline: $+4.9 \pm 0.8\%$, baclofen: $+4.7 \pm 0.7\%$; paired t test: $p = 0.69$; $n = 15$; Fig. 7G). When the AOC was light stimulated in addition to odor presentation, we observed a decrease in the M/T cell odor-driven responses (one-way ANOVA: $F_{(1,461,20,46)} = 13.25$, $p = 0.0006$, Holm–Sidak’s multiple-comparisons test: $p < 0.01$ for 10, 33, and 67 Hz frequencies, $n = 15$; Fig. 7G). Similar to the electrophysiological recordings, we found that baclofen depressed the light-induced reduction of M/T cell odor-evoked activity and this effect was significant at all frequencies (baclofen: $F_{(1,14)} = 4.7$, $p = 0.048$, baclofen \times stimulation: $F_{(2,28)} = 1.9$, $p < 0.17$, $p < 0.001$ *post hoc* for 10, 33, and 67 Hz frequencies, $n = 15$; Fig. 7G). Together with our *in vivo* electrophysiological recordings, these data show that activation of presynaptic GABA_BRs at AOC axon terminals profoundly remodels M/T cell responses to simultaneous sensory and top-down inputs.

Discussion

Cortical projections influence olfactory information processing as early as in the first central relay of the olfactory system, namely the OB. In this region, cortico-bulbar feedback transfers information about, for example, brain states, attention, and prior sensory experience. Because these top-down inputs convey signals relative to dynamic internal states, their regulation must be an essential feature for their precise function. In this study, we revealed a GABA_BR-dependent mechanism to modulate cortico-bulbar feedback. Using a combination of genetics, pharmacology, electrophysiology, and Ca^{2+} imaging of neuronal population, we found that: (1) activation of presynaptic GABA_BRs reduces the direct glutamatergic inputs

onto GCs, but not M/T cells; (2) GABA_BR activation blocks cortical-driven feedforward inhibition of M/T cells’ spontaneous and odor-evoked firing activity; (3) GABA_BR activation biases M/T cell excitatory/inhibitory response ratio to cortical stimulation toward excitation; and (4) depressing glutamate release from AOC axons reduces beta, but not gamma oscillations. Interestingly, GABA_BR activation does not shunt the overall AOC feedback to the OB, but instead refines the functional connectivity between the AOC and OB.

In this study, we introduced ChR2 into the two olfactory primary cortices, the AON and APC, to gain control over the main source of cortico-bulbar projections. Despite the anatomical distinction of the two olfactory cortices, there is no clear evidence that they affect OB function differentially. Both areas mainly target the GCL and GL of the OB (Boyd et al., 2012; Markopoulos et al., 2012; Lepousez et al., 2014) and, even though distinction in the precise connectivity patterns seems to exist, such subtle differences can also be found within specific area subdivisions (Haberly and Price, 1978a, 1978b; Davis and Macrides, 1981). Moreover, recent studies investigating either AON or APC inputs reported a comparable connectivity pattern (NBQX-sensitive inputs to GCs, MCs, and GL neurons such as periglomerular neurons and superficial short axon cells) and similar functional impact on M/T cell odor-evoked responses (Boyd et al., 2012; Markopoulos et al., 2012). Therefore, we chose here to consider the AON and APC as a single functional entity that we collectively named the anterior (primary) olfactory cortex (or AOC). Further work would be required to investigate potential differences in top-down functions of AON and APC.

GABA_BRs are widely expressed in the OB. In addition to cortico-bulbar terminals, GABA_BRs are expressed at olfactory sensory neuron terminals to depress glutamate release. Sensory inputs drive M/T cell activity (Cang and Isaacson, 2003; Margrie and Schaefer, 2003; Phillips et al., 2012) and generate theta OB oscillations (for review, see Kay et al., 2009). In our condition, neither M/T cell spontaneous firing rate nor theta rhythms was sensitive to local baclofen infusion in the GCL. Therefore, it seems apparent that baclofen did not diffuse superficially to sensory axon terminals in the GL. Recordings of fEPSPs at different depths in the GCL further confirmed the drug diffusion area to be $< 600 \mu\text{m}$. GABA_BRs are also expressed at GC apical dendrites, where they depress GABA release, as reported *in vitro* (Isaacson and Vitten, 2003; Valley et al., 2013). Surprisingly, we did not observe any effect of baclofen on light-evoked feedforward inhibition onto M/T cells in AOC^{GABAB^{-/-}} mice (Fig. 3F). Given the remoteness of the virus injection site to the OB, the unaltered GABA_BR1 immunoreactivity in the EPL of AOC^{GABAB^{-/-}} mice and with the near absence of labeled GCs in the OB, it is highly unlikely that the virus diffused to the OB and altered GABA_BR expression at GC dendrites. Moreover, spontaneous gamma oscillations, which rely on dendrodendritic reciprocal synapses (Rall and Shepherd, 1968; Lepousez and Lledo, 2013), were strongly reduced after GABA_BR activation in AOC^{GABAB^{-/-}}. Therefore, the lack of effect of baclofen on M/T cell feedforward inhibition in AOC^{GABAB^{-/-}} mice suggests that distal stimulation of GCs by M/T cell dendrites triggers GABA_BR-sensitive GABA release, whereas AOC terminal proximal stimulation of GCs triggers GABA release in a GABA_BR-independent manner. An alternate hypothesis could be that AOC axon stimulation preferentially engages adult-born GCs, which have been proven to be GABA_BR insensitive (Valley et al., 2013). In any case, because GABA_BR activation had no effect in AOC^{GABAB^{-/-}} mice, we further reasoned that AOC inputs trigger feedforward inhibi-

←

(Figure legend continued.) in M/T cells. Right, Higher-magnification image showing the track of the implanted 400 μm optic fiber above intact GCaMP6f-expressing M/T cells and dendrites in the dorsolateral part of the OB. C, Average photometry traces (mean \pm SE, average of 10 traces) in baseline with red (589 nm, 5–10 mW) or blue light stimulation (473 nm, 0.4–0.5 mW) and in baclofen with red light stimulation (589 nm, 5–10 mW). D, Summary of fluorescence changes during light stimulation in baseline and baclofen conditions ($n = 6$). E, Representative individual trace showing M/T cell fluorescence changes with odor presentation. Note the breathing modulation on top of the odor-evoked response. Odor dynamic was measured using a PID. F, Average photometry traces (mean \pm SE, average of 10 traces) with odor presentation (black) and with odor + 33 Hz light stimulation (red) in baseline condition. G, Summary of odor- and odor + light-evoked changes in M/T cell fluorescence across all odor-recording pairs ($n = 15$). ## $p < 0.01$, comparing odor and odor + light responses with a Holm–Sidak’s multiple-comparisons test after one-way ANOVA, ** $p < 0.01$, *** $p < 0.001$, **** $p < 0.0001$ with a Sidak’s multiple-comparisons test after two-way ANOVA.

tion but do not drive significant dendrodendritic recurrent inhibition between M/T cells.

To our knowledge, the present study is the first to show the presence of GABA_BRs in a cortico-bulbar synapse. Using selective GABA_BR knock-down in cortico-bulbar projections, we discovered an additional site of GABA_BR expression that adds more insight into the understanding of GABA_BR-dependent modulation of OB activity. We showed that activation of presynaptic GABA_BRs depresses the AOC-to-GC excitatory synapse, thereby blocking AOC-driven feedforward inhibition onto M/T cells. In contrast, we did not find any evidence for GABA_BR-dependent modulation of the AOC-to-M/T cell synapse. The target-dependent expression of presynaptic GABA_BR could reflect the diversity of AOC-projecting cells or it could be determined by the activity or the nature of the postsynaptic target (i.e., glutamatergic or GABAergic), as reported in cultured hippocampal neurons (Schinder et al., 2000). This target-dependent functional expression of GABA_BRs modifies the balance between cortical excitation and feedforward inhibition received by M/T cells. Because the temporal window M/T cells use to integrate cortical excitatory events is tightly controlled by GABA_BR-sensitive feedforward inhibition, GABA_BR activation enlarges this integration windows as observed in thalamo-cortical feedforward circuits (Chittajallu et al., 2013). Using patterned light stimulation of cortico-bulbar inputs at different frequencies, we observed that this differential GABA_BR sensitivity extends the coupling between M/T cell responses and AOC axon stimulations to beta frequencies (10–50 Hz; Fig. 3F). Given that cortical activity can operate at such rhythms, we propose that GABA_BR modulation participates in gating the transfer of the beta regimes on M/T cell firing activity. Consistent with this, we found that GABA_BR activation at cortico-bulbar inputs selectively depresses spontaneous beta oscillations.

Recent evidence suggests a role for top-down inputs on temporal activity of the targeted structure. Top-down inputs might affect ongoing oscillations, synchronicity of postsynaptic cells, and coherence between brain areas (Engel et al., 2001). In the olfactory system, by acting at the AOC axon terminals, we demonstrated that GABA_BRs are well positioned to regulate coherence between distant structures, such as the AOC and the OB, a phenomenon likely to emerge in behaviorally relevant tasks (Chabaud et al., 1999; Kay and Beshel, 2010; Cohen et al., 2015). In particular, beta oscillations were depressed by cortical GABA_BR activation and have been proposed to be supported by a reentry of cortical input in the OB (Gray and Skinner, 1988; Neville and Haberly, 2003; Martin et al., 2014). GABA_BR could thereby regulate the shift in coherence between cortical structures and the OB under different sensory experiences (adaptation, learning, memory, etc.). In the near future, it will be of great interest to investigate the behavioral impact of this GABA_BR-dependent presynaptic modulation of top-down activity and to decipher in which context it is engaged.

References

- Balu R, Pressler RT, Strowbridge BW (2007) Multiple modes of synaptic excitation of olfactory bulb granule cells. *J Neurosci* 27:5621–5632. [CrossRef Medline](#)
- Boyd AM, Sturgill JF, Poo C, Isaacson JS (2012) Cortical feedback control of olfactory bulb circuits. *Neuron* 76:1161–1174. [CrossRef Medline](#)
- Boyd AM, Kato HK, Komiyama T, Isaacson JS (2015) Broadcasting of cortical activity to the olfactory bulb. *Cell Rep* 10:1032–1039. [CrossRef Medline](#)
- Cang J, Isaacson JS (2003) In vivo whole-cell recording of odor-evoked synaptic transmission in the rat olfactory bulb. *J Neurosci* 23:4108–4116. [Medline](#)
- Chabaud P, Ravel N, Wilson DA, Gervais R (1999) Functional coupling in rat central olfactory pathways: a coherence analysis. *Neurosci Lett* 276:17–20. [CrossRef Medline](#)
- Chen T-W, Wardill TJ, Sun Y, Pulver SR, Renninger SL, Baohan A, Schreier ER, Kerr RA, Orger MB, Jayaraman V, Looger LL, Svoboda K, Kim DS (2013) Ultrasensitive fluorescent proteins for imaging neuronal activity. *Nature* 499:295–300.
- Chittajallu R, Pelkey KA, McBain CJ (2013) Neurogliaform cells dynamically regulate somatosensory integration via synapse-specific modulation. *Nat Neurosci* 16:13–15. [CrossRef Medline](#)
- Cohen Y, Putrino D, Wilson DA (2015) Dynamic cortical lateralization during olfactory discrimination learning. *J Physiol* 593:1701–1714. [CrossRef Medline](#)
- Davis BJ, Macrides F (1981) The organization of centrifugal projections from the anterior olfactory nucleus, ventral hippocampal rudiment, and piriform cortex to the main olfactory bulb in the hamster: an autoradiographic study. *J Comp Neurol* 203:475–493. [Medline](#)
- Engel AK, Fries P, Singer W (2001) Dynamic predictions: oscillations and synchrony in top-down processing. *Nat Rev Neurosci* 2:704–716. [CrossRef Medline](#)
- Franks KM, Russo MJ, Sosulski DL, Mulligan AA, Siegelbaum SA, Axel R (2011) Recurrent circuitry dynamically shapes the activation of piriform cortex. *Neuron* 72:49–56. [CrossRef Medline](#)
- Gray CM, Skinner JE (1988) Centrifugal regulation of neuronal activity in the olfactory bulb of the waking rabbit as revealed by reversible cryogenic blockade. *Exp Brain Res* 69:378–386. [Medline](#)
- Gunaydin LA, Grosenick L, Finkelstein JC, Kauvar IV, Fenno LE, Adhikari A, Lammel S, Mirzabekov JJ, Airan RD, Zalocusky KA, Tye KM, Anikeeva P, Malenka RC, Deisseroth K (2014) Natural neural projection dynamics underlying social behavior. *Cell* 157:1535–1551. [CrossRef Medline](#)
- Haberly LB, Price JL (1978a) Association and commissural fiber systems of the olfactory cortex of the rat. II Systems originating in the olfactory peduncle. *J Comp Neurol* 181:781–807. [CrossRef Medline](#)
- Haberly LB, Price JL (1978b) Association and commissural fiber systems of the olfactory cortex of the rat. I. Systems originating in the piriform cortex and adjacent areas. *J Comp Neurol* 178:711–740. [CrossRef Medline](#)
- Haddad R, Lanjuin A, Madisen L, Zeng H, Murthy VN, Uchida N (2013) Olfactory cortical neurons read out a relative time code in the olfactory bulb. *Nat Neurosci* 16:949–957. [CrossRef Medline](#)
- Haller C, Casanova E, Müller M, Vacher CM, Vigot R, Doll T, Barbieri S, Gassmann M, Bettler B (2004) Floxed allele for conditional inactivation of the GABAB(1) gene. *Genesis* 40:125–130. [CrossRef Medline](#)
- Isaacson JS, Strowbridge BW (1998) Olfactory reciprocal synapses: dendritic signaling in the CNS. *Neuron* 20:749–761. [CrossRef Medline](#)
- Isaacson JS, Vitten H (2003) GABA(B) receptors inhibit dendrodendritic transmission in the rat olfactory bulb. *J Neurosci* 23:2032–2039. [Medline](#)
- Kay LM, Beshel J (2010) A beta oscillation network in the rat olfactory system during a 2-alternative choice odor discrimination task. *J Neurophysiol* 104:829–839. [CrossRef Medline](#)
- Kay LM, Beshel J, Brea J, Martin C, Rojas-Libano D, Kopell N (2009) Olfactory oscillations: the what, how and what for. *Trends Neurosci* 32:207–214. [CrossRef Medline](#)
- Klapoetke NC, Murata Y, Kim SS, Pulver SR, Birdsey-Benson A, Cho YK, Morimoto TK, Chuong AS, Carpenter EJ, Tian Z, Wang J, Xie Y, Yan Z, Zhang Y, Chow BY, Surek B, Melkonian M, Jayaraman V, Constantine-Paton M, Wong GK, et al. (2014) Independent optical excitation of distinct neural populations. *Nat Methods* 11:338–346. [CrossRef Medline](#)
- Lepousez G, Lledo PM (2013) Odor discrimination requires proper olfactory fast oscillations in awake mice. *Neuron* 80:1010–1024. [CrossRef Medline](#)
- Lepousez G, Nissant A, Bryant AK, Gheusi G, Greer CA, Lledo PM (2014) Olfactory learning promotes input-specific synaptic plasticity in adult-born neurons. *Proc Natl Acad Sci U S A* 111:13984–13989. [CrossRef Medline](#)
- Linster C, Fontanini A (2014) Functional neuromodulation of chemosensation in vertebrates. *Curr Opin Neurobiol* 29:82–87. [CrossRef Medline](#)
- Ma M, Luo M (2012) Optogenetic activation of basal forebrain cholinergic neurons modulates neuronal excitability and sensory responses in the main olfactory bulb. *J Neurosci* 32:10105–10116. [CrossRef Medline](#)
- Manabe H, Kusumoto-Yoshida I, Ota M, Mori K (2011) Olfactory cortex

- generates synchronized top-down inputs to the olfactory bulb during slow-wave sleep. *J Neurosci* 31:8123–8133. [CrossRef Medline](#)
- Margeta-Mitrovic M, Mitrovic I, Riley RC, Jan LY, Basbaum AI (1999) Immunohistochemical localization of GABA(B) receptors in the rat central nervous system. *J Comp Neurol* 405:299–321. [CrossRef Medline](#)
- Margrie TW, Schaefer AT (2003) Theta oscillation coupled spike latencies yield computational vigour in a mammalian sensory system. *J Physiol* 546:363–374. [CrossRef Medline](#)
- Markopoulos F, Rokni D, Gire DH, Murthy VN (2012) Functional properties of cortical feedback projections to the olfactory bulb. *Neuron* 76:1175–1188. [CrossRef Medline](#)
- Martin C, Ravel N (2014) Beta and gamma oscillatory activities associated with olfactory memory tasks: different rhythms for different functional networks? *Front Behav Neurosci* 8:218. [CrossRef Medline](#)
- Martin C, Gervais R, Messaoudi B, Ravel N (2006) Learning-induced oscillatory activities correlated to odour recognition: a network activity. *Eur J Neurosci* 23:1801–1810. [CrossRef Medline](#)
- Matsutani S, Yamamoto N (2008) Centrifugal innervation of the mammalian olfactory bulb. *Anat Sci Int* 83:218–227. [CrossRef Medline](#)
- Neville KR, Haberly LB (2003) Beta and gamma oscillations in the olfactory system of the urethane-anesthetized rat. *J Neurophysiol* 90:3921–3930. [CrossRef Medline](#)
- Otazu GH, Chae H, Davis MB, Albeanu DF (2015) Cortical feedback decorrelates olfactory bulb output in awake mice. *Neuron*:1–17.
- Petzold GC, Hagiwara A, Murthy VN (2009) Serotonergic modulation of odor input to the mammalian olfactory bulb. *Nat Neurosci* 12:784–791. [CrossRef Medline](#)
- Phillips ME, Sachdev RN, Willhite DC, Shepherd GM (2012) Respiration drives network activity and modulates synaptic and circuit processing of lateral inhibition in the olfactory bulb. *J Neurosci* 32:85–98. [CrossRef Medline](#)
- Poo C, Isaacson JS (2009) Odor representations in olfactory cortex: “sparse” coding, global inhibition, and oscillations. *Neuron* 62:850–861. [CrossRef Medline](#)
- Rall W, Shepherd GM (1968) Theoretical reconstruction of field potentials and dendrodendritic synaptic interactions in olfactory bulb. *J Neurophysiol* 31:884–915. [Medline](#)
- Schinder AF, Berninger B, Poo M (2000) Postsynaptic target specificity of neurotrophin-induced presynaptic potentiation. *Neuron* 25:151–163. [CrossRef Medline](#)
- Shea SD, Katz LC, Mooney R (2008) Noradrenergic induction of odor-specific neural habituation and olfactory memories. *J Neurosci* 28:10711–10719. [CrossRef Medline](#)
- Soria-Gómez E, Bellocchio L, Reguero L, Lepousez G, Martin C, Bendahmane M, Ruehle S, Remmers F, Desprez T, Matias I, Wiesner T, Cannich A, Nissant A, Wadleigh A, Pape HC, Chiarlone AP, Quarta C, Verrier D, Vincent P, Massa F, et al. (2014) The endocannabinoid system controls food intake via olfactory processes. *Nat Neurosci* 17:407–415. [CrossRef Medline](#)
- Valley MT, Henderson LG, Inverso SA, Lledo PM (2013) Adult neurogenesis produces neurons with unique GABAergic synapses in the olfactory bulb. *J Neurosci* 33:14660–14665. [CrossRef Medline](#)
- Youngstrom IA, Strowbridge BW (2015) Respiratory modulation of spontaneous subthreshold synaptic activity in olfactory bulb granule cells recorded in awake, head-fixed mice. *J Neurosci* 35:8758–8767. [CrossRef Medline](#)

1.2 Supplementary results

In addition to these results, other experiments aiming at tackling several remaining questions have been performed.

To ask whether or not GABA_BR at AOC axons are tonically activated *in vivo*, I performed direct injections of the antagonist CGP. This direct injection had no effect on the light-evoked fEPSP slope or amplitude ($p > 0.05$, $n = 5$) or on light-evoked feedforward inhibition of M/T cell multi-units ($F(1,10) = 0.86$, $p = 0.37$ with a two-way ANOVA, $n = 11$). These results suggest the lack of tonic activation of these GABA_BRs, at least under spontaneous activity.

Next, I tried to induce activation of these GABA_BRs using classic protocols to evoke repetitive and synchronous GABA release from GCs. Using different protocols with seconds-long stimulation of AOC axons at high frequency (> 40 Hz), I aimed at evoking massive GABA release from AOC postsynaptic targets, both GCs and dSACs. Repeated and synchronous GABA release would then bind GABA_BRs at AOC axons to depress glutamate release and thus the light-evoked fEPSPs. Repeated stimulation of AOC axons at various frequencies produced different short-term plasticity behavior at the AOC-to-GC membrane, as measured by fEPSP recordings. Yet, application of CGP failed to induce a significant modification of this short-term plasticity. Direct stimulation of OB GABAergic neurons using conditional ChR expression in VGAT-Cre animals (Vong et al., 2011) is another possibility to drive local GABA release. This will require to express a version of ChR that is activated by a different wavelength in the AOC. However, excitation spectra of ChR2 and ChRmison, a red-shifted version of ChR, overlap and thus care should be taken in the choice of which structure would express which version of ChR (see "Discussion" part). The use of electrical stimulation is another possibility, and since this technique it is possible to avoid stimulation of the LOT and trigger anti-dromic spikes in M/T cells, but one should bear in mind that this method of stimulation is not specific and will likely stimulate other centrifugal fibers. In addition, this method of stimulation produces deflections in the LFP that are much slower than what we observed using ChR stimulation (see for example Manabe et al., 2011; Neville and Haberly, 2003), thus it is not clear to me what is measured utilizing this protocol.

I next aimed at increasing the extracellular concentration of GABA to investigate whether GABA_BRs at AOC axons could be activated by broad an increase in the extracellular tone of GABA. To do so, I first locally applied GABA uptake blockers (such as NO 711, NPPB and SNAP 5114 to block GABA transporter 1, 2 and 3) and then perfused CGP. Again, CGP had no effect in these conditions ($n = 3$). Because we did not measure whether our cocktail or GABA uptake inhibitor did increase the extracellular concentra-

tion of GABA, these results should be interpreted with caution. Nevertheless, together with the experiments aiming at releasing GABA from local OB neurons, these data suggest that presynaptic GABA_BR at the AOC-to-GC synapse are not spill-over detectors under spontaneous activity.

Chapter 2

GABAergic cortico-bulbar
projections to the olfactory bulb
alter olfactory perception (Article 2,
in preparation)

2.1 Results from the article in preparation

Long-range GABAergic projections from the olfactory cortex control olfaction

Camille Mazo, Gabriel Lepousez, Antoine Nissant, Enzo Peroni, Julien Grimaud, Lucie Dixsaut
and Pierre-Marie Lledo¹.

Laboratory for *Perception and Memory*, Institut Pasteur, F-75015 Paris, France.
Centre National de la Recherche Scientifique (CNRS), Unité Mixte de Recherche (UMR-3571), F-75015
Paris, France.

¹To whom correspondence should be addressed: Laboratory for Perception and Memory,
Institut Pasteur and CNRS, 25 rue du Dr. Roux, 75 724 Paris Cedex 15, France.
Tel: (33) 1 45 68 88 03 — **Fax:** (33) 1 45 68 83 69 — **E-mail:** pmlledo@pasteur.fr

Manuscript information:

Format: Article

Number of pages:

Number of figures:

Total word count: . **Abstract;**; **Introduction;**; **Discussion:**.

Running title: Long-range GABAergic projections control olfaction.

Keywords: Sensory circuits, Top-down, Long-range inhibitory projections, Behavior, Fiber photometry, Calcium Imaging, optogenetic, pharmacogenetic.

The authors declare no conflict of interest.

Author contributions: CM, GL, AN and PML designed the experiments, CM, GL, AN, EP, JG and LD performed and analyzed the experiments. CM, GL and PML wrote the manuscript.

Abstract

Sensory perception is shaped greatly by feedback inputs. In olfaction, top-down inputs from the olfactory cortex innervate the earliest brain region for olfaction, the olfactory bulb. As in other sensory systems, this feedback has been widely described as being only glutamatergic. Here we reveal that part of the cortical feedback arise from a subset of GABAergic neurons that mainly express somatostatin. Selective expression of genetics tools in cortical GABAergic neurons reveals that these projection neurons target a variety of bulbar neurons, which results in disinhibition of olfactory bulb principal cells *in vivo*. Monitoring of cortical GABAergic feedback confirmed their involvement during olfactory behavior and selective manipulation of their activity altered odor detection. We thus demonstrate for the first time the existence of a GABAergic feedback in a sensory system, and showed that it tunes olfactory abilities.

Introduction

Sensory perception results from the interaction between feedforward and feedback inputs. This convergence occurs at early brain levels emerging from the sensory thalamus in vision, audition, gustation and somatosensation, and as early as the first brain relay in olfaction in the olfactory bulb (OB). Long-range projections from cortical regions are mainly glutamatergic, while GABAergic projections are often considered local, giving rise to the metonymy “interneuron” to refer to GABAergic neurons. Yet long-range GABAergic projections associating brain areas with distinct functions are found in the forebrain (for reviews, see Tamamaki and Tomioka, 2010; Caputi et al., 2013). For instance, reciprocal long-range GABAergic projections have been reported between the hippocampus and the entorhinal cortex (Melzer et al., 2012; Basu et al., 2016), between the hippocampus and the septum (Jinno and Kosaka, 2002; Takács et al., 2008) and also between neocortical areas (Tomioka et al., 2005). However, long-range GABAergic projections between different stages of a sensory system have never been reported.

In the olfactory bulb (OB), sensory input from olfactory sensory neurons is transmitted to mitral and tufted cells (M/T cells), the principal output neurons of the OB. Information is first locally processed by different microcircuits embedded in different layers, before being transmitted to the downstream olfactory cortex (Wilson and Mainen, 2006; Murthy, 2011; Uchida et al., 2013). Like the corticothalamic pathway, the olfactory cortex, and mainly the anterior olfactory nucleus (AON) and anterior piriform cortex (APC) in return send massive glutamatergic innervation back to the OB (de Olmos et al., 1978; Haberly and Price, 1978a, 1978b; Davis and Macrides, 1981; Luskin and Price, 1983; Carson, 1984; Shipley and Adamek, 1984; Padmanabhan et al., 2016; Mazo et al., 2017). Glutamatergic feedback from the AON and APC have been reported to target almost every type of neuron in the OB, with a main effect on inhibitory neurons which results in feedforward inhibition of odor responses in OB principal cells (Boyd et al., 2012; Markopoulos et al., 2012).

In addition to the cortico-bulbar glutamatergic projections, the OB also receives external GABAergic inputs from the basal forebrain (Zaborszky et al., 1986; Kunze et al., 1992a, 1992b; Gracia-Llanes et al., 2010; Nunez-Parra et al., 2013). Descriptive observations from two studies only reported the presence of very rare inhibitory OB-projecting neurons in the olfactory cortex, but the exact anatomical characterization was kept succinct and the function unaddressed (Zaborszky et al., 1986; Diodato et al., 2016).

In this study, we used anterograde and retrograde viral-genetic based tracing techniques to first demonstrate that a subpopulation of GABAergic neurons in the olfactory cortex send long-range GABAergic projection to the OB. These GABAergic projections originate in the AON and APC, and particularly in the AON *pars posterioralis* (AONpp). Combining *in vitro* and *in vivo* approaches, together with selective genetic manipulation, we further studied the activity dynamics of the GABAergic feedback, their cellular targets in the OB and the impact of manipulating their activity on the OB network and behavior.

Results

The olfactory cortex sends GABAergic projections back to the olfactory bulb.

To investigate whether or not the anterior olfactory cortex (AOC) sends GABAergic projections to the OB, we injected the AON and APC of VGAT-Cre mice with a conditional adeno-associated virus (AAV) expressing channelrhodopsin-2 (ChR2) fused to eYFP in a Cre-dependant manner (AAV-Flex-ChR2-eYFP; **Figure 1A-C**). Following injection, top-down fibers were visualized in the OB (**Figure 1D,E**). We confirmed the GABAergic nature of the ChR2+ fibers by Immunohistological labeling against GAD65 and GAD67 (**Figure 1F**). Fluorescence was predominantly found in the granule cell layer (GCL), but peaks of fluorescence were also detected in the deepest part of the glomerular layer and surrounding the mitral cell layer (**Figure 1D,E**). A similar distribution pattern among OB layers was observed when using a GAD1-Cre mouse line (data not shown). To clarify the exact origin of these OB-projecting GABAergic cells, we injected the right OB of VGAT-Cre animals with the retrogradely transported herpes simplex virus (HSV) expressing the green fluorescent reporter GCaMP6f in a Cre-dependant manner (HSV-Flex-GCaMP6f; **Figure 2A**). In addition to retrogradely labeled cells in the HDB/MCPO nucleus of the basal forebrain (Zaborszky et al., 1986; Gracia-Llanes et al., 2010; Nunez-Parra et al., 2013), a significant number of scattered cells were detected in the AON or APC (**Figure 2B,C**). Very rare cells were visible in the olfactory tubercle or posterior regions of the olfactory cortex (posterior piriform cortex, cortical amygdala or lateral entorhinal cortex) and no cells were visible either in the left contralateral side. Both spiny and aspiny neurons were retrogradely labeled (**Figure 2D**), and immunohistochemistry confirmed their GABAergic nature (**Figure 2E**). We also observed neurites, presumably from GABAergic AONpp neurons, passing between the OT and APC reaching the LOT. Finally, axons from cortical GABAergic cells appeared to enter the OB *via* both the ventral and dorsal LOT in the olfactory peduncle.

Interestingly, we found a higher concentration of labeled neurons at the border between the APC and olfactory tubercle (**Figure 2B,C**). Careful anatomical observation suggests that this GABAergic cell cluster belongs to a caudal subdivision of the AON, namely the AONpp. In the medio-lateral axis, AONpp GABAergic cell cluster extends from the lateral half of the olfactory peduncle to half the APC (preliminary results, **Figure S1C**). In the antero-posterior axis, it spreads from the caudal end of the AON to half of the APC.

Overall, 45% of the retrogradely-labeled GABAergic cells were found in the basal forebrain (HDB/MCPO), 38% in the AONpp and the remaining 17% scattered between different subdivisions of the AON (mainly in *par externa*) and in the APC (in layer 1 and 3; **Figure S1C**). Counting across successive sagittal and coronal sections allowed us to obtain a coarse 3D reconstruction of the region sending these cortical GABAergic inputs to the OB.

To confirm our observations in the AON and APC, OB-projecting cells were labeled by injecting a fluorophore-conjugated cholera toxin subunit B retrograde tracer (CTB) into the OB, and GABAergic cells of the AON, APC, OT and striatum were injected with AVV-Flex-GCamp6f in VGAT-Cre mice (**Figure 3A**). Analysis of the CTB+ cell distribution eased the delimitation between the APC, containing densely labeled layer 2b cells (Haberly and Price, 1978b; Diodato et al., 2016; Padmanabhan et al., 2016), and AONpp, containing a more homogenous distribution of projecting cells (Haberly and Price, 1978a; Padmanabhan

et al., 2016). In these sections, a large proportion of CTB+ / GCaMP6+ dually labeled cells were found in a cluster inside the AONpp, while lower cell densities were observed in the APC or other subdivision of the AON (**Figure 3B,C**). Immunostaining against the cholinergic marker ChAT confirmed that this cluster did not contain cholinergic cells (**Figure S1B**), thus ruling out the possibility that these GABAergic OB-projecting cells belong to the basal forebrain or the ventral pallidum, as suggested previously (de Olmos et al., 1978; Shipley and Adamek, 1984). Taken together, these results demonstrate that the AON and APC contain GABAergic cells sending projections to the OB, with a significant proportion of these long-range projecting GABAergic cells being concentrated in the AONpp. To our knowledge, this is the first description of OB GABAergic feedback innervation emanating from the olfactory cortex.

OB-projecting GABAergic cells from the cortex mainly express somatostatin.

Long-range projecting cells in the brain are diverse with regards to their protein expression patterns (Tamamaki and Tomioka, 2010; Caputi et al., 2013). Therefore, we examined the molecular markers expressed by the OB-projecting cells from the AOC. Using viral-genetic tracing in specific mouse Cre lines, we focused on the expression of somatostatin (SOM), parvalbumin (PV) or the vasoactive intestinal peptide (VIP) because they are found in largely non-overlapping populations of both the AON (Kay and Brunjes, 2014) and APC (Suzuki and Bekkers, 2010). We first injected an AAV-Flex-ChR2-TdTomato into the AOC of VIP-Cre, SOM-cre and PV-Cre mice. Substantial innervation in the OB of SOM-Cre mice was observed, while we detected only very sparse labeling in PV-Cre and VIP-Cre mice (**Figure 4**). Importantly, the density of GABAergic fibers in the OB were 50% lower in SOM-Cre mice compared to VGAT-Cre mice, suggesting that SOM is expressed in only a sub-population of the OB-projecting cortical GABAergic cells. To confirm these observations by another method, we next injected the retrograde virus HSV-Flex-GCaMP6f in the OB. We found a large number of retrogradely-labeled cells in SOM-Cre mice, whereas only few cells were labeled in VIP-Cre and PV-Cre mice (**Figure 4**), thus confirming the higher proportion of SOM-expressing cells in the OB-projecting cortical GABAergic neurons. However, only few cells were labeled in the AONpp of SOM-Cre mice.

Cortical GABAergic projecting cells target various OB neurons

Given that cortico-bulbar GABAergic fibers innervate all layers of the OB (**Figure 1**), we investigated the functional connectivity of these fibers with multiple targets in the OB. To tackle this issue, we injected AAV-Flex-ChR2 in the AOC of VGAT-Cre mice and obtained acute OB slices (**Figure 5A**). In the GCL, light stimulation of ChR2-expressing fibers elicited IPSCs in most of the deep short-axon cells recorded (5/6 cells connected, 38.3 ± 4.7 pA, low light intensity), while granule cells (GCs) displayed a lower degree of connectivity (15/39 cells connected, 22.2 ± 3.2 pA, low light intensity). These light-evoked IPSCs display fast latencies, were completely suppressed by the GABA_A receptor antagonist gabazine (5 μ M), and resistant to the AMPAR blocker NBQX, consistently with monosynaptic GABAergic transmission (**Figure 5B,C**). In contrast, no inputs were found in glomerular layer neurons (periglomerular cells: 0/17 or external tufted cells: 0/2) or in mitral cells (0/7).

Inhibition of cortical GABAergic feedback improves odor detection performance at low concentrations

To test the impact of cortical GABAergic feedback on olfactory behavior, we specifically manipulated the activity of GABAergic axons targeting the OB. Designer receptors exclusively activated by designer drugs (DREADD) were specifically expressed in AOC neurons (AAV-Flex-DREADD in VGAT-CRE mice). DREADD⁺ GABAergic axons projecting to the OB were then selectively targeted by an intrabulbar infusion of the ligand clozapine-N oxide (CNO; **Figure 6A**). To manipulate GABAergic axons in a bidirectional manner, the excitatory (hM3D, AAV2.5-hM3D-eYFP, n = 10) and the inhibitory (hM4D, AAV2.5-hM4D-eYFP, n = 8) versions of DREADDs were expressed in separate groups of animals. The control group included mice expressing hM4D or hM3D infused with saline in the OB (n = 4) or mice not transfected with a virus and infused with CNO in the OB (n = 5).

Following CNO or saline intrabulbar infusion, mice were placed in an olfactometer to perform a Go/No-Go odor-reward association task (**Figure 6A**). We did not observe any significant effect of either activation or inhibiting cortical GABAergic fibers in monomolecular odor discrimination learning, reversal learning or during a discrimination task using binary mixtures with increasing similarity (L+/L- 75/25 vs. 25/75, 60/40 vs 40/60 and 55/45 vs. 45/55). However, we found an effect of inhibiting the cortical GABAergic feedback when the odors to be discriminated were highly diluted (10^{-6} in mineral oil, but not for 10^{-3} , 10^{-4} or 10^{-5} ; **Figure 6B**). When behavioral performances were segregated according to the odor value (rewarded or not), we observed that there was a significantly greater decrease in the number of false alarms of the hM4D group at dilution of 10^{-6} (Two-way repeated measure ANOVA, block x group interaction: $F(9,135) = 1.956$, $p = 0.0492$), but not for other tasks, notably when mice had to discriminate the same odor couple at a dilution of 10^{-5} ($p > 0.05$; **Figure 6C**).

Discussion

Anatomical characterization of olfactory cortical regions sending GABAergic projections to the OB

In this study, we demonstrate that GABAergic neurons of the olfactory cortex send feedback projections to the OB. Projecting neurons were found scattered in the AON and APC, with a substantial concentration forming a cluster in the AONpp, located in the ventro-medial region of the APC, at the border with the OT. The cluster of OB-projecting cells in the AONpp has already been reported in non-specific retrograde labeling studies in hamster (Davis et al., 1978; Davis and Macrides, 1981), rats (de Olmos et al., 1978; Haberly and Price, 1978a) and mice (Shiple and Adamek, 1984; Miyamichi et al., 2013). Yet no study determined the nature of the neurotransmitter release by projecting cells in this region, probably because the vast majority of AON projection neurons, taken as a whole, are glutamatergic (Markopoulos et al., 2012). The AON comprises two main regions: *pars principalis* and *pars externa*, the former being further divided according to cardinal points in *pars dorsalis*, *pars lateralis*, *pars medialis*, *pars ventralis* and *pars posterioralis* (Herrick, 1910; Haberly and Price, 1978a; Brunjes et al., 2005). Different AON subdivisions (Brunjes et al., 2005) as well as different regions of the APC (anterior or posterior) (Hintiryan et al., 2012) send glutamatergic projections with distinct patterns across OB layers. However, addressing AON subregion input and output organization is particularly challenging since AON subdivisions are arbitrary and exhibit wide variations. Among them, the boundary between the AONpp and *ventralis* is very poorly defined, and the two subregions have often been combined to form the AON *pars ventroposterioralis* (Haberly and Price, 1978a; Brunjes et al., 2005). As for the APC, output channels were found to be segregated with regards to their projections targets (Chen et al., 2014; Diodato et al., 2016; Mazo et al., 2017). In this study, we show that AOC subdivisions exhibit further differences when considering the neurochemical nature of their projections to the OB. Here we focused on GABAergic projections to the OB, but more comprehensive studies looking at the detailed output organization of AOC subdivisions with regards to their neurochemical features and targets might shed light on additional differences defining the functional organization of the output of the AOC.

Detailed examination of the OB-projecting GABAergic cells revealed several interesting anatomical features. First, we observed that GABAergic projecting neurons in the AONpp extend neurites in between the OT and APC to receive inputs from the LOT. Extension of dendrites of AONpp neurons have been reported in hamster, although the dendrites seemed to pass through the OT to receive inputs from the LOT (Davis et al., 1978). Second, we did not find significant numbers of GABAergic projection axons or retrogradely-labeled GABAergic projecting cells in the AONpp, in contrast to the bilateral projections of unspecified neurochemical nature emanating from the hamster AONpp (Davis et al., 1978). Therefore, differences in contralateral projection patterns might arise either from species differences, or could alternatively be a signature of the difference between the glutamatergic and GABAergic projection systems of the AONpp. Third, we noticed that the caudal extension of the AONpp seems to spread in relative close proximity to another nucleus of the basal forebrain sending GABAergic projections, namely the HDB/MCPO. Interestingly, we observed axons connecting the two structures. However, immunohistochemistry labeling confirmed that the cluster we identified was not cholinergic, ruling out the possibility that it forms a rostral extension of the basal forebrain under the olfactory cortex (de Olmos et al., 1978; Shiple and Adamek, 1984). It worth noting here that the identified basal

forebrain nucleus location matched well with the nucleus of the horizontal band of Broca and magnocellular preoptic nucleus (HDB/MCPO) in medial slices, but we find extension of that basal forebrain division much more laterally than reported by classical anatomy studies.

Methods

Animals. Adult GAD1-Cre ($Gad1^{tm2(cre)Mony}$, MGI ID: 4830465) or VGAT-Cre mice ($Slc32a1^{tm(cre)Lowl}$, MGI ID: 5141270) (both maintained on a C57Bl/6 background) were used in this study. This work was performed in compliance with the French application of the European Communities Council Directive of 22 September 2010 (2010/63/EEC) and approved by the local ethics committee (CETEA 89, project #01126.02).

Stereotaxic injections. Adeno-associated viruses (AAV; capsid serotype 2/5 or 2/9) were generated by the Penn Vector Core, University of North Carolina Vector core, or produced by the Institut National de la Santé et de la Recherche Médicale (INSERM, UMR 1089, IRT1 Vector platform Nantes, www.atlantic-gene-therapies.fr). Herpes simplex viruses (HSV) were produced by the MIT gene transfer core. CTB conjugated to either Alexa Fluor 555 (C34776) or biotinylated (C34779) were obtained from Molecular probes. Viral injections were performed as previously describe (Soria-Gómez et al., 2014; Mazo et al., 2016a). Briefly, mice were deeply anesthetized with a ketamine and xylazine mixture (150 mg/kg Imalgene and 5mg/kg Rompun, respectively; i.p.) and placed in a stereotaxic apparatus. A small craniotomy was performed and viral solution was injected into the brain bilaterally through a glass micropipette attached to a Nanoinjector system (Nanoject II). Coordinates for the injections; AON: 2.3 mm anterior from Bregma, 1.1 mm lateral and 3.3 and 3.5 mm deep from the brain surface, 100nL/site; APC: 1.9 mm anterior from Bregma, 2.25 mm lateral and 3.8 and 4.2 mm deep from the brain surface; 150-200 nL/site, 300-400 nL total; OB: AP: 5 mm, ML: 1.0 mm, DV: several injections from 1mm to 2 mm deep, 300 nL total.

For electrophysiology experiments, high titer stock of either AAV2/5-EF1a-Flex-ChR2-eYFP or AAV2/9-EF1a-Flex-ChR2-mCherry-WPRE (viral titer, 1.8×10^{13} or 1.4×10^{13} genome copies per ml) were injected in VGAT-IRES-Cre.

For photometry experiments, high titer stock of AAV2/9-hSyn-flex-ChRimson-TdTomato-WPRE (viral titer, 2.2×10^{13}) were injected in the APC and AON, and/or AAV-hSyn-DIO-GCaMP6f-WPRE constructs (viral titer: 1.1×10^{13}) were injected in the OB of VGAT-IRES-Cre mice.

For behavior experiments, an AAV2.5-Flex-hM4D-eYFP or AAV2.5-Flex-h3MD-eYFP was injected in the AON and APC.

For anatomy experiments, HSV-hEF1-Flex-GCaMP6f were injected in the OB, and AAV2/9-hSyn-flex-ChRimson-TdTomato-WPRE (viral titer, 2.2×10^{13}) and/or AAV2/1-hSyn-DIO-GCaMP6f-WPRE construct (viral titer: 1.1×10^{13}) and/or AAV2/9-CaMKII-hM4D-mCherry (1.1×10^{13}) were injected in VGAT-Cre or GAD1-Cre mice. For the dual-conditional experiment, a HSV-hEF1-Flex-mCherry-IRES-Flp was injected in the OB, and an AAV2/5-EF1a-fDIO-hChR2(H134R)-eYFP (4.2×10^{12}) was injected in the AON and APC. Larger volumes were used for identification of GABAergic neurons (Figure 3): 150nL/site in the AON and 300nL/site in the APC.

Histology.

Tissue preparation. Animals were intracardially perfused (4% paraformaldehyde (PFA) in 0.1M phosphate buffer) and the brains were removed and post-fixed in the same fixative overnight. Brain sections were then cut with a vibratome. For post-hoc analyses of recording sites and viral expression, 100 μ m-thick

sections were sliced. OB sections were inspected to check for proper axonal expression, absence of virus diffusion into the OB, and for the absence of significant somatic labeling in the OB. 50 μm -thick sections were used for anatomical analyzes.

Immunohistochemistry. Primary and secondary antibodies used in this study are summarized in Table 1. Immunohistochemistry labelings were performed as follow: slices were rinsed, permeabilized and blocked in 10% serum and PBST for 2 h, and incubated in primary antibodies for up to 48 h at 4°C. Secondary antibodies was then incubated for 2 h. Slices were then rinsed and counterstained with DAPI, mounted and imaged with a confocal microscope (LSM 700, Zeiss).

Cell counting of retrogradely-labeled cells. Series of 50 μm -thick coronal or sagittal slices were taken for cell quantification. Regions were manually determined using morphological parameters, DAPI staining and immunohistochemistry labeling. Antero-posterior or medio-lateral coordinates were determined in coronal and sagittal slices, respectively, using a reference atlas and position relative to following and preceding slices.

Quantification of labeled fibers in the OB. Density of GABAergic, ChR2+ fibers was determine using the ImageJ plugin “plot profile” across OB layers. Multiple measurements were performed and a representative example is shown.

Electrophysiology.

Slice recording. Tissue preparation was carried out as described in Valley et al. (2013). Briefly, tissue was dissected in ACSF and three-hundred-micrometer-thick slices were vibrosectioned. Recordings were made with borosilicate glass pipettes with a tip resistance between 3 and 6 M Ω . Recordings were discarded if the access resistance exceeded half the input resistance of the cell or if the access resistance varied by $\sim 30\%$ during the experiment. Data were digitized at 10kHz (EPC9double; HEKA). ChR2 stimulation used a 470 nm light-emitting diode array (Bridgelux). Light duration was controlled using a digital sequencer (Master-8; A.M.P.I.), and all stimulations were given with an inter-stimulus interval of 20 s.

In vivo recording. Awake recordings were performed as previously described (Lepousez and Lledo, 2013; Soria-Gómez et al., 2014; Mazo et al., 2016b). Mice were anesthetized and an L-shaped metal bar as well as a silver reference electrode were fixed to the caudal part of the skull. Optic fibers (multimode, 430 μm diameter, NA 0.39, Thorlabs) were bilaterally implanted above the anterior commissure (400 μm posterior to the sinus of the olfactory bulb, 0.9 mm lateral and 2.3 mm deep from the brain surface with an angle of $\sim 30^\circ$). After greater than a week of recovery, mice were slowly and progressively trained for head-restraint habituation and a 5% sucrose solution was given as a reward. The craniotomy was performed the day before recording and protected with silicone sealant (KwikCast). An array of four tungsten electrodes (~ 3 M Ω , FHC) glued to one or two miniature cannulas (polymide tubing, 0.0035”, Neuralynx; positioned 100-200 μm above the electrode tips, connected to a 10 μL -Hamilton syringe) was slowly lowered into the OB and a drop of silicone sealant was applied to the brain surface to increase recording stability. Both LFP and spiking signals were continuously recorded 40 min before and 60 min after local drug microinjection through the miniature cannula (injection speed: 0.05 $\mu\text{L}/\text{min}$; 0.15-0.3 μL total). Signals were pre-amplified (HS-18, Neuralynx), amplified (x 1000 Lynx8, Neuralynx) and digitized

at 20 kHz (Power 1401 A/D interface, CED). The identity of M/T cells units were established on the basis of several criteria: 1) stereotaxic coordinates of the mitral cell layer, 2) decrease in both gamma oscillation amplitude and light-evoked fEPSP in the mitral cell layer, compared to the LFP recorded in the GCL or EPL, where the current sources/sinks are localized (Neville and Haberly, 2003), 3) increase in background spiking activity in a narrow band of 100–150 μ m, 4) typical spontaneous activity patterns coarsely time-locked to the respiration rhythm and, 5) odor-evoked responses. Light stimulation of Chr2+ axons was performed using either an optic fiber placed on the OB brain surface or with implanted optical fibers coupled to a DPSS laser (473 nm, 150 mW, CNI Lasers; output fiber intensity, 20mW) via a custom-built fiber launcher and controlled by a PS-H-LED laser driver connected to the CED interface. Light stimulation consisted in train stimulation (10 – 67 Hz) of 5 ms-long light pulses. The craniotomy was cleaned and covered with Kwik-Cast between sessions. We performed four recording sessions per mice (two per hemisphere), which were made at least 1-2 d apart.

Odor presentation. We used a custom-built flow-dilution olfactometer controlled by the CED interface. Pure monomolecular odorants (Sigma-Aldrich) were diluted in mineral oil (5%) in odorless glass vials. Saturated odor vapor was further diluted with humidified clean air (1:10) by means of computer-controlled solenoid pinch valves. Odor presentation dynamics were monitored and calibrated using a miniPID (Aurora). Cycles of odor, light and odor + light presentations were repeated at least 7 times for each condition. Stimuli were applied for 1 s and a given odorant was presented every 50 s to prevent sensory adaptation. The odorants used were: ethyl butyrate, ethyl valerate, 1-pentanol, 1,4 cineole, valeraldehyde, ethyl tiglate, (S)-limonene, 2-hexanone, butyric acid, valeric acid, acetophenone, hexanoic acid, amyl acetate, geraniol, benzaldehyde and carvone-(+).

Calcium imaging using fiber photometry. We used a fiber photometry system adapted from Gunaydin et al., 2014. Immediately following GCaMP6f virus injection in the OB or AOC, optical fibers (multimode, 430 μ m in diameter, NA 0.48, LC zirconia ferrule) were bilaterally implanted in the dorso-lateral part of the OB above the virus injection site. Three weeks post-injection, GCaMP6f was continuously excited using a 473 nm DPSS laser (output fiber intensity, 0.4-0.5mW; CNI Lasers) reflected on a dichroic mirror (452-490 nm/505-800 nm) and collimated into a 400 μ m multimode optical fiber (NA, 0.48) with a convergent lens ($f = 30$ mm). The emitted fluorescence was collected in the same fiber and transmitted by the dichroic mirror, filtered (525 ± 19 nm) and focused on a NewFocus 2151 femtowatt photoreceptor (Newport; DC mode). Reflected blue light along the light path was also measured with another amplified photodetector (PDA36A, Thorlabs) for monitoring light excitation and fiber coupling. Signals from both photodetectors were digitized by a digital-to-analog converter (DAC; Power 1401, CED) at 5000 Hz and recorded using Spike2 software. For AOC stimulation using ChRimson, an optic fiber (multimode, 430 μ m diameter, NA 0.39, with LC zirconia ferrule; Thorlabs; 5-10 mW output fiber intensity) were bilaterally implanted above the AOC and connected to a DPSS laser (589 nm, 200 mW, CNI Lasers) via a custom-built fiber launcher.

Mice were placed in small ventilated cage (~ 0.5 L) for passive odor presentation, and in a custom-built olfactometer for the odor discrimination tasks (see “Behavior” section for the training protocol and

for the performances measurement). Pure monomolecular odorants were diluted in mineral oil (1%) and saturated odor vapor was delivered into the ventilated cage or olfactometer at a flow rate of 3L/min. Odors were presented every 30 s and odor presentation dynamics in the cage were constantly monitored using a miniPID (Aurora).

Behavior. Guide cannulas (26 gauge, 8 mm long) were bilaterally implanted over the OB on the same day as viral injections. Guide cannulas were stabilized using dental cement and a dummy cannula was positioned in the guide cannula to prevent blocking. On the day of the experiments, dummies were retrieved, cannulas (8 mm long to reach the GCL, 33-gauge and connected to a 10 μ l Hamilton syringe) were placed for injections in the GCL. Dummies were replaced a few minutes after the end of the injection.

Behavior experiments were conducted using a go/no- go operant conditioning scheme as previously described (Alonso et al., 2012; Lepousez and Lledo, 2013). 2 weeks after the surgery, aged-matched adult male VGAT-IRES-Cre mice (10-12 weeks old, n = 27) were water deprived and trained in custom-built olfactometers. The weight of the animals was strictly monitored and kept >85% of the initial body weight. Mice had first to learn the procedure before being tested. To do so, mice were placed in an olfactometer to explore the set-up and to learn that water can only be obtained by licking at a metal tube placed 5 cm left to the odor port. Then, mice had to learn to insert their snout into the odor sampling port for at least 1.2 s to obtain the water reward. Once mice exhibited high behavioral robustness, a first odor-reward association learning was performed for them to learn the procedure. Mice were then tested for olfactory-guided behaviors (see below). Odor-reward association tasks were performed as following: mice self-initiated a trial by poking their head into the sampling port and breaking an infrared light beam. Mice needed to wait 1.2 s at the odor port for the final valve to open and the odor to be delivered at the animal's nose, so that the odorant was present at the appropriate concentration. Then, the odor was applied for 2 s. If mice failed to wait up to 1.2 s in the odor port, airflow was directed to the exhaust and the trial was aborted. Inter-trial intervals were 5 s-long.

Two odors were presented in a pseudo-random order, such that both odors were presented ten times at the end of the block and not more than 3 times in a row. One odor was associated to a water reward (S+), the other not (S-). Mice had to lick to the S+ in a 2 ms time-window to get a water drop. In contrast, they had to refrain licking in that time-window for the S-. Correct behavior to the S+ is a "hit", while uncorrected behavior is a "miss". For the S-, correct and incorrect behaviors are "Correct rejection" and "false alarm", respectively. The percentage of correct responses was determined for each block of 20 trials and each mouse performed a maximum of 10 blocks (200 trials) per session. Mice were weighted and given sufficient water for their body weight to stay > 85%.

Initial odor-reward learning, without intrabulbar injection, was performed using Anisol (S+) and Heptanone (S-). Mice learned the behavioral procedure and were able to discriminate the two odors (behavioral performance > 85%) within three days. Three additional days of training were performed to ensure performance homogeneity and to increase the speed at which the animals executed the task.

Then, mice underwent bilateral intrabulbar injection of CNO or vehicle (saline) through the guide cannula (CNO final concentration: 0.1 mg/mL, injection speed: 0.33 μ L/min for 3 min, 1 μ L total/bulb) and

left in their home cage to recover for ~15min before being placed in the olfactometer. Mice expressing hM3D or h4MD in cortical GABAergic neurons could be injected with either CNO or saline, thereby allowing us to homogenize the group performances before starting a new task.

Odor used for discrimination learning, reversal learning, mixture discrimination and detection were anisole vs. heptanone, amylacetate vs. ethylbutyrate, (+)-carvone vs. (-)-carvone, (+)-limonene vs. (-)-limonene. Odor presentation dynamics were monitored and calibrated using a miniPID (Aurora). Odors were delivered for 2 seconds when mice poked their snout odor port for at least 1 second (if not, the trial is considered a short sample and is not counted), with an inter trial interval of 5 seconds

Data analysis.

For measurements of M/T cell spiking activity, signals were high-pass filtered (0.3 – 9 kHz) and spike detection, sorting, clustering and spike waveform analysis were performed using Spike2 software (CED) followed by manual cluster adjustment. For single-unit validation, all sorted cells displaying more than 1% of their interspike intervals below a 3.5 ms refractory period were discarded from the analysis. Careful attention was taken to discard any unit that showed some significant change in spike amplitude or waveform caused by the local infusion of drugs.

The change in firing rate to repeated light stimulation was calculated as following:

$$MC \text{ firing rate change} = \frac{\text{firing rate (stimulus, 1s)} - \text{basal firing rate(1s)}}{\text{basal firing rate (1s)}} \times 100$$

For photometry experiments, signals were smoothed (0.02 s window) and down-sampled to 500 Hz. For each trial, the signal was normalized to the averaged fluorescence of the trial using the $\Delta F/F$ ratio:

$$\frac{\Delta F}{F}(t) = \frac{F(t) - F_0}{F_0}$$

With F_0 being the average fluorescence over the trial. Sessions with significant averaged changes in the reflected blue light (>1% $\Delta F/F$) were discarded from the analysis.

Statistics. The mean is represented in all graphs and reported variances are SEM. All statistical analyses were performed using commercial analysis software (Graphpad Prism) with $p < 0.05$ considered significant.

Acknowledgements. We thank Carine Moigneu for viral injections and all members of the Lledo laboratory for their insights during the course of these experiments. We also wish to thank our colleagues Uwe Maskos and David DiGregorio at the Institut Pasteur for the gift of SST-Cre, PV-Cre and VIP-Cre mice. We thank Hannah Monyer for providing us with the GAD1-Cre mice and Bradford B. Lowell for the VGAT-Cre mice. The authors also thank Rachael L. Neve (Viral Gene Transfer Core, MIT) for the

HSV viruses, Karl Deisseroth and Bryan Roth for the optogenetic tools, and the Genetically-Encoded Neuronal Indicator and Effector (GENIE) Project and the Janelia Farm Research Campus of the Howard Hughes Medical Institute for sharing GCaMP6f constructs. This work was supported by the life insurance company “AG2R-La-Mondiale”, the Agence Nationale de la Recherche (ANR-15-CE37-0004) and the Laboratoire d'Excellence Revive (Investissement d'Avenir, ANR-10-LABX-73). Our laboratory is part of the Ecole des Neurosciences de Paris (ENP) Ile-de-France network, and is affiliated with the *Bio-Psy* Laboratory of Excellence. C.M. is a recipient of a fellowship from the French Ministère de l'Éducation Supérieure et de la Recherche and was also supported by the Fondation de la Recherche Médicale (FDT20160435483), the Bio-Psy Laboratory of excellence and an intramural fellowship from the Institut Pasteur.

References

- Alonso M, Lepousez G, Wagner S, Bardy C, Gabellec M-M, Torquet N, Lledo P-M (2012) Activation of adult-born neurons facilitates learning and memory. *Nat Neurosci* 2:1–10.
- Basu J, Zaremba JD, Cheung SK, Hitti FL, Zemelman B V, Losonczy A, Siegelbaum SA (2016) Gating of hippocampal activity, plasticity, and memory by entorhinal cortex long-range inhibition. *Science* (80-) 351:aaa5694-aaa5694.
- Boyd AM, Sturgill JF, Poo C, Isaacson JS (2012) Cortical feedback control of olfactory bulb circuits. *Neuron* 76:1161–1174.
- Brunjes PC, Illig KR, Meyer EA (2005) A field guide to the anterior olfactory nucleus (cortex). *Brain Res Rev* 50:305–335.
- Caputi A, Melzer S, Michael M, Monyer H (2013) The long and short of GABAergic neurons. *Curr Opin Neurobiol* 23:179–186.
- Carson K a (1984) Quantitative localization of neurons projecting to the mouse main olfactory bulb. *Brain Res Bull* 12:635–639.
- Chen C-FF, Zou D-J, Altomare CG, Xu L, Greer CA, Firestein SJ (2014) Nonsensory target-dependent organization of piriform cortex. *Proc Natl Acad Sci* 111:16931–16936.
- Davis BJ, Macrides F (1981) The Organization of Centrifugal Projections From the Anterior Olfactory Nucleus, Ventral Hippocampal Rudiment, and Piriform Cortex to the Main Olfactory Bulb in the Hamster : An Autoradiographic Study. *J Comp Neurol* 493:475–493.
- Davis BJ, Macrides F, Youngs WM, Schneider SP, Rosene DL (1978) Efferents and centrifugal afferents of the main and accessory olfactory bulbs in the hamster. *Brain Res Bull* 3:59–72.
- de Olmos J, Hardy H, Heimer L (1978) The afferent connections of the main and the accessory olfactory bulb formations in the rat: an experimental HRP-study. *J Comp Neurol* 181:213–244.
- Diodato A, Brimont MR De, Yim YS, Derian N, Perrin S, Pouch J, Klitzmann D, Garel S, Choi GB, Fleischmann A (2016) Molecular signatures of neural connectivity in the olfactory cortex. *Nat Commun* 7:1–10.
- Gracia-Llanes FJ, Crespo C, Blasco-Ibáñez JM, Nacher J, Varea E, Rovira-Esteban L, Martínez-Guijarro FJ (2010) GABAergic basal forebrain afferents innervate selectively GABAergic targets in the main olfactory bulb. *Neuroscience* 170:913–922.
- Gunaydin L a, Grosenick L, Finkelstein JC, Kauvar I V, Fenno LE, Adhikari A, Lammel S, Mirzabekov JJ, Airan RD, Zalocusky K a, Tye KM, Anikeeva P, Malenka RC, Deisseroth K (2014) Natural neural projection dynamics underlying social behavior. *Cell* 157:1535–1551.
- Haberly LB, Price JL (1978a) Association and Commissural Fiber Systems of the Olfactory Cortex of the Rat. II Systems originating in the olfactory peduncle. *J Comp Neurol*:781–807.
- Haberly LB, Price JL (1978b) Association and commissural fiber systems of the olfactory cortex of the rat. I. Systems originating in the piriform cortex and adjacent areas. *J Comp Neurol* 178:711–740.

- Herrick CJ (1910) The morphology of the forebrain in amphibia and reptilia. *J Comp Morph (Neurol?)* 20:129–162.
- Hintiryan H, Gou L, Zingg B, Yamashita S, Lyden HM, Song MY, Grewal AK, Zhang X, Toga AW, Dong H-W (2012) Comprehensive connectivity of the mouse main olfactory bulb: analysis and online digital atlas. *Front Neuroanat* 6:1–16.
- Jinno S, Kosaka T (2002) Immunocytochemical characterization of hippocamposeptal projecting GABAergic nonprincipal neurons in the mouse brain: A retrograde labeling study. *Brain Res* 945:219–231.
- Kay RB, Brunjes PC (2014) Diversity among principal and GABAergic neurons of the anterior olfactory nucleus. *Front Cell Neurosci* 8:111.
- Kunze W a, Shafton a D, Kemm RE, McKenzie JS (1992a) Olfactory bulb output neurons excited from a basal forebrain magnocellular nucleus. *Brain Res* 583:327–331.
- Kunze WAA, Shafton AD, Kemm RE, McKenzie JS (1992b) Intracellular responses of olfactory bulb granule cells to stimulating the horizontal diagonal band nucleus. *Neuroscience* 48:363–369.
- Lepousez G, Lledo P-M (2013) Odor discrimination requires proper olfactory fast oscillations in awake mice. *Neuron* 80:1010–1024.
- Luskin MB, Price JL (1983) The topographic organization of associational fibers of the olfactory system in the rat, including centrifugal fibers to the olfactory bulb. *J Comp Neurol* 216:264–291.
- Markopoulos F, Rokni D, Gire DH, Murthy VN (2012) Functional properties of cortical feedback projections to the olfactory bulb. *Neuron* 76:1175–1188.
- Mazo C, Grimaud J, Murthy VN, Lau CG (2017) Distinct projection patterns of different classes of layer 2 principal neurons in the olfactory cortex. *bioRxiv*.
- Mazo C, Lepousez G, Nissant A, Valley MT, Lledo P-M (2016a) GABAB Receptors Tune Cortical Feedback to the Olfactory Bulb. *J Neurosci* 36:8289–8304.
- Mazo C, Lepousez G, Nissant A, Valley MT, Lledo P-M (2016b) GABAB Receptors Tune Cortical Feedback to the Olfactory Bulb. *J Neurosci* 36:8289–8304.
- Melzer S, Michael M, Caputi A, Eliava M, Fuchs EC, Whittington M a, Monyer H (2012) Long-range-projecting GABAergic neurons modulate inhibition in hippocampus and entorhinal cortex. *Science* 335:1506–1510.
- Miyamichi K, Shlomag-Fuchs Y, Shu M, Weissbourd BC, Luo L, Mizrahi A (2013) Dissecting local circuits: Parvalbumin interneurons underlie broad feedback control of olfactory bulb output. *Neuron* 80:1232–1245.
- Murthy VN (2011) Olfactory maps in the brain. *Annu Rev Neurosci* 34:233–258.
- Nunez-Parra A, Maurer RK, Krahe K, Smith RS, Araneda RC (2013) Disruption of centrifugal inhibition to olfactory bulb granule cells impairs olfactory discrimination. *Proc Natl Acad Sci U S A* 2013:1–3.
- Padmanabhan K, Osakada F, Tarabrina A, Kizer E, Callaway EM, Gage FH, Sejnowski TJ (2016) Diverse

- Representations of Olfactory Information in Centrifugal Feedback Projections. *J Neurosci* 36:7535–7545.
- Shiple MT, Adamek GD (1984) The connections of the mouse olfactory bulb: A study using orthograde and retrograde transport of wheat germ agglutinin conjugated to horseradish peroxidase. *Brain Res Bull* 12:669–688.
- Soria-Gómez E et al. (2014) The endocannabinoid system controls food intake via olfactory processes. *Nat Neurosci* 17:407–415.
- Suzuki N, Bekkers JM (2010) Inhibitory neurons in the anterior piriform cortex of the mouse: classification using molecular markers. *J Comp Neurol* 518:1670–1687.
- Takács VT, Freund TF, Gulyás AI (2008) Types and synaptic connections of hippocampal inhibitory neurons reciprocally connected with the medial septum. *Eur J Neurosci* 28:148–164.
- Tamamaki N, Tomioka R (2010) Long-range GABAergic connections distributed throughout the neocortex and their possible function. *Front Neurosci* 4:1–8.
- Tomioka R, Okamoto K, Furuta T, Fujiyama F, Iwasato T, Yanagawa Y, Obata K, Kaneko T, Tamamaki N (2005) Demonstration of long-range GABAergic connections distributed throughout the mouse neocortex. *Eur J Neurosci* 21:1587–1600.
- Uchida N, Poo C, Haddad R (2013) Coding and Transformations in the Olfactory System. *Annu Rev Neurosci*:363–385.
- Valley MT, Henderson LG, Inverso S a, Lledo P-M (2013) Adult neurogenesis produces neurons with unique GABAergic synapses in the olfactory bulb. *J Neurosci* 33:14660–14665.
- Wilson RI, Mainen ZF (2006) Early events in olfactory processing. *Annu Rev Neurosci* 29:163–201.
- Zaborszky L, Carlsen J, Brashear HR, Heimer L (1986) Cholinergic and GABAergic Afferents to the Olfactory-Bulb in the Rat with Special Emphasis on the Projection Neurons in the Nucleus of the Horizontal Limb of the Diagonal Band. *J Comp Neurol* 243:488–509.

Figure legends

Figure 1. Anterograde labeling of cortico-bulbar GABAergic axons.

A. Schematic representing anterograde virus injection in the AOC and projections in the OB. Chr2 is fused to a green reporter gene.

B-C. Sagittal section of the injection site, showing that injection targeted the AON but spared the striatum (Str.) and the OT (B). Higher magnification of the AON (boxed area in B.) displaying infected neurons (arrowheads, C).

D. Distribution of the GABAergic fibers across layers of the ipsilateral OB. Right: The fluorescence intensity profile show three peaks in the deep GL, MCL and GCL.

E. High magnification in the layers with fluorescence peaks illustrating fiber densities.

F. Labeled axon fiber boutons colocalized with GAD 65/67 staining, confirming their GABAergic nature. Scale bars in E and F are 20 μm .

GL: glomerular layer; EPL/IPL: external/internal plexiform layer; MCL: mitral cell layer; GCL: granule cell layer

Figure 2. Retrograde labeling of cortico-bulbar GABAergic neuron somas.

A. Schematic representing retrograde virus injection in the OB and back-labeled somas in the AOC. Retrogradely-labeled cells express GCaMP6f and appear in green.

B Sagittal slices with identified brain regions showing two main clusters of retrogradely-labeled cells along the medio-lateral axis: in the AONpp and the HDB/MCPO.

C. Coronal slice depicting the localization of the AONpp cluster and the neurites passing in between the APC and OT.

C. Example AON GABAergic neurons projecting to the OB. Spiny (left) and unspiny (right) neurons could be observed. Inset in the left image is from the boxed area. Scale bars in inset are 10 μm .

D. Retrogradely-labeled neurons colocalize with GAD 67 staining, confirming again their GABAergic nature.

LOT: lateral olfactory tract; Str: striatum

Figure 3. Dual labeling strategy confirms that AONpp sends cortico-bulbar GABAergic projections.

A. Schematic representing CTB injection in the OB and virus injection in the AOC. CTB labels OB-projecting cells in red and GCaMP6 labels GABAergic neurons in green.

B. Coronal slice showing dually labeled cells in the AONpp, at the border between the APC and OT (arrowhead). Note the homogenous CTB labeling in the AONpp compared to the labeling concentrated in layer 2b and 3 in the nearby APC.

C. Example dually-labeled neurons from B (stared arrowheads).

Figure 4. Molecular expression pattern of cortico-bulbar GABAergic neurons.

Anterograde and retrograde labeling in SOM-Cre (left), VIP-Cre (middle) and PV-Cre mice (right). Specific anterograde and retrograde labelings were achieved as before. Insets show example retrogradely

labeled neurons. Cortico-bulbar GABAergic neurons are mainly expressing SOM. Scale bars are 200 μm (up), 500 μm (bottom) and 10 μm (insets).

Figure 5. Cortico-bulbar GABAergic axons form functional synapses onto OB neurons.

- A. Recording schematic. Periglomerular (PG) cells, external tufted cells (eTCs), mitral cells (MCs), granule cells (GCs) and deep short-axon cells (dSACs) were patched and GABAergic cortico-bulbar axons were light-stimulated. Connections were found only on GCs and dSACs.
- B. Representative example trace of a GC recorded at 0 mV. Light-stimulation of GABAergic axons induced fast IPSCs. Blue square: light onset.
- C. Histogram reporting the connectivity probabilities (left) and connectivity strength (right) of the GABAergic axon-to-OB neuron synapse.

Figure 6. Cortico-bulbar GABAergic axons decrease odor discrimination at very low thresholds.

- A. Top: Schematic showing the injection of DREADD in the AOC and the local perfusion of the ligand CNO in the OB. Bottom: Go / No-go task with odor-reward association. When smelling the rewarded odor (S+), the mouse had to lick a water port to get a reward (“HIT”). Failing to lick to the S+ is a “MISS”. Following presentation of the unrewarded odor (S-), the mouse had to refrain licking (correct rejection, “CR”). If the mouse licked to the S-, the behavior was called a false alarm (“FA”).
- B. Performances of the animals across blocks (20 trials composed of 10 S+ and 10 S- odor presentation) for the limonene (L) odor couple with increasing dilution. Mice performed well in all groups to discriminate between the enantiomers (+) and (-) of the limonene at the dilution 10^{-5} . At the 10^{-6} dilution, hM4D mice performed significantly better than the control and h3MD groups.
- C. Increase in performances to discriminate L+ vs. L- at the 10^{-6} dilution was due to a decrease in the number of false alarms in h4MD mice.

Supplementary Figure 1. Anatomical characterization of cortico-bulbar GABAergic neurons.

- A. Retrograde labeling using HSV-Flex-GCaMP6f injection in the OB shows that GABAergic axons from cortical neurons lies superficial to both the ventral and dorsal lateral olfactory tract (vLOT and dLOT, respectively; left). Right: neurites presumably from AONpp neurons passes in between the APC and OT to gain access to the LOT.
- B. Retrogradely-labeled neurons of the AONpp are not in a cholinergic structure, arguing against the hypothesis of a rostral extension of the HDB/MCPO.
- C. *Preliminary*. Left: Relative numbers of OB-projecting cells in the AONpp, in other parts of the AON, in the APC and HDB/MCPO. Right: Distribution of the OB-projecting GABAergic neurons from the same brain regions across the medio-lateral axis (sagittal sections). Data are normalized such that each brain region maximum is set to 1.

ChAT: choline acetyltransferase.

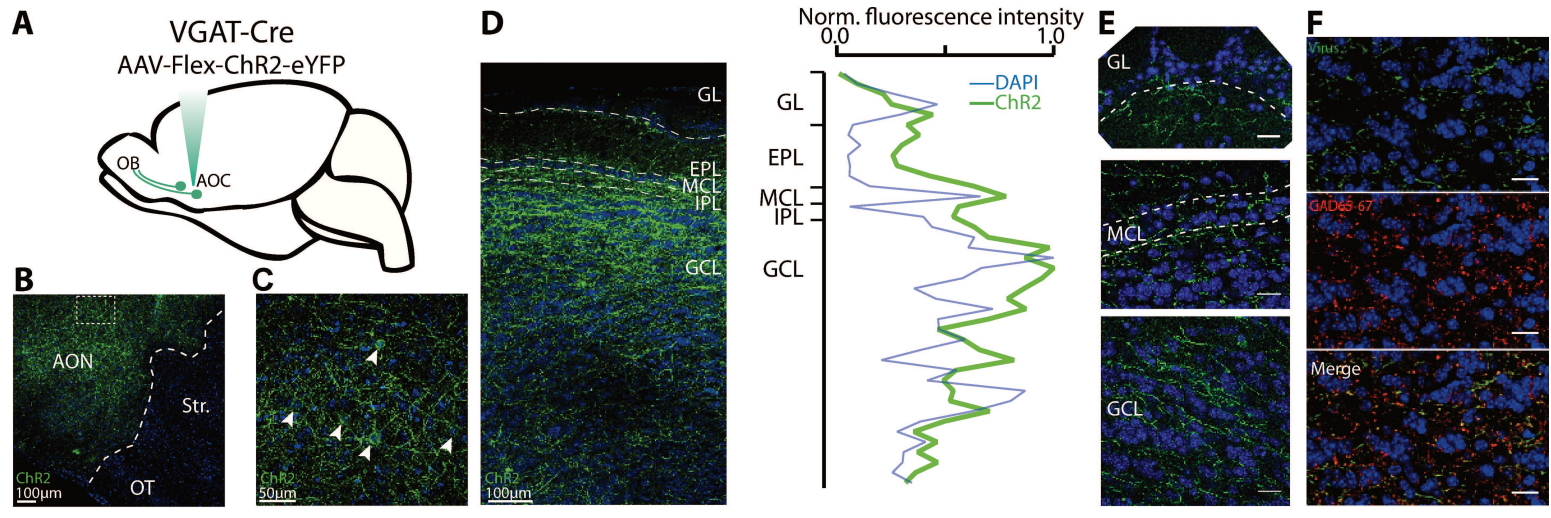


Figure 1

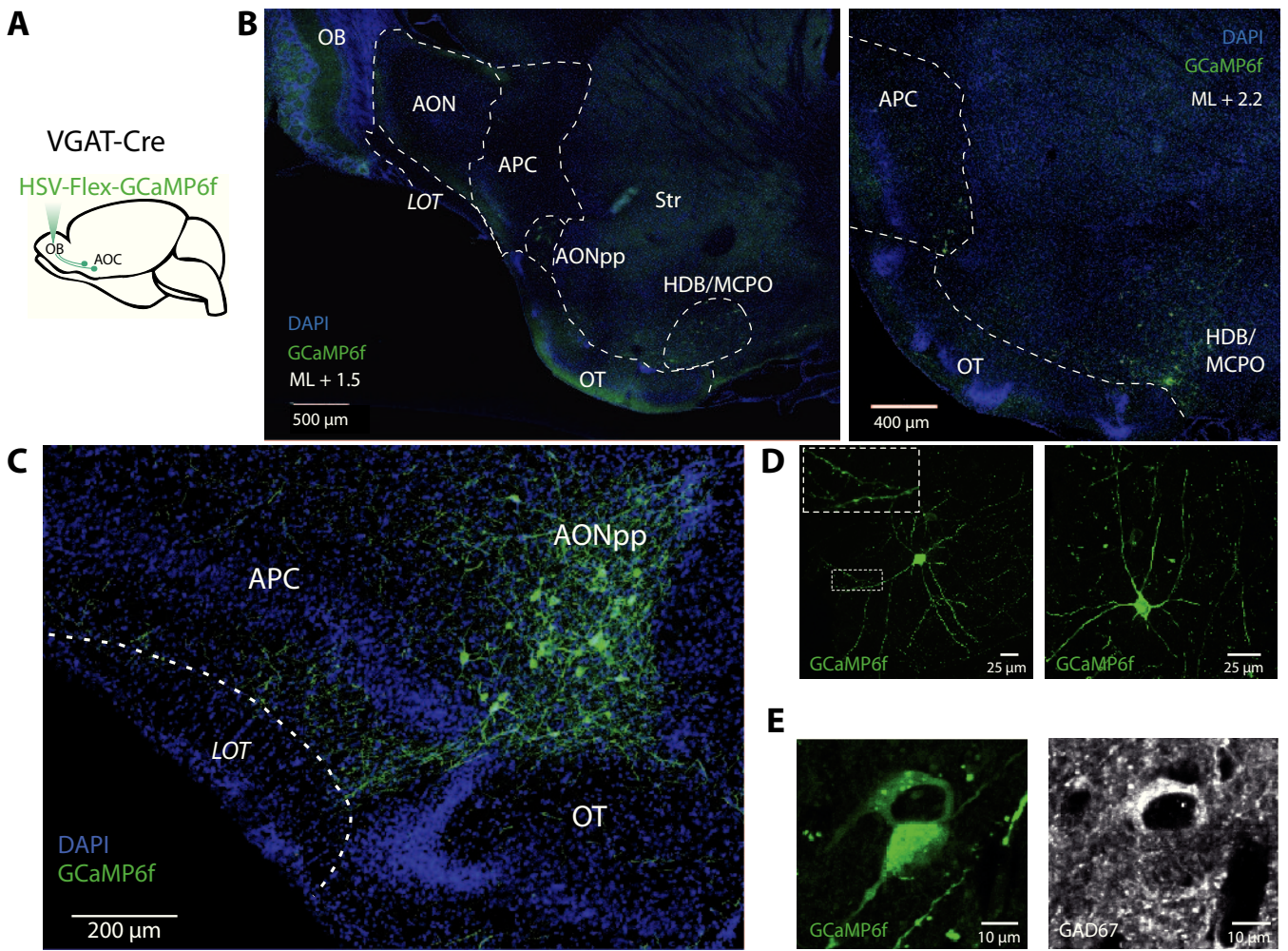


Figure 2

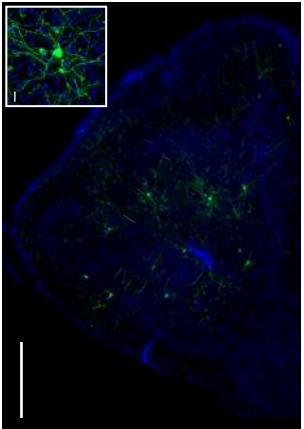
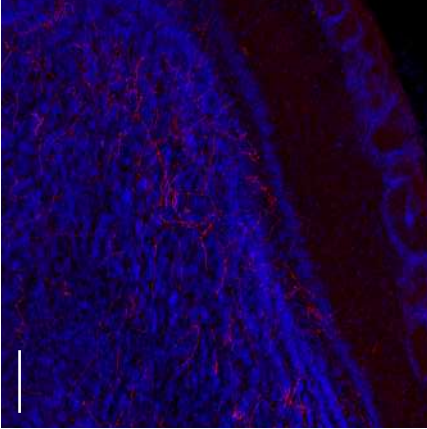
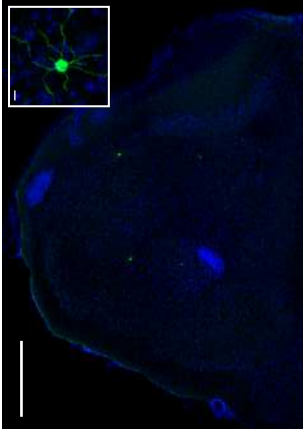
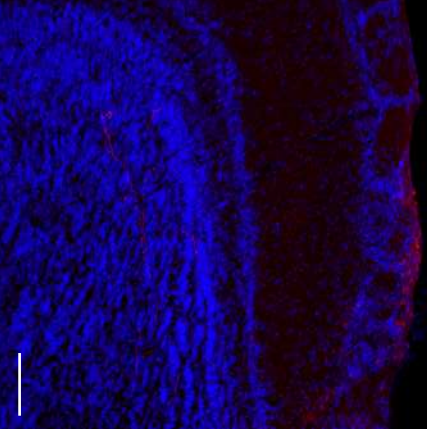
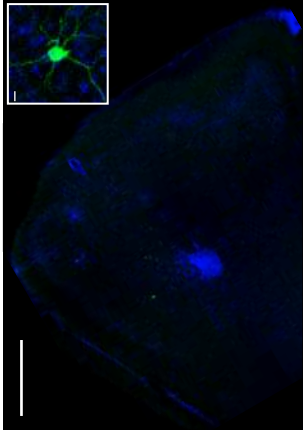
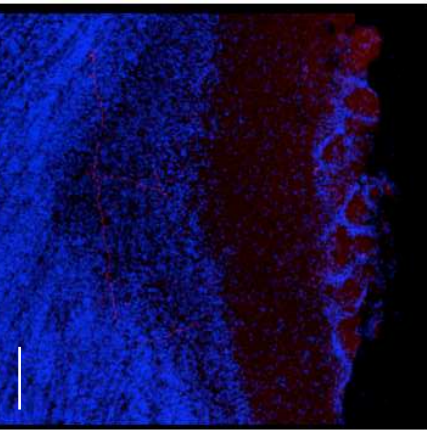
Retrograde labeling OB: HSV-Flex-GCaMP6f	Anterograde labeling AOC: AAV-Flex-TdTomato	
 <p>Fluorescence micrograph of a brain section from a SOM-Cre mouse. The image shows green retrograde labeling (GCaMP6f) in the olfactory bulb (OB) and blue anterograde labeling (TdTomato) in the olfactory cortex (AOC). A white scale bar is present in the bottom right corner. An inset in the top right shows a magnified view of a single green-labeled neuron.</p>	 <p>Fluorescence micrograph of a brain section from a SOM-Cre mouse. The image shows blue anterograde labeling (TdTomato) in the olfactory cortex (AOC). A white scale bar is present in the bottom right corner.</p>	SOM-Cre
 <p>Fluorescence micrograph of a brain section from a VIP-Cre mouse. The image shows green retrograde labeling (GCaMP6f) in the olfactory bulb (OB) and blue anterograde labeling (TdTomato) in the olfactory cortex (AOC). A white scale bar is present in the bottom right corner. An inset in the top right shows a magnified view of a single green-labeled neuron.</p>	 <p>Fluorescence micrograph of a brain section from a VIP-Cre mouse. The image shows blue anterograde labeling (TdTomato) in the olfactory cortex (AOC). A white scale bar is present in the bottom right corner.</p>	VIP-Cre
 <p>Fluorescence micrograph of a brain section from a PV-Cre mouse. The image shows green retrograde labeling (GCaMP6f) in the olfactory bulb (OB) and blue anterograde labeling (TdTomato) in the olfactory cortex (AOC). A white scale bar is present in the bottom right corner. An inset in the top right shows a magnified view of a single green-labeled neuron.</p>	 <p>Fluorescence micrograph of a brain section from a PV-Cre mouse. The image shows blue anterograde labeling (TdTomato) in the olfactory cortex (AOC). A white scale bar is present in the bottom right corner.</p>	PV-Cre

Figure 4

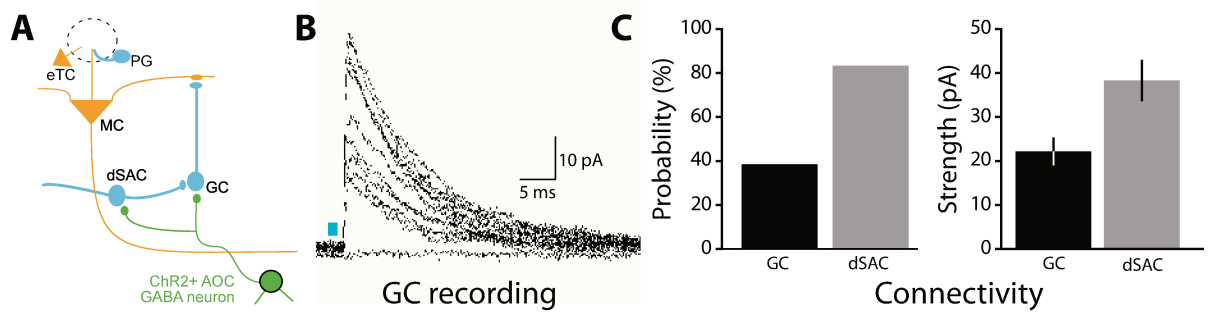


Figure 5

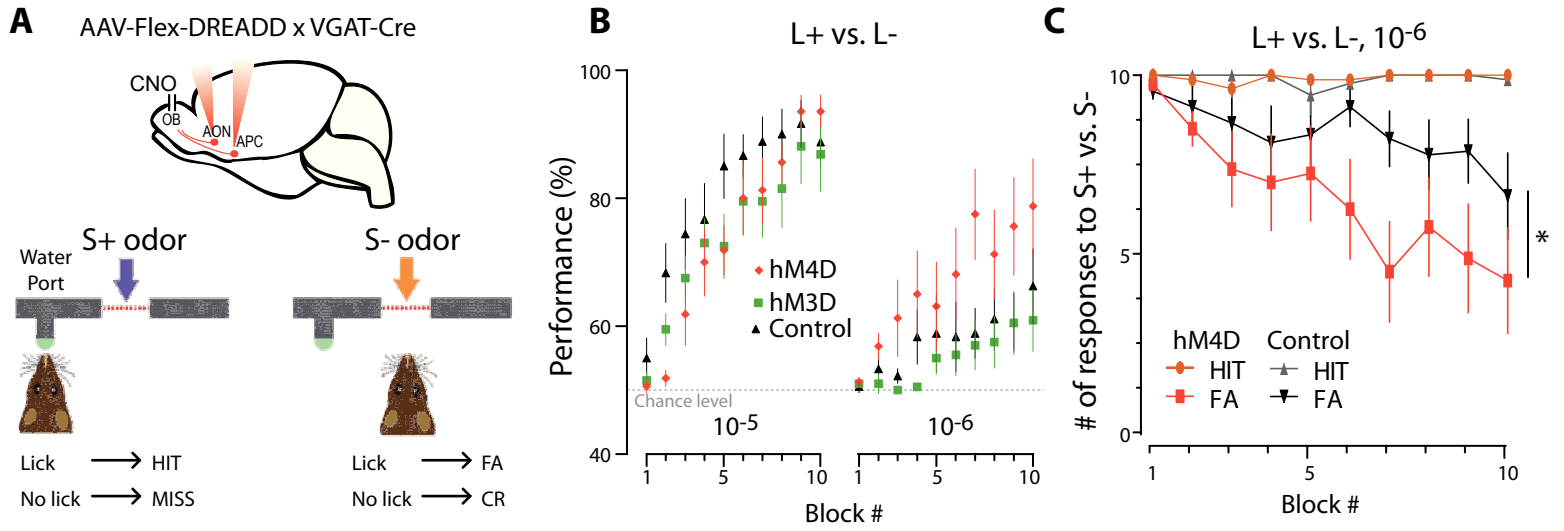
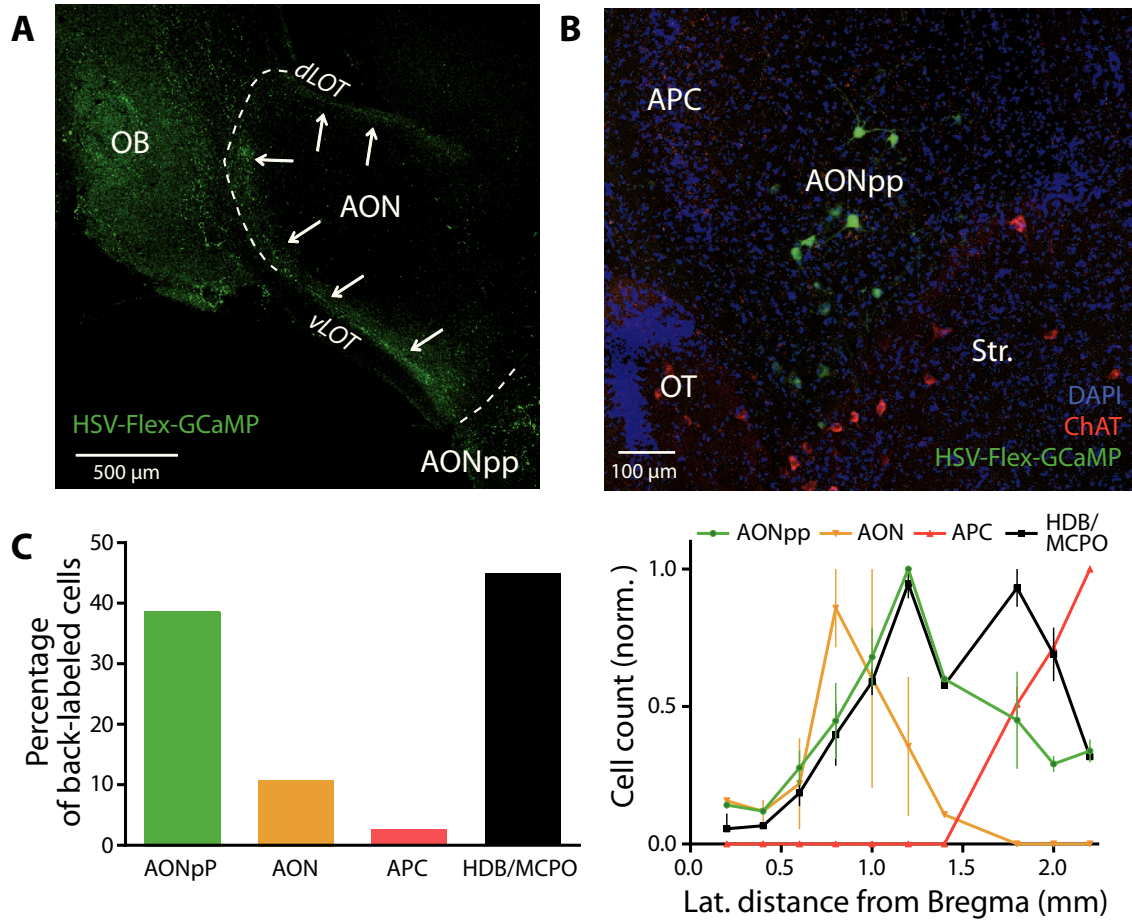


Figure 6



Supplementary Figure 1

2.2 Preliminary results

To investigate the activity dynamics of cortico-bulbar GABAergic axons in olfactory behavior, we developed a fiber photometry approach combined with an odor-reward association task. GCaMP6f was selectively expressed in GABAergic cells (AAV-DIO-GCaMP6f in VGAT-Cre mice) and an optical fiber was placed above the GCL of the OB to record axonal Ca^{2+} activity (Figure 2.1,A,B), while mice performed a Go/No-Go odor-reward association task (Figure 2.1,C). In mice performing above criterion ($> 85\%$), we observed that axonal Ca^{2+} activity decreased at odor onset. Interestingly, in presence of the rewarded odors (Benzaldehyde: B+ and ethyl butyrate: EB+), the activity level strongly decreased, whereas this decrease was weaker and transient with the non-rewarded odors (Ethyl Tiglate: Et- and amyl acetate:AA-; Figure 2.1,D). Thus it seems that cortico-bulbar GABAergic axon activity can discriminate the odors based on their value (rewarded or not). Consistent with this hypothesis is the observation that the divergences in the Ca^{2+} transient kinetics to the reward and unrewarded odors appear later than the divergence in the licking activities. To confirm these results, we are currently performing experiments where odor values are switched (reversal learning). If GABAergic cortical axon activity does reflect the contingencies of the odors, activity profiles to the odor should switch with the switch in their associated value.

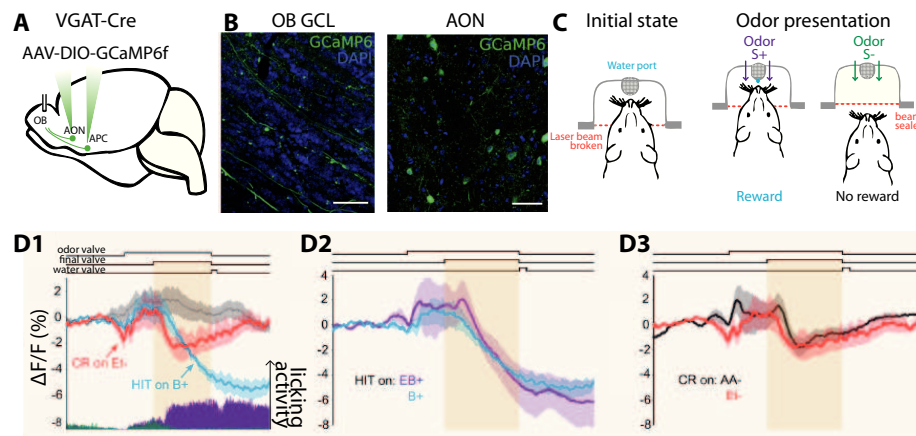


Figure 2.1 – Cortico-bulbar GABAergic axon activity discriminates odor values.

A. Conditional expression of GCaMP6f in AOC GABAergic neurons, and axon terminals activity recording in the OB.

B. Expression of GCaMP6f in the GCL of the OB (left) and at the injection site (AON, right). Scale bars are $50\mu m$

C. Behavioral paradigm. Mice had to performed a Go / No-go task similar to behavior experiments in Figure 6 of the article in preparation. D. Photometry traces for mice performing at accuracy $> 85\%$. Orange shading represent odor presentation duration and fluorescence traces are mean and SEM. Histograms in D1 represent the licking frequency in case of a HIT on B+ (purple) or a CR on Et- (green). Gray trace in D1 represents axonal calcium activity in the absence of odor stimulation. D1: Axonal calcium transients for an example odor couple S+ (B+, blue) / S- (Et-, red) couple. D2, D3: Superimposed traces elicited by 2 different odor couples. Rewarded odors are shown in D2 (EB+, purple; B+, blue), unrewarded odors in D3 (AA-, black; Et-, red).

Part III

Discussion

Discussion

In the two studies, I investigated the influence of cortical top-down inputs to the OB. The first study explores a regulation of glutamatergic transmission mediated by the activation of metabotropic receptors for GABA, while the second study focuses on a GABAergic top-down innervation of the OB. In both works, I labeled, manipulated and recorded specific circuits utilizing a combination of modern genetic tools. This manuscript is good example illustrating that combining multiple, always more specific genetic tools is instrumental in modern neurosciences. For instance, development of calcium indicators or optogenetic tools activated by distinct wavelength, or ligand with distinct exogenous ligand is also fundamental for multiplexing activity manipulation and recordings. Optical stimulation of cortical top-down inputs while recording optically the postsynaptic target in the OB has proven successful and efficient to investigate functional connectivity *in vivo*. Increasing selectivity in genetically-encoded protein expression, permitting neuronal subtype-specific investigation is also decisive to understand precise circuit functions. Combining dual conditional genetics and retrograde labeling, we could specifically labeled OB-projecting neurons from the AONpp. This is critical for anatomical observation and will refine circuit-base analyses in the near future. For further details on modern techniques to label, record and manipulate neurons, see 1.3 A and a excellent review by Deisseroth (Kim et al., 2017).

In this discussion part, I will first extend the discussion on Article 1. Then, I will discuss important points brought up by the second work, some of which are currently undertaken in the laboratory, other are possible future directions. Lastly, I will discuss broader aspects, that my thesis work has raised.

1.1 Extended discussion on Article 1

Because of space limitations, there are several points we did not address in the discussion of our work entitled "GABA_B Receptors Tune Cortical Feedback to the Olfactory Bulb". In this section, I would like to come back on a few of them.

Bell-shaped inhibition of M/T cells. The frequency-dependence is a striking characteristic of the light-evoked feedforward inhibition of M/T cell spiking (Figure 3F). Upon increasing light frequencies, M/T cell inhibition increases and peaks at 33 – 50Hz, before decreasing with higher stimulation frequencies. There are at least two parameters that could participate in this resonance/filtering effect: 1) GC spike-coupling to AOC axon stimulation and 2) ChR2 kinetics.

Parameter #1: occasional GC extracellular recordings *in vivo* showed an optimal excitation to 40Hz stimulation. Interestingly, the number of spike emitted per light pulse (fidelity) diminished with increasing light frequencies, but the concomitant increase in the number of light pulses during a 1s-long stimulus overcome that decrease in fidelity for frequencies up to 40Hz. For frequencies higher than 40Hz, the decrease in fidelity dominates over the increase in the number of light pulses. This optimal GC coupling to 40Hz light stimulation could account for the observed bell-shaped inhibition on M/T cells. However, we can not distinguish from these data whether intrinsic properties from either AOC axon terminals or GCs (thus mediating synaptic filtering), or both account mostly for this optimum. Nonetheless, it seems that bell-shaped inhibition of M/T cells does not occur from synaptic filtering at the GC-to-M/T cell synapse.

Importantly, decrease in inhibition with light frequencies higher than 40Hz, and up to 67 – 83Hz, is likely not due to ChR2 kinetics (Parameter #2). Indeed, we observed in the laboratory that when the same version of ChR2 (with the H134R mutation) was introduced in M/T cells (using Tbet-Cre mice), synchrony in M/T cell activity generates a band in the LFP at the stimulation frequency that increased until frequencies up to 67 – 83Hz (unpublished material). This result suggests that population-wise, ChR2 is able to follow such high light frequencies. Thus, intrinsic properties of the AOC-GC-M/T cell pathway, rather than of the ChR2 itself, are likely responsible for the light-driven bell-shape inhibition of M/T cells, and in particular the synaptic coupling between AOC axons and GC spiking activity.

Source of disynaptic inhibition. The main source of inhibition driven by AOC axon light stimulation has been reported to be GCs in acute OB slices (Markopoulos et al., 2012). However, about a third of the inhibition on M/T cells originates from GL interneurons (Markopoulos et al., 2012).

In our experiments, we did not assess whether GABA_BRs also modulate the AOC axon-to-PG cell synapse, but since 1) we estimate baclofen diffusion to be restricted to a radius of $\sim 600\mu m$, and 2) theta oscillations were not affected by baclofen application (Figure 5C), we reasoned that baclofen did not diffuse significantly up to the GL.

Therefore, the remaining light-evoked inhibition following baclofen application results either from: Hypothesis #1: non-saturating baclofen binding of GABA_BR at AOC axon-to-GC synapse and/or a not fully efficient pharmacological block of glutamate release or Hypothesis #2: GL neurons (free of baclofen).

Hypothesis #1: Baclofen was used at a concentration of $2.5mM$ in our experiments, therefore it seems unlikely that baclofen was applied at non-saturating doses (EC50: several μM in other brain networks). However, baclofen might induce a not fully efficient block of AOC synaptic transmission. Indeed, even though baclofen suppressed a substantial amount of the evoked inhibition at low light stimulation frequencies, it was reported at the GC-to-MC synapse that GABA_BR activation was less efficient to block GABA release at higher frequencies (Isaacson and Vitten, 2003). The decreased efficiency of baclofen suppression of inhibition at higher frequencies could thus be explained by higher proportions of GABA release that escape GABA_BR-mediated inhibition.

Hypothesis #2: Another possibility is that baclofen-resistant feedforward inhibition onto M/T cell is mediated by GL neurons, free of baclofen. Because feedforward inhibition of M/T cells becomes less sensitive to baclofen with increasing light stimulation frequencies, Hypothesis #2 involves that light-driven inhibition of M/T cells largely depends on GCs at low frequency, but the contribution of PG cells increases with higher light stimulation, such that the ratio of feedforward inhibition mediated by GCs and PG cells would shift with increasing AOC axon stimulation frequencies. A similar switch between two sources of feedforward inhibition has been demonstrated in the neocortex (Tremblay et al., 2016) and olfactory cortex (Stokes and Isaacson, 2010). In these brain regions, differences in short-term synaptic plasticity account for this switch. In the OB, AOC axon-to-GC synaptic strength was indeed observed to decrease both in slice (Balu et al., 2007) and in our experiments, as measured by fEPSP recordings (unpublished data), consistent with a decrease in GC contribution to feedforward inhibition at high stimulation frequencies. However, the short-term synaptic plasticity of the AOC axon-to-PG cell synapse remains unknown.

In conclusion, increasing frequency stimulation of AOC axons could trigger glutamate release on GCs in a GABA_BR-independent manner, or alternatively could mediate a switch in the local source of inhibition received by M/T cells.

GABA_BR1 staining in the GCL. In Figure 2G of the article, we showed that GABA_BR1 immunolabeling is specifically decreased in the GCL of AOC^{GABAB^{-/-}} animals, yet some signal remains. Several factors can account for the remaining signal.

First, it can be due, or partially due to background fluorescence (i.e. fluorescence that is not specific to the GABA_B1 receptor signal, such as autofluorescence or non-specific labeling). Background fluorescence is hard to quantify since there is no layer that does not express GABA_BRs in the OB.

Second, it is also possible that all the GABA_BRs at AOC axon terminals have not been degraded by the cellular machinery.

Third, centrifugal fibers originating from brain regions that we did not target with our viral injection might also express GABA_BRs at their axon terminals. As we have seen in the Chapter "3" (Figure 2.5), the OB is innervated by multiple brain regions, different from the anterior olfactory cortex. For instance, the lateral entorhinal cortex has been recently reported to send projections back to the OB (Leitner et al., 2016).

Lastly, signal can partially come from OB neurons in the GCL. Baclofen was found to have no postsynaptic effect on GCs Isaacson and Vitten (2003); Valley et al. (2013), but it is unknown whether dSACs do express GABA_BRs or not. In this study, we found that disynaptic inhibition onto GCs – likely originating from dSACs – was blocked by baclofen, but we did not dissect the circuit further. We have evidence for a GABA_BR-dependent regulation of the AOC-to-dSAC synapse (recordings from putative dSAC show depression of evoked transmission with baclofen; $n = 2$, excluded from the study). This suggests that GABA_BRs expression at the pre- or postsynaptic site, or both. In addition, GABA_BR could be expressed at the dSAC-to-GC synapse to depress AOC-driven disynaptic inhibition onto GCs. These three sites of expression are not mutually exclusive. dSAC patch-clamp recordings, as well as pair-recordings of GC and dSAC, will permit to decipher where are GABA_BRs effectively expressed in the AOC-dSAC-GC pathway.

Baclofen failed to depress GC-mediated GABA release onto M/T cells. In the discussion of the article, we have raised the point that we did not observe any depression of inhibition mediated by baclofen in AOC^{GABAB^{-/-}} animals (Figure 3F, 4B). This is somewhat surprising since GABA_BRs are expressed at the GC dendrites to suppress GABA release (Isaacson and Vitten, 2003; Valley et al., 2013), and indirect evidence suggests that baclofen did diffuse up to the EPL (baclofen application altered gamma oscillations, Figure 5, and DAPI diffused up to 500 – 600 μ m away from the injection site). Therefore we conclude that: Hypothesis #1: cortical feedback preferentially engages disynaptic inhibition on M/T cells through new-born GCs, which express non-functional GABA_BRs (Valley et al., 2013), or Hypothesis

#2: GC stimulation evoked by our cortical top-down stimulation protocol triggers GABA release in a GABA_BR-independent fashion.

Hypothesis #1 is that cortically-driven inhibition on M/T cells is mostly driven by newborn GCs, produced through adult neurogenesis. Two mechanisms may account for this: newborn neurons might be more excited by AOC stimulation and therefore release more GABA on M/T cells, and/or they can release more GABA for the same depolarization, i.e more efficiently. Notably, differences in intrinsic properties or spontaneous GABA release between newborn and pre-existing GCs have been observed (Breton-Provencher et al., 2009; Carleton et al., 2003, but see also Valley et al., 2013). However their contribution to different level of inhibition on M/T cells in response to cortical stimulation remains unknown .

The latter mechanism implies that GABA release from newborn GCs is more efficiently coupled to similar AOC-mediated depolarization. If there is no work directly investigating this issue, indirect evidence suggests that it is not the case. Indeed, in previous work from the laboratory, we demonstrated that direct light-stimulation of newborn *vs.* pre-existing GC evoke IPSCs of similar amplitude in M/T cells in slice (Valley et al., 2013). However, this was assessed by direct ChR2-mediated excitation and no exact characterization was performed for minimal *vs.* stronger light-stimulation. Therefore, it remains unclear whether newborn GCs are more efficiently eliciting inhibition on M/T cells for a similar excitation.

Stronger excitation of newborn GCs in response to similar cortical inputs is an alternate mechanism that could account for a greater contribution of newborn GCs in mediating M/T cell inhibition. Although single stimulation of cortical axons evokes greater EPSCs in early postnatal born GCs than in newborns ones (Nissant et al., 2009), two observations still support this hypothesis. 1) Synaptic short-term plasticity is in favor of a greater contribution of newborn GC to M/T cell inhibition upon repetitive stimulation of AOC axons. Indeed, upon 20 Hz stimulation AOC axon-to-newborn GC synapse is facilitating while AOC-to-early postnatally-born GC is depressing (Nissant et al., 2009). 2) Excitation/Inhibition ratio might also ease spike emission by newborn GCs compared to pre-existing ones. In the hippocampus for example, EPSCs are bigger in pre-existing neurons than in newborn ones, but inhibition is also bigger. This results in an excitation/inhibition ratio more in favor of spike emission in newborn GCs, as confirmed by cell-attached recordings in hippocampal slices (Marín-Burgin et al., 2012). Similarly in the OB, cell-attached recordings of GCs would address the question whether newborn GC are more likely to spike than pre-existing ones in response to AOC axon stimulation.

To go further, hypothesis #1 could be tackled *in vivo*. To ask whether newborn or pre-existing GCs contribute more to the cortically-evoked synaptic inhibition on M/T cells, one can introduce ChR2 in AOC axons (sim-

ilarly to what has been done in this study), and inhibitory DREADD (for instance, but genetic ablation can also be achieved, see Arruda-Carvalho et al., 2014) selectively in newborn *vs.* pre-existing GCs. Injection of lentivirus in the rostral migratory stream of mice at different ages is a technique routinely used in the laboratory to selectively label a GC population or the other (see for example, Alonso et al., 2012; Lepousez et al., 2014; Nissant et al., 2009). Light-stimulation of AOC axons while specifically inhibiting a GC population or the other will address whether or not newborn GCs play a predominant role in M/T cell disynaptic inhibition.

Hypothesis #2 is that cortical axons evoke GC GABA release in a GABA_R-independent manner in our experiments.

First, this could imply that GABA release following distal *vs.* proximal stimulation is mediated through different mechanisms, or in a different chemical context. Distal and proximal modes of GC excitation differs in several points. Dendrodendritic inhibition was shown to be dependent on slow kinetics of NMDAR and on high-voltage activated Ca²⁺ channels (N and P/Q-type) (Isaacson, 2001; Isaacson and Strowbridge, 1998). In contrast, cortical axon stimulation was shown to produce fast inhibition on M/T cells in a NMDAR-independent manner (Boyd et al., 2012). The mechanism associated with GABA release upon back-propagating somatic Na⁺ spike depolarization is not known. Yet if GABA release is mediated by distinct mechanisms, it requires that GABA_BR activation acts on effectors upstream of the final common pathway for GABA release. In line with this, Isaacson and Vitten (2003) found that GABA_BR activation blocks high-voltage (N and P/Q-type), but not low-voltage (T-type), activated calcium channels. Low-threshold calcium spikes have been reported (Egger et al., 2003, 2005), thus Na⁺ spike could recruit GABA_BR-insensitive Ca²⁺ channels (T-type). Differential recruitment of calcium channels with distal *vs.* proximal stimulation would thus be the cellular basis for a differential sensitivity to GABA_BR activation.

Alternatively, GABA release triggered by distal *vs.* proximal stimulation might be mediated by similar cellular effectors, but these effectors might be recruited differently depending on the regime of activity at the synapse. GABA_BR-mediated depression of GABA release was interestingly found to decrease upon repetitive GC dendrite stimulation or upon increased dendrodendritic inhibition (Isaacson and Vitten, 2003). Since AOC axon stimulation has been proposed to potentiate dendrodendritic inhibition (Balu et al., 2007) and because we used repetitive light stimulation in our study, it is possible that our protocol induces GC dendritic GABA release that is little sensitive to GABA_BR activation. Therefore, the GABA_BR-independent GABA release mechanism triggered by AOC inputs (which we observed in this study) might activate the same GABA release mechanism as for dendrodendritic inhibition, but the high regime of activity we used might have

induced little sensitivity to GABA_BR-dependent regulation.

These two scenarios of hypothesis #2 are addressable experimentally. Indeed, the nature of the voltage-gated calcium channels involved in cortically-evoked GABA release can be tested with pharmacology in acute slice, as it was done for the dendrodendritic inhibition. *In vivo*, comparison of the impact of baclofen on cortically-evoked inhibition *vs.* dendrodendritic inhibition can also be addressed. Dendrodendritic inhibition can be evoked by direct ChR2 stimulation of M/T cells (using Tbet-Cre animals, for example) or LOT electrical stimulation, which produces back-propagating action potentials. The second scenario can be investigated by single light-pulse activation of AOC axons and careful study of the effect of baclofen on M/T cell feedforward inhibition.

Natural context of AOC GABA_BR activation. In this work, we failed to find the natural context of activation of these GABA_BRs. Previous studies showed that wake and sleep states modulate AOC axon synaptic transmission strength, as measured by LFP recordings (Manabe et al., 2011), and fasting induced endocannabinoid production in rodents, which activate cannabinoid receptors at AOC axons to depress glutamate release (Soria-Gómez et al., 2014). To ask whether we could find a condition where the GABA_B system similarly modulate AOC axon input strength, I performed chronic recordings in freely behaving animals. I confirmed that both sleep-wave cycles and 24 hours of fasting could modulate the light-evoked fEPSPs (although the fasting-dependent modulation of AOC transmission was opposite to what has been described by Soria-Gómez et al. (2014)). Local perfusion of CGP in the OB through a cannula would address whether these modulations are mediated by activation of the GABA_BR system. Unfortunately, in my pilot experiments, injection of the positive control baclofen failed to modulate the fEPSP (probably due to a bad cannula implantation). However, these first results are promising and at least open a promising avenues for deciphering the natural context of the modulations at AOC axons, whether this is mediated by the GABA_B system or not.

Functional impact on behavior. We did not evaluate the impact on behavior of selective GABA_BR activation at AOC axon terminals because we could not find an experimental condition allowing specific manipulation of these GABA_BRs.

First, in the OB, GABA_BRs are also expressed at OSN axons and at GC apical dendrites in the EPL. Since we have evidence for a diffusion of baclofen in that layer using our injection protocol, any change in behavior with baclofen could be a mix of effects at AOC axons and at GC apical

dendrites.

Second, GABA_BRs are also expressed in the APC (Franks and Isaacson, 2005; Poo and Isaacson, 2009), thus removing GABA_BRs in cortico-bulbar axons also removes GABA_BRs expressed in intracortical fibers and prevent the selective manipulation of cortico-bulbar inputs. This was not a major issue in our experiments investigating synaptic physiology but this would have been a major drawback for behavioral investigation. Therefore, the use of the transgenic animals cannot overcome the lack of specificity of pharmacological injection, and the ubiquitous expression of GABA_BRs both in the OB and AOC precludes the investigation of the selective impact of GABA_BR activation at AOC axon terminals.

Canabinoid receptors are also expressed at AOC axon terminals and their activation lower odor detection threshold (Soria-Gómez et al., 2014). Because canabinoid receptors activation also depresses the AOC-to-GC synaptic transmission, it is tempting to draw a parallel between the GABA_B and canabinoid regulation mechanisms. However, 1) canabinoid-dependent modulation of the AOC-to-M/T cell synapse has not been tested, and 2) AOC axons target many neurons in the OB whose regulation by either of these systems is largely unknown. Therefore, further dissection of synaptic transmission regulation by both GABA_B and canabinoid receptors is needed before comparing the function of the two modulations.

Regime of activation. Finally, the source of GABA of these GABA_BRs remains to be determine. Experiences aiming to address whether these GABA_BRs are tonically activated by GABA, or whether GABA_BRs can be activated by synaptically- and/or pharmacologically-evoked increase in the extracellular concentration of GABA failed to induce a significant activation of GABA_BRs as measured by fEPSP measurement. Even though we did not measure whether our protocols did increase the extracellular level of GABA, these experiments suggest that GABA does not activate GABA_BRs expressed at AOC axon terminals by spill-over or volume transmission. Rather, consistently with growing evidence suggesting a role for GABA_BR in fast inhibition (see 1.3), we think that these GABA_BRs might detect phasic, synaptically-released GABA. Putative sources for synaptically released GABA are either intrinsic (such as dSACs or astrocytes) or extrinsic, and notably the GABAergic projections we investigate in the second section.

To test whether extrinsic or intrinsic GABAergic neurons can activate GABA_BRs expressed at cortical glutamatergic axons, one could take advantage of ChR spectral variants and transgenic animals. In VGAT-Cre or GAD1-Cre animals, injection of a Cre-dependent, red-shifted ChR (ChRimson) in the AONpp (or OB) and injection of a non-conditional blue ChR

(ChR2) in the AOC would allow selective expression of ChRimson in GABAergic neurons and non-selective expression of ChR2 in cortical top-down inputs, mainly composed of glutamatergic axons. Comparing the fEPSPs evoked by light stimulation of AOC axons before and after specific light stimulation of GABAergic axons (or OB neurons) would address whether or not AOC-to-GC synaptic transmission is modulated by the light-evoked GABA release. Application of the GABA_BR antagonist GCP will permit to validate that this is mediated through GABA_BR activation. Furthermore, comparison of the two conditions (ChRimson injection in the AONpp *vs.* in the OB) would assess the contribution of the intrinsic and extrinsic sources of GABA in GABA_BR activation.

In this first study, we showed that GABA_BR expressed at AOC axons gate the window for M/T cells to integrate AOC feedback inputs, and thus are poised to heavily shape centrifugal influence on sensory perception. GABA_BR modulation might shift the computation performed by the OB since it reshapes the interplay between M/T cells and GCs. Furthermore, we demonstrate in this first article that GABA_BRs also play a role in beta and gamma (fast) oscillations. Therefore, in line with accumulating evidence, GABA_BRs at cortical top-down axons alter fast network and cellular activities in the OB.

1.2 Discussion on Article 2 and future directions

In this second study, we demonstrate the existence of GABAergic cells sending projections back to the OB. We claim that a substantial proportion of OB-projecting GABAergic neurons originate from a cluster of cells belonging to the AON pars posterioris (AONpp; see discussion of the article in preparation). In addition to the anatomical characterization of this cluster of cells and its projections to the OB, we tackle the question of the functional connectivity of this cortical GABAergic feedback and its impact on odor-driven behavior. Currently, we are also investigating 1) its natural context of activation in an odor-reward association task, 2) the functional impact of its stimulation on spontaneous and odor-evoked activity of postsynaptic OB cells – and notably on M/T cell firing activity –, and 3) its functional impact on the OB network. The discovery of this cortico-bulbar GABAergic top-down raise many questions. I will review a few of them in the following paragraphs.

GABAergic feedback: Considerations on previous studies. The first obvious consequence of the existence of this GABAergic feedback is that previous studies supposedly investigating glutamatergic cortical feed-

back likely comprise GABAergic axons too. It seems very probable that viral injections targeting the APC diffused in the AONpp (because of the spatial proximity). In addition, first evidence from our ongoing study highly suggests that at least a subpopulation of these GABAergic cells express the CaMKIIa promoter – widely used as a glutamatergic neuron specific promoter. Therefore, even in studies using this promoter to restrict labeling to excitatory neurons, feedback axons are probably contaminated by GABAergic axons. We should still precise that this contamination is probably minor regarding the total number of feedback axons or boutons. Indeed, using our injection protocol, we estimate the density of cortical GABAergic top-down fibers to be roughly one to two order of magnitude less numerous than their glutamatergic counterparts.

In the first study presented here, in spite of using of a CaMKIIa promoter driving ChR2 expression, we also probably stimulated the GABAergic feedback in addition to the glutamatergic one. However, we believe that it does not impact our findings, given 1) the relative low proportion of the GABAergic fibers compared to the glutamatergic ones, and 2) because fEPSP recordings are due to glutamatergic depolarization of the GCs (and a GABAergic component will only lead to an underestimation of it), and M/T cells light-evoked inhibition was not observed when GABA inputs were directly stimulated.

Characterization of the cortical GABAergic projecting cells. Getting insights in the molecular, anatomical and electrical properties is necessary for characterizing the OB-projecting GABAergic cells and determining what subtype they belong to. Characterization of these GABAergic projecting cells might be helpful to refine hypotheses regarding their functions.

First, we aim at characterizing the molecular expression pattern of the GABAergic projecting cells. Examples from the literature illustrate that GABAergic projecting cells within a brain region are often heterogeneous (in the hippocampus for instance, Jinno, 2009; Jinno et al., 2007), but might be more homogeneous when a specific projection is considered: 90% of hippocampo-septal neurons are SOM⁺ for example (Jinno and Kosaka, 2002). Are the cortico-bulbar GABAergic neurons heterogeneous in term of protein expression pattern or do they mainly fall into a category, such as PV, VIP or SOM? Utilizing transgenic animal-based labeling, we showed that a sizable fraction of cells are SOM-expressing. In addition, we are currently using immunohistochemical labelings to 1) confirm above results and 2) investigate whether the GABAergic projecting cells might express additional molecular markers widely express in the AON (Brunjes et al., 2005) and APC (Suzuki and Bekkers, 2010), such as calbindin and calretinin. We aim at confirming the results obtained with the transgenic animals because using genetic mouse lines might restrict viral expression to a subset of cells (i.e, a

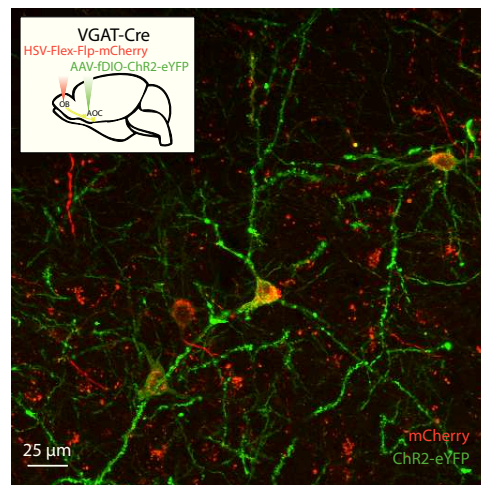


Figure 1.1 – Dual conditional labeling of cortico-bulbar GABAergic neurons. Confocal image of dually-labeled AOC neurons projecting to the OB. OB-projecting GABAergic neurons express the flipase (Flp) recombinase as well as mCherry. Anterior olfactory cortex neurons expressing the flipase are then transfected by a virus delivering the flipase-dependent (fDIO) ChR2 fused to eYFP.

subset of PV cells would only express Cre in PV-Cre mice), or in contrast might "leak" to other cell types (Cre expression might by-pass the promoter or arise from transient promoter expression that lead to permanent genetic rearrangement).

Second, it would be interesting to study the morphology of these neurons in greater details. For instance, the use of dual-conditional labeling allowed us to specifically label the cortical GABAergic cells projecting to the OB, but not any other GABAergic OB-projecting cells, emanating from the basal forebrain for example (Figure 1.1). First investigations of ChR2 expression elsewhere in the brain suggest that OB-projecting cells of the AONpp also project locally and in other brain regions. This also appears to be a common feature of long-distance projecting GABAergic cells, and notably in the GABAergic projecting cells from the hippocampal formation (Jinno et al., 2007). "Pioneer" GABAergic cells, born as early as embryonic day 10, were found to send long-range projections to various brain regions and persist into adulthood. Hub neurons of the hippocampus are classically described pioneer cells (Picardo et al., 2011), but pioneer cells produce projecting neurons in many other brain regions. Interestingly, they seem to exhibit a wide axonal arborization. Thus, widely branching axon collaterals from projecting GABAergic cells might arise from their development origin. Tissue clearing or serial reconstruction techniques would be instrumental in efficiently appreciating the 3D organization of the projections across the full brain.

Intrinsic electrophysiological properties are another important parameter to characterize a cell population. Our retrograde labeling technique utiliz-

ing HSV virus allow us to perform such investigation. Retrograde labeling with a fluorescent reporter allows OB-projecting cell identification in acute slices to obtain electrical recordings from. Cells can subsequently be filled with biocytin for post-hoc reconstruction and more detailed morphological analyses. Greater knowledge about their intrinsic properties and notably their firing activity pattern would allow refinement of working hypothesis regarding their function and their impact on the OB network.

Odor response properties. In addition to these morphological and electrical properties, determining the odor-response properties of the cortico-bulbar GABAergic neurons, or their axon terminals in the OB, is crucial.

Recording the axon terminal activity can be achieved by simple anterograde labeling with a Cre-dependent GCaMP combined with calcium imaging. Superficial two-photon imaging of GABAergic fibers in the GL could be compared to deep imaging in the GCL, as it was performed for the glutamatergic axons (Boyd et al., 2015; Otazu et al., 2015).

Selective recordings of the somas can also be achieved since our retrograde labeling protocol allows GCaMP6f expression in GABAergic projecting cells specifically. Fiber photometry recordings would give a first, fast general idea of the odor population coding, but single cell recording would permit embracing the response diversity in the population. So deep (about 2.5 mm deep from the brain surface), single cell recording is now possible using GRIN lenses and microendoscopes (Flusberg et al., 2005). Recording resolution should be good enough to identify putative cells under the lens.

The first biological questions one should ask (looking either at the axon terminals or cell bodies) have been addressed recently for the glutamatergic cortical feedback (Boyd et al., 2015; Otazu et al., 2015): 1) how are these projecting GABAergic cells/axons tuned to odor? Can the odor respond both inhibitory and excitatory? 2) What are the kinetics of the responses? And 3) are these neurons/axons diverse in their responses polarity, kinetics and tuning or are they homogeneous? Finally, it would be interesting to find out whether there is a topographical organization of this GABAergic feedback, such that axons tuned to the same odors are clustered, or are the axons tuned for different odors intermingled?

Natural conditions of activation. To investigate the activity dynamics of cortico-bulbar GABAergic axons in olfactory behavior, we developed a fiber photometry approach combined with an odor-reward association task. In mice that had already learned the discrimination task, we observed in the OB that Ca^{2+} activity in cortico-bulbar GABAergic axons decreased substantially more for the S+ compared to the S- (see Figure 2.1). This data suggests that cortico-bulbar GABAergic axons code for odor quality (or valence) rather than for odor identity. Therefore, it appears that odor

valence coding in the olfactory system might start as early as in the OB, the first brain relay for olfactory information, through top-down innervation. In line with this, unpublished data from the laboratory shows that blocking glutamatergic feedback impairs reversal learning, where odor contingencies are switched. If this assumption is true, valence coding in the first brain region will be a particular signature of the olfactory system. This might not be too surprising given the strong relation between odor and innate behavior (see for example Root et al. (2014a)).

Functional connectivity of GABAergic cortico-bulbar axons. The first question we asked is the functional connectivity between cortico-bulbar GABAergic axons and OB neurons. Using patch-clamp recordings in acute OB slices, we found that GABAergic cortico-bulbar axons target GCs and dSACs, but apparently not MCs, PG cells and eTCs (Figure 5). This was surprising given the cortical GABAergic neurons innervate all layers in the OB (Figure 1). Slicing artifacts might lead to an underestimation of the number of connected cells, although sliced axons are still able to release neurotransmitter upon ChR2 activation. In any case, this observation is in strong contrast with the connectivity matrix obtain with glutamatergic cortico-bulbar axons.

Impact of cortico-bulbar GABAergic projections on odor coding and perception. GABAergic feedback projections raise the question of the function of long-distance inhibitory projections in the brain. Both GABAergic projections from the septum or enthorinal cortex were shown to disinhibit hippocampal principal cells (Basu et al., 2016; Tóth et al., 1997). Our ongoing *in vivo* experiments are investigating the functional impact of cortical GABAergic projections on the OB *in vivo*.

First, using fiber photometry coupled to optogenetic stimulation, preliminary data suggests that cortico-bulbar GABAergic axon stimulation depresses spontaneous and odor-evoked GCs activity. We additionally found that Ca^{2+} activity decreases following odor onset (Figure 2.1), suggesting that GABAergic fibers are tonically active. Thus, GABAergic feedback might contribute to the sparse odor code in the GC population.

Second, I am currently investigating the resulting impact of OB network inhibition by GABAergic feedback axons on M/T cells. Are M/T cells disinhibited by long-range GABAergic projections? To address this question, I perform extracellular recordings of spontaneous and odor-evoked M/T cells activity upon stimulation of GABAergic projection axons. Technically, these experiments are based on the techniques we developed in the article 1 "GABA_B receptors tune cortical feedback to the olfactory bulb".

Long-range GABAergic projections from the septum end entorhinal cortex

were also shown to generate – or at least modulate – theta oscillations in the hippocampus (Brandon et al., 2014; Melzer et al., 2012). Importantly, synchronized oscillatory activity is thought to be crucial for olfaction (Laurent, 2002). Using *in vivo* electrophysiological recordings, it will be interesting to investigate whether or not cortico-bulbar GABAergic projections similarly regulate rhythms in the OB.

Finally, enthorinal cortex-to-hippocampus (Basu et al., 2016) as well as mesolimbic (Brown et al., 2012) GABAergic projections perturbation were shown to impair stimuli discrimination. Our behavioral experiments show alteration of behavioral performances as well when cortical GABAergic axon activity was manipulated. Long-range GABAergic projections, despite their relative sparseness, might therefore have significant impact on behavior.

1.3 General discussion

These studies raise two important points about feedback function that have rarely been addressed in the rapidly increasing amount of studies investigating centrifugal inputs to the OB. The first article shed light on a novel presynaptic regulation of glutamatergic feedback transmission to the OB, while the second study put in the forefront the diversity of the cortical feedback inputs as well as the functional diversity of the projecting regions. These findings highlight the need for finer dissection of feedback functions, with regard to their neurochemical nature, origin, and their regulation, to better understand their key role in OB odor coding. Towards this aim, a recent work investigated the specific function of the AONpm in olfactory guided behavior, although this study lacks specificity towards the cortico-bulbar projections (Aqrabawi et al., 2016).

Subregion specificities in centrifugal fibers. In the Introduction part (Chapter 3), we saw that different regions from the anterior olfactory cortex, and notably the AON, project differentially among the OB layers (Figure 3.1). Furthermore, we showed in the second study that long-range GABAergic projections exist in the cortical feedback, and they originate mainly within a precise region: the AONpp. Therefore, cortical feedback diversity is represented both at the level of their distribution pattern across the OB layers, and regarding their neurochemical nature. Within a layer, fiber originating from different regions might also contact different types of postsynaptic cells. First studies shed light on the vast diversity of the OB neurons connected by top-down axons (Boyd et al., 2012; Markopoulos et al., 2012), but further effort should be made to bring that issue at the neuronal subtype

level. Indeed, greater feedback specialization might arise from more precise circuit dissection. Studies considering cortical feedback from a region, or from whole centrifugal system have been instrumental to shed light on the substantial impact of centrifugal regulations to the OB, yet the diversity of cortical feedback might be greater than usually assumed. Thus, the impact of cortical feedback originating from different subregions of the anterior olfactory cortex might influence odor coding in the OB in different manners and serve different functions in the OB. Study of cortical feedback will greatly benefit from more specific manipulations and better understanding of their heterogeneity.

Cross-regulations of centrifugal fibers. In addition to directly acting on post-synaptic cells, it would be interesting to investigate whether long-range inhibition acts on parallel glutamatergic axon terminal to depress neurotransmitter release. Inhibition of glutamate release could be mediated by GABA_B heteroreceptors activation, through shunting inhibition of Ca²⁺ currents or direct inhibition of neurotransmitter release. As discussed before, an interesting hypothesis is that cortical GABAergic inputs are the source of GABA activating GABA_B heteroreceptors at glutamatergic axon terminals. This hypothesis is addressable with the tools we have in the laboratory (see discussion above). Cannabinoid receptors have also been shown to regulate the glutamatergic cortico-bulbar transmission. In addition, first evidence in the laboratory suggests that GABA_B and cannabinoid receptor activation block AOC-to-GC GABAergic transmission. The presynaptic regulations of cortico-bulbar terminals have only be found to be inhibitory so far. It would be interesting to investigate if cortical feedback is tonically active, and is down-regulated *via* presynaptic signaling mechanisms during appropriate behavior (i.e, during fasting Soria-Gómez et al., 2014).

Data from the laboratory shows that cortical glutamatergic and GABAergic top-down transmissions are regulated by at least two independent systems (GABA_B and cannabinoid). Neuromodulatory fibers (serotonergic, cholinergic or noradrenergic) might also influence –and be influenced by– glutamate or GABAergic release from the cortico-bulbar axons. Cross-interactions between centrifugal inputs could thus be prevalent in the OB, but the consequences on odor coding remain unclear. Yet we reasoned that it makes sense for the OB to be able to block a class of top-down inputs selectively, in order to allow another top-down modality to influence the network. Comprehensive studies on centrifugal fiber synaptic transmission regulation, and possibly on cross-regulation between centrifugal inputs, would greatly contribute to a better knowledge about top-down inputs functions in the OB.

Parallel inhibition in the brain. In the olfactory cortex – or at least in the AONpp –, GABAergic projections are sent in parallel to the glutamater-

gic ones. What is the function of parallelizing excitatory and inhibitory inputs? In the *Drosophila* olfactory system, glutamatergic and GABAergic neurons from the antennal lobe (the functional equivalent of the OB) project to the lateral horn (Liang et al., 2013; Parnas et al., 2013). In this system, GABAergic projection neurons selectively inhibit olfactory responses to food odor, but not to pheromones (Liang et al., 2013). Food odor and pheromones channels are segregated in *Drosophila*, and thus GABAergic projections provide another level of specificity, based on odor quality, of the higher-order neuronal responses to olfactory inputs. In a reward-association task, we found evidence for a differential activity of the GABAergic feedback based on the odor contingencies. Therefore, it seems that GABAergic feedback in mice does also respond differentially to behavioral relevant *vs.* non-relevant odors. In *Drosophila*, in contrast with the broad innervation pattern by glutamatergic feedforward and feedback inputs (which is optimal for the functions they are thought to serve, such as gain control and pattern separation/completion), GABAergic projection pattern seems to be spatially restricted to food odor channels specifically. It would be interesting to address whether GABAergic feedback boutons in the OB have a particular topography and whether they are tuned to qualitatively similar odors.

In addition, long-range GABAergic inhibition in *Drosophila* has also been shown to facilitate discrimination of mostly food odors (Parnas et al., 2013). In our experiments, we show that cortical GABAergic top-down inputs decrease odor detection threshold. Odor detection and discrimination are often thought to be balanced in olfaction, such that the ability increase of one results in ability decrease of the other. It is therefore tempting to suggest that the decrease of odor detection by cortical GABAergic feedback permits finer odor discrimination, although our behavior experiments did not allow us to detect such subtle changes.

We raised here several similarities between parallel inhibition in *Drosophila* and mice, but we should also point major differences. Parallel excitation and inhibition in *Drosophila* are ascending inputs, while the projections I refer to in mice are descending. A more straightforward anatomical comparison could be made with projections from dSACs and M/T cells. In addition, inhibitory projection neurons in *Drosophila* were shown to selectively innervate the lateral horn, but spare the mushroom body, while such differences in innervation patterns are not clear between glutamatergic and GABAergic feedback in mice.

Another feature of parallel inhibition is the timing of inhibition. Inhibition arising from feedforward and feedback motifs are delayed compared to excitation, restricting the postsynaptic cell response to a narrow time-window. However, parallel inhibition theoretically arrives at the same time as excitation (direct inhibition), as observed in *Drosophila*, and possibly al-

lows complete suppression of the incoming excitatory input. Thus, parallel inhibition seems ideally suited for information gating.

GABAergic projection loop. Additionally, a few dSACs in the GCL of the OB have been shown to project to the cortical structures, and particularly the AON (Eyre et al., 2008). Using both Cre-dependent anterograde labeling of dSACs and retrograde labeling of cortical projecting GABAergic neurons, it would be interesting to investigate whether dSAC projections terminates in the region where the cluster of GABAergic cells projecting back to the OB is found. If so, AONpp and the OB form a reciprocally connected inhibitory loop. Bidirectional GABAergic projections between the hippocampus and the entorhinal cortex and between the hippocampus and the medial septum have already been reported (Caputi et al., 2013). What are the functions of these GABAergic loop connecting two different brain regions? This is largely unknown, but one can speculate that they serve as functional negative feedback to regulate incoming GABAergic activity and finely regulate oscillatory couplings between the brain regions involved.

Thus, long-distance GABAergic projections are more prominent in the mammalian brain than usually considered, even in cortical structures where glutamate is the main output. Therefore, parallel excitation and inhibition might potentially be widely used in the brain. Here, we report the first GABAergic feedback projections in a sensory system. Further anatomical and functional investigation are currently conducted and will provide great insight into the enigmatic role of GABAergic projections.

Bibliography

Bibliography

- Abraham, N. M., V. Egger, D. R. Shimshek, R. Renden, I. Fukunaga, R. Sprengel, P. H. Seeburg, M. Klugmann, T. W. Margrie, A. T. Schaefer, and T. Kuner
2010. Synaptic inhibition in the olfactory bulb accelerates odor discrimination in mice. *Neuron*, 65(3):399–411.
- Abraham, N. M., H. Spors, A. Carleton, T. W. Margrie, T. Kuner, and A. T. Schaefer
2004. Maintaining accuracy at the expense of speed: Stimulus similarity defines odor discrimination time in mice. *Neuron*, 44(5):865–876.
- Adesnik, H., W. Bruns, H. Taniguchi, Z. J. Huang, and M. Scanziani
2012. A neural circuit for spatial summation in visual cortex. *Nature*, 490(7419):226–231.
- Allen, K. and H. Monyer
2014. Interneuron control of hippocampal oscillations. *Current Opinion in Neurobiology*, 31:81–87.
- Alonso, M., G. Lepousez, S. Wagner, C. Bardy, M.-M. Gabellec, N. Torquet, and P.-M. Lledo
2012. Activation of adult-born neurons facilitates learning and memory. *Nature Neuroscience*, 2(May):1–10.
- Angelo, K., E. a. Rancz, D. Pimentel, C. Hundahl, J. Hannibal, A. Fleischmann, B. Pichler, and T. W. Margrie
2012. A biophysical signature of network affiliation and sensory processing in mitral cells. *Nature*, 488(7411):375–378.
- Apicella, a., Q. Yuan, M. Scanziani, and J. S. Isaacson
2010. Pyramidal cells in piriform cortex receive convergent input from distinct olfactory bulb glomeruli. *J Neurosci*, 30(42):14255–14260.

- Aqrabawi, A., C. Browne, Z. Dargaei, D. Garand, C. Khademullah, M. Woodin, and J. Kim
2016. A bidirectional switch for olfaction: top-down modulation of olfactory-guided behaviours by the anterior olfactory nucleus pars medialis and ventral hippocampus. *Nature Communications*, Under Re-r:1–9.
- Aroniadou-Anderjaska, V., F. M. Zhou, C. A. Priest, M. Ennis, and M. T. Shipley
2000. Tonic and synaptically evoked presynaptic inhibition of sensory input to the rat olfactory bulb via GABA(B) heteroreceptors. *Journal of neurophysiology*, 84(3):1194–1203.
- Arruda-Carvalho, M., K. G. Akers, A. Guskjolen, S. Masanori, S. A. Josse-lyn, and P. W. Frankland
2014. Posttraining ablation of adult-generated olfactory granule cells degrades odor-reward memories.
- Ascoli, G. a., L. Alonso-Nanclares, S. a. Anderson, G. Barrionuevo, R. Benavides-Piccione, A. Burkhalter, G. Buzsáki, B. Cauli, J. Defelipe, A. Fairén, D. Feldmeyer, G. Fishell, Y. Fregnac, T. F. Freund, D. Gardner, E. P. Gardner, J. H. Goldberg, M. Helmstaedter, S. Hestrin, F. Karube, Z. F. Kisvárdy, B. Lambolez, D. a. Lewis, O. Marin, H. Markram, A. Muñoz, A. Packer, C. C. H. Petersen, K. S. Rockland, J. Rossier, B. Rudy, P. Somogyi, J. F. Staiger, G. Tamas, A. M. Thomson, M. Toledo-Rodriguez, Y. Wang, D. C. West, and R. Yuste
2008. Petilla terminology: nomenclature of features of GABAergic interneurons of the cerebral cortex. *Nature reviews. Neuroscience*, 9(7):557–568.
- Atallah, B. V., W. Bruns, M. Carandini, and M. Scanziani
2012. Parvalbumin-Expressing Interneurons Linearly Transform Cortical Responses to Visual Stimuli. *Neuron*, 73(1):159–170.
- Atallah, B. V. and M. Scanziani
2009. Instantaneous Modulation of Gamma Oscillation Frequency by Balancing Excitation with Inhibition. *Neuron*, 62(4):566–577.
- Aungst, J. L., P. M. Heyward, A. C. Puche, S. V. Karnup, A. Hayar, G. Szabo, and M. T. Shipley
2003. Centre-surround inhibition among olfactory bulb glomeruli. *Nature*, 426(6967):623–629.
- Balu, R., R. T. Pressler, and B. W. Strowbridge
2007. Multiple modes of synaptic excitation of olfactory bulb granule cells. *The Journal of neuroscience : the official journal of the Society for Neuroscience*, 27(21):5621–5632.

Balu, R. and B. W. Strowbridge

2007. Opposing inward and outward conductances regulate rebound discharges in olfactory mitral cells. *Journal of neurophysiology*, 97(3):1959–68.

Banerjee, A., F. Marbach, F. Anselmi, M. S. Koh, M. B. Davis, P. Garcia da Silva, K. Delevich, H. K. Oyibo, P. Gupta, B. Li, and D. F. Albeanu
2015. An Interglomerular Circuit Gates Glomerular Output and Implements Gain Control in the Mouse Olfactory Bulb. *Neuron*, 87(1):193–207.

Barth, A. M. I., I. Ferando, and I. Mody

2014. Ovarian cycle-linked plasticity of δ -GABAA receptor subunits in hippocampal interneurons affects γ oscillations in vivo. *Frontiers in cellular neuroscience*, 8(August):222.

Basu, J., J. D. Zaremba, S. K. Cheung, F. L. Hitti, B. V. Zemelman, A. Losonczy, and S. A. Siegelbaum

2016. Gating of hippocampal activity, plasticity, and memory by entorhinal cortex long-range inhibition. *Science*, 351(6269):aaa5694–aaa5694.

Bathellier, B.

2005. Circuit Properties Generating Gamma Oscillations in a Network Model of the Olfactory Bulb. *Journal of Neurophysiology*, 95(4):2678–2691.

Bathellier, B., D. L. Buhl, R. Accolla, and A. Carleton

2008. Dynamic Ensemble Odor Coding in the Mammalian Olfactory Bulb: Sensory Information at Different Timescales. *Neuron*, 57(4):586–598.

Bathellier, B., S. Lagier, P. Faure, and P.-M. Lledo

2006. Circuit properties generating gamma oscillations in a network model of the olfactory bulb. *Journal of neurophysiology*, 95(4):2678–91.

Ben-Ari, Y.

2014. The GABA excitatory/inhibitory developmental sequence: A personal journey. *Neuroscience*, 279:187–219.

Beshel, J., N. Kopell, and L. M. Kay

2007. Olfactory bulb gamma oscillations are enhanced with task demands. *Journal of Neuroscience*, 27(31):8358–8365.

Blumhagen, F., P. Zhu, J. Shum, Y.-P. Z. Schärer, E. Yaksi, K. Deisseroth, and R. W. Friedrich

2011. Neuronal filtering of multiplexed odour representations. *Nature*, 479(7374):493–8.

- Bolding, K. A. and K. M. Franks
2017. Complementary codes for odor identity and intensity in olfactory cortex. *eLife*, 6(919).
- Booker, S. a., a. Gross, D. Althof, R. Shigemoto, B. Bettler, M. Frotscher, M. Hearing, K. Wickman, M. Watanabe, a. Kulik, and I. Vida
2013. Differential GABAB-Receptor-Mediated Effects in Perisomatic- and Dendrite-Targeting Parvalbumin Interneurons. *Journal of Neuroscience*, 33(18):7961–7974.
- Bowery, N. G.
2010. Historical perspective and emergence of the GABAB receptor. *Advances in Pharmacology*, 58(C):1–18.
- Boyd, A. M., H. K. Kato, T. Komiyama, and J. S. Isaacson
2015. Broadcasting of Cortical Activity to the Olfactory Bulb. *Cell Reports*, 10(7):1032–1039.
- Boyd, A. M., J. F. Sturgill, C. Poo, and J. S. Isaacson
2012. Cortical feedback control of olfactory bulb circuits. *Neuron*, 76(6):1161–74.
- Brandon, M. P., J. Koenig, J. K. Leutgeb, and S. Leutgeb
2014. New and Distinct Hippocampal Place Codes Are Generated in a New Environment during Septal Inactivation. *Neuron*, 82(4):789–796.
- Brazhnik, E., F. Shah, and J. M. Tepper
2008. GABAergic afferents activate both GABAA and GABAB receptors in mouse substantia nigra dopaminergic neurons in vivo. *The Journal of neuroscience : the official journal of the Society for Neuroscience*, 28(41):10386–98.
- Breton-Provencher, V., M. Lemasson, M. Peralta, and A. Saghatelian
2009. Interneurons produced in adulthood are required for the normal functioning of the olfactory bulb network and for the execution of selected olfactory behaviors. *The Journal of neuroscience : the official journal of the Society for Neuroscience*, 29(48):15245–15257.
- Brickley, S. G. and I. Mody
2012. Extrasynaptic GABA A Receptors: Their Function in the CNS and Implications for Disease. *Neuron*, 73(1):23–34.
- Brill, J., Z. Shao, A. C. Puche, M. Wachowiak, and M. T. Shipley
2015. Serotonin increases synaptic activity in olfactory bulb glomeruli. *Journal of Neurophysiology*, 115(3):jn.00847.2015.

- Brill, M. S., J. Ninkovic, E. Winpenny, R. D. Hodge, I. Ozen, R. Yang, A. Lepier, S. Gascon, F. Erdelyi, G. Szabo, C. Parras, F. Guillemot, M. Frotscher, B. Berninger, R. F. Hevner, O. Raineteau, and M. Gotz
2009. Adult generation of glutamatergic olfactory bulb interneurons. *Nature Neuroscience*, 12(12):1524–1533.
- Brown, J. T., C. H. Davies, and A. D. Randall
2007. Synaptic activation of GABA(B) receptors regulates neuronal network activity and entrainment. *The European journal of neuroscience*, 25(10):2982–90.
- Brown, M. T. C., K. R. Tan, E. C. O’Connor, I. Nikonenko, D. Muller, and C. Lüscher
2012. Ventral tegmental area GABA projections pause accumbal cholinergic interneurons to enhance associative learning. *Nature*, 492(7429):452–456.
- Brown, S. L., J. Joseph, and M. Stopfer
2005. Encoding a temporally structured stimulus with a temporally structured neural representation. *Nature neuroscience*, 8(11):1568–76.
- Brunert, D., X. Y. Tsuno, M. Rothermel, X. M. T. Shipley, and M. Wachowiak
2016. Cell-Type-Specific Modulation of Sensory Responses in Olfactory Bulb Circuits by Serotonergic Projections from the Raphe Nuclei. *The Journal of Neuroscience*, 36(25):6820–6835.
- Brunjes, P. C., K. R. Illig, and E. A. Meyer
2005. A field guide to the anterior olfactory nucleus (cortex). *Brain Research Reviews*, 50(2):305–335.
- Buck, L. and R. Axel
1991. A novel multigene family may encode odorant receptors: a molecular basis for odor recognition. *Cell*, 65(1):175–87.
- Buetfering, C., K. Allen, and H. Monyer
2014. Parvalbumin interneurons provide grid cell-driven recurrent inhibition in the medial entorhinal cortex. *Nature neuroscience*, 17(5):710–8.
- Buonviso, N., C. Amat, P. Litaudon, S. Roux, J. P. Royet, V. Farget, and G. Sicard
2003. Rhythm sequence through the olfactory bulb layers during the time window of a respiratory cycle. *European Journal of Neuroscience*, 17(9):1811–1819.
- Buonviso, N., M. a. Chaput, and F. Berthommier
1992. Temporal pattern analyses in pairs of neighboring mitral cells. *Journal of neurophysiology*, 68(2):417–424.

- Burton, S. D., G. LaRocca, A. Liu, C. E. Cheetham, and N. N. Urban
2017. Olfactory Bulb Deep Short-Axon Cells Mediate Widespread Inhibition of Tufted Cell Apical Dendrites. *The Journal of Neuroscience*, 37(5):1117–1138.
- Burton, S. D. and N. N. Urban
2014. Greater excitability and firing irregularity of tufted cells underlies distinct afferent-evoked activity of olfactory bulb mitral and tufted cells. *J Physiol*, 59210(59210):2097–2118.
- Burton, S. D. and N. N. Urban
2015. Rapid Feedforward Inhibition and Asynchronous Excitation Regulate Granule Cell Activity in the Mammalian Main Olfactory Bulb. *Journal of Neuroscience*, 35(42):14103–14122.
- Bushdid, C., M. O. Magnasco, L. B. Vosshall, and a. Keller
2014. Humans can discriminate more than 1 trillion olfactory stimuli. *Science (New York, N.Y.)*, 343(6177):1370–2.
- Bywalez, W. G., D. Patirniche, V. Rupprecht, M. Stemmler, A. V. M. Herz, D. Palfi, B. Rozsa, and V. Egger
2015. Local postsynaptic voltage-gated sodium channel activation in dendritic spines of olfactory bulb granule cells. *Neuron*, 85(3):590–601.
- Cang, J. and J. S. Isaacson
2003. In vivo whole-cell recording of odor-evoked synaptic transmission in the rat olfactory bulb. *The Journal of neuroscience : the official journal of the Society for Neuroscience*, 23(10):4108–16.
- Caputi, A., S. Melzer, M. Michael, and H. Monyer
2013. The long and short of GABAergic neurons. *Current opinion in neurobiology*, 23(2):179–186.
- Carleton, A., L. T. Petreanu, R. Lansford, A. Alvarez-Buylla, and P. M. Lledo
2003. Becoming a new neuron in the adult olfactory bulb. *Nature Neuroscience*, 6(5):507–518.
- Carlson, G. C., M. T. Shipley, and a. Keller
2000. Long-lasting depolarizations in mitral cells of the rat olfactory bulb. *The Journal of neuroscience : the official journal of the Society for Neuroscience*, 20(5):2011–21.
- Carson, K. a.
1984. Quantitative localization of neurons projecting to the mouse main olfactory bulb. *Brain research bulletin*, 12(6):635–9.

- Castillo, P. E., a. Carleton, J. D. Vincent, and P. M. Lledo
1999. Multiple and opposing roles of cholinergic transmission in the main olfactory bulb. *The Journal of neuroscience : the official journal of the Society for Neuroscience*, 19(21):9180–91.
- Cazakoff, B. N., B. Y. B. Lau, K. L. Crump, H. S. Demmer, and S. D. Shea
2014. Broadly tuned and respiration-independent inhibition in the olfactory bulb of awake mice. *Nature neuroscience*, 17(4):569–76.
- Chabaud, P., N. Ravel, D. a. Wilson, a. M. Mouly, M. Vigouroux, V. Farget, and R. Gervais
2000. Exposure to behaviourally relevant odour reveals differential characteristics in rat central olfactory pathways as studied through oscillatory activities. *Chemical Senses*, 25(5):561–573.
- Chen, C.-f. F., D.-j. Zou, C. G. Altomare, L. Xu, C. A. Greer, and S. J. Firestein
2014. Nonsensory target-dependent organization of piriform cortex. 111(47).
- Chittajallu, R., K. a. Pelkey, and C. J. McBain
2013. Neurogliaform cells dynamically regulate somatosensory integration via synapse-specific modulation. *Nature neuroscience*, 16(1):13–15.
- Choy, J. M. C., N. Suzuki, Y. Shima, T. Budisantoso, S. B. Nelson, and J. M. Bekkers
2015. Optogenetic Mapping of Intracortical Circuits Originating from Semilunar Cells in the Piriform Cortex. *Cerebral cortex (New York, N.Y. : 1991)*, Pp. 1–13.
- Christie, J. M. and G. L. Westbrook
2006. Lateral Excitation within the Olfactory Bulb. *Journal of Neuroscience*, 26(8):2269–2277.
- Chu, M. W., W. L. Li, and T. Komiyama
2016. Balancing the Robustness and Efficiency of Odor Representations during Learning. *Neuron*, 92(1):174–186.
- Cleland, T. A.
2010. Early transformations in odor representation. *Trends in Neurosciences*, 33(3):130–139.
- Cleland, T. A. and P. Sethupathy
2006. Non-topographical contrast enhancement in the olfactory bulb. *BMC Neuroscience*, 7:7.

- Collins, C. E., D. C. Lyon, and J. H. Kaas
2005. Distribution across cortical areas of neurons projecting to the superior colliculus in new world monkeys. *The anatomical record. Part A, Discoveries in molecular, cellular, and evolutionary biology*, 285(1):619–27.
- Courtiol, E., C. Amat, M. Thévenet, B. Messaoudi, S. Garcia, and N. Buono-viso
2011. Reshaping of bulbar odor response by nasal flow rate in the Rat. *PLoS ONE*, 6(1).
- Courtiol, E. and D. a. Wilson
2014. Thalamic olfaction: characterizing odor processing in the mediodorsal thalamus of the rat. *Journal of neurophysiology*, 111(6):1274–85.
- Craig, M. T., E. W. Mayne, B. Bettler, O. Paulsen, and C. J. McBain
2013. Distinct roles of GABAB1a- and GABAB1b-containing GABAB receptors in spontaneous and evoked termination of persistent cortical activity. *The Journal of physiology*, 591(Pt 4):835–43.
- Craig, M. T. and C. J. McBain
2014. The emerging role of GABAB receptors as regulators of network dynamics: Fast actions from a 'slow' receptor? *Current Opinion in Neurobiology*, 26:15–21.
- Cryan, J. F. and D. A. Slattery
2010. GABAB receptors and depression. Current status. *Advances in Pharmacology*, 58(C):427–451.
- Cury, K. M. and N. Uchida
2010. Robust odor coding via inhalation-coupled transient activity in the mammalian olfactory bulb. *Neuron*, 68(3):570–85.
- Davis, B. J. and F. Macrides
1981. The Organization of Centrifugal Projections From the Anterior Olfactory Nucleus, Ventral Hippocampal Rudiment, and Piriform Cortex to the Main Olfactory Bulb in the Hamster : An Autoradiographic Study. *The Journal of comparative neurology*, 493:475–493.
- Davison, I. G. and M. D. Ehlers
2011. Neural Circuit Mechanisms for Pattern Detection and Feature Combination in Olfactory Cortex. *Neuron*, 70(1):82–94.
- Davison, I. G. and L. C. Katz
2007. Sparse and selective odor coding by mitral/tufted neurons in the main olfactory bulb. *The Journal of neuroscience : the official journal of the Society for Neuroscience*, 27(8):2091–101.

- de Olmos, J., H. Hardy, and L. Heimer
1978. The afferent connections of the main and the accessory olfactory bulb formations in the rat: an experimental HRP-study. *The Journal of comparative neurology*, 181(2):213–244.
- De Saint Jan, D., D. Hirnet, G. L. Westbrook, and S. Charpak
2009. External Tufted Cells Drive the Output of Olfactory Bulb Glomeruli. *Journal of Neuroscience*, 29(7):2043–2052.
- De Saint Jan, D. and G. L. Westbrook
2007. Disynaptic amplification of metabotropic glutamate receptor 1 responses in the olfactory bulb. *The Journal of neuroscience : the official journal of the Society for Neuroscience*, 27(1):132–140.
- DeFelipe, J., P. L. López-Cruz, R. Benavides-Piccione, C. Bielza, P. Larrañaga, S. Anderson, A. Burkhalter, B. Cauli, A. Fairén, D. Feldmeyer, G. Fishell, D. Fitzpatrick, T. F. Freund, G. González-Burgos, S. Hestrin, S. Hill, P. R. Hof, J. Huang, E. G. Jones, Y. Kawaguchi, Z. Kisvárdy, Y. Kubota, D. a. Lewis, O. Marín, H. Markram, C. J. McBain, H. S. Meyer, H. Monyer, S. B. Nelson, K. Rockland, J. Rossier, J. L. R. Rubenstein, B. Rudy, M. Scanziani, G. M. Shepherd, C. C. Sherwood, J. F. Staiger, G. Tamás, A. Thomson, Y. Wang, R. Yuste, and G. A. Ascoli
2013. New insights into the classification and nomenclature of cortical GABAergic interneurons. *Nature reviews. Neuroscience*, 14(3):202–16.
- Deisseroth, K.
2011. Optogenetics. *Nature methods*, 8(1):26–29.
- Devore, S. and C. Linster
2012. Noradrenergic and cholinergic modulation of olfactory bulb sensory processing. *Frontiers in behavioral neuroscience*, 6(August):52.
- Devore, S., L. C. Manella, and C. Linster
2012. Blocking muscarinic receptors in the olfactory bulb impairs performance on an olfactory short-term memory task. *Frontiers in behavioral neuroscience*, 6(September):59.
- Dhawale, A. K., A. Hagiwara, U. S. Bhalla, V. N. Murthy, and D. F. Albeanu
2010. Non-redundant odor coding by sister mitral cells revealed by light addressable glomeruli in the mouse. *Nature neuroscience*, 13(11):1404–12.
- Diodato, A., M. R. D. Brimont, Y. S. Yim, N. Derian, S. Perrin, J. Pouch, D. Klatzmann, S. Garel, G. B. Choi, and A. Fleischmann
2016. Molecular signatures of neural connectivity in the olfactory cortex. *Nature Communications*, 7:1–10.

- Donato, F., S. B. Rompani, and P. Caroni
2013. Parvalbumin-expressing basket-cell network plasticity induced by experience regulates adult learning. *Nature*, 504(7479):272–276.
- Doucette, W., D. H. Gire, J. Whitesell, V. Carmean, M. T. Lucero, and D. Restrepo
2011. Associative cortex features in the first olfactory brain relay station. *Neuron*, 69(6):1176–87.
- Doucette, W. and D. Restrepo
2008. Profound context-dependent plasticity of mitral cell responses in olfactory bulb. *PLoS biology*, 6(10):e258.
- D’Souza, R. D. and S. Vijayaraghavan
2012. Nicotinic receptor-mediated filtering of mitral cell responses to olfactory nerve inputs involves the alpha3beta4 subtype. *J Neurosci*, 32(9):3261–3266.
- Eckmeier, D. and S. D. Shea
2014. Noradrenergic plasticity of olfactory sensory neuron inputs to the main olfactory bulb. Technical Report 46.
- Economo, M. N., K. R. Hansen, and M. Wachowiak
2016. Control of Mitral/Tufted Cell Output by Selective Inhibition among Olfactory Bulb Glomeruli. *Neuron*, 91(2):397–411.
- Egger, V., K. Svoboda, and Z. F. Mainen
2003. Mechanisms of lateral inhibition in the olfactory bulb: efficiency and modulation of spike-evoked calcium influx into granule cells. *The Journal of neuroscience : the official journal of the Society for Neuroscience*, 23(20):7551–7558.
- Egger, V., K. Svoboda, and Z. F. Mainen
2005. Dendrodendritic Synaptic Signals in Olfactory Bulb Granule Cells: Local Spine Boost and Global Low-Threshold Spike. *Journal of Neuroscience*, 25(14):3521–3530.
- Eyre, M. D., M. Antal, and Z. Nusser
2008. Distinct deep short-axon cell subtypes of the main olfactory bulb provide novel intrabulbar and extrabulbar GABAergic connections. *The Journal of neuroscience : the official journal of the Society for Neuroscience*, 28(33):8217–29.
- Eyre, M. D., K. Kerti, and Z. Nusser
2009. Molecular diversity of deep short-axon cells of the rat main olfactory bulb. *The European journal of neuroscience*, 29(7):1397–1407.

- Ferando, I. and I. Mody
2014. Interneuronal GABAA receptors inside and outside of synapses. *Current Opinion in Neurobiology*, 26:57–63.
- Flusberg, B. A., E. D. Cocker, W. Piyawattanametha, J. C. Jung, E. L. M. Cheung, and M. J. Schnitzer
2005. Fiber-optic fluorescence imaging. *Nature Methods*, 2(12):941–950.
- Franks, K. M. and J. S. Isaacson
2005. Synapse-specific downregulation of NMDA receptors by early experience: A critical period for plasticity of sensory input to olfactory cortex. *Neuron*, 47(1):101–114.
- Franks, K. M., M. J. Russo, D. L. Sosulski, A. A. Mulligan, S. A. Siegelbaum, and R. Axel
2011. Recurrent Circuitry Dynamically Shapes the Activation of Piriform Cortex. *Neuron*, 72(1):49–56.
- Freund, T. F. and M. Antal
1988. GABA-containing neurons in the septum control inhibitory interneurons in the hippocampus. *Nature*, 336(6195):170–173.
- Freund, T. F. and V. Meskenaite
1992. gamma-Aminobutyric acid-containing basal forebrain neurons innervate inhibitory interneurons in the neocortex. *Proceedings of the National Academy of Sciences of the United States of America*, 89(2):738–42.
- Friedrich, R. W., C. J. Habermann, and G. Laurent
2004. Multiplexing using synchrony in the zebrafish olfactory bulb. *Nature neuroscience*, 7(8):862–71.
- Friedrich, R. W. and G. Laurent
2001. Dynamic optimization of odor representations by slow temporal patterning of mitral cell activity. *Science (New York, N.Y.)*, 291(5505):889–894.
- Fritschy, J. M. and P. Panzanelli
2014. GABAA receptors and plasticity of inhibitory neurotransmission in the central nervous system. *European Journal of Neuroscience*, 39(11):1845–1865.
- Fukunaga, I., M. Berning, M. Kollo, A. Schmaltz, and A. T. Schaefer
2012. Two distinct channels of olfactory bulb output. *Neuron*, 75(2):320–9.
- Fukunaga, I., J. T. Herb, M. Kollo, E. S. Boyden, and A. T. Schaefer
2014. Independent control of gamma and theta activity by distinct interneuron networks in the olfactory bulb. *Nature neuroscience*, 17(July):1208–1216.

- Gao, Z., G. M. van Woerden, Y. Elgersma, C. I. De Zeeuw, and F. E. Hoebeek
2014. Distinct roles of α - and β CaMKII in controlling long-term potentiation of GABAA-receptor mediated transmission in murine Purkinje cells. *Frontiers in cellular neuroscience*, 8(February):16.
- Gassmann, M. and B. Bettler
2012. Regulation of neuronal GABAB receptor functions by subunit composition. *Nature Reviews Neuroscience*, 13(June):380–394.
- Geng, Y., M. Bush, L. Mosyak, F. Wang, and Q. R. Fan
2013. Structural mechanism of ligand activation in human GABAB receptor. *Nature*, 504(7479):254–259.
- Gentet, L. J., Y. Kremer, H. Taniguchi, Z. J. Huang, J. F. Staiger, and C. C. Petersen
2012. Unique functional properties of somatostatin-expressing GABAergic neurons in mouse barrel cortex. *Nat Neurosci*, 15(4):607–612.
- Ghosh, S., S. D. Larson, H. Hefzi, Z. Marnoy, T. Cutforth, K. Dokka, and K. K. Baldwin
2011. Sensory maps in the olfactory cortex defined by long-range viral tracing of single neurons. *Nature*, 472(7342):217–220.
- Gire, D. H., K. M. Franks, J. D. Zak, K. F. Tanaka, J. D. Whitesell, A. a. Mulligan, R. Hen, and N. E. Schoppa
2012. Mitral cells in the olfactory bulb are mainly excited through a multistep signaling path. *The Journal of neuroscience : the official journal of the Society for Neuroscience*, 32(9):2964–75.
- Gire, D. H. and N. E. Schoppa
2009. Control of on/off glomerular signaling by a local GABAergic microcircuit in the olfactory bulb. *The Journal of neuroscience : the official journal of the Society for Neuroscience*, 29(43):13454–64.
- Gire, D. H., J. D. Whitesell, W. Doucette, and D. Restrepo
2013. Information for decision-making and stimulus identification is multiplexed in sensory cortex. *Nature neuroscience*, 16(8):991–993.
- Gómez, C., J. G. Briñón, M. V. Barbado, E. Weruaga, J. Valero, and J. R. Alonso
2005. Heterogeneous targeting of centrifugal inputs to the glomerular layer of the main olfactory bulb. *Journal of Chemical Neuroanatomy*, 29(4):238–254.

- Grabska-Barwińska, A., S. Barthelmé, J. Beck, Z. F. Mainen, A. Pouget, and P. E. Latham
2017. A probabilistic approach to demixing odors. *Nature neuroscience*, 20(1):98–106.
- Gracia-Llanes, F. J., J. M. Blasco-Ibáñez, J. Nácher, E. Varea, T. Liberia, P. Martínez, F. J. Martínez-Guijarro, and C. Crespo
2010a. Synaptic connectivity of serotonergic axons in the olfactory glomeruli of the rat olfactory bulb. *Neuroscience*, 169(2):770–780.
- Gracia-Llanes, F. J., C. Crespo, J. M. Blasco-Ibáñez, A. I. Marqués-Marí, and F. J. Martínez-Guijarro
2003. VIP-containing deep short-axon cells of the olfactory bulb innervate interneurons different from granule cells. *European Journal of Neuroscience*, 18(7):1751–1763.
- Gracia-Llanes, F. J., C. Crespo, J. M. Blasco-Ibáñez, J. Nacher, E. Varea, L. Rovira-Esteban, and F. J. Martínez-Guijarro
2010b. GABAergic basal forebrain afferents innervate selectively GABAergic targets in the main olfactory bulb. *Neuroscience*, 170(3):913–922.
- Gray, C. M. and J. E. Skinner
1988. Centrifugal regulation of neuronal activity in the olfactory bulb of the waking rabbit as revealed by reversible cryogenic blockade. *Experimental brain research*, 69(2):378–86.
- Gschwend, O., N. M. Abraham, S. Lagier, F. Begnaud, I. Rodriguez, and A. Carleton
2015. Neuronal pattern separation in the olfactory bulb improves odor discrimination learning. *Nature neuroscience*, 18(10):1474–82.
- Gschwend, O., J. Beroud, and A. Carleton
2012. Encoding odorant identity by spiking packets of rate-invariant neurons in awake mice. *PloS one*, 7(1):e30155.
- Gschwend, O., J. Beroud, R. Vincis, I. Rodriguez, and A. Carleton
2016. Dense encoding of natural odorants by ensembles of sparsely activated neurons in the olfactory bulb. *Scientific Reports*, 6(1):36514.
- Haberly, L. B.
2001. Parallel-distributed processing in olfactory cortex: new insights from morphological and physiological analysis of neuronal circuitry. *Chemical senses*, 26(5):551–576.
- Haberly, L. B. and J. L. Price
1978a. Association and commissural fiber systems of the olfactory cortex of the rat. I. Systems originating in the piriform cortex and adjacent areas. *The Journal of comparative neurology*, 178(4):711–40.

- Haberly, L. B. and J. L. Price
1978b. Association and Commissural Fiber Systems of the Olfactory Cortex of the Rat. II Systems originating in the olfactory peduncle. *The Journal of comparative neurology*, Pp. 781–807.
- Hack, M. a., A. Saghatelyan, A. de Chevigny, A. Pfeifer, R. Ashery-Padan, P.-M. Lledo, and M. Götz
2005. Neuronal fate determinants of adult olfactory bulb neurogenesis. *Nature neuroscience*, 8(7):865–872.
- Haddad, R., A. Lanjuin, L. Madisen, H. Zeng, V. N. Murthy, and N. Uchida
2013. Olfactory cortical neurons read out a relative time code in the olfactory bulb. *Nature neuroscience*, 16(7):949–957.
- Hagiwara, A., S. K. Pal, T. F. Sato, M. Wienisch, and V. N. Murthy
2012. Optophysiological analysis of associational circuits in the olfactory cortex. *Frontiers in neural circuits*, 6(April):18.
- Haider, B., M. Häusser, and M. Carandini
2012. Inhibition dominates sensory responses in the awake cortex. *Nature*, 493(7430):97–100.
- Haller, C., E. Casanova, M. Müller, C. M. Vacher, R. Vigot, T. Doll, S. Barbieri, M. Gassmann, and B. Bettler
2004. Floxed allele for conditional inactivation of the GABAB(1) gene. *Genesis*, 40(3):125–130.
- Hardy, A., B. Palouzier-Paulignan, A. Duchamp, J.-P. Royet, and P. Duchamp-Viret
2005. 5-hydroxytryptamine action in the rat olfactory bulb: In vitro electrophysiological patch-clamp recordings of juxtglomerular and mitral cells. *Neuroscience*, 131(3):717–731.
- Harris, K. D. and T. D. Mrsic-Flogel
2013. Cortical connectivity and sensory coding. *Nature*, 503(7474):51–8.
- Harris, K. D. and G. M. G. Shepherd
2015. The neocortical circuit: themes and variations. *Nature Neuroscience*, 18(2):170–181.
- Hayar, A., P. M. Heyward, T. Heinbockel, M. T. Shipley, and M. Ennis
2001. Direct excitation of mitral cells via activation of alpha1-noradrenergic receptors in rat olfactory bulb slices. *Journal of neurophysiology*, 86(5):2173–2182.
- Hayar, A., S. Karnup, M. Ennis, and M. T. Shipley
2004. External tufted cells: a major excitatory element that coordinates

- glomerular activity. *The Journal of neuroscience : the official journal of the Society for Neuroscience*, 24(30):6676–85.
- He, M., J. Tucciarone, S. Lee, M. J. Nigro, Y. Kim, J. M. Levine, S. M. Kelly, I. Krugikov, P. Wu, Y. Chen, L. Gong, Y. Hou, P. Osten, B. Rudy, and Z. J. Huang
2016. Strategies and Tools for Combinatorial Targeting of GABAergic Neurons in Mouse Cerebral Cortex. *Neuron*, (In Press):1–16.
- Heaney, C. F. and J. W. Kinney
2016. Role of GABAB receptors in learning and memory and neurological disorders. *Neuroscience and Biobehavioral Reviews*, 63:1–28.
- Higley, M. J.
2014. Localized GABAergic inhibition of dendritic Ca²⁺ signalling. *Nature Reviews Neuroscience*, 15(9):567–72.
- Hintiryan, H., L. Gou, B. Zingg, S. Yamashita, H. M. Lyden, M. Y. Song, A. K. Grewal, X. Zhang, A. W. Toga, and H.-W. Dong
2012. Comprehensive connectivity of the mouse main olfactory bulb: analysis and online digital atlas. *Frontiers in Neuroanatomy*, 6(August):1–16.
- Hirano, T. and S.-y. Kawaguchi
2014. Regulation and functional roles of rebound potentiation at cerebellar stellate cell-Purkinje cell synapses. *Frontiers in cellular neuroscience*, 8(February):42.
- Homma, R., Y. Kovalchuk, A. Konnerth, L. B. Cohen, and O. Garaschuk
2013. In vivo functional properties of juxtglomerular neurons in the mouse olfactory bulb. *Frontiers in Neural Circuits*, 7(February):23.
- Hu, H., J. Gan, and P. Jonas
2014. Interneurons. Fast-spiking, parvalbumin+ GABAergic interneurons: from cellular design to microcircuit function. *Science (New York, N.Y.)*, 345(6196):1255–263.
- Huang, L., I. Garcia, H.-I. Jen, and B. R. Arenkiel
2013. Reciprocal connectivity between mitral cells and external plexiform layer interneurons in the mouse olfactory bulb. *Frontiers in neural circuits*, 7(March):32.
- Huang, L., K. Ung, I. Garcia, K. B. Quast, K. Cordiner, P. Saggau, and B. R. Arenkiel
2016. Task Learning Promotes Plasticity of Interneuron Connectivity Maps in the Olfactory Bulb. *The Journal of Neuroscience*, 36(34):8856–8871.

- Huang, Z., N. Thiebaud, and D. A. Fadool
2017. Differential serotonergic modulation across the main and accessory olfactory bulbs. *The Journal of physiology*, Pp. 1–44.
- Ichikawa, T. and Y. Hirata
1986. Organization of choline acetyltransferase-containing structures in the forebrain of the rat. *The Journal of neuroscience : the official journal of the Society for Neuroscience*, 6(1):281–292.
- Igarashi, K. M., N. Ieki, M. An, Y. Yamaguchi, S. Nagayama, K. Kobayakawa, R. Kobayakawa, M. Tanifuji, H. Sakano, W. R. Chen, and K. Mori
2012. Parallel Mitral and Tufted Cell Pathways Route Distinct Odor Information to Different Targets in the Olfactory Cortex. *The Journal of Neuroscience*, 32(23):7970–7985.
- Illig, K. R. and L. B. Haberly
2003. Odor-Evoked Activity is Spatially Distributed in Piriform Cortex. *The Journal of comparative neurology*, 373(October 2002):361–373.
- Imamura, F., A. E. Ayoub, P. Rakic, and C. A. Greer
2011. Timing of neurogenesis is a determinant of olfactory circuitry. *Nature Neuroscience*, 14(3):331–337.
- Imamura, F. and C. A. Greer
2015. Segregated labeling of olfactory bulb projection neurons based on their birthdates. *European Journal of Neuroscience*, 41(2):147–156.
- Inaki, K., S. Nishimura, T. Nakashiba, S. Itoharu, and Y. Yoshihara
2004. Laminar organization of the developing lateral olfactory tract revealed by differential expression of cell recognition molecules. *The Journal of Comparative Neurology*, 479(3):243–256.
- Iremonger, K. J., J. I. Wamsteeker Cusulin, and J. S. Bains
2013. Changing the tune: Plasticity and adaptation of retrograde signals. *Trends in Neurosciences*, 36(8):471–479.
- Isaacson, J. S.
1999. Glutamate Spillover Mediates Excitatory Transmission in the Rat Olfactory Bulb. *Neuron*, 23:377–384.
- Isaacson, J. S.
2001. Mechanisms governing dendritic gamma-aminobutyric acid (GABA) release in the rat olfactory bulb. *Proc Natl Acad Sci U S A*, 98(1):337–342.
- Isaacson, J. S. and M. Scanziani
2011. How inhibition shapes cortical activity. *Neuron*, 72(2):231–43.

- Isaacson, J. S. and B. W. Strowbridge
1998. Olfactory reciprocal synapses: dendritic signaling in the CNS. *Neuron*, 20(4):749–61.
- Isaacson, J. S. and H. Vitten
2003. GABA(B) receptors inhibit dendrodendritic transmission in the rat olfactory bulb. *The Journal of neuroscience : the official journal of the Society for Neuroscience*, 23(6):2032–9.
- Jasnow, A. M., P. K. Cullen, and D. C. Riccio
2012. Remembering another aspect of forgetting. *Frontiers in Psychology*, 3(JUN):1–8.
- Jinno, S.
2009. Structural organization of long-range GABAergic projection system of the hippocampus. *Frontiers in neuroanatomy*, 3(July):13.
- Jinno, S., T. Klausberger, L. F. Marton, Y. Dalezios, J. D. B. Roberts, P. Fuentealba, E. a. Bushong, D. Henze, G. Buzsáki, and P. Somogyi
2007. Neuronal diversity in GABAergic long-range projections from the hippocampus. *The Journal of neuroscience : the official journal of the Society for Neuroscience*, 27(33):8790–804.
- Jinno, S. and T. Kosaka
2002. Immunocytochemical characterization of hippocamposeptal projecting GABAergic nonprincipal neurons in the mouse brain: A retrograde labeling study. *Brain Research*, 945(2):219–231.
- Jinno, S. and T. Kosaka
2004. Parvalbumin is expressed in glutamatergic and GABAergic cortico-striatal pathway in mice. *Journal of Comparative Neurology*, 477(2):188–201.
- Kapoor, V., A. C. Provost, P. Agarwal, and V. N. Murthy
2016. Activation of raphe nuclei triggers rapid and distinct effects on parallel olfactory bulb output channels. *Nature Neuroscience*, (November 2015):1–14.
- Kapoor, V. and N. N. Urban
2006. Glomerulus-Specific , Long-Latency Activity in the Olfactory Bulb Granule Cell Network. 26(45):11709–11719.
- Kasten, C. R. and S. L. Boehm
2015. Identifying the role of pre-and postsynaptic GABA<inf>B</inf> receptors in behavior. *Neuroscience and Biobehavioral Reviews*, 57:70–87.

- Kato, H. K., M. W. Chu, J. S. Isaacson, and T. Komiyama
2012. Dynamic sensory representations in the olfactory bulb: modulation by wakefulness and experience. *Neuron*, 76(5):962–975.
- Kato, H. K., S. N. Gillet, A. J. Peters, J. S. Isaacson, and T. Komiyama
2013. Parvalbumin-expressing interneurons linearly control olfactory bulb output. *Neuron*, 80(5):1218–1231.
- Kay, L. M.
2014. *Circuit oscillations in odor perception and memory*, volume 208, 1 edition. Elsevier B.V.
- Kay, L. M., J. Beshel, J. Brea, C. Martin, D. Rojas-Libano, and N. Kopell
2009. Olfactory oscillations: the what, how and what for. *Trends in neurosciences*, 32(4):207–14.
- Kay, L. M. and G. Laurent
1999. Odor- and context-dependent modulation of mitral cell activity in behaving rats. *Nature Neuroscience*, 2(11):1003–1009.
- Kay, L. M. and S. M. Sherman
2007. An argument for an olfactory thalamus. *Trends in Neurosciences*, 30(2):47–53.
- Kepecs, A. and G. Fishell
2014. Interneuron cell types are fit to function. *Nature*, 505(7483):318–26.
- Kepecs, A., N. Uchida, and Z. F. Mainen
2007. Rapid and Precise Control of Sniffing During Olfactory Discrimination in Rats. *Journal of Neurophysiology*, 98(1):205–213.
- Kikuta, S., M. L. Fletcher, R. Homma, T. Yamasoba, and S. Nagayama
2013. Odorant Response Properties of Individual Neurons in an Olfactory Glomerular Module. *Neuron*, 77(6):1122–1135.
- Kim, C. K., A. Adhikari, and K. Deisseroth
2017. Integration of optogenetics with complementary methodologies in systems neuroscience. *Nature Reviews Neuroscience*, 18(4):222–235.
- Kiselycznyk, C. L., S. Zhang, and C. Linstner
2006. Role of centrifugal projections to the olfactory bulb in olfactory processing. *Learning & Memory*, 13(5):575–579.
- Klausberger, T. and P. Somogyi
2008. Neuronal diversity and temporal dynamics: the unity of hippocampal circuit operations. *Science (New York, N.Y.)*, 321(5885):53–7.

- Kohl, M. M. and O. Paulsen
2010. *The Roles of GABA B Receptors in Cortical Network Activity*, volume 58, first edition. Elsevier Inc.
- Kollo, M., A. Schmaltz, M. Abdelhamid, I. Fukunaga, and A. T. Schaefer
2014. 'Silent' mitral cells dominate odor responses in the olfactory bulb of awake mice. *Nature neuroscience*, 17(10):1313–1315.
- Kosaka, T. and K. Kosaka
2010. Heterogeneity of calbindin-containing neurons in the mouse main olfactory bulb: I. General description. *Neuroscience Research*, 67(4):275–292.
- Koulakov, A. A. and D. Rinberg
2011. Sparse Incomplete Representations: A Potential Role of Olfactory Granule Cells. *Neuron*, 72(1):124–136.
- Kunze, W. a., a. D. Shafton, R. E. Kemm, and J. S. McKenzie
1992a. Olfactory bulb output neurons excited from a basal forebrain magnocellular nucleus. *Brain Res*, 583(1-2):327–331.
- Kunze, W. A. A., A. D. Shafton, R. E. Kemm, and J. S. McKenzie
1992b. Intracellular responses of olfactory bulb granule cells to stimulating the horizontal diagonal band nucleus. *Neuroscience*, 48(2):363–369.
- Kvitsiani, D., S. Ranade, B. Hangya, H. Taniguchi, J. Z. Huang, and A. Kepecs
2013. Distinct behavioural and network correlates of two interneuron types in prefrontal cortex. *Nature*, 498(7454):363–366.
- Laaris, N., A. Puche, and M. Ennis
2007. Complementary postsynaptic activity patterns elicited in olfactory bulb by stimulation of mitral/tufted and centrifugal fiber inputs to granule cells. *Journal of neurophysiology*, 97(1):296–306.
- Labarrera, C., M. London, and K. Angelo
2013. Tonic inhibition sets the state of excitability in olfactory bulb granule cells. *The Journal of physiology*, 591(Pt 7):1841–50.
- Lagier, S., A. Carleton, and P.-M. Lledo
2004. Interplay between local GABAergic interneurons and relay neurons generates gamma oscillations in the rat olfactory bulb. *The Journal of neuroscience : the official journal of the Society for Neuroscience*, 24(18):4382–4392.
- Larkum, M. E., J. J. Zhu, and B. Sakmann
2001. Dendritic mechanisms underlying the coupling of the dendritic with

the axonal action potential initiation zone of adult rat layer 5 pyramidal neurons. *Journal of Physiology*, 533(2):447–466.

Laurent, G.

2002. Olfactory network dynamics and the coding of multidimensional signals. *Nature reviews. Neuroscience*, 3(11):884–895.

Laurent, G. and H. Davidowitz

1994. Encoding of olfactory information with oscillating neural assemblies. *Science (New York, N.Y.)*, 265(5180):1872–5.

Lazarini, F., M. A. Mouthon, G. Gheusi, F. de Chaumont, J. C. Olivo-Marin, S. Lamarque, D. N. Abrous, F. D. Boussin, and P. M. Lledo

2009. Cellular and behavioral effects of cranial irradiation of the subventricular zone in adult mice. *PLoS ONE*, 4(9):1–11.

Lecca, S., A. Pelosi, A. Tchenio, I. Moutkine, R. Lujan, D. Hervé, and M. Mameli

2016. Rescue of GABAB and GIRK function in the lateral habenula by protein phosphatase 2A inhibition ameliorates depression-like phenotypes in mice. *Nature medicine*, 22(3).

Lee, A. T., D. Vogt, J. L. Rubenstein, and V. S. Sohal

2014. A class of GABAergic neurons in the prefrontal cortex sends long-range projections to the nucleus accumbens and elicits acute avoidance behavior. *The Journal of neuroscience : the official journal of the Society for Neuroscience*, 34(35):11519–25.

Leitner, F. C., S. Melzer, H. Lütcke, R. Pinna, P. H. Seeburg, F. Helmchen, and H. Monyer

2016. Spatially segregated feedforward and feedback neurons support differential odor processing in the lateral entorhinal cortex. *Nature Neuroscience*, 19(7):935–44.

Lepousez, G. and G. Gheusi

2011. Olfaction: Quand le cortex redistribue les cartes. *Medecine/Sciences*, 27(8-9):687–689.

Lepousez, G. and P.-M. Lledo

2013. Odor discrimination requires proper olfactory fast oscillations in awake mice. *Neuron*, 80(4):1010–24.

Lepousez, G., A. Nissant, A. K. Bryant, G. Gheusi, C. a. Greer, and P.-M. Lledo

2014. Olfactory learning promotes input-specific synaptic plasticity in adult-born neurons. *Proceedings of the National Academy of Sciences*, 111(38):13984–13989.

- Lepousez, G., M. T. Valley, and P.-M. Lledo
2013. The impact of adult neurogenesis on olfactory bulb circuits and computations. *Annual review of physiology*, 75:339–363.
- Letzkus, J. J., S. B. E. Wolff, E. M. M. Meyer, P. Tovote, J. Courtin, C. Herry, and A. Lüthi
2011. A disinhibitory microcircuit for associative fear learning in the auditory cortex. *Nature*, 480(7377):331–335.
- Li, a., D. H. Gire, and D. Restrepo
2015. Spike-Field Coherence in a Population of Olfactory Bulb Neurons Differentiates between Odors Irrespective of Associated Outcome. *Journal of Neuroscience*, 35(14):5808–5822.
- Liang, L., Y. Li, C. J. Potter, O. Yizhar, K. Deisseroth, R. W. Tsien, and L. Luo
2013. Article GABAergic Projection Neurons Route Selective Olfactory Inputs to Specific Higher-Order Neurons. *Neuron*, 79(5):917–931.
- Lin, C. S., M. A. Nicolelis, J. S. Schneider, and J. K. Chapin
1990. A major direct GABAergic pathway from zona incerta to neocortex. *Science*, 248(4962):1553–6.
- Liu, B.-h., P. Li, Y. J. Sun, Y.-t. Li, L. I. Zhang, and H. W. Tao
2010. Intervening inhibition underlies simple-cell receptive field structure in visual cortex. *Nature Neuroscience*, 13(1):89–96.
- Liu, S., J. L. Aungst, a. C. Puche, and M. T. Shipley
2012. Serotonin modulates the population activity profile of olfactory bulb external tufted cells. *Journal of Neurophysiology*, 107(1):473–483.
- Liu, Z., J. Zhou, Y. Li, F. Hu, Y. Lu, M. Ma, Q. Feng, J. en Zhang, D. Wang, J. Zeng, J. Bao, J. Y. Kim, Z. F. Chen, S. ElMestikawy, and M. Luo
2014. Dorsal raphe neurons signal reward through 5-HT and glutamate. *Neuron*, 81(6):1360–1374.
- Livneh, Y., Y. Adam, and A. Mizrahi
2014. Odor processing by adult-born neurons. *Neuron*, 81(5):1097–1110.
- Lois, C. and A. Alvarez-Buylla
1994. Long-distance neuronal migration in the adult mammalian brain. *Science*, 264(5162):1145–1148.
- Lottem, E., M. L. Lörincz, and Z. F. Mainen
2016. Optogenetic Activation of Dorsal Raphe Serotonin Neurons Rapidly Inhibits Spontaneous But Not Odor-Evoked Activity in Olfactory Cortex. *The Journal of neuroscience : the official journal of the Society for Neuroscience*, 36(1):7–18.

- Luskin, M. B. and J. L. Price
1983. The topographic organization of associational fibers of the olfactory system in the rat, including centrifugal fibers to the olfactory bulb. *The Journal of comparative neurology*, 216(3):264–291.
- Ma, M. and M. Luo
2012. Optogenetic activation of basal forebrain cholinergic neurons modulates neuronal excitability and sensory responses in the main olfactory bulb. *The Journal of neuroscience : the official journal of the Society for Neuroscience*, 32(30):10105–16.
- Macrides, F., B. J. Davis, W. M. Youngs, N. S. Nadi, and F. L. Margolis
1981. Cholinergic and catecholaminergic afferents to the olfactory bulb in the hamster: a neuroanatomical, biochemical, and histochemical investigation. *The Journal of comparative neurology*, 203(3):495–514.
- Manabe, H., I. Kusumoto-Yoshida, M. Ota, and K. Mori
2011. Olfactory Cortex Generates Synchronized Top-Down Inputs to the Olfactory Bulb during Slow-Wave Sleep. *Journal of Neuroscience*, 31(22):8123–8133.
- Manabe, H. and K. Mori
2013. Sniff rhythm-paced fast and slow gamma-oscillations in the olfactory bulb: relation to tufted and mitral cells and behavioral states. *Journal of neurophysiology*, 110(7):1593–9.
- Margrie, T. W., B. Sakmann, and N. N. Urban
2001. Action potential propagation in mitral cell lateral dendrites is decremental and controls recurrent and lateral inhibition in the mammalian olfactory bulb. *Proceedings of the National Academy of Sciences of the United States of America*, 98(1):319–24.
- Margrie, T. W. and A. T. Schaefer
2003. Theta oscillation coupled spike latencies yield computational vigour in a mammalian sensory system. *The Journal of Physiology*, 546(2):363–374.
- Marín, O.
2012. Interneuron dysfunction in psychiatric disorders. *Nature reviews. Neuroscience*, 13(2):107–20.
- Marín-Burgin, A., L. a. Mongiat, M. B. Pardi, and A. F. Schinder
2012. Unique processing during a period of high excitation/inhibition balance in adult-born neurons. *Science (New York, N. Y.)*, 335(6073):1238–42.
- Markopoulos, F., D. Rokni, D. H. Gire, and V. N. Murthy
2012. Functional properties of cortical feedback projections to the olfactory bulb. *Neuron*, 76(6):1175–88.

- Martin, C., R. Gervais, B. Messaoudi, and N. Ravel
2006. Learning-induced oscillatory activities correlated to odour recognition: a network activity. *The European journal of neuroscience*, 23(7):1801–10.
- Matsutani, S.
2010. Trajectory and terminal distribution of single centrifugal axons from olfactory cortical areas in the rat olfactory bulb. *Neuroscience*, 169(1):436–448.
- Matsutani, S. and N. Yamamoto
2008. Centrifugal innervation of the mammalian olfactory bulb. *Anatomical Science International*, 83(4):218–227.
- Mazor, O. and G. Laurent
2005. Transient dynamics versus fixed points in odor representations by locust antennal lobe projection neurons. *Neuron*, 48(4):661–673.
- McLean, J. H. and M. T. Shipley
1987. Serotonergic afferents to the rat olfactory bulb: I. Origins and laminar specificity of serotonergic inputs in the adult rat. *The Journal of neuroscience : the official journal of the Society for Neuroscience*, 7(10):3016–3028.
- McLean, J. H., M. T. Shipley, W. T. Nickell, G. Aston-Jones, and C. K. H. Reyher
1989. Chemoanatomical organization of the noradrenergic input from locus coeruleus to the olfactory bulb of the adult rat. *Journal of Comparative Neurology*, 285(3):339–349.
- Melzer, S., M. Michael, A. Caputi, M. Eliava, E. C. Fuchs, M. a. Whittington, and H. Monyer
2012. Long-range-projecting GABAergic neurons modulate inhibition in hippocampus and entorhinal cortex. *Science (New York, N.Y.)*, 335(6075):1506–10.
- Merkle, F. T., L. C. Fuentealba, T. a. Sanders, L. Magno, N. Kessaris, and A. Alvarez-Buylla
2014. Adult neural stem cells in distinct microdomains generate previously unknown interneuron types. *Nature neuroscience*, 17(2):207–214.
- Miyamichi, K., F. Amat, F. Moussavi, C. Wang, I. Wickersham, N. R. Wall, H. Taniguchi, B. Tasic, Z. J. Huang, Z. He, E. M. Callaway, M. A. Horowitz, and L. Luo
2011. Cortical representations of olfactory input by trans-synaptic tracing. *Nature*, 472(7342):191–196.

- Miyamichi, K., Y. Shlomai-Fuchs, M. Shu, B. C. Weissbourd, L. Luo, and A. Mizrahi
2013. Dissecting local circuits: parvalbumin interneurons underlie broad feedback control of olfactory bulb output. *Neuron*, 80(5):1232–45.
- Mombaerts, P.
1996. Targeting olfaction. *Current Opinion in Neurobiology*, 6(4):481–486.
- Morrisett, R. A., D. D. Mott, D. V. Lewis, H. S. Swartzwelder, and W. A. Wilson
1991. GABAB-receptor-mediated inhibition of the N-methyl-D-aspartate component of synaptic transmission in the rat hippocampus. *J. Neurosci.*, 11(January):203–209.
- Mott, D. and D. Lewis
1991. Facilitation of the induction of long-term potentiation by GABAB receptors. *Science*, 252(5013):1718–1720.
- Murphy, G. J., D. P. Darcy, and J. S. Isaacson
2005. Intraglomerular inhibition: signaling mechanisms of an olfactory microcircuit. *Nature neuroscience*, 8(3):354–64.
- Nagayama, S., R. Homma, and F. Imamura
2014. Neuronal organization of olfactory bulb circuits. *Frontiers in neural circuits*, 8(September):98.
- Nagayama, S., Y. K. Takahashi, Y. Yoshihara, and K. Mori
2004. Mitral and tufted cells differ in the decoding manner of odor maps in the rat olfactory bulb. *Journal of neurophysiology*, 91(6):2532–2540.
- Nai, Q., H. Dong, C. Linster, and M. Ennis
2010. Activation of $\alpha 1$ and $\alpha 2$ noradrenergic receptors exert opposing effects on excitability of main olfactory bulb granule cells. *Neuroscience*, 169(2):882–892.
- Nai, Q., H.-W. Dong, A. Hayar, C. Linster, and M. Ennis
2009. Noradrenergic Regulation of GABAergic Inhibition of Main Olfactory Bulb Mitral Cells Varies as a Function of Concentration and Receptor Subtype. *J Neurophysiol*, 101:2472–2484.
- Najac, M., A. Sanz Diez, A. Kumar, N. Benito, S. Charpak, and D. De Saint Jan
2015. Intraglomerular lateral inhibition promotes spike timing variability in principal neurons of the olfactory bulb. *Journal of neuroscience*, 35(10):4319–31.

- Neville, K. R. and L. B. Haberly
2003. Beta and gamma oscillations in the olfactory system of the urethane-anesthetized rat. *Journal of neurophysiology*, 90(6):3921–30.
- Nicholas, A. P., V. Pieribone, and T. Hökfelt
1993a. Distributions of mRNAs for alpha-2 adrenergic receptor subtypes in rat brain: An in situ hybridization study. *Journal of Comparative Neurology*, 328(4):575–594.
- Nicholas, a. P., V. a. Pieribone, and T. Hokfelt
1993b. Cellular localization of messenger RNA for beta-1 and beta-2 adrenergic receptors in rat brain: An in situ hybridization study. *Neuroscience*, 56(4):1023–1039.
- Nissant, A., C. Bardy, H. Katagiri, K. Murray, and P.-M. Lledo
2009. Adult neurogenesis promotes synaptic plasticity in the olfactory bulb. *Nature neuroscience*, 12(6):728–30.
- Nunes, D. and T. Kuner
2015. Disinhibition of olfactory bulb granule cells accelerates odour discrimination in mice. *Nature Communications*, 6:8950.
- Nunez-Parra, A., R. K. Maurer, K. Krahe, R. S. Smith, and R. C. Araneda
2013. Disruption of centrifugal inhibition to olfactory bulb granule cells impairs olfactory discrimination. *Proceedings of the National Academy of Sciences of the United States of America*, 2013:1–3.
- Nusser, Z., L. M. Kay, G. Laurent, I. Mody, and G. E. Homanics
2001. Disruption of GABA(A) receptors on GABAergic interneurons leads to increased oscillatory power in the olfactory bulb network. *Journal of Neurophysiology*, 86(6):2823–2833.
- Oettl, L. L., N. Ravi, M. Schneider, M. F. Scheller, P. Schneider, M. Mitre, M. da Silva Gouveia, R. C. Froemke, M. V. Chao, W. S. Young, A. Meyer-Lindenberg, V. Grinevich, R. Shusterman, and W. Kelsch
2016. Oxytocin Enhances Social Recognition by Modulating Cortical Control of Early Olfactory Processing. *Neuron*, 90(3):609–621.
- Oláh, S., M. Füle, G. Komlósi, C. Varga, R. Báldi, P. Barzó, and G. Tamás
2009. Regulation of cortical microcircuits by unitary GABA-mediated volume transmission. *Nature*, 461(7268):1278–81.
- Orona, E., E. C. Rainer, and J. W. Scott
1984. Dendritic and axonal organization of mitral and tufted cells in the rat olfactory bulb. *Journal of Comparative Neurology*, 226(3):346–356.

- Oswald, A.-m. M., B. Doiron, J. Rinzel, and A. D. Reyes
2009. Spatial profile and differential recruitment of GABAB modulate oscillatory activity in auditory cortex. *The Journal of neuroscience : the official journal of the Society for Neuroscience*, 29(33):10321–34.
- Otazu, G., H. Chae, M. Davis, and D. Albeanu
2015. Cortical Feedback Decorrelates Olfactory Bulb Output in Awake Mice. *Neuron*, Pp. 1–17.
- Padmanabhan, K., F. Osakada, A. Tarabrina, E. Kizer, E. M. Callaway, F. H. Gage, and T. J. Sejnowski
2016. Diverse Representations of Olfactory Information in Centrifugal Feedback Projections. *The Journal of neuroscience : the official journal of the Society for Neuroscience*, 36(28):7535–45.
- Pager, J.
1983. Unit responses changing with behavioral outcome in the olfactory bulb of unrestrained rats. *Brain Research*, 289(1-2):87–98.
- Palmer, L. M., J. M. Schulz, S. C. Murphy, D. Ledergerber, M. Murayama, and M. E. Larkum
2012. Interhemispheric Inhibition. *Science*, 335(February):989–993.
- Pan, B. X., Y. Dong, W. Ito, Y. Yanagawa, R. Shigemoto, and A. Morozov
2009. Selective Gating of Glutamatergic Inputs to Excitatory Neurons of Amygdala by Presynaptic GABA_B Receptor. *Neuron*, 61(6):917–929.
- Parnas, M., A. Lin, W. Huetteroth, and G. Miesenböck
2013. Odor Discrimination in *Drosophila*: From Neural Population Codes to Behavior. *Neuron*, 79(5):932–944.
- Pérez-Garci, E., M. Gassmann, B. Bettler, and M. E. Larkum
2006. The GABAB1b Isoform Mediates Long-Lasting Inhibition of Dendritic Ca²⁺ Spikes in Layer 5 Somatosensory Pyramidal Neurons. *Neuron*, 50(4):603–616.
- Pérez-Garci, E., M. E. Larkum, and T. Nevian
2013. Inhibition of dendritic Ca²⁺ spikes by GABAB receptors in cortical pyramidal neurons is mediated by a direct Gi/o- β -subunit interaction with Cav1 channels. *The Journal of physiology*, 591(Pt 7):1599–612.
- Perez-Orive, J., O. Mazor, G. C. Turner, S. Cassenaer, R. I. Wilson, and G. Laurent
2002. Oscillations and sparsening of odor representations in the mushroom body. *Science (New York, N.Y.)*, 297(5580):359–365.

- Petreaanu, L., D. Huber, A. Sobczyk, and K. Svoboda
2007. Channelrhodopsin-2-assisted circuit mapping of long-range callosal projections. *Nature neuroscience*, 10(5):663–8.
- Pettersen, K. H., A. M. Dale, G. T. Einevoll, and H. Lindén
2011. Extracellular spikes and CSD. *Handbook of Neural Activity Measurement*, (April):92–135.
- Petzold, G. C., A. Hagiwara, and V. N. Murthy
2009. Serotonergic modulation of odor input to the mammalian olfactory bulb. *Nature neuroscience*, 12(6):784–91.
- Phillips, M. E., R. N. S. Sachdev, D. C. Willhite, and G. M. Shepherd
2012. Respiration Drives Network Activity and Modulates Synaptic and Circuit Processing of Lateral Inhibition in the Olfactory Bulb. *Journal of Neuroscience*, 32(1):85–98.
- Pi, H.-J., B. Hangya, D. Kvitsiani, J. I. Sanders, Z. J. Huang, and A. Kepecs
2013. Cortical interneurons that specialize in disinhibitory control. *Nature*, 503(7477):521–4.
- Picardo, M. A., P. Guigue, P. Bonifazi, R. Batista-Brito, C. Allene, A. Ribas, G. Fishell, A. Baude, and R. Cossart
2011. Pioneer GABA cells comprise a subpopulation of hub neurons in the developing hippocampus. *Neuron*, 71(4):695–709.
- Pignatelli, A. and O. Belluzzi
2008. Cholinergic modulation of dopaminergic neurons in the mouse olfactory bulb. *Chemical Senses*, 33(4):331–338.
- Pimentel, D. O. and T. W. Margrie
2008. Glutamatergic transmission and plasticity between olfactory bulb mitral cells. *The Journal of physiology*, 586(8):2107–19.
- Pin, J.-P. and B. Bettler
2016. Organization and functions of mGlu and GABAB receptor complexes. *Nature*, 540(7631):60–68.
- Pinard, A., R. Seddik, and B. Bettler
2010. GABAB receptors. Physiological functions and mechanisms of diversity. *Advances in Pharmacology*, 58(C):231–255.
- Pinching, a. J. and T. P. Powell
1971a. The neuron types of the glomerular layer of the olfactory bulb. *Journal of cell science*, 9(2):305–345.
- Pinching, A. J. and T. P. Powell
1971b. The neuropil of the periglomerular region of the olfactory bulb. *Journal of cell science*, 9(2):379–409.

- Poo, C. and J. S. Isaacson
2009. Odor representations in olfactory cortex: "sparse" coding, global inhibition, and oscillations. *Neuron*, 62(6):850–61.
- Poo, C. and J. S. Isaacson
2011. A Major Role for Intracortical Circuits in the Strength and Tuning of Odor-Evoked Excitation in Olfactory Cortex. *Neuron*, 72(1):41–48.
- Pouille, F., A. Marin-Burgin, H. Adesnik, B. V. Atallah, and M. Scanziani
2009. Input normalization by global feedforward inhibition expands cortical dynamic range. *Nature neuroscience*, 12(12):1577–85.
- Pouille, F. and M. Scanziani
2001. Enforcement of temporal fidelity in pyramidal cells by somatic feedforward inhibition. *Science (New York, N. Y.)*, 293(5532):1159–63.
- Pressler, R. T., T. Inoue, and B. W. Strowbridge
2007. Muscarinic receptor activation modulates granule cell excitability and potentiates inhibition onto mitral cells in the rat olfactory bulb. *Journal of Neuroscience*, 27(41):10969–10981.
- Pressler, R. T., P. a. Rozman, and B. W. Strowbridge
2013. Voltage-dependent intrinsic bursting in olfactory bulb Golgi cells. *Learning & memory*, 20:459–466.
- Pressler, R. T. and B. W. Strowbridge
2006. Blanes cells mediate persistent feedforward inhibition onto granule cells in the olfactory bulb. *Neuron*, 49(6):889–904.
- Price, C. J., R. Scott, D. A. Rusakov, and M. Capogna
2008. {GABAB} Receptor Modulation of Feedforward Inhibition through Hippocampal Neurogliaform Cells. *The Journal of Neuroscience*, 28(27):6974–6982.
- Price, J. L. and T. P. Powell
1970a. The synaptology of the granule cells of the olfactory bulb. *Journal of cell science*, 7(1):125–155.
- Price, J. L. and T. P. S. Powell
1970b. The Mitral and Short Axon Cells of the Olfactory Bulb. *Journal of Cell Science*, 7(3):631–651.
- Quraish, A. U., J. Yang, K. Murakami, S. Oda, M. Takayanagi, A. Kimura, S. Kakuta, and K. Kishi
2004. Quantitative analysis of axon collaterals of single superficial pyramidal cells in layer IIb of the piriform cortex of the guinea pig. *Brain Research*, 1026(1):84–94.

- Raimondo, J. V., H. Markram, and C. J. Akerman
2012. Short-term ionic plasticity at GABAergic synapses. *Frontiers in Synaptic Neuroscience*, 4(OCT):1–9.
- Rall, W. and G. M. Shepherd
1968. Theoretical reconstruction of field potentials and dendrodendritic synaptic interactions in olfactory bulb. *Journal of neurophysiology*, 31(6):884–915.
- Rennaker, R. L., C.-F. F. Chen, A. M. Ruyle, A. M. Sloan, and D. a. Wilson
2007. Spatial and temporal distribution of odorant-evoked activity in the piriform cortex. *The Journal of neuroscience : the official journal of the Society for Neuroscience*, 27(7):1534–1542.
- Resulaj, A. and D. Rinberg
2015. Novel Behavioral Paradigm Reveals Lower Temporal Limits on Mouse Olfactory Decisions. *Journal of Neuroscience*, 35(33):11667–11673.
- Rinberg, D. and A. Gelperin
2006. Olfactory neuronal dynamics in behaving animals. *Seminars in cell & developmental biology*, 17(4):454–461.
- Rinberg, D., A. Koulakov, and A. Gelperin
2006. Sparse odor coding in awake behaving mice. *The Journal of neuroscience : the official journal of the Society for Neuroscience*, 26(34):8857–8865.
- Rokni, D., V. Hemmelder, V. Kapoor, and V. N. Murthy
2014. An olfactory cocktail party: figure-ground segregation of odorants in rodents. *Nature neuroscience*, 17(9):1225–32.
- Root, C. M., C. a. Denny, R. Hen, and R. Axel
2014a. The participation of cortical amygdala in innate, odour-driven behaviour. *Nature*, (V).
- Root, D. H., C. a. Mejias-Aponte, S. Zhang, H. L. Wang, a. F. Hoffman, C. R. Lupica, and M. Morales
2014b. Single rodent mesohabenular axons release glutamate and GABA. *Nature neuroscience*, 17(11):1543–1551.
- Rost, B. R., P. Nicholson, G. Ahnert-Hilger, A. Rummel, C. Rosenmund, J. Breustedt, and D. Schmitz
2011. Activation of metabotropic GABA receptors increases the energy barrier for vesicle fusion. *Journal of cell science*, 124(Pt 18):3066–3073.
- Roth, B. L.
2016. DREADDs for Neuroscientists. *Neuron*, 89(4):683–694.

- Rothermel, M., R. M. Carey, A. Puche, M. T. Shipley, and M. Wachowiak
2014. Cholinergic inputs from Basal forebrain add an excitatory bias to odor coding in the olfactory bulb. *The Journal of neuroscience : the official journal of the Society for Neuroscience*, 34(13):4654–4664.
- Rothermel, M. and M. Wachowiak
2014. Functional imaging of cortical feedback projections to the olfactory bulb. *Frontiers in Neural Circuits*, 8(July):1–14.
- Roux, L. and G. Buzsáki
2015. Tasks for inhibitory interneurons in intact brain circuits. *Neuropharmacology*, 88:10–23.
- Roux, L., E. Stark, L. Sjulson, and G. Buzsáki
2014. In vivo optogenetic identification and manipulation of GABAergic interneuron subtypes.
- Royer, S., B. V. Zemelman, A. Losonczy, J. Kim, F. Chance, J. C. Magee, and G. Buzsáki
2012. Control of timing, rate and bursts of hippocampal place cells by dendritic and somatic inhibition. *Nature neuroscience*, 15(5):769–75.
- Sachidhanandam, S., B. S. Sermet, and C. C. H. Petersen
2016. Parvalbumin-Expressing GABAergic Neurons in Mouse Barrel Cortex Contribute to Gating a Goal-Directed Sensorimotor Transformation. *Cell Reports*, 15(4):700–706.
- Sailor, K. A., M. T. Valley, M. T. Wiechert, H. Riecke, G. J. Sun, W. Adams, J. C. Dennis, S. Sharafi, G. li Ming, H. Song, and P. M. Lledo
2016. Persistent Structural Plasticity Optimizes Sensory Information Processing in the Olfactory Bulb. *Neuron*, 91(2):384–396.
- Salin, P. a., P. M. Lledo, J. D. Vincent, and S. Charpak
2001. Dendritic glutamate autoreceptors modulate signal processing in rat mitral cells. *Journal of neurophysiology*, 85(3):1275–1282.
- Scanziani, M.
2000. GABA Spillover Activates Postsynaptic GABAB Receptors to Control Rhythmic Hippocampal Activity. *Neuron*, 25(3):673–681.
- Schaefer, A. T., K. Angelo, H. Spors, and T. W. Margrie
2006. Neuronal oscillations enhance stimulus discrimination by ensuring action potential precision. *PLoS biology*, 4(6):e163.
- Schmidt, L. J. and B. W. Strowbridge
2014. Modulation of olfactory bulb network activity by serotonin: synchronous inhibition of mitral cells mediated by spatially localized GABAergic microcircuits. *Learning & Memory*, 21(8):406–416.

- Schoppa, N. E. and N. N. Urban
2003. Dendritic processing within olfactory bulb circuits. *Trends in Neurosciences*, 26(9):501–506.
- Schoppa, N. E. and G. L. Westbrook
2001. Glomerulus-specific synchronization of mitral cells in the olfactory bulb. *Neuron*, 31(4):639–651.
- Schoppa, N. E. and G. L. Westbrook
2002. AMPA autoreceptors drive correlated spiking in olfactory bulb glomeruli. *Nature neuroscience*, 5(11):1194–1202.
- Schwarz, L. A., K. Miyamichi, X. J. Gao, K. T. Beier, B. Weissbourd, K. E. DeLoach, J. Ren, S. Ibanes, R. C. Malenka, E. J. Kremer, and L. Luo
2015. Viral-genetic tracing of the input-output organization of a central noradrenergic circuit. *Nature*, 524(7563):88–92.
- Schwenk, J., A. Schneider, A. Kollwe, A. Gauthier-Kemper, T. Fritzius, A. Raveh, M. C. Dinamarca, A. Hanuschkin, W. Bildl, R. Klingauf, M. Gassmann, U. Schulte, B. Bettler, and B. Fakler
2015. Modular composition and dynamics of native GABAB receptors identified by high-resolution proteomics. *Nature Neuroscience*, 19(2):233–242.
- Scimemi, A.
2014. Structure, function, and plasticity of GABA transporters. *Frontiers in Cellular Neuroscience*, 8(June):161.
- Shea, S. D., L. C. Katz, and R. Mooney
2008. Noradrenergic induction of odor-specific neural habituation and olfactory memories. *The Journal of neuroscience : the official journal of the Society for Neuroscience*, 28(42):10711–10719.
- Shepherd GM, Chen WR, G.
2004. *Olfactory bulb. In: The synaptic organization of the brain.* Oxford University Press.
- Shipley, M. T. and G. D. Adamek
1984. The connections of the mouse olfactory bulb: A study using orthograde and retrograde transport of wheat germ agglutinin conjugated to horseradish peroxidase. *Brain Research Bulletin*, 12(6):669–688.
- Shipley, M. T., F. J. Halloran, and J. de la Torre
1985. Surprisingly rich projection from locus coeruleus to the olfactory bulb in the rat. *Brain research*, 329(1-2):294–299.

- Shusterman, R., M. C. Smear, A. a. Koulakov, and D. Rinberg
2011. Precise olfactory responses tile the sniff cycle. *Nature neuroscience*, 14(8):1039–44.
- Smear, M., A. Resulaj, J. Zhang, T. Bozza, and D. Rinberg
2013. Multiple perceptible signals from a single olfactory glomerulus. *Nature neuroscience*, 16(11):1687–91.
- Smear, M., R. Shusterman, R. O’Connor, T. Bozza, and D. Rinberg
2011. Perception of sniff phase in mouse olfaction. *Nature*, 479(7373):397–400.
- Soria-Gómez, E., L. Bellocchio, L. Reguero, G. Lepousez, C. Martin, M. Bendahmane, S. Ruehle, F. Remmers, T. Desprez, I. Matias, T. Wiesner, A. Cannich, A. Nissant, A. Wadleigh, H.-C. Pape, A. P. Chiarlone, C. Quarta, D. Verrier, P. Vincent, F. Massa, B. Lutz, M. Guzmán, H. Gurdén, G. Ferreira, P.-M. Lledo, P. Grandes, and G. Marsicano
2014. The endocannabinoid system controls food intake via olfactory processes. *Nature neuroscience*, 17(3):407–15.
- Sosulski, D. L., M. L. Bloom, T. Cutforth, R. Axel, and S. R. Datta
2011. Distinct representations of olfactory information in different cortical centres. *Nature*, 472(7342):213–6.
- Soucy, E. R., D. F. Albeanu, A. L. Fantana, V. N. Murthy, and M. Meister
2009. Precision and diversity in an odor map on the olfactory bulb. *Nature neuroscience*, 12(2):210–20.
- Steinfeld, R., J. T. Herb, R. Sprengel, A. T. Schaefer, and I. Fukunaga
2015. Divergent innervation of the olfactory bulb by distinct raphe nuclei. *The Journal of comparative neurology*, 523(5):805–13.
- Stettler, D. D. and R. Axel
2009. Representations of Odor in the Piriform Cortex. *Neuron*, 63(6):854–864.
- Stokes, C. C. and J. S. Isaacson
2010. From Dendrite to Soma: Dynamic Routing of Inhibition by Complementary Interneuron Microcircuits in Olfactory Cortex. *Neuron*, 67(3):452–465.
- Stopfer, M., V. Jayaraman, and G. Laurent
2003. Intensity versus identity coding in an olfactory system. *Neuron*, 39(6):991–1004.
- Sturgill, J. F. and J. S. Isaacson
2015. Somatostatin cells regulate sensory response fidelity via subtractive inhibition in olfactory cortex. *Nature neuroscience*, (November 2014):1–7.

- Succol, F., H. Fiumelli, F. Benfenati, L. Cancedda, and A. Barberis
2012. Intracellular chloride concentration influences the GABAA receptor subunit composition. *Nature Communications*, 3:738.
- Sultan, S., N. Mandairon, F. Kermen, S. Garcia, J. Sacquet, and a. Didier
2010. Learning-dependent neurogenesis in the olfactory bulb determines long-term olfactory memory. *The FASEB journal : official publication of the Federation of American Societies for Experimental Biology*, 24(7):2355–2363.
- Suzuki, N. and J. M. Bekkers
2006. Neural Coding by Two Classes of Principal Cells in the Mouse Piriform Cortex. *The Journal of Neuroscience*, 26(46):11938–11947.
- Suzuki, N. and J. M. Bekkers
2010. Inhibitory neurons in the anterior piriform cortex of the mouse: classification using molecular markers. *The Journal of comparative neurology*, 518(10):1670–1687.
- Suzuki, N. and J. M. Bekkers
2011. Two layers of synaptic processing by principal neurons in piriform cortex. *The Journal of neuroscience : the official journal of the Society for Neuroscience*, 31(6):2156–66.
- Suzuki, N. and J. M. Bekkers
2012. Microcircuits Mediating Feedforward and Feedback Synaptic Inhibition in the Piriform Cortex. *Journal of Neuroscience*, 32(3):919–931.
- Suzuki, Y., E. Kiyokage, J. Sohn, H. Hioki, and K. Toida
2015. Structural basis for serotonergic regulation of neural circuits in the mouse olfactory bulb. *Journal of Comparative Neurology*, 523(2):262–280.
- Takács, V. T., T. F. Freund, and A. I. Gulyás
2008. Types and synaptic connections of hippocampal inhibitory neurons reciprocally connected with the medial septum. *European Journal of Neuroscience*, 28(1):148–164.
- Tamamaki, N. and R. Tomioka
2010. Long-range GABAergic connections distributed throughout the neocortex and their possible function. *Frontiers in Neuroscience*, 4(Article 202):1–8.
- Tamas, G.
2003. Identified Sources and Targets of Slow Inhibition in the Neocortex. *Science*, 299(5614):1902–1905.

- Terunuma, M., R. Revilla-Sanchez, I. M. Quadros, Q. Deng, T. Z. Deeb, M. Lumb, P. Sicinski, P. G. Haydon, M. N. Pangalos, and S. J. Moss
2014. Postsynaptic GABAB receptor activity regulates excitatory neuronal architecture and spatial memory. *The Journal of neuroscience : the official journal of the Society for Neuroscience*, 34(3):804–16.
- Tomioka, R., K. Okamoto, T. Furuta, F. Fujiyama, T. Iwasato, Y. Yanagawa, K. Obata, T. Kaneko, and N. Tamamaki
2005. Demonstration of long-range GABAergic connections distributed throughout the mouse neocortex. *European Journal of Neuroscience*, 21(6):1587–1600.
- Tomioka, R., K. Sakimura, and Y. Yanagawa
2015. Corticofugal GABAergic projection neurons in the mouse frontal cortex. *Frontiers in neuroanatomy*, 9(October):133.
- Tóth, K., T. F. Freund, and R. Miles
1997. Disinhibition of rat hippocampal pyramidal cells by GABAergic afferents from the septum. *The Journal of Physiology*, 500(2):463–74.
- Tovote, P., M. S. Esposito, P. Botta, F. Chaudun, J. P. Fadok, M. Markovic, S. B. E. Wolff, C. Ramakrishnan, L. Fenno, K. Deisseroth, C. Herry, S. Arber, and A. Luthi
2016. Midbrain circuits for defensive behaviour. *Nature*, 534(7606):206–212.
- Tremblay, R., S. Lee, and B. Rudy
2016. GABAergic Interneurons in the Neocortex: From Cellular Properties to Circuits. *Neuron*, 91(2):260–292.
- Tsuno, Y., H. Kashiwadani, and K. Mori
2008. Behavioral state regulation of dendrodendritic synaptic inhibition in the olfactory bulb. *The Journal of neuroscience : the official journal of the Society for Neuroscience*, 28(37):9227–38.
- Uchida, N., N. Eshel, and M. Watabe-Uchida
2013a. Division of labor for division: Inhibitory interneurons with different spatial landscapes in the olfactory system. *Neuron*, 80(5):1106–1109.
- Uchida, N. and Z. F. Mainen
2003. Speed and accuracy of olfactory discrimination in the rat. *Nature neuroscience*, 6(11):1224–1229.
- Uchida, N., C. Poo, and R. Haddad
2013b. Coding and Transformations in the Olfactory System. *Annual review of neuroscience*, (May):363–385.

- Urban, N. N. and B. Sakmann
2002. Reciprocal intraglomerular excitation and intra- and interglomerular lateral inhibition between mouse olfactory bulb mitral cells. *The Journal of physiology*, 542(2):355–367.
- Vaaga, C. E., J. T. Yorgason, J. T. Williams, and G. L. Westbrook
2017. Presynaptic gain control by endogenous cotransmission of dopamine and GABA in the olfactory bulb. *Journal of neurophysiology*, 117(3):1163–1170.
- Valley, M. T., L. G. Henderson, S. a. Inverso, and P.-M. Lledo
2013. Adult neurogenesis produces neurons with unique GABAergic synapses in the olfactory bulb. *The Journal of neuroscience : the official journal of the Society for Neuroscience*, 33(37):14660–5.
- van den Pol, A. N.
2012. Neuropeptide Transmission in Brain Circuits. *Neuron*, 76(1):98–115.
- Vigot, R., S. Barbieri, H. Bräuner-Osborne, R. Turecek, R. Shigemoto, Y. P. Zhang, R. Luján, L. H. Jacobson, B. Biermann, J. M. Fritschy, C. M. Vacher, M. Müller, G. Sansig, N. Guetg, J. F. Cryan, K. Kaupmann, M. Gassmann, T. G. Oertner, and B. Bettler
2006. Differential Compartmentalization and Distinct Functions of GABAB Receptor Variants. *Neuron*, 50(4):589–601.
- Vincent, S. R., T. Hökfelt, L. R. Skirboll, and J. Y. Wu
1983. Hypothalamic gamma-aminobutyric acid neurons project to the neocortex. *Science (New York, N.Y.)*, 220(4603):1309–11.
- Vincis, R., S. Lagier, D. Van De Ville, I. Rodriguez, and A. Carleton
2015. Sensory-Evoked Intrinsic Imaging Signals in the Olfactory Bulb Are Independent of Neurovascular Coupling. *Cell Reports*, 12(2):313–325.
- Vogel, E., S. Krabbe, J. Gründelmann, J. I. Cusulin Wamstecker, E. Vogel, and A. Lüthi
2016. Projection-Specific Dynamic Regulation of Inhibition Article Projection-Specific Dynamic Regulation of Inhibition in Amygdala Micro-Circuits. *Neuron*, Pp. 644–651.
- Vong, L., C. Ye, Z. Yang, B. Choi, S. Chua, and B. B. Lowell
2011. Leptin Action on GABAergic Neurons Prevents Obesity and Reduces Inhibitory Tone to POMC Neurons. *Neuron*, 71(1):142–154.
- Wachowiak, M., M. N. Economo, M. Díaz-Quesada, D. Brunert, D. W. Wesson, J. a. White, and M. Rothermel
2013. Optical dissection of odor information processing in vivo using

- GCaMPs expressed in specified cell types of the olfactory bulb. *The Journal of neuroscience : the official journal of the Society for Neuroscience*, 33(12):5285–300.
- Wehr, M. S. and A. M. Zador
2003. Balanced inhibition underlies tuning and sharpens spike timing in auditory cortex. *Nature*, 426(6965):442–6.
- Wesson, D. W., R. M. Carey, J. V. Verhagen, and M. Wachowiak
2008a. Rapid encoding and perception of novel odors in the rat. *PLoS Biology*, 6(4):717–729.
- Wesson, D. W., J. V. Verhagen, and M. Wachowiak
2008b. Why Sniff Fast? The Relationship Between Sniff Frequency, Odor Discrimination, and Receptor Neuron Activation in the Rat. *Journal of Neurophysiology*, 101(2):1089–1102.
- Wiegand, H. F., P. Beed, M. H. K. Bendels, C. Leibold, D. Schmitz, and F. W. Jochenning
2011. Complementary Sensory and Associative Microcircuitry in Primary Olfactory Cortex. *Journal of Neuroscience*, 31(34):12149–12158.
- Wienisch, M. and V. N. Murthy
2016. Population imaging at subcellular resolution supports specific and local inhibition by granule cells in the olfactory bulb. *Scientific Reports*, 6:29308.
- Wilent, W. B. and D. Contreras
2004. Synaptic responses to whisker deflections in rat barrel cortex as a function of cortical layer and stimulus intensity. *J Neurosci*, 24(16):3985–3998.
- Wilent, W. B. and D. Contreras
2005. Dynamics of excitation and inhibition underlying stimulus selectivity in rat somatosensory cortex. *Nature Neuroscience*, 8(10):1364–70.
- Wilson, D. a.
1998. Habituation of odor responses in the rat anterior piriform cortex. *Journal of neurophysiology*, 79(3):1425–1440.
- Wilson, D. A. and R. M. Sullivan
2011. Cortical Processing of Odor Objects. *Neuron*, 72(4):506–519.
- Wilson, M. A. and B. L. McNaughton
1993. Dynamics of the hippocampal ensemble code for space. *Science*, 261(5124):1055–1058.

- Wilson, N. R., C. A. Runyan, F. L. Wang, and M. Sur
2012. Division and subtraction by distinct cortical inhibitory networks in vivo. *Nature*, 488(7411):343–348.
- Woo, C. C. and M. Leon
1995. Distribution and development of beta-adrenergic receptors in the rat olfactory bulb. *The Journal of comparative neurology*, 352(1):1–10.
- Woodin, M. A., K. Ganguly, and M. ming Poo
2003. Coincident pre- and postsynaptic activity modifies GABAergic synapses by postsynaptic changes in Cl⁻ transporter activity. *Neuron*, 39(5):807–820.
- Xue, M., B. V. Atallah, and M. Scanziani
2014. Equalizing excitation-inhibition ratios across visual cortical neurons. *Nature*, 511(7511):596–600.
- Yamada, Y., K. Bhaukaurally, T. J. Madarász, A. Pouget, I. Rodriguez, and A. Carleton
2017. Context- and Output Layer-Dependent Long-Term Ensemble Plasticity in a Sensory Circuit. *Neuron*, Pp. 1–15.
- Yang, J., A. ul Quraish, K. Murakami, Y. Ishikawa, M. Takayanagi, S. Kakuta, and K. Kishi
2004. Quantitative Analysis of Axon Collaterals of Single Neurons in Layer IIa of the Piriform Cortex of the Guinea Pig. *The Journal of comparative neurology*, 42(December 2003):30–42.
- Youngstrom, I. a. and B. W. Strowbridge
2015. Respiratory Modulation of Spontaneous Subthreshold Synaptic Activity in Olfactory Bulb Granule Cells Recorded in Awake, Head-Fixed Mice. *Journal of Neuroscience*, 35(23):8758–8767.
- Younts, T. J. and P. E. Castillo
2014. Endogenous cannabinoid signaling at inhibitory interneurons. *Current Opinion in Neurobiology*, 26:42–50.
- Younts, T. J., H. R. Monday, B. Dudok, M. E. Klein, B. A. Jordan, I. Katona, and P. E. Castillo
2016. Presynaptic Protein Synthesis Is Required for Long-Term Plasticity of GABA Release. *Neuron*, 92(2):479–492.
- Zaborszky, L., J. Carlsen, H. R. Brashear, and L. Heimer
1986. Cholinergic and Gabaergic Afferents to the Olfactory-Bulb in the Rat with Special Emphasis on the Projection Neurons in the Nucleus of the Horizontal Limb of the Diagonal Band. *Journal of Comparative Neurology*, 243(4):488–509.

- Zacchi, P., R. Antonelli, and E. Cherubini
2014. Gephyrin phosphorylation in the functional organization and plasticity of GABAergic synapses. *Frontiers in cellular neuroscience*, 8(April):103.
- Zhang, S., M. Xu, T. Kamigaki, J. P. Hoang Do, W.-C. Chang, S. Jenvay, K. Miyamichi, L. Luo, and Y. Dan
2014. Long-range and local circuits for top-down modulation of visual cortex processing. *Science*, 345(6197):660–665.
- Zhang, X. and S. Firestein
2002. The olfactory receptor gene superfamily of the mouse. *Nature neuroscience*, 5(2):124–133.
- Zhaoping, L.
2016. Olfactory object recognition, segmentation, adaptation, target seeking, and discrimination by the network of the olfactory bulb and cortex: Computational model and experimental data. *Current Opinion in Behavioral Sciences*, 11:30–39.
- Zhou, F.-W., H.-W. Dong, and M. Ennis
2016. Activation of β -noradrenergic receptors enhances rhythmic bursting in mouse olfactory bulb external tufted cells. *Journal of Neurophysiology*, 116(6):2604–2614.

Appendices

Appendix A

Genetic tools to label, monitor and manipulate cell-type specific activity

Advances in genetics and associated technologies have greatly contributed to the exponential increase of publications in modern Neuroscience. Indeed, restricted expression and manipulation of proteins is instrumental for deciphering neuronal coding and functions. Conditional expression of genetically encoded proteins – whose fluorescence is activity-dependent or whose activity is light or drug-sensitive – permit monitoring and manipulating neuronal activity in intact brain circuits. Pharmacology and endogenous neuronal activity can also be used to restrict the expression of genetically encoded proteins. For an excellent, up-to-date review on this issue, see Kim et al. (2017).

Among genes of interest, extensive use is made of the Ca^{2+} activity reporter GCaMPs and opto- and pharmacogenetic proteins. GCaMP are Ca^{2+} binding proteins whose fluorescence intensity increases with Ca^{2+} concentration. GCaMP imaging permit investigating how labeled neurons are recruited during a determined stimulus. Combined with two-photon imaging, it allows large-scale imaging with single cell or axon resolution. However, optical access limits monitoring to superficial layer. In contrast, fiber photometry permits imaging of Ca^{2+} transients in deep brain regions. Indeed, fluorescence light is collected through an optical fiber, which can be implanted in the brain. However, spatial resolution is lost and fluorescence of the whole population is collected. GCaMP slow kinetics precludes investigation of fast neuronal activity. Voltage indicators are developed to overcome this issue, but for now their signal-to-noise ratio remains too low. Optogenetic tools are light-sensitive channels genetically engineered from bacterian or archean opsins (Deisseroth, 2011). Channelrhodopsin (ChR) and ChR2 are light-activated cation selective channels that induce cell depolarization upon activation. Halorhodopsin and ArCh are pumps inducing hyperpolarization

of the cell. Controlling neuronal activity allow functional connectivity, or synaptic physiology properties investigation. It can also reveal causal relationship between neuronal activity and behavior. However, optical control of a cell population can lead to oversynchrony of cells, recruitment of non-physiologic cell assemblies, or at non-physiological frequencies and thus give rise to function that are not supported by a given circuit in natural conditions. Pharmacogenetic tools are genetically encoded receptors activated by drugs. Derived human muscarinic (metabotropic) receptors activated by a biologically inert ligand are now widely use to manipulate neuronal activity. These technology has been named DREAD (designer receptors exclusively activated by designer drugs) and can both activate (hM3D, couple to a Gs protein) on inhibit (hM4D, coupled to Gi proteins) the cell through activation by a clozapine derivative (clozapine-N-oxyde, CNO; Roth, 2016). Rather than controlling activity, pharmacogenetics tools alter the excitability of the cells, and thus presumably preserves better the natural activity dynamics (but the question of cell population recruitment holds true). In contrast, pharmacological activation lack precise temporal resolution and permit long lasting manipulation of activity, well suited for behavioral investigation. Although ligand can be injected locally in the brain, diffusion and kinetics of activation of the molecule is not well controlled.

Injection of viruses encoding these proteins in wild-type animals allow direct labeling, monitoring or manipulating of neuronal activity. Virus-mediated expression of the gene of interest is spatially restricted by the injection site and volume (and thus diffusion). Virus themselves have different tropism (due to the protein expressed at the envelope) and therefore often bias expression to different cell populations. Cell-type preference can be further achieved by the promoter of the gene of interest (such as CaMKIIa, preferentially expressed in glutamatergic cells in the cortex or the somatostatin promoter). More powerfull cell-type specificity is achieved with the use of conditional genetics. Cre recombinase is a protein from bacteriophages that selectively acts on recognition (LoxP) sites to allow either genetic expression ("flex" gene, or DIO sequence) or deletion ("flox" genes). Transgenic animals have been obtained to express Cre under a variety of promoters, and among them those regulating the expression of GABAergic markers such as SOM, PV or VIP. Injection of virus containing the Cre-dependent gene of interest permit restrained expression of that gene to the virus injection site. This strategy is the more widely used but conversely, one can inject a Cre expression virus in mice floxed for a given gene of interest.

Because neurons in a given brain areas often project to many different brain region, further circuit specificity can be obtained utilizing the location of injection and the recording or the manipulation, together with even more complex transgenic animals/virus strategies. Indeed, different virus have distinct preferences regarding neuronal infection, with those infecting preferentially cell somas and producing anterograde labeling of the neurites (most of the

adeno-associated viruses, AAV), and those preferentially infecting axons and being retrogradely propagated to the neuronal body (such as modified herpes simplex virus, HSV). Thus optical manipulation or activity recording can be restricted to axonal projections or to neuron projecting to a specific location.

In addition, different opsins and Ca^{2+} indicators have different peaks of activation across light wavelengths, allowing parallel or simultaneous, and near-independent manipulation and recording of activity. These investigations can be targeted to the same brain region or distant, connected ones for the study of causal relationship between neuronal populations.

However, these strategies do not allow one to distinguish between different subpopulations of GABAergic neurons (for instance) collectively expressing the recombinase Cre. In other words, PV-Cre mice express Cre in all types of PV neurons, with no further discrimination (based on i.e, other markers, morphology, activity etc.) that might be necessary for dissecting precise functions bared by inhibitory neuron diversity. Intersectional genetics is one way to tackle this issue. Intersectional approaches rely on the expression of two recombinase, Cre and the Flipase (Flp, from yeast), and viral injections encoding proteins whose expression is conditioned by both recombinase. Gene expression can be restricted by expression of both recombinase in the cell or if one, and only one is expressed (equivalent to the "AND" and "OR" logic, respectively). Recent articles made pertinent use of this intersectional approach to dissect the circuits of fear response (Tovote et al., 2016; Vogel et al., 2016). In addition, endogenous neuronal activity can also drive Cre expression. Neuronal activity induces transcription of the immediate early gene *cfos*, together with Cre. Activity-dependent expression of Cre can also be limited in time through pharmacological manipulation (CreER, dependent on tamoxifen). This strategy has already proven useful for specific monitoring or manipulating of a cell population activated in a given context. Therefore, appropriate combination of transgenic animals and virus allows powerful deciphering of specific circuits.

In combination with electrophysiology, Ca^{2+} imaging, opto- and pharmacogenetics have already greatly improved dissection of brain circuits and they relation to behavior. These advances benefit from advances in molecular biology, such as genetics, but also the study of a great diversity of organism at origin of the opsins, Ca^{2+} indicator and recombinases. These proteins are then engineered to best fit the use they are serving. Research in engineering better genetically encoded proteins is an active field of research and promises other conceptual leverage in the near future. In this insert, I reviewed classic strategies for labeling, monitoring and manipulating brain activity but many different techniques or combination of them exist, allowing always more refined dissection of circuit and function of even better defined neuronal cell types.

Appendix B

GABA_BRs form large complexes.

Recently, it was found that native GABA_BRs are associated with auxiliary subunits, namely KCTD proteins (proteins that contains a K⁺ channel tetramerization domain). When expressed exogenously together with GABA_{B1} and GABA_{B2}, the KCTDs confer the receptor some of the missing kinetics and pharmacological features (Gassmann and Bettler, 2012). Notably, the composition of GABA_BRs in main and auxiliary subunits influences the receptor subcellular location, kinetics and desensitization (Gassmann and Bettler, 2012). While GABA_{B1} and GABA_{B2} are found in both vertebrates and invertebrates, KCTDs are evolutionary more recent and found only in vertebrates (Gassmann and Bettler, 2012; Pin and Bettler, 2016). Principal GABA_{B1} and GABA_{B2} subunits and auxiliary KCTDs subunits, together with the G protein, are now viewed as the core building blocks of GABA_BRs (Pin and Bettler, 2016). In addition, peripheral building blocks bind to the core binding block and generate receptor complexes with unique function and localization. Peripheral interactors comprise effector channels, elements of the presynaptic release machinery, and proteins that regulate G protein signaling (Pin and Bettler, 2016; Schwenk et al., 2015).

Appendix C

Supplemental methods

The only method I used that is not explain in one of the article is the procedure used for chronic recordings. Below, I detail the experimental procedure.

First WT mice were deeply anesthetized using a ketamine and xylazine mixture, and injected with an AAV2.9-CaMKIIa-hChR2(H134R)-eYFP-WPRE as described in the "Material and methods" section of the article. For LFP recordings, AOC axon light stimulation and local drug perfusion, I glued together two tungsten electrodes twisted together, a $400\mu m$ -diameter optical fiber and a guide cannula. It was designed such that the tip of the twisted electrodes was $1.5mm$ deeper than the tip of the optical fiber and the guide cannula. Two of these devices were hold together and implanted bilaterally in a way that the optical fibers and the guide cannula sit on the top of the OB while the twisted tungsten electrodes reached the GCL. For EEG recording, silver electrodes were placed on top of the pia, above the hippocampus, while EMG electrodes consisted in teflon-insulated stainless-steel wire implanted in the neck muscle. Reference electrodes were made of teflon-insulated silver wire. LFP, EEG, EMG and two references electrodes were solder to a 8-pin connector and lowered close to the brain surface to permit implantation of the LFP, EEG, EMG and reference electrodes bilaterally in the OB, occipital cortex and cerebellum respectively. EMG electrodes were twisted with neck muscle. The skull was next covered with a thick layer of dental cement. On the day of the experiment, the connectors was connected to a flexible wire linked to an amplifier and a signal acquisition interface board and the optical fiber to a patch cord connected to a computer-controlled laser as described in the article. Cannulas were connected to $10\mu L$ hamilton syringes and placed in the guide cannula to reach the GCL as described in the "material and methods" section of the following article. Sleep-wake cycles were analyzed using a plugin in Spike 2 and LFP recordings were analyzed as for the acute recordings.

Abstract

Cortical feedback conducts information towards earlier relays of information processing. It is instrumental for sensory perception. In the olfactory system, odorants are never experienced in isolation by the nose, and they might be meaningful to the animal or not depending on the context. Feedback inputs onto early processing stages are poised to permit selective attention to the relevant odorants in the olfactory scene. During my thesis work, I focused on understanding the key role that inhibitory GABAergic signaling plays in the cortical feedback to the olfactory bulb in mice.

The first part of my work started with the discovery of excitatory transmission between cortical feedback inputs and the olfactory bulb is modulated by metabotropic receptors for GABA. Next, the impact of this regulation on the olfactory bulb network was investigated. We found that GABAergic signaling at cortical feedback axons profoundly changes the response of the olfactory bulb output cells to odor stimulation.

In the second part of my thesis, I found that the cortical projections to the olfactory bulb not only comprises of excitatory components, but also inhibitory components. The precise origin of this GABAergic feedback was then determined and its impact on the olfactory bulb network is currently assessed. In particular, we observed that manipulating the activity of this GABAergic feedback perturbs olfactory behavior.

Résumé

Les projections corticales de retour conduisent l'information vers des relais de traitement de l'information plus précoces. Elles sont essentielles pour la perception sensorielle. En ce qui concerne l'olfaction, l'information sensorielle est constituée d'une multitude de molécules odorantes, et c'est ce mélange complexe qui pénètre dans la cavité nasale. En fonction du contexte, c'est une partie ou une autre de cet ensemble de molécules qui va être importante d'un point de vue comportemental. Les signaux corticaux de retour permettraient de focaliser son attention sur les odeurs pertinentes de l'environnement. Au cours de mon doctorat, j'ai étudié le rôle de la signalisation inhibitrice GABAergique dans ces retours corticaux vers le bulbe olfactif, le premier relais de l'information olfactive.

La première partie de mon travail a mis en évidence une modulation métabotrope GABAergique du retour cortical excitateur. Nos expériences caractérisent ensuite l'effet produit par cette modulation sur le bulbe olfactif. Nous avons ainsi démontré que la signalisation GABAergique au niveau de retours corticaux change de manière profonde la réponse du bulbe olfactif aux stimuli olfactifs.

Dans un deuxième temps, j'ai trouvé que le cortex olfactif envoie non seulement des projections de retour excitatrices, mais aussi des retours inhibiteurs. Des expériences précisent ensuite la localisation de ce retour GABAergique, ainsi que son impact sur le bulbe olfactif. Nous avons notamment observé qu'en manipulant l'activité de ces fibres GABAergiques, nous pouvions modifier le comportement olfactif.